

No. 6, Vol. 51, 1985

PIPSBD 51 (6) 905-1053

ISSN 0370-0046

Part A  
Physical  
Sciences

# PROCEEDINGS OF THE INDIAN NATIONAL SCIENCE ACADEMY



INDIAN NATIONAL SCIENCE ACADEMY  
NEW DELHI

# **Proceedings of the Indian National Science Academy**

## **Part A**

**(Physical Sciences)**

### **Editor**

**A N Mitra, Department of Physics, University of Delhi, Delhi**

### **Editorial Board**

**Sadhan Basu, Department of Chemistry, Calcutta University, Calcutta**

**J C Bhattacharyya, Indian Institute of Astrophysics, Bangalore**

**T R Govindachari, 22 Crescent Park Street, T. Nagar, Madras**

**P K Kaw, Plasma Physics Programme, Physical Research Laboratory, Navrangpura, Ahmedabad**

**A Mani (Miss), Wind Energy Project, Indian Institute of Tropical Meteorology, Raman Research Institute, Bangalore**

**G Mehta, School of Chemistry, University of Hyderabad, Hyderabad**

**K K Rohatgi-Mukherjee (Mrs), Department of Physical Chemistry, Faculty of Science, Jadavpur University, Calcutta**

**A P B Sinha, Physical Chemistry Division, National Chemical Laboratory, Pune**

**B M Udgaonkar, Tata Institute of Fundamental Research, Homi Bhabha Road, Bombay**

**R C Mehrotra, Department of Chemistry, University of Rajasthan, Jaipur**

**S P Pandya, Physical Research Laboratory, Navrangpura, Ahmedabad**

### **Assistant Executive Secretary**

**(Associate Editor/Publications)**

**M Dhara**

### **Assistant Editor**

**J. Saketharaman**

### **Annual Subscription Rates**

**(Including postage)**

**Inland : Rs 150.00**

**Foreign : US \$ 50.00**

### **Single Issue**

**Inland : Rs 30.00**

**Foreign : US \$ 10.00**

### **Editorial Office**

**The Indian National Science Academy, Bahadur Shah Zafar Marg, New Delhi 110 002, India**

**© The Indian National Science Academy, 1986. All rights reserved.**

**Proceedings of the Indian National Science Academy, Part A, is published in alternate months, i.e., January, March, May, July, September and November.**

---

## **Information to Contributors**

### **Purpose and Scope**

**PART 'A' of the Proceedings of the Indian National Science Academy is an interdisciplinary Journal in Physical Sciences devoted to publication of papers embodying results of original research in any branch of Physics, Chemistry and Geology. Contributions in Biophysics, Biochemistry, Geochemistry, Hydrology, Meteorology, Radio-Physics, Soil Physics, Soil Chemistry, and Oceanography are also accepted.**

**Papers presented at the Academy's Symposia, Special Academy Lectures and Original Review articles relating to research and concepts fundamental to Physical Sciences would also be published in the Proceedings.**

**(Continued on inside back cover)**

## SISIR KUMAR MITRA MEMORIAL LECTURE—1984

### SECOLOGANIN DERIVED BIO-DYNAMIC INDOLE ALKALOIDS

(Mrs) ASIMA CHATTERJEE FNA

Member, Rajya Sabha

and

Former Khaira Professor and Head, Department of Pure Chemistry,  
University College of Science, 92 APC Road, Calcutta-700009, INDIA

(Delivered 1 January 1985)

MR CHAIRMAN, DISTINGUISHED FELLOW COLLEAGUES AND GUESTS, LADIES AND GENTLEMEN,

At the outset I would like to express my sincere thanks to INSA and particularly to Professor A K Sharma, President, Indian National Science Academy for awarding me the *Sisir Kumar Mitra Memorial Lectureship* for the year 1984.

Before I proceed to deliver my lecture I would like to pay my respectful homage to Professor S. K. Mitra who dedicated his life to teaching and research. He established an active school of research on ionosphere, the "radio-roof" of the world, in Calcutta and was the pioneer in the field of radio research in India.

In recognition of his outstanding contributions to the field of radio research, specially in research of the upper atmospheric phenomenon, Professor Mitra was elected to the Fellowship of the Royal Society, London in 1958. He was President of the Asiatic Society during the period 1951-52, General President of the Indian Science Congress in 1955 and President of the National Institute of Sciences of India during the period 1959-60. His book on *Upper Atmosphere* received worldwide recognition. Professor Mitra had been associated with many scientific organisations.

I was fortunate to come in close association with Professor Mitra since my student days. He always encouraged me in my studies and research. His dedication and devotion infused the spirit of hard work. His affection and kindness for students irrespective of different disciplines and his sincere friendliness towards his colleagues show the humane aspects of his life. He was indeed a man of wide culture and liberal outlook.

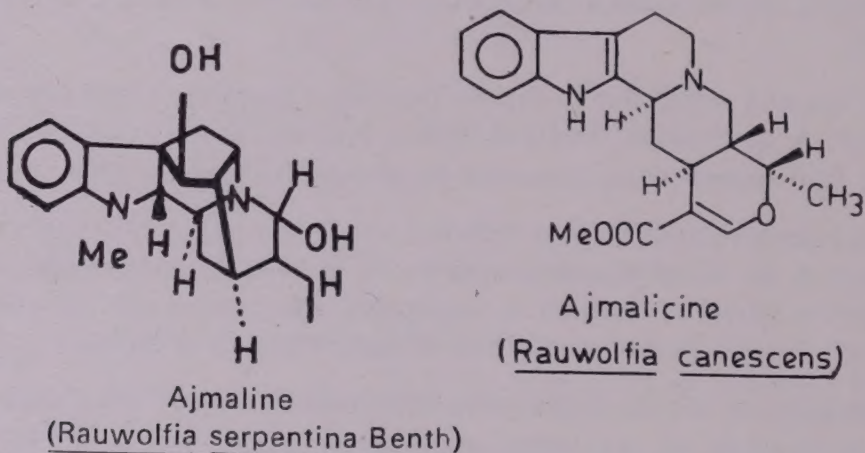
Professor Mitra was a lover of Nature and always took a keen interest in the maintenance of the gardens at Science College, University of Calcutta.

I will speak today on some aspects of Natural Products, the topic being "Secologanin Derived Bio-Dynamic Indole Alkaloids."

Since 1803 when Derosne isolated the alkaloid narcotine from opium (*Papaver somniferum* Fam. Papaveraceae) followed by the discovery of morphine, the painkiller, by Sertürner the alkaloids have grown to become the largest group of natural products. The impetus for pursuit of research in these compounds has come largely from the interest in their biological activity and their molecular complexities displaying a diversity of structure unmatched by any other group of natural products. A Russian review to the middle of 1973 reported the isolation of 4,959 alkaloids of which 3,293 had known structures. In 1976, the number was closer to 4000 structurally defined alkaloids.<sup>1</sup>

The therapeutic values of alkaloids are well documented and do not need any elaboration. It may be mentioned, however, that intensive studies on medicinal properties of alkaloids have culminated in the discovery of many valuable drugs including hypotensive and antileukemics.

Recently, two indole alkaloids—ajmaline and ajmalicine are being used extensively as coronary dilator and antiarrhythmic.



Alkaloids have been extensively evaluated by those interested in evolutionary relationships. Since the biosynthetic pathways could be delineated it has been possible to attach taxonomic significance to their distribution.

Although most alkaloids occur in the flowering plants, the Angiosperms, they are also produced in animals, marine organisms, microorganisms and the lower plants as evidenced from the examples cited herein (Chart 1).

According to Engler there are 60 orders in the higher plant system. Of these, 34 contain alkaloid-bearing species. The major alkaloid-bearing orders are the Campanulales, Centrospermae, Gentianales, Geraniales, Liliflorae, Ranales, Rhoedales, Rosales, Rubiales, Sapindales and Tubiflorae. Within these orders the most important alkaloid-containing families are the Amaryllidaceae, Apocynaceae, Euphorbiaceae, Lauraceae, Leguminosae, Liliaceae, Loganiaceae, Menispermaceae, Papaveraceae, Ranunculaceae, Rubiaceae, Rutaceae and Solanaceae.

The greatest number of alkaloids isolated and characterised during the past three decades have been indole compounds which have been derived from isovinco-side (Strictosidine).

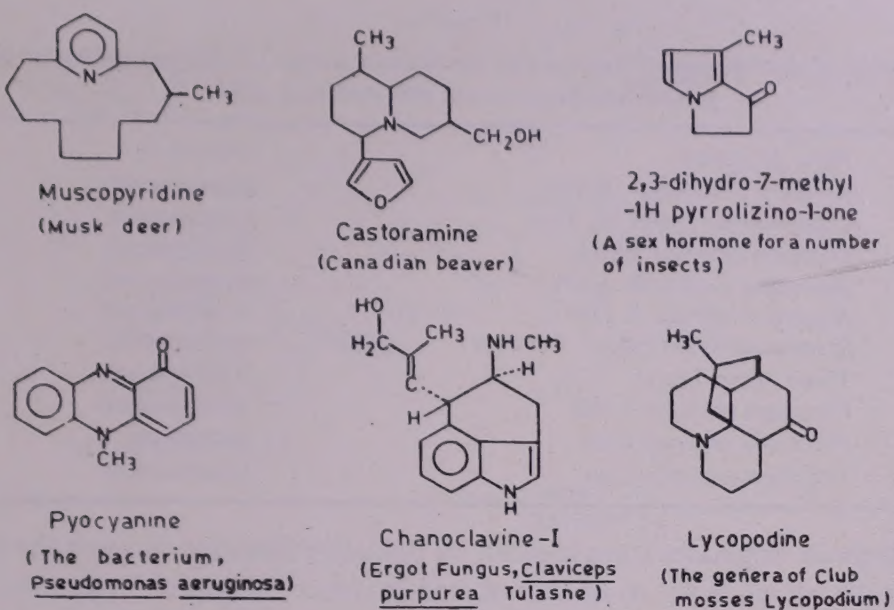
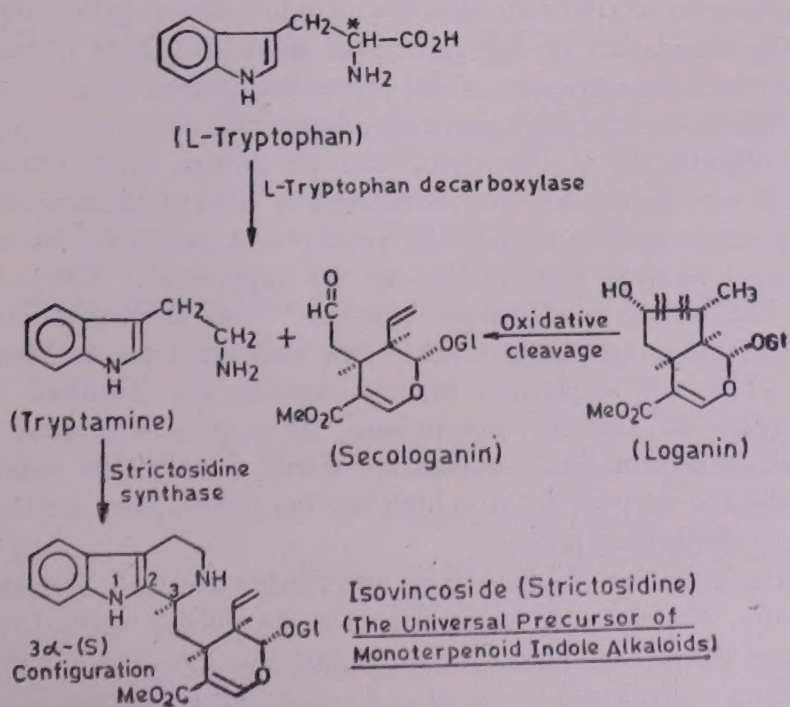


CHART 1

In this context, it deserves mention that isovincoside occupies the crucial position in the biosynthesis<sup>2</sup> of monoterpenoid indole alkaloids in higher plants. The enzyme catalyzing the Pictet-Spengler type condensation of tryptamine and the monoterpenoid, secologanin, is strictosidine synthase.<sup>2a</sup> This enzyme has been isolated from eight species belonging to different genera of Apocynaceae, the pH optimum for enzyme reaction being pH 6.0–7.0.



## CHART 2

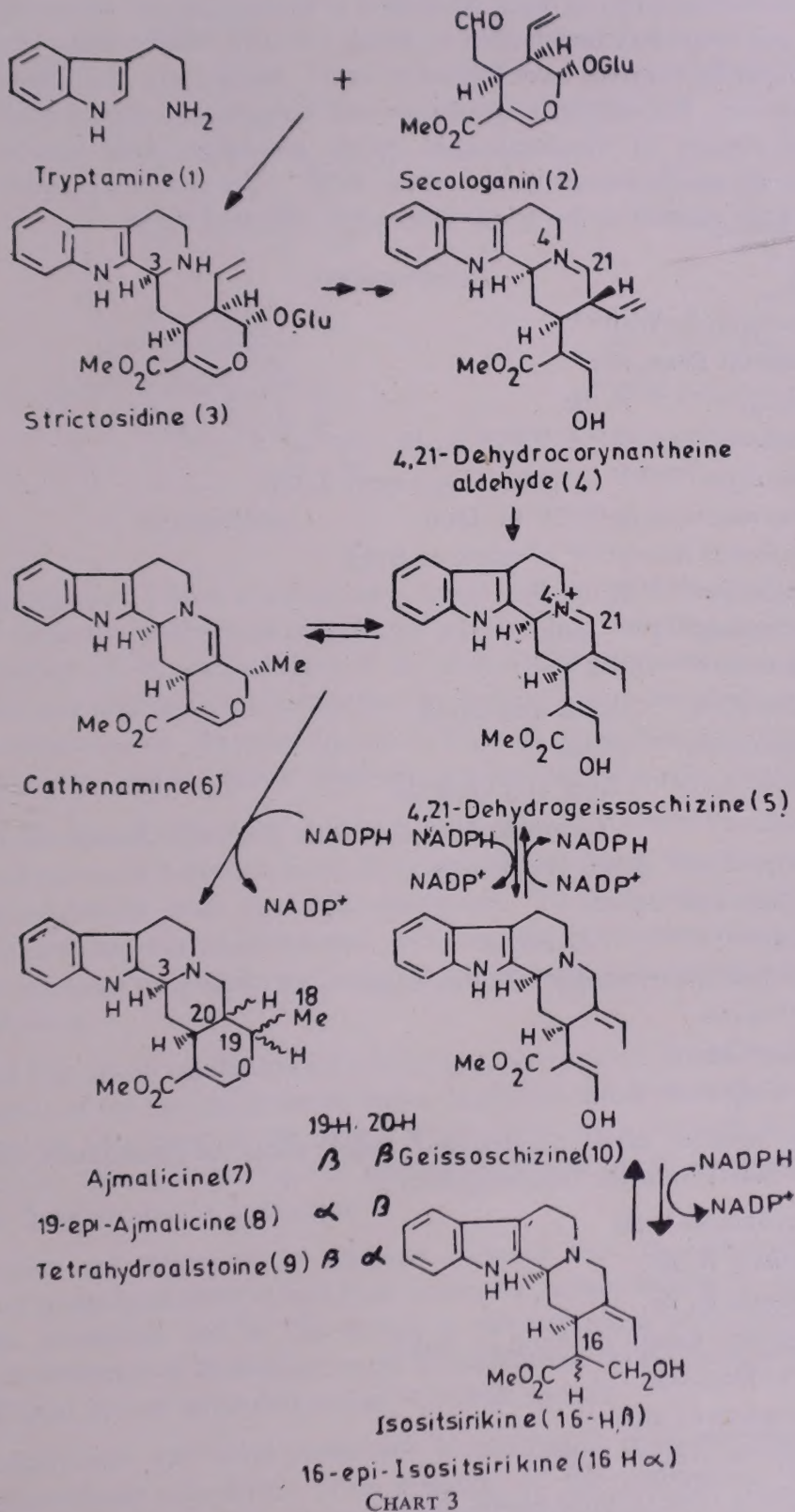
*Survey of distribution of Strictosidine Synthase in species of different genera of the family Apocynaceae and two unrelated species*

<i>Plant Material</i>	<i>Family</i>
<i>Amsonia salicifolia</i> Pursh	Apocynaceae
<i>Catharanthus roseus</i> G. Don	Apocynaceae
<i>Ochrosia elliptica</i> Labill	Apocynaceae
<i>Rauwolfia vomitoria</i> Afzel	Apocynaceae
<i>Rhazya orientalis</i> A. DC	Apocynaceae
<i>Stemmadenia tomentosa</i> Greenm	Apocynaceae
<i>Vinca minor</i> Linn	Apocynaceae
<i>Voacanga africana</i> Rolfe	Apocynaceae
<i>Nicotiana tabacum</i> Linn	Solanaceae
<i>Trifolium pratense</i> Linn	Leguminosae

Secologanin originates from loganin by oxidative cleavage through the participation of enzyme which is yet to be reproduced *in vitro*. Loganin<sup>3,4</sup> was first isolated from *Strychnos nux vomica* of the family Loganiaceae (hence the name, loganin) by Dunstan and Short in 1884, later by Rosenthaler in 1928 from *Menyanthes trifoliata*, a plant species of the family Gentianaceae and subsequently from *Vinca rosea* L. (*Catharanthus roseus* G. Don).<sup>3</sup> The enzyme which is involved in the oxidative cleavage of loganin does not occur in either of these plants viz. *Strychnos nux vomica* and *Menyanthes trifoliata* but in *Catharanthus roseus* G. Don of the family Apocynaceae. Loganin when fed to *Catharanthus roseus* (earlier known as *Vinca rosea* L.)<sup>3</sup> is metabolized to secologanin.<sup>5</sup>

Isovincoside (Strictosidine) undergoes various reactions including rearrangements leading to diverse skeleta<sup>6,7</sup> apparently having no similarity. Since isovincoside<sup>2,2a</sup> is the universal precursor of all the monoterpenoid indole alkaloids investigation is being pursued for the elucidation of biosynthesis of alkaloids (Chart 3) and biosynthetic interconversions with the assistance of cell suspension culture techniques and with the application of highly sensitive analytical methods e.g. radioimmunoassay.<sup>2a</sup> An obvious advantage of cultured cells is that tissue can be grown under exactly controlled conditions and on a large scale thus providing any desired amount of homogeneous plant material as an enzyme source. By appropriate growth conditions, the formation of potential enzyme inactivators can be suppressed. These are the main reasons that the isolation of cell-free systems from suspension cultures is more promising than from intact plants which often contain high amounts of enzyme inactivators. The cell suspension cultures provide an excellent material for enzymatic studies on alkaloid biosynthesis. It is quite likely that the biogenetic potential of alkaloid formation is genetically fixed, thereby the callus tissue and suspension cultures derived from a high yielding parent plant are to be expected to retain this biosynthetic capacity.

In fact after initiation of callus tissue and further selection for high producing cell strains, the alkaloid production in suspension cultures derived from the plants exceeded that of the original plants, *Catharanthus roseus*.<sup>6</sup> The composition of the nutrient medium controls the synthesis and accumulation of alkaloidal constituents,



the secondary metabolites of the plant cells. This is augmented by supplementing the medium with the biogenetic precursor viz., *L*-tryptophan. Another important

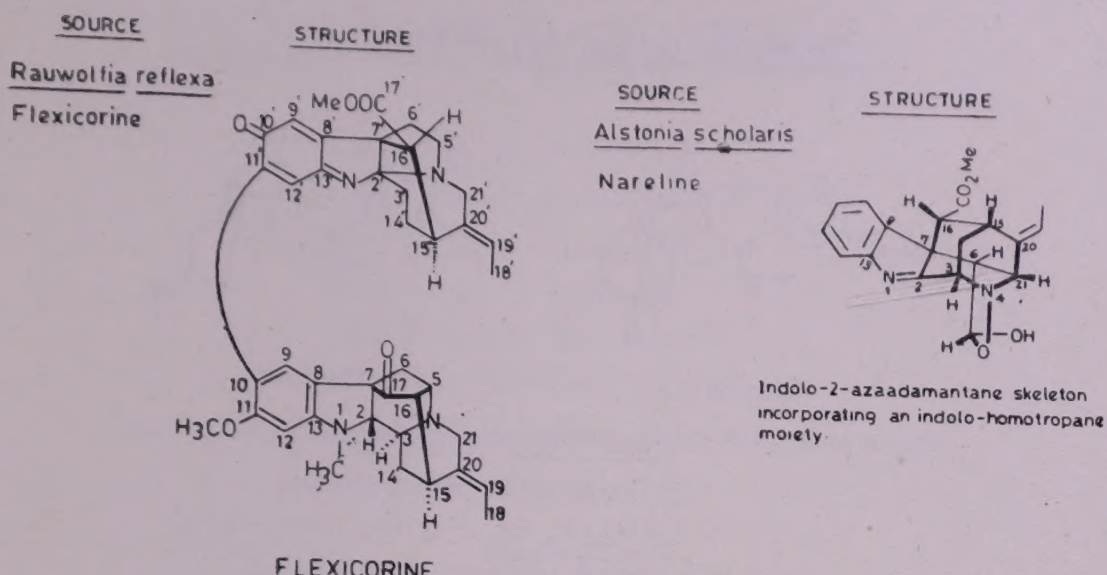
area viz., chemotaxonomy is being developed to understand the relationship between taxonomy and secondary metabolites to which category alkaloids are considered. In these cases specific enzymes have the major role. Studies on the chemotaxonomy of Apocynaceae, Rubiaceae, Loganiaceae and Nyssaceae, have revealed that these are the rich sources of monoterpenoid indole alkaloids. Our interest has been centered round apocynaceous species since 1939. The particular genus and species which had been studied so far in our laboratory are cited below :

#### APOCYNACEAE

- Alstonia macrophylla* Wall<sup>7,8</sup>
- Alstonia nerifolia* Denn. Sci.<sup>9</sup>
- Alstonia scholaris*<sup>10,11,12</sup> R. Br.
- Alstonia venenata*<sup>13,14,15,16,17,18,19,20,21</sup> R. Br.
- Catharanthus roseus*<sup>22,23,24</sup> G. Don (*Vinca rosea* Linn)
- Chonemorpha macrophylla*<sup>25,26,27</sup> G. Don
- Kopsia pruniformis* Reichl<sup>28,29</sup> of etzoll ex Bakh
- Rauwolfia beddomei*<sup>22,30</sup> Hook F
- Rauwolfia canescens*<sup>22,30,31</sup> Linn
- Rauwolfia decurva*<sup>22,30</sup> Hook F
- Rauwolfia densiflora*<sup>22,30</sup> Benth and Hook
- Rauwolfia micrantha*<sup>22,30</sup> Hook F
- Rauwolfia perakensis*<sup>22,30</sup> King and Gamble
- Rauwolfia reflexa*<sup>22,30,32,33</sup> Teijsm & Binn Syn with *Rauwolfia Sumatrana* (Mig) Jack
- Rauwolfia serpentina*<sup>31</sup> Benth Hook
- Rauwolfia vomitoria*<sup>35</sup> Afzel
- Rhazya stricta*<sup>36,37,38,39,40,41</sup> Decaisne
- Tabernaemontana sphaerocarpa*<sup>42</sup> Blume, Bijdr
- Vinca major*<sup>43</sup> Linn
- Vinaca pusilla*<sup>44</sup> Murr
- Voacanga grandifolia*<sup>45</sup> Rolfe

A large number of monoterpenoid indole alkaloids (monomeric and dimeric) have been isolated from the following taxa :

- Alstonia macrophylla* Wall
- Alstonia scholaris* R. Br.
- Alstonia venenata* R. Br.
- Kopsia pruniformis* Reichl of etzoll ex Bakh
- Rhazya stricta* Decaisne
- Rauwolfia canescens* Linn
- Rauwolfia reflexa*—Teijsm & Binn
- Tabernaemontana sphaerocarpa* Blume, Bijdr
- Vinaca major* Linn
- Voacanga grandifolia* Rolfe



On this occasion, I have selected two novel indole alkaloids—"Nareline and flexicorine" from the plethora of compounds we have been working on. Nareline is a minor component of *Alstonia scholaris* R. Br. and is still being used as an antimalarial in the traditional medicine in combination with other herbal materials. It bears an indolo-2-azaadamantane skeleton incorporating an indolohomotropane moiety hitherto unknown among indole alkaloids and has opened a new chapter in indole chemistry.

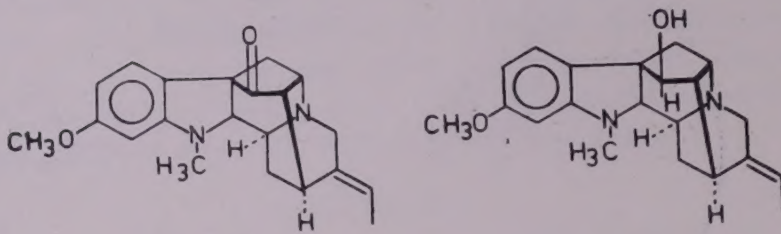
The second one is a dimeric base, flexicorine<sup>33</sup> occurring in *Rauwolfia reflexa* which is synonymous with *Rauwolfia sumatrana*. To my knowledge, flexicorine is the first 10'-hydroxy-Na-unsubstituted indoline derivative which preferentially exists in the oxidised iminoquinone form. Such iminoquinone indole alkaloids were hitherto unknown.

I would first speak on flexicorine which is an unusual red dimeric indole alkaloid and a congener of the two monomeric bases, rauflexine and reflexine.<sup>17</sup> Rauflexine and reflexine are two new indole bases which had been isolated and studied in our laboratory. The co-occurrence of rauflexine and reflexine is significant as they are found to be incorporated in flexicorine.

Flexicorine was reluctant to undergo cleavage into its monomers. Neither reductive nor hydrolytic method had been successful in such fission of the molecule. Any drastic procedure led to the complete disintegration of the molecule. The molecular architecture of flexicorine could be established mainly from detailed studies of <sup>1</sup>H NMR and proton noise-decoupled <sup>13</sup>C NMR spectra.

The amorphous red solid could only be purified by repeated preparative TLC followed by treatment with ether. The presence of the conjugated chromophore could be recognised from the electromagnetic radiation spectra as evidenced from the strong light absorption in the visible region coupled with the bright colour of the compound.

Rauwolfia reflexa Teijsm and Binn  
(Leaves)



Rauflexine

Reflexine

Red Dimeric Alkaloid

Flexicorine (Amorphous)

C<sub>41</sub>H<sub>44</sub>N<sub>4</sub>O<sub>5</sub>; Purified by repeated

TLC followed by treatment with Ether.

The proton-noise-decoupled <sup>13</sup>C NMR spectrum of flexicorine exhibited unique resonances for 39 carbons and a double intensity signal at 50ppm representing two non-protonated carbons.

From ND and SFORD spectra which correspond to 41 carbon atoms it could be established that below 80ppm (Chart 4).

ND and SFORD spectra correspond to 41 C atoms

Below 80 ppm : 2 Nonprotonated carbons

2 Methines (-CH)

8 Methylenes (-CH<sub>2</sub>)

5 Methyls

Above 90 ppm : 13 Quaternary carbons (-C-)

6 Methine carbons (-CH-)

<sup>1</sup>H-<sup>13</sup>C coupling patterns (SFORD): 44 Hydrogens are bonded directly to carbons.

## CHART 4

From a careful analysis of the electromagnetic radiation spectra and 270MHz <sup>1</sup>H NMR spectra, it has been possible to ascertain some of the functionalities as also the total number of protons in flexicorine.

The <sup>1</sup>H NMR spectra showed 4 well separated signals in the aromatic region ( $\delta$  7.35, 7.01, 6.58 and 6.31). The special feature is the presence of 4 well separated

**UV, IR,  $^1\text{H}$  NMR Spectra (270 MHz)**

---

$-\text{COOCH}_3 \longrightarrow 1$   
 Indoline- $\text{NCH}_3 \longrightarrow 1$   
 $\text{Ar}-\text{OCH}_3 \longrightarrow 1$   
 $\equiv \text{CH}-\text{CH}_3 \longrightarrow 2$   
 $>\text{C=O}$  (saturated)  $\rightarrow 1$   
 $>\text{C=O}$  (Conjugated)  $\rightarrow 1$

and 4 well separated singlets in the aromatic region  
 ( 8 7.35, 7.01, 6.58 and 6.31 )

Flexicorine     $\text{C}_{41}\text{H}_{44}\text{N}_4\text{O}_5$

CHART 5

singlets and the absence of *ortho* and *meta* protons. This observation has proved useful in ascertaining the substitution pattern in the aromatic ring (Chart 5).

Now the question is what would be the structural feature of flexicorine in conformity with these observations.  $^{13}\text{C}$  NMR spectra were highly complicated because of the combined spectra of two monomers. However, after careful scanning and critical analysis of the combined spectra, several important informations regarding one of the monomers were available. Twenty one carbon signals showed striking resemblance to that of rauflexine (Chart 6).

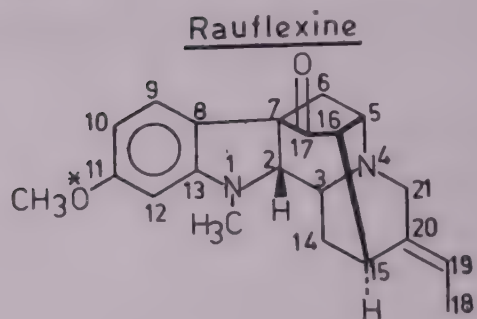
From a comparison of the  $^1\text{H}$  NMR spectra of rauflexine and flexicorine the nature of the substitution pattern in the aromatic ring could be ascertained. Both  $\text{C}_{10}$  and  $\text{C}_{11}$  in flexicorine were found to be substituted which confirmed the earlier observation that *ortho* and *meta* protons were absent. Interestingly all the non-aromatic resonances in rauflexine were reproduced in the  $^{13}\text{C}$  NMR spectra of flexicorine thus identifying rauflexine as half of the bis alkaloid. From  $^1\text{H}$ - $^{13}\text{C}$  coupling pattern it became clear that rauflexine which constitutes one of the monomers was attached to the other half of the molecule through its aromatic ring at  $\text{C}_{10}$ ,  $\text{C}_{11}$  being associated with a methoxyl group.

Coming to other functionalities viz., the carbo-methoxyl, the conjugated ketone and ketone geminal diamino system ( $-\text{N}(\text{---})\overset{\text{---}}{\text{C}}(\text{---})\text{N}(\text{---})$ )

it was the apparent that these must reside in the remaining half which also bears which the second ethyldiene function.

Regarding the information of the skeletal pattern of the second half we had to depend on  $^{13}\text{C}$  NMR spectra as no other method could be evolved to isolate and identify this unit by suitable chemical processes.

From a literature survey of indole alkaloids it came to our notice that the functional groups distribution including geminal diaminosystem ( $-\text{N}(\text{---})\overset{\text{---}}{\text{C}}(\text{---})\text{N}(\text{---})$ ) and



(C<sub>21</sub>H<sub>24</sub>N<sub>2</sub>O<sub>2</sub>)

Carbon Chemical Shift (ppm)

Carbon	Rauflexine	Flexicorine	Carbon	Rauflexine	Flexicorine
2	78.4	78.1 d	13	155.1	155.7 s
3	50.1	50.0 d	14	35.3	35.0 t
5	53.1	52.8 d	15	28.5	28.3 d
6	31.5	31.5 t	16	50.3	50.0 d
7	57.8	57.5 s	17 (>C=O)	214.0	212.7 s
8	121.6	120.6 s	18	12.9	12.8 q
9	122.5	124.1 d	19	115.7	115.7 d
*10	103.8(d)	115.5 s	20	137.3	136.8 s
11	160.1	157.8 s	21	55.7	55.4 t
12	97.5	94.4 d	-N-CH <sub>3</sub>	34.2	33.9 q
			Ar-OCH <sub>3</sub>	55.3	55.5 q

\* <sup>1</sup>H-<sup>13</sup>C coupling pattern is different (C<sub>10</sub> in flexicorine is substituted)

Functionalities in Flexicorine (C<sub>41</sub>H<sub>44</sub>N<sub>4</sub>O<sub>5</sub>)

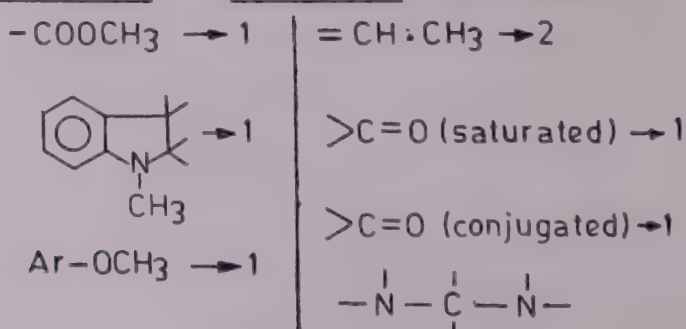
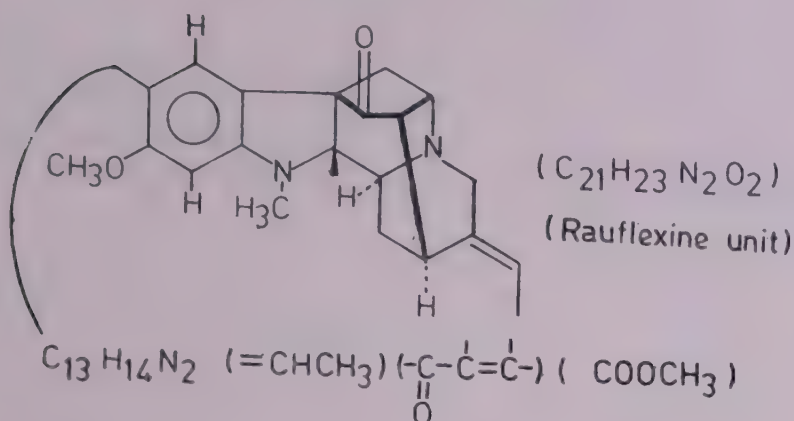
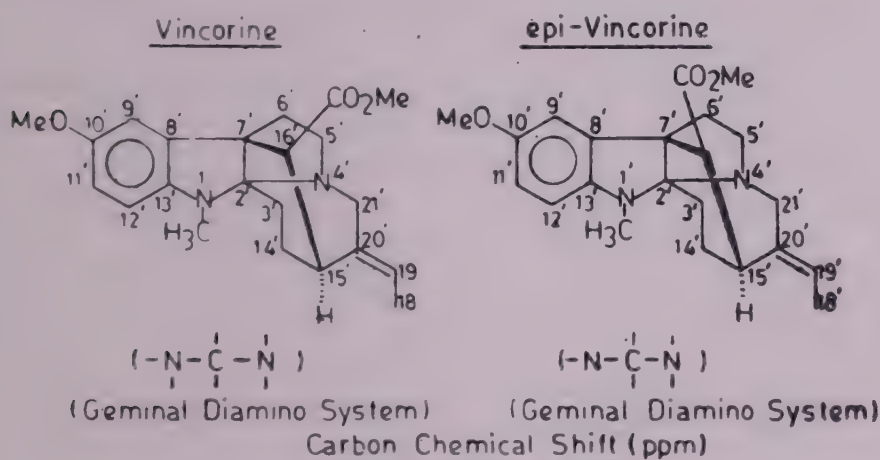


CHART 6

almost all the nonaromatic signals in flexicorine had been reminiscent of that of vincorine,<sup>40</sup> an alkaloid of *Alstonia deplanchei* (Apocynaceae). Disparities were observed only for the C<sub>2'</sub> and C<sub>6'</sub>-resonances and the carbon values in the aromatic region.

Flexicorine ( $C_{41}H_{44}N_4O_5$ )

The variation in the carbon signals at  $C_{6'}$  may be accommodated by the removal of the  $\gamma$ -effect at  $C_{6'}$  from the  $C_{16'}$ -carbomethoxyl. This implied that the configuration of  $C_{16'}$ -carbomethoxyl is opposite to that of vincorine and the same as that of  $C_{16'}$  in epivincorine (Chart 7).



Carbon	Vincorine	Flexicorine	Carbon	Vincorine	Flexicorine
*2'	97.9	103.6	14'	26.3	27.5
3'	40.6	40.7	15'	34.8	35.4
5'	56.1	53.5	16'	50.7	49.8
*6'	20.4	26.5	17'	173.5	172.2
7'	57.3	56.5	18'	13.6	13.6
8'	138.2	144.4	19'	123.2	122.7
*9'	105.5	122.9	20'	138.2	138.8
*10'	152.3	186.6	-COOCH <sub>3</sub>	51.7	51.6
*11'	111.7	157.5	-NCH <sub>3</sub>	28.3	—
*12'	112.1	130.5	-O-CH <sub>3</sub>	54.9	—
*13'	143.6	164.0			

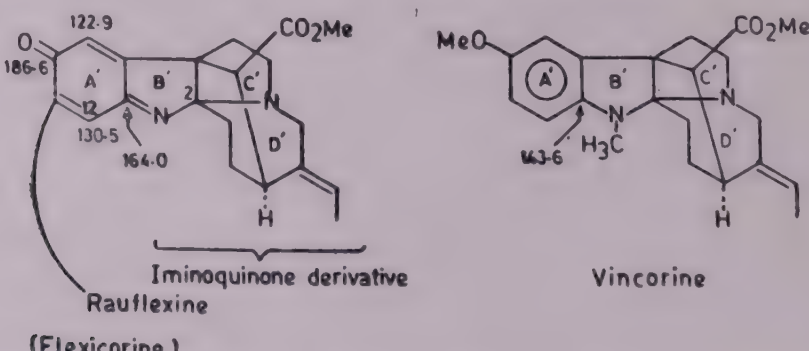
CHART 7

So far as the disparity of  $C_{2'}$  resonance is concerned the value is close to that of the carbon involved in the geminal diaminosystem (i.e. — $\begin{array}{c} | & | \\ N & C \\ | & | \\ N & — \end{array}$ ). However, the difference in values by 5ppm at  $C_{2'}$  was due to the oxidation state of the aromatic ring system. This was also apparent from the resonances of the aromatic carbon at  $C_9'$ ,  $C_{10'}$ ,  $C_{11'}$ ,  $C_{12'}$  and  $C_{13'}$ . The values of the carbon chemical shifts provided ample evidence regarding the modification of the aromatic ring A of the vincorine unit.

Coming to the carbon signal at  $C_{10'}$  we observed that the chemical shift appeared at 186.6ppm, a field position 20ppm lower than any known heterosubstituted dihydroindole resonance. This was typical of quinone carbonyl revealing that the aromatic ring had been modified to a quinone structure. The resonances at 186.6ppm and the nonprotonated carbon signal at 164.0ppm each revealed a single long range  $^1\text{H}$ — $^{13}\text{C}$  coupling constant of 8.5Hz, typical of  $3 J_{\text{CH}}$  transmitted through a trigonal path.

In this context, it would be worthwhile to mention that the carbonyl resonances of 2,6-di-tert-butylquinones appear at 187.2 and 188.2 ppm, ( $3 J_{\text{CH}} = 9.5\text{Hz}$ ). These observations and the disparities in the  $C_{2'}$ ,  $C_9'$ ,  $C_{10'}$ ,  $C_{11'}$ ,  $C_{12'}$  &  $C_{13'}$  carbon resonances as mentioned earlier indicated that the benzpyrrole i.e. the indole moiety (A' B' ring system) had been modified to an iminoquinone form.

In order to substantiate this unusual feature which is hitherto unknown in indole alkaloids the proton-noise-decoupled  $^{13}\text{C}$  NMR spectra of a model system of iminoquinone derivative were examined. Surprisingly, all the values for  $C_9'$ ,  $C_{10'}$ ,  $C_{11'}$ ,  $C_{12'}$  and  $C_{13'}$  were in consonance with the iminoquinone structure. This



A' ring in Vincorine has been modified to Iminoquinone derivative.



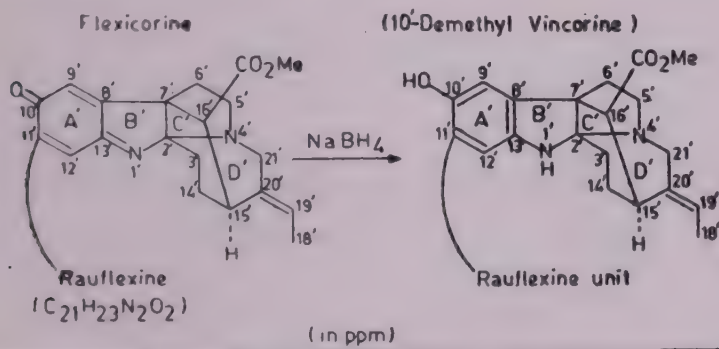
iminoquinone structure could explain the difference in carbon resonances at C<sub>2'</sub> of flexicorine and vincorine. The unusual oxidation state of the aromatic ring i.e. iminoquinone form was reflected in the downfield shift of the C<sub>2'</sub> signal.

The observation on the modification of the aromatic ring A' could be substantiated by appropriate experiments. When treated with NaBH<sub>4</sub> in methanolic solution in an argon atmosphere flexicorine underwent an interesting transformation. The deep red colour of the base changed to pale yellow. The product on examination showed the reduction of the C<sub>17</sub>-keto carbonyl to the 17- $\alpha$ -hydroxyl. Further change was observed in the ring A'. It was converted to an aromatic system with the generation of a phenolic—OH arising out of the reduction of quinone carbonyl and with the simultaneous appearance of an indoline—NH due to the reduction of the indolenine moiety. The change induced major chemical shift alterations of the aromatic carbon resonances of flexicorine.

In NaBH<sub>4</sub> reduction product of flexicorine (Chart 8) the carbon signal at 186.6 ppm at the quinone carbon was altered remarkably. This signal and the nonprotonated carbon resonances at 164.00 ppm changed to 147.8 and 142.4 ppm respectively.

Both the aromatic and nonaromatic carbon signals in NaBH<sub>4</sub> reduction product were compatible with that of vincorine (Chart 8).<sup>21</sup>

Further interesting observation was the regeneration of the deep red colour when the methanolic solution of the sodium borohydride reduction product was

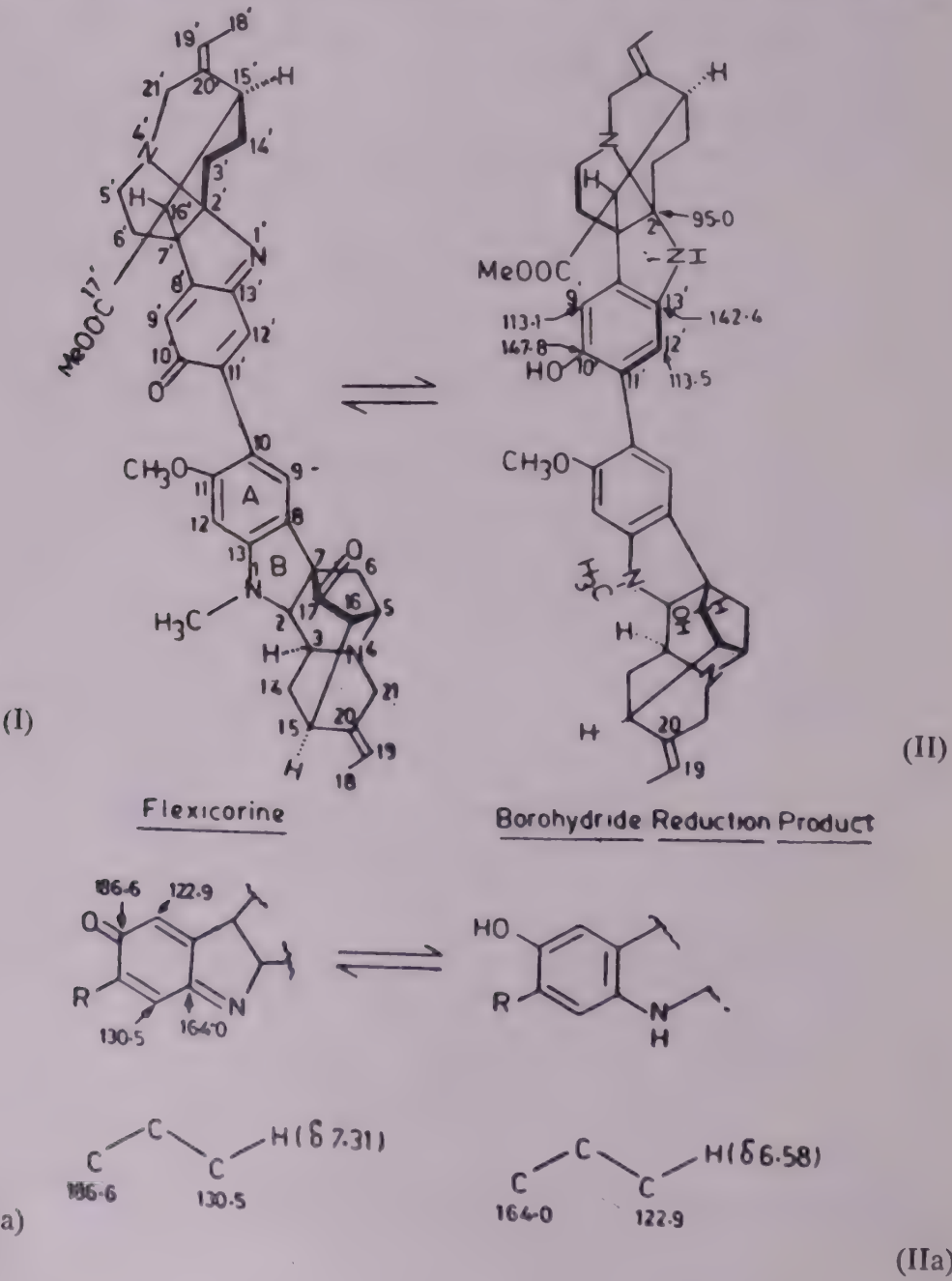


Carbon	Vincorine	Flexicorine	NaBH <sub>4</sub> Reduction Product	Carbon	Vincorine	Flexicorine	NaBH <sub>4</sub> Reduction Product.
• 2'	97.9	103.6	95.0	14'	26.3	27.50	26.2
• 3'	40.6	40.7	• 40.5	15'	34.8	35.4	35.1
• 5'	56.1	53.5	56.3	16'	50.7	49.8	50.5
• 6'	20.4	26.5	26.5	17'	173.5	172.2	173.2
• 7'	57.3	56.5	57.3	18'	13.6	13.6	13.6
• 8	138.2	144.4	137.9	19'	123.2	122.7	122.9
• 9'	105.5	122.9	113.1	20'	138.2	138.8	138.4
• 10'	152.3	186.6	147.8	-COOCH <sub>3</sub>	51.7	51.6	51.6
• 11'	111.7	157.5	126.9	-N-CH <sub>3</sub>	28.3	—	—
• 12'	112.1	130.5	113.5	-O-CH <sub>3</sub>	54.9	—	—
• 13	143.6	164.0	142.4				

### ND(Noise decoupled) & SFORD Spectra of Flexicorine

CHART 8

exposed to air. The oxidation product was found to be identical with flexicorine. This is what is exactly expected from an iminoquinone derivative. In this context, studies on  $^1\text{H}$ - $^{13}\text{C}$  cross-coupling experiments had proved useful.  $^1\text{H}$ - $^{13}\text{C}$  cross-coupling experiments showed that the proton at  $\delta$  7.31 corresponding to the proton at  $\text{C}_{12'}$  exhibited one and three bond coupling to the carbon resonances at 130.5 and 186.6 ppm whereas the proton at  $\text{C}_9'$  ( $\delta$  6.58) exhibited one and three bond coupling to the carbon resonances at 122.9 and 164.00 ppm. Since the methines at 130.5 and 122.9 ppm were shifted upfield strongly in the borohydride reduction product four of the six carbon resonances of the A' ring of the alkaloid that were altered in the borohydride reduction product may be grouped into two geminally



related pairs (Ia) and (IIa). These fragments, together with the constraint of the proton substitution pattern are in complete harmony with the iminoquinone structure which confirmed flexicorine to have structure (I) and its  $\text{NaBH}_4$  product to have structure (II).

The two remaining methines which suffer minimal perturbation between flexicorine and its sodium borohydride reduction product belong to A ring. One of these shifts, 94.4 ppm was diagnostic for  $\text{C}_{11}$  oxygen substituent establishing  $\text{C}_{10}$  as the linkage site in this base. This was confirmed by the field position of the remaining aromatic methine, 124.1 ppm, which cannot be situated ortho to the oxygen-bearing carbon.

Thereby flexicorine is the first 10'-hydroxy-Na-substituted indoline derivative which preferentially exists in the oxidised iminoquinone form (I).

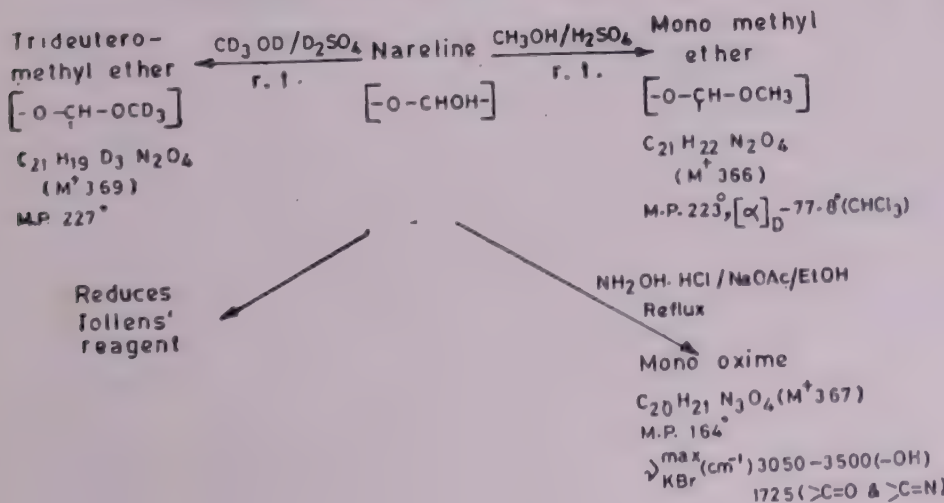
### NARELINE

Nareline is a novel indole alkaloid isolated from *Alstonia scholaris* R. Br. To establish the indolo-2-azaadamantane structure of this basic constituent where an indole homotropane unit is incorporated it took us more than six years to settle the structure of this complex base and its derivatives. Even after publishing our first paper, we are still working on the structures of some of its reaction products. I would be discussing today some of the more interesting reactions of nareline typical of indolo-2-azaadamantane skeleton.

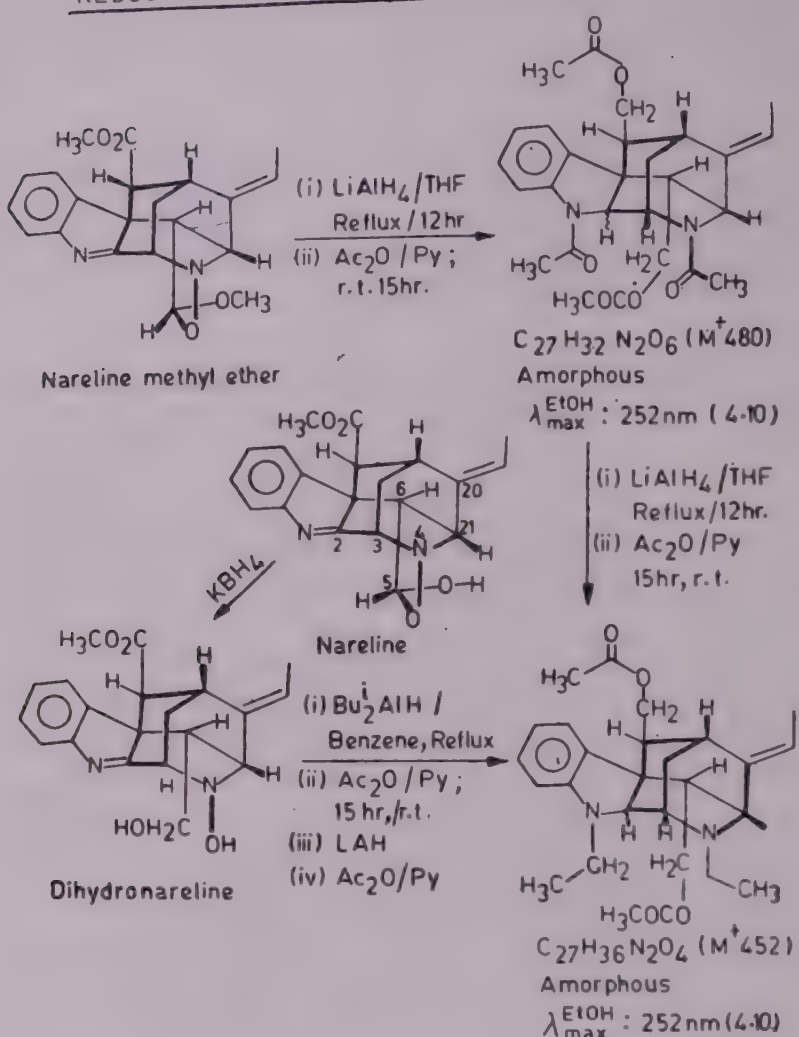
The most unusual feature in this alkaloid is the presence of Nb-hydroxylamine moiety involved in a hemiacetal formation with the formyl group of the tryptophal derivative through the neighbouring group participation.

$^1\text{H}$  NMR spectra of nareline methyl ether could provide important structural information. Particularly useful were the decoupling experiments with nareline methyl ether and acetyl to establish the sequence of carbon linkages in the alkaloid

### REACTIONS OF NARELINE



## REDUCTION OF NARELINE DERIVATIVES



skeleton. A methine group at  $C_3$  appeared as a triplet at  $\delta$  4.65 with coupling constant of 3Hz. Irradiation of this signal caused the double triplets at  $\delta$  2.10 and  $\delta$  2.36, the signals for geminal protons at  $C_{21}$  to collapse to double doublet. Similarly, the irradiation of one proton quartet at  $\delta$  2.27 at  $C_{16}$  also collapsed to a singlet during the irradiation of the signals from  $\delta$  2.0-2.5. This confirmed the linkage of  $C_3-C_{14}-C_{15}-C_{16}$ . The unusual attachment between  $C_6$  and  $C_{21}$  could be recognised from decoupling experiments. However,  $C_3$  and  $C_{21}$ —two methine protons appeared at low-field at  $\delta$  4.65 and  $\delta$  4.06 because of their attachment to heteroatoms. From the sequence of carbon linkages as shown it was apparent that nareline has modified C ring picraline skeleton (Charts 9 and 10).

With methanolic sulphuric acid at room temperature nareline formed a mono-methyl derivative. This change corresponded to the conversion of the hemiacetal grouping to an acetal. When the reaction was performed in  $\text{CD}_3\text{OD}/\text{H}_2\text{SO}_4$  the corresponding trideuteromethyl ether was obtained.

25 MHz CMR( $\text{CDCl}_3$ ) ASSIGNMENTS OF NARELINE DERIVATIVES  
 (Chemical shifts in ppm)

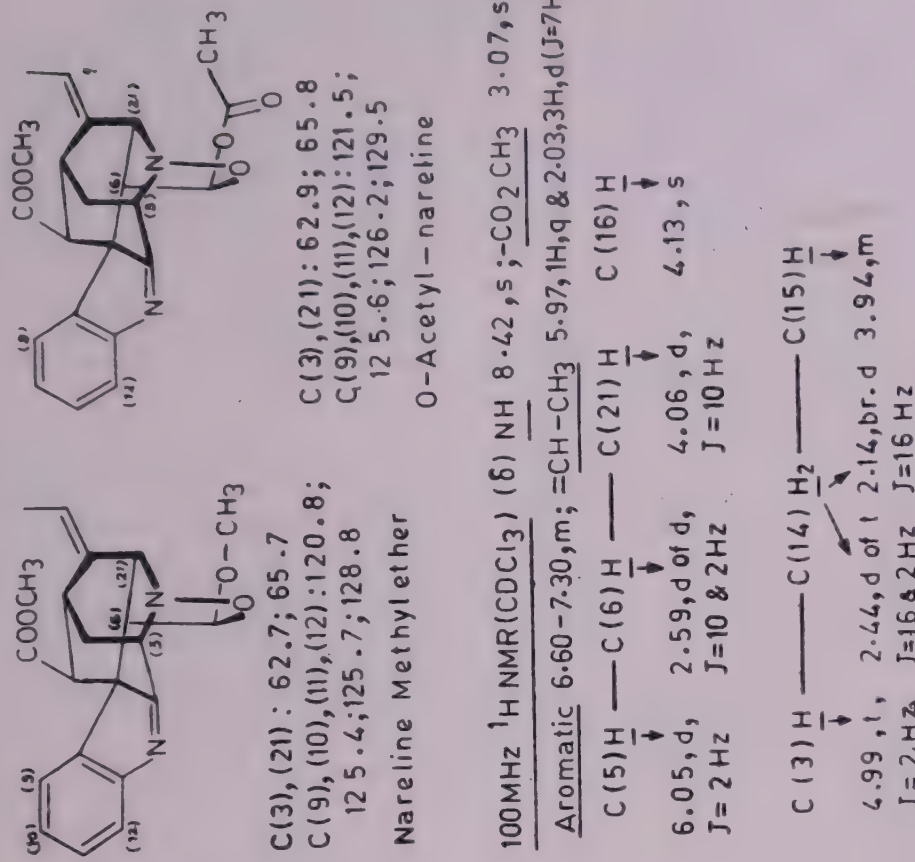
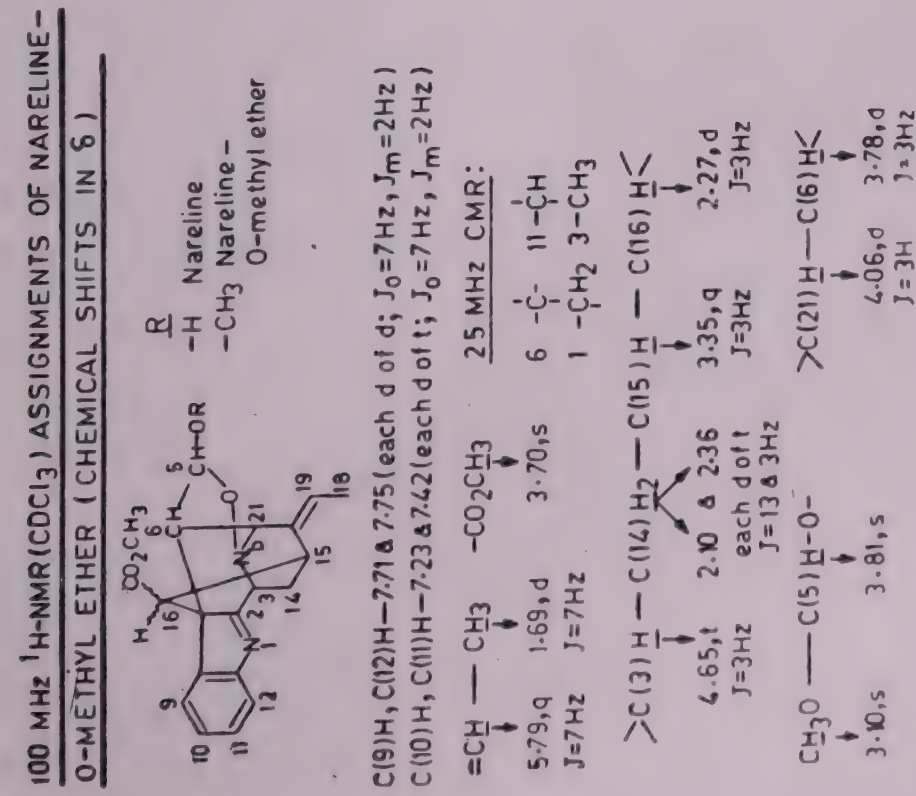


CHART 9

CHART 9

CHART 10

On treatment with  $\text{NH}_2\text{OH HCl/NaOAc}$  the base afforded a monoxime.

The high resolution mass spectra (Chart 11) of nareline and its acetate showed the loss of  $-\text{CHO}$  (formyl group) while its methyl and trideuteromethyl ethers revealed the loss of  $\text{NO}$  from the molecular ion. Such loss of  $\text{NO}$  is typical of 3,5-ditaryl and 3-tolyl-5-phenylisooxazolines. Another characteristic feature is the observance of the peak at  $m/z$  307 in the mass spectrum of nareline ( $M\text{-O-CHO}$ ), its methyl ether ( $M\text{-C}_2\text{H}_3\text{O}_2$ ), its trideuteromethyl ether ( $M\text{-C}_2\text{D}_3\text{O}_2$ ) and its oxime ( $M\text{-CH}_2\text{NO}_2$ ). This type of fragmentation is reminiscent of the loss of  $\text{C}_5\text{H}_9\text{O}_2$  moiety in 5-butyloxy-2-methyl-3-phenyl-isooxazoline. Such fragmentation is typical of a  $-\text{N-O-CHOH}$  linkage. This could explain the ejection of  $-\text{CHO}$  from nareline and  $\text{NO}$  from the monomethyl ether and *not*  $-\text{CHO}$  because of  $-\text{CHO}$  being bound into acetal form.

Nareline had been subjected to reduction with various reagents under different conditions. The unusual hemiacetal was affected as also the indolenine and carbomethoxyl. Controlled reduction of nareline in methanol with  $\text{KBH}_4$  gave a dihydroderivative in which the marked aldehydic function was reduced to a primary alcohol with the generation of hydroxylamine  $\text{N}_b\text{OH}$ . During reduction nareline monomethyl ether, however, suffered reductive demethylation.

The UV spectrum of this compound was unchanged and exhibited peak at 218 and 256nm characteristic of an indolenine chromophore. Dihydronareline on acetylation yielded a diacetyl derivative as would be expected from the assigned structure.

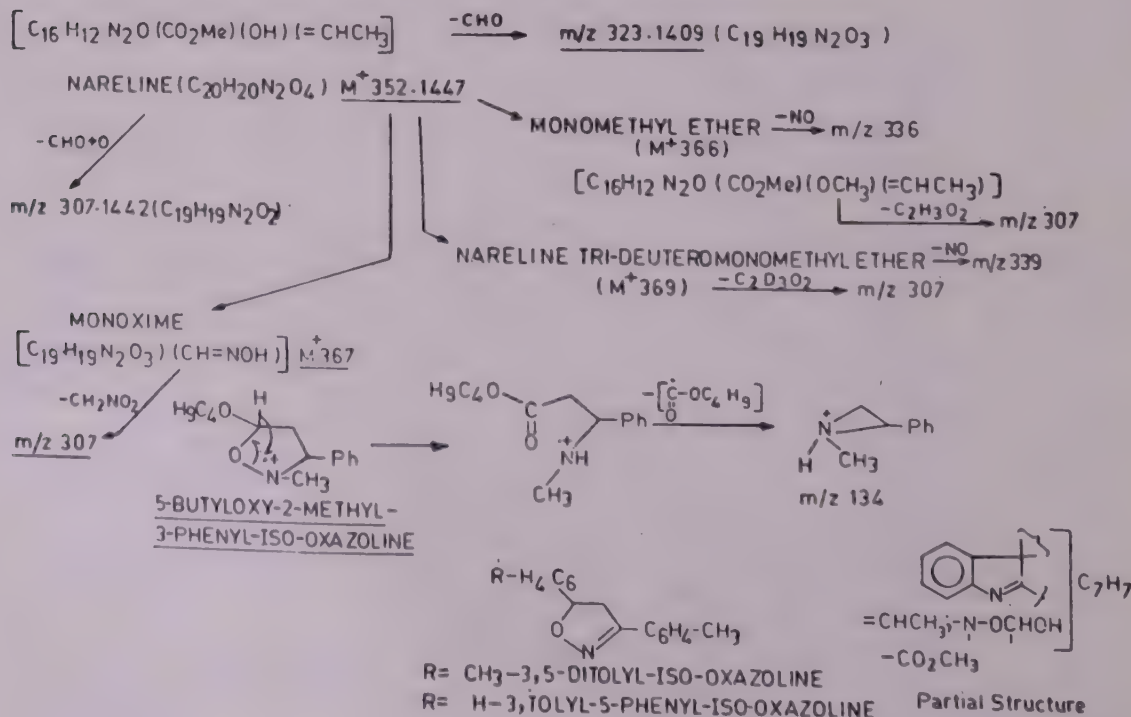
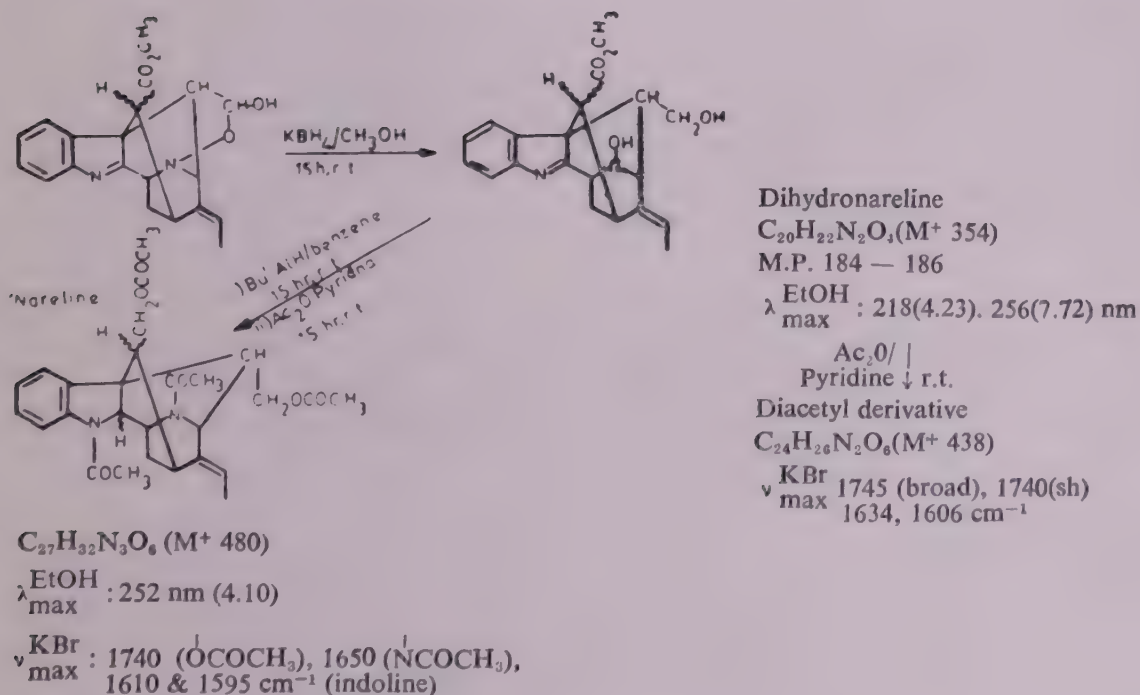
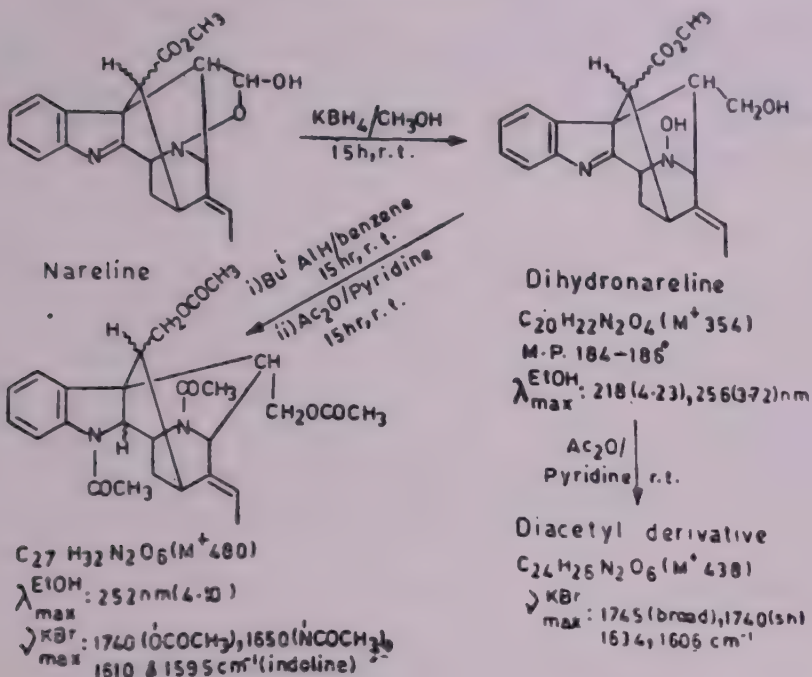


CHART 11

REDUCTION OF NARELINE

Dihydronareline thus obtained on further reduction with diisobutylaluminium hydride (DBA) in benzene afforded a compound which was characterised as its tetraacetyl derivative. This exhibited typical Na-acylindoline UV absorption and showed bands for both O- and N-acetyl groups.

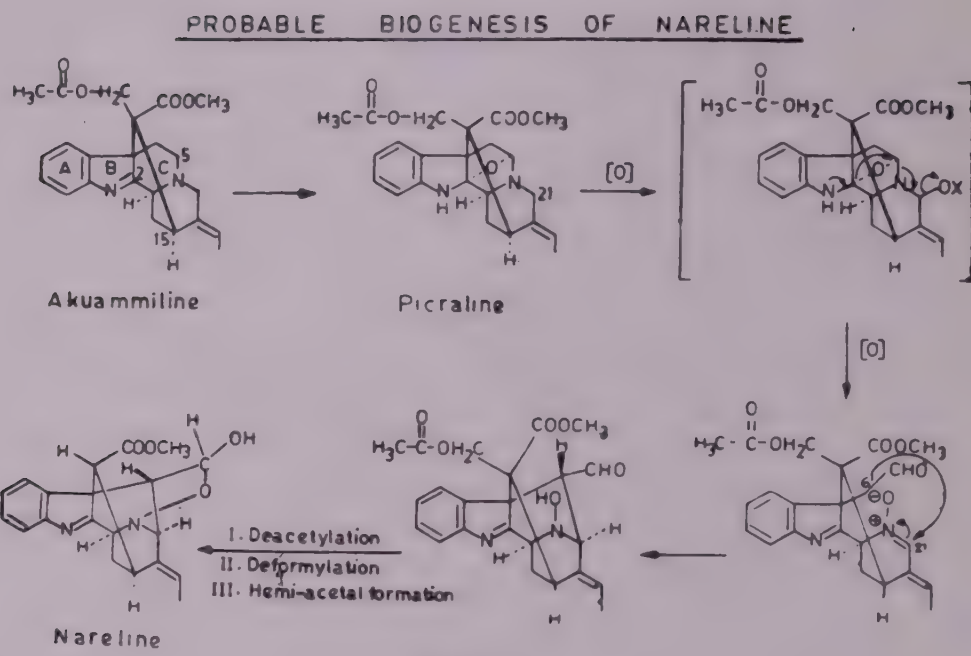
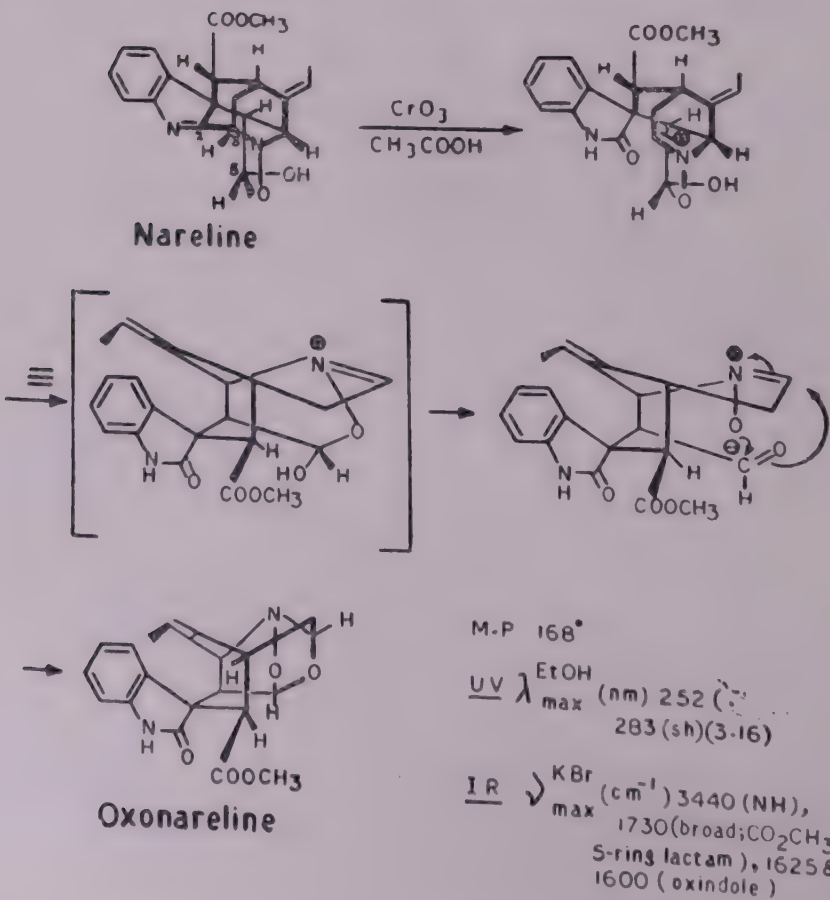


CHART 12

FORMATION OF OXONARELINE

The same product was also obtained by lithium aluminium hydride reduction of nareline methyl ether followed by acetylation. Further reduction of the acetylated product with lithium aluminium hydride followed by acetylation gave an indoline derivative. During reductive cleavage of nareline monomethyl ether with lithium aluminium hydride, in addition to the reduction of the formyl of the hemiacetal, carbomethoxyl and indolenine groups, an oxygen was lost. This is typical of  $\text{—N}_\text{b}\text{—O—CHOH}$  system.

One of the most interesting reactions of nareline is its conversion to an oxindole, oxonareline, on treatment with chromic acid in acetic acid. A comparison of  $^1\text{H}$  and  $^{13}\text{C}$ NMR spectra of oxonareline with those of nareline and its derivatives confirmed the structure of this compound.  $^1\text{HNMR}$  spectrum showed the signal for indole —NH at  $\delta$  8.42 and also the characteristic of an oxindole was the splitting pattern of the aromatic protons.  $\text{C}_3\text{H}$  resonated at  $\delta$  4.99, about 0.5ppm downfield than in nareline. The carbon bearing this proton was situated next to a methylene group, viz., C(14) which had  $\text{—CH}(15)$  as its neighbour.

This sequence was confirmed by decoupling experiments. On the basis of chemical shifts it was apparent that compared to nareline, C(3) in oxonareline was bonded to an extra heteroatom.

In the  $^{13}\text{C}$  NMR spectrum the changes in chemical shifts for the carbon atoms 3, 12 and 13 were well pronounced. C(3) appeared 30ppm downfield. C(12), 11ppm and C(13) 18ppm upfield whereas the carbonyl carbon absorbed at almost the same value as the indolenine carbon C(2). The chemical shift of C(3) from 63ppm to 92.7ppm indicated a change in its oxidation state. The other chemical shifts of C(12) and C(13) were in complete agreement with the changes in chromophore from indolenine to oxindole.

Thus we find that nareline is a unique base with modified C and E rings both being seco with an unusual linkage between C(6)-C(21) rather than the usual  $\text{N}_\text{4}\text{—C}_\text{5}$  bond significant from biogenetic aspect. The oxocyclic C(5) is present as an aldehyde and forms a cyclic hemiacetal with a hydroxyl group attached to N(4).

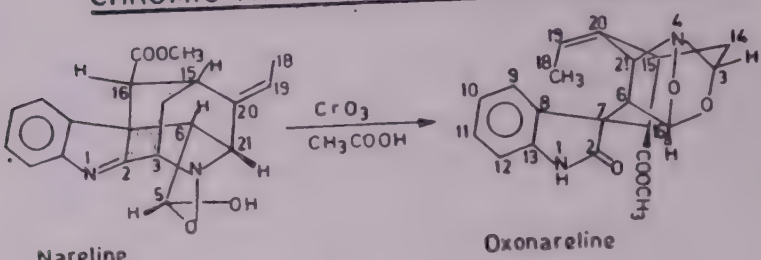
The probable biogenesis of nareline has been postulated (Chart 12).

The author expresses her deep sense of gratitude to her collaborators—Drs Avijit Banerji and Julie Banerji, Department of Chemistry, Calcutta University, Dr Y. Morita, Professors Hans Schmid and Manfred Hesse of the Institute of Organic Chemistry University of Zürich, Dr James N. Shoolery, Varian Associates, Palo Alto, U.S.A., and Dr Ashim K. Ghosh Department of Chemistry, Washington University. Thanks are also accorded to the University Grants Commission and the Council of Scientific and Industrial Research, New Delhi for financial assistance.

---

<sup>\*</sup>Since deceased.

## CHROMIC ACID OXIDATION OF NARELINE



### <sup>1</sup>H-NMR Spectra of Oxonareline in S

NH	$\text{CH}_3(\text{C}_{18})$	$\text{C}_{19}-\text{H}$	$\text{C}_3-\text{H}$	$\text{C}_5-\text{H}$	$\text{C}_{21}-\text{H}$
8.42(s) $J = 7 \text{ Hz}$	2.03(d)	5.97(q) $J = 7 \text{ Hz}$	4.99	6.05(d)-s on irr. of $\text{C}_6-\text{H}$	4.06(d)-s on irr. of $\text{C}_6-\text{H}$

<sup>13</sup>C NMR Signals of Oxonoreline in ppm

C <sub>2</sub> 180.4(s)	C <sub>3</sub> 91.4(d)	C <sub>5</sub> 103.9(d)	C <sub>6</sub> 49.3(d)	C <sub>7</sub> 56.4(s)	C <sub>8</sub> 133.3(s)	C <sub>9</sub> 126.2(d)
C <sub>10</sub> 125.8(d)	C <sub>11</sub> 128.6(d)	C <sub>12</sub> 109.7(d)	C <sub>13</sub> 140.0(d)	C <sub>14</sub> 26.0(t)	C <sub>15</sub> 36.1(d)	
C <sub>16</sub> 51.9(d)	C <sub>17</sub> 173.1(s)	C <sub>18</sub> 13.5(q)	C <sub>19</sub> 122.6(d)	C <sub>20</sub> 132.7(s)	C <sub>21</sub> 66.8(d)	-OCH <sub>3</sub> (-COOMe)

## REFERENCES

1. G A Cordell and Kirk Othmer *Encyclopaedia of Chemical Technology* 1 Third Edn. John Wiley and Sons Inc. (1978)
  2. A Chatterjee B Mukherjee and A Banerji Current awareness on the biogenesis of C<sub>19</sub>-indole alkaloids *J scient ind Res.* **29** (1970) 29
  - 2a. J Stöckigt *The Biosynthesis of Heteroyohimbine-type Alkaloids* Ch 6 (1980) 113–141; Johannes F Treimer and Meinhert Zenk Strictosidine synthase from cell cultures of apocynaceous plants *FEBS Lett.* **97**(1979) 159–162; J Stockigt 4,21-Dihydrogeissoschizine, an intermediate in heteroyohimbine alkaloid biosynthesis *JCS chem Commun* (1979) 1016
  3. G Büchi A John J E Carleson Jr Powell and L F Tietze *J Am chem Soc* **92** (1970) 2165
  4. Boon-Wai Au-Young and I Fleming, *JCS chem Commun* (1977) 81
  5. A Battersby A R Burnett and P G Parsons Preparation and isolation of deoxyloganin : its role as precursor of loganin *JCS chem Commun* (1970) 826
  6. W Barz E Reinhard and M H Zenk *Plant Tissue Culture and its Bio-technological Application* Springer-Verlag (Berlin) 27–43
  7. B Mukherjee A B Ray A Chatterjee and B C Das O-Benzoylvincamajine, a new alkaloid from the leaves of *Alstonia Macrophylla* Wall *Chemistry Ind* (1969) 1387
  8. A Chatterjee *Recent Developments in the Chemistry of Natural Products* (Eds S Rangaswami and N V Subba Rao) Prentice Hall of India Privated Limited (New Delhi) **1** (1972)
  9. A Chatterjee S Ghosh and S Ghosal Nerifoline—an alkaloid of *Alstonia macrophylla* Den *Sci Cult* **26** (1960) 238
  10. A Chatterjee S Ghosal and S Ghosh Majumdar Echitamine, the major alkaloid of *Alstonia scholaris* R Br *Chemistry Ind* (1960) 265
  11. A Chatterjee B Mukherjee A B Ray and B Das The alkaloid of the leaves of *Alstonia scholaris* R Br *Tetrahedron Lett* (1965) 3633

12. A Chatterjee J Banerji and A Banerji Alkaloids of *Alstonia scholaris* R Br *Indian J Pharma Edu* (1977) 80
13. B Das K Biemann A Chatterjee A B Ray and P L Majumder The alkaloids of bark of *Alstonia venenata* R Br *Tetrahedron Lett* (1965) 2239
14. B Das K Biemann A Chatterjee A B Ray and P L Majumdar The alkaloids of the fruits of *Alstonia venenata* R Br : Echitovenedine and (+) minovincinine *Tetrahedron Lett* (1966) 2483
15. A Chatterjee P L Majumdar and B C Das Structure of veneserpine, a new alkaloid of *Alstonia venenata* R Br *Chem Ind* (1969) 1381
16. L A Mitscher A B Ray and A Chatterjee Identity of RW-47 and venoterpine and determination of their absolute configuration *Experientia* 27 (1971) 16
17. A Chatterjee and S Mukhopadhyay Anhydroalstanoline—a new indole alkaloid from *Alstonia venenata* R. Br *Indian J Chem* 15B (1977) 183
18. A Chatterjee S Mukhopadhyay and A B Ray Alkaloids of *Alstonia venenata* R Br *J scient ind Res* 37 (1978) 187
19. A Chatterjee D J Roy and S Mukhopadhyay 5, 22-Dioxokopsane—a minor indole alkaloid isolated from *Alstonia venenata* R Br *Indian J Chem* 17B (1979) 651
20. A Chatterjee D J Roy and S Mukhopadhyay New stereomers : 16 epivenenatine and 16 epialstovenine from *Alstonia venenata* R Br *Phytochem* (1981) 1981
21. J Banerji A Chatterjee D J Roy and J N Shoolery 5-methoxy-1-oxo-tetrahydro-β-Carboline, a new alkaloid from *Alstonia venenata* R Br *Phytochem* 21 (1982) 2765
22. A Chatterjee S C Pakrashi and G Werner Recent development in the chemistry and pharmacology of *Rauwolfia* alkaloids *Z f Chem Organisc Naturstoff* 13 (1956) 346-443
23. Asima Chatterjee (Mrs) Indole alkaloids and their transformation *Trans Bose Res Inst* 47 (1984) 1-11
24. A Chatterjee S Bandyopadhyay and J N Shoolery Chemical transformation of ajmalicine : structure and stereochemistry of some interchangeable transformation products *J org Chem* (1982) 4333
25. A Chatterjee and B C Das Constitution of chonemorphine and synthesis of desamino-oxychonemorphine *Chem Ind* (1960) 1247
26. A Chatterjee and B Das Structure and synthesis of chonemorphine the steroid alkaloid of *Chonemorpha macrophylla* G. Don *Indian J Chem* 5 (1967) 146
27. J Banerjee A Chatterjee Y Itoh and T Kikuchi New steroid alkaloids from *Chonemorpha macrophella* G Don (*C. fragrans* Moon Alston) *Indian J Chem* 11 (1973) 1057; J Banerji A Chatterjee Y Itoh and T Kikuchi Constituents of *Chonemorpha macrophylla* G. Don *Indian J Chem* 16B (1978) 731
28. A Bhattacharjee A Chatterjee and P K Bose On the alkaloids of *Kopsia fruticosa* A DC *J Am chem Soc* 71 (1949) 3310
29. G Spitteler A Chatterjee A Bhattacharya and A Deb Anwendung der Massen spektromeric Zür Struktur aufklärung von alkaloiden *Monats f Chem* 93 (1961) 1220
30. A Chatterjee Rauwolfia alkaloids *Z f Chem Organis Naturstoff* 10 (1953) 382
31. A Chatterjee Chemistry of the alkaloids of *Rauwolfia canescens* Linn *Indian J Pharma* 18 (1956) 232
32. A Chatterjee M Chakraborty A K Ghosh E O Hagaman and E Wenkert Indole alkaloids of *Rauwolfia reflexa* the structures of rauflexine and reflexine *Tetrahedron Lett* (1978) 3879
33. A Chatterjee and A K Ghosh Indole Alkaloids of *Rauwolfia reflexa*, carbon-13-nuclear magnetic resonance structural analysis of the bis (indole) alkaloid flexicorine *J org Chem* 47 (1982) 1732
34. A Chatterjee and A B Ray Recent development in the chemistry of indole alkaloids *J scient ind Res (India)* 21A (1962) 515
35. A Chatterjee and S Bandopadhyay Vellosimine—an alkaloid of *Rauwolfia vomitoria* Afzel *Indian J Chem* 18B (1979) 87

36. A Banerji P L Majumder and A Chatterjee Occurrence of Geissoschizine and other minor biogenetically related alkaloids in *Rhazya stricta* Decrigne *Phytochem* **9** (1970) 1491
37. A Chatterjee C R Ghosal and N Adityachaudhury Alkaloids of *Rhazya stricta* Decaisne : The structure of Rhazine *J scient ind Res* **21B** (1962) 147
38. M Spitteler Friedmann R Kaschnitz G Spitteler A Chatterjee N Adityachaudaury and G Ganguli Anwendung der Massenpektrometrie Zur Struktur aufklärung von Alkaloiden 4 Mitt Zur struktur des Rhazidine *Monats f Chem* **95** (1964) 1228
39. K Schnoes K Biemann J Mokry I Kompis A Chatterjee and G Ganguly Strictamine *J org Chem* **31** (1966) 1641
40. A Chatterjee (Mrs) A Banerji P L Majumdar and (Mrs.) R Majumdar Alkaloids of *Rhazya stricta* Decaisne : studies on rhazinaline and geissoschizine *Bull chem Soc Japan* **49** (1976) 17
41. A Chatterjee (Mrs.) J Banerji and A Banerji *Rhazya* alkaloids *J Indian chem Soc (Golden Jubilee)* **51** (1974) 156
42. A Chatterjee A Banerji and P L Majumdar Occurrence of tabernaemontanine and dregamine in *Tabernaemontana sphaerocarpa* BL *Indian J Chem* **6** (1968) 545
43. A Chatterjee M Chakraborty and A Banerjee Monoterpeneoid alkaloid from *Vinca major* Linn *Planta Medica* **28** (1975) 109
44. A Chatterjee G K Biswas and A B Kundu Indole alkaloids of *Vinca pusilla* *Indian J Chem* **11** (1973) 7
45. V C Agwada J Naranjo M Hesse H Schmid Y Rolland N Kunesch J Poisson and A Chatterjee Die Struktur des Bisindolkaloids Amatin (= Grandifolin Subsessilin) *Helv Chim Acta* **60** (1977) 2830
46. B C Das J P Cosson J Lukaces and P Potier Vincorme the Alkaloid of *Alstonia deplanche* *Tetrahedron Lett* (1974) 4299
47. Y Morita M Hesse H Schmid A Banerji J Banerjee A Chatterjee and W E Oberhansli *Alstonia scholaris* R. Br Struktur des indolalkaloide : nareline *Helv Chim Acta* **60** (1977) 1419

# THERMO- AND PHOTO-MAGNETIC EFFECTS IN POLY-CRYSTALLINE META DINITROBENZENE INVOLV- ING TIME-VARIATION OF DIELECTRIC CONSTANT

A K CHATTERJEE\* and S D CHATTERJEE FNA

*Department of Physics, Jadavpur University, Calcutta-700 032, India*

(Received 9 April 1985)

Samples prepared from pure meta dinitrobenzene are treated thermally in dark in the presence of steady magnetic field and time variation of dielectric constant of the samples are subsequently studied over a period of three weeks. Also an analogous experiment is performed by replacing the thermal treatment of the material with photo-irradiation again in the presence of a steady magnetic field and time variation of dielectric constant is studied subsequently. These after-effects are mutually compared and attempts are made to provide explanations for the observed results mostly on the basis of a generalized theory due to Rose<sup>1</sup> and Fowler.<sup>2</sup> Subsequent observations concerning the process of photo-depolarization of the thermally and optically activated samples are also done and tentative explanation for the results is provided.

**Key Words :** Thermo-and Photo-magnetic Effect; Perforated Electrode Surface;  
Photo-depolarization; Migrating Charge Carriers; Iso-Charge

## INTRODUCTION

THE effect of thermal treatment of meta dinitrobenzene, a polar molecular crystal, when the material placed within a dark cover was taken through a course of melting, resolidification and slow return to the ambient temperature in the presence of a steady magnetic field and was subsequently studied in terms of time variation in the value of electrical capacitance of the condenser which contained the experimental material as medium. The capacitance was measured with an universal L-C-R bridge (Simpson model 901-I) powered with a source of 1kHz signal following a method due to Chatterjee and Bhadra.<sup>3</sup> The method for activation of the experimental material was basically similar to that followed by Agarwal and Bhatnagar.<sup>4</sup> The samples and the controls were kept in total darkness throughout the course of the experiment. Four to five different sets of experiments were usually performed to establish the typical behaviour of these samples. Each set of experiments was of about three to four weeks' duration at the end of which the samples were found to attain practically a steady state. Subsequently, the photo-depolarisation of these samples were also studied.

The influence of photo-irradiation on solid polycrystalline metadinitrobenzene regarding its electrical polarization under the simultaneous action of steady

\*Department of Physics, Presidency College, Calcutta.

magnetic field was also studied, which also involved the time variation of the dielectric constant of the activated material. Subsequently, these activated samples were re-exposed to light only, and their photo-depolarisation were studied.

### EXPERIMENTAL

Experimental material was prepared by dissolving reagent quality of meta dinitrobenzene in pure ethyl alcohol. The solute was filtered through glass wool fibres and allowed to crystallise by slow evaporation. Large needle-shaped crystals were selected from the crystallized material. These were again dissolved in absolute alcohol and the whole process was repeated twice to have pure experimental material.

#### (A) Study of Thermo-Magnetic Effect

The electrical capacitor used for this experiment was specially prepared. A nichrome wire resistor (nearly 50ohms) closely wound over a porcelain pipe was inserted in to a thin brass pipe, closed at one end, and having a diameter slightly larger than the outer diameter of the resistor. These two were placed co-axially by introducing a long brass screw through the bore of the porcelain and a previously made central hole at the closed face of the brasspipe, where the screw was soldered. This formed a cylindrical condenser about 3.5cm in length. Initially, the condenser was thoroughly washed with carbon tetrachloride and then treated with pure absolute alcohol before storing it in a desiccator for a period of twenty four hours. Then the condenser was placed inside molten meta dinitrobenzene where it was throughly stirred with a clean glass rod in order to drive out trapped air bubbles and to ensure proper filling up of the space between the condenser plates with meta dinitrobenzene. Finally, it was taken out of the molten liquid, keeping the open end upwards and held vertically. Next, the material inside the condenser was remelted under dark cover by connecting the leads from the ends of the nichrome resistor to a 24V d c supply for a suitable period. Subsequently, the power supply was switched off and the molten material was allowed to cool down slowly to the ambient temperature. The capacitance was then measured with a universal L-C-R bridge after short-circuiting the two leads of the nichrome resistor. The dielectric medium of the condenser was again taken through a course of melting and subsequent solidification and the value of the electrical capacitance was remeasured after the system cooled down. The process was repeated in order to ensure that the value of the capacitance remained practically unchanged.

Next the condenser was placed vertically between the pole pieces of an electromagnet within dark cover and meta dinitrobenzene located between the plates of the cylindrical condenser was remelted in the presence of 6.8 K oersted magnetic field and then allowed to cool down to the room temperature ( $\approx 290^{\circ}\text{K}$ ) with magnetic field constantly on. The field was removed subsequently and the electrical capacitance of the sample was measured at regular intervals of time for the next

three weeks. The results of the experiment are shown graphically in Fig. 1. This figure also includes the curve showing the time variations of capacitance of a control sample treated similarly as before but without exposure to any magnetic field.

After studying the time variation of capacitance for three weeks the activated sample was reexposed to light from a 200 Watt lamp held at a distance of 100cm above the open end of the cylindrical condenser for a period of 10 hours. A prolonged exposure was given because of the low transmission of light through the thick medium of metadinitrobenzene. The exposed sample was then placed once again within dark cover and its capacitance was measured at regular intervals of time for the next 72 hours. A nearly complete depolarization was observed.

(B) *Study of the influence of Photo-irradiation of Solid Sample in the Presence of Magnetic Field*

Experimental samples were prepared by melting pure meta dinitrobenzene in a clean small petri dish and then slowly cooled between two brass electrodes in the form of thin wafers. Small mica spacers of thickness about 0.5mm were used at the opposite edges of the rectangular electrodes ( $2\text{cm} \times 1.5\text{cm}$ ) to ensure a more or less uniform thickness. Excess material from the outer surfaces was removed. The plates had presoldered colour codified lead wires at the outer faces. Two such samples were then stored in a desiccator with electrodes short circuited for a period of twenty four hours and finally stored inside a metal container. The capacitances of these samples were then successively measured after a lapse of 24 hours by connecting the colour codified leads coming out through light-tight small holes on the surface of the metal container, to the L-C-R bridge. These measurements were repeated at the end of further periods of 24 and 48 hours to ensure that the values remained unchanged.

Next, one of the condensers was taken out of the dark container and photo-irradiated in the presence of a steady magnetic field with its electrodes short circuited. It was illuminated for a specified length of time by means of a 6.3V, 0.3amp miniature lamp run at 10 per cent over voltage placed at distance of about 10cm. This sample had one of its electrode surfaces perforated with small holes (1 mm) about 30 in number. The sample was placed between the pole pieces so that the perforated electrode faced the light source. The sample was so placed that its thickness was oriented at an angle of  $45^\circ$  to the direction of the applied magnetic field. The sample was retransferred to the dark container after cessation of irradiation and its c-value was then measured after a rest period of ten minutes when it was presumed that the sample had returned to the room temperature. Furthermore any substantial rise in temperature of the sample was prevented by circulation of air current during the irradiation process. The c-value of the other condenser (control) unexposed to light and without application of magnetic field was also measured. Actually, the capacitances of these two condensers were measured at regular intervals of time for a period of about three weeks.

Finally the activated sample was taken out of the dark container and was exposed to light from a 100 watt lamp placed at a distance of 1 metre for a period

of 100 minutes, with electrodes short-circuited. Air was circulated during photo irradiation to prevent any rise in temperature of the sample. The sample was then transferred into the dark container and the C-value was again measured after a rest period of 10 minutes at regular intervals of time for the next 72 hours.

### RESULTS

Typical results of the experiments are shown in Fig. 1.

$\frac{C_m}{C_0} \times 100$  values, plotted as ordinates represent the percentage changes in the value of electrical capacitances of the experimental samples with time plotted as abscissa.

$C_m$  denotes the modified c-value while  $C_0$  represents that prior to activation of the experimental sample.

### DISCUSSION

The change in permittivity of the samples on activation is not explainable in terms of reorientation of permanent dipoles of meta dinitrobenzene since no electric field was used for poling. However, trapping of mobile charges in the conduction and valence bands generated due to thermal effect or action of light may lead to subsequent formation of charge layers that might alter the permittivity of the material. Rose<sup>1</sup> and Fowler<sup>2</sup> introduced concepts like carrier excitation and carrier trapping in the defect levels located in the band gap. When a polycrystalline

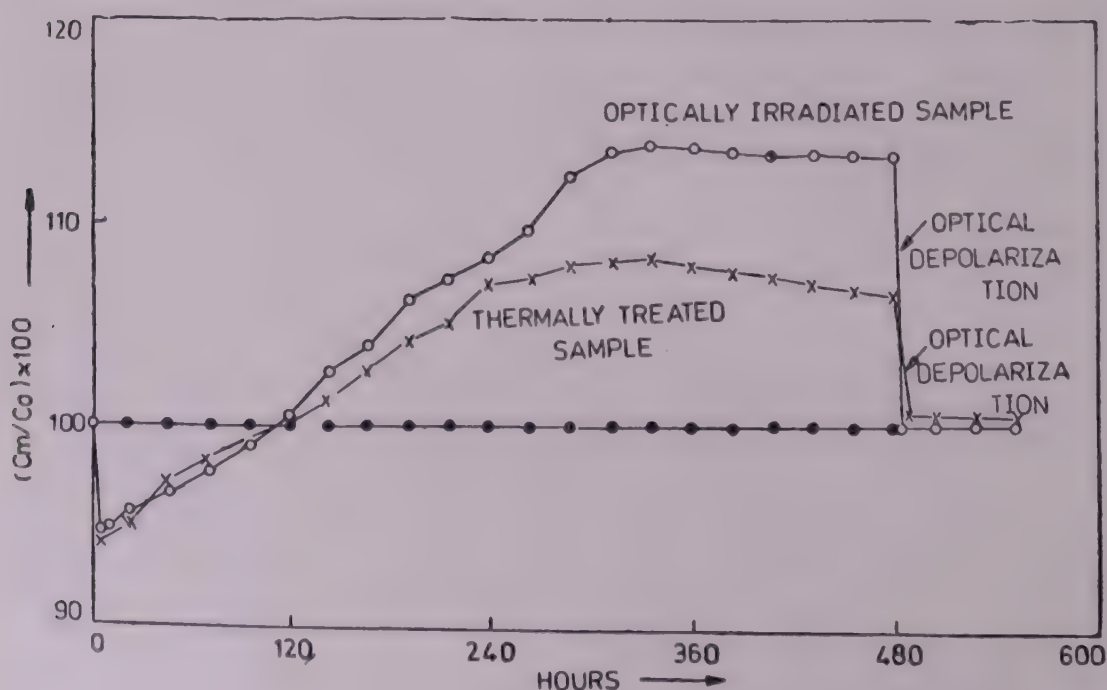


FIG 1

dielectric material is allowed to return to the temperature of the ambient following its melting or if it is irradiated non-uniformly for a prolonged period, in the presence of an external magnetic field, the trap levels in the band gap are filled up more and more with electrons from the valence band. Some of these elevated electrons located closer to the conduction band edge may jump further into the conduction band giving rise to the generation of free electrons. These together with the holes in the valence band constitute the non-equilibrium carriers of the material. Consequently, some diffusion current may appear, which interacting with external magnetic field causes a drift of these charge carriers along the third perpendicular direction.

The cylindrical condenser of the thermo-magnetic experiment, however when allowed to cool down slowly after molten state of the material, a temperature gradient most probably is formed along radial and other directions inclined to the radial. Thus charge carriers are non-uniformly generated along these directions due to unequal phonon interactions with the lattice. Consequently, diffusion currents are generated along these directions which have non-zero components in general along the central axis. These components of diffusion currents interact with external magnetic field causing drifts of the charge carriers along the third perpendicular directions along which they are likely to be trapped at grain boundaries and at defect centres. Similar trappings of migrating charge carriers are also expected in the bulk of a non uniformly illuminated polycrystalline sample simultaneously exposed to a magnetic field. Thus the mechanism of charge separation may be understood to some extent.

The pattern and effects of charge separation in a solid homogeneous dielectric medium bounded by two parallel metal electrodes of thickness 's' may now be theoretically examined. Let us consider a monopolar charge layer of density  $\sigma_s$  which develops at a distance  $x$  from the left hand side electrode. This layer should induce an equal amount of charge of opposite sign on the parallel electrodes (appearance of isocharge) located at  $x = 0$  and  $x = s$  having surface densities  $\sigma_0$  and  $\sigma_s$  respectively. Considering the electrode cross sections to be the same and to be externally short-circuited and applying laws of parallel combination of condensers, it can be shown that

$$\sigma_s = -\sigma_s(x/s) \quad \dots(1)$$

$$\text{Lt } s \rightarrow 0,$$

where

$$\sigma_0 + \sigma_s = -\sigma_s \quad \dots(2)$$

whence

$$\sigma_0 = -\sigma_s \frac{s-x}{s} \quad \dots(3)$$

If there be a number of monocharge layers of the same or different kind at  $x_1, x_2, x_3, \dots, x_n$  having charge densities  $\sigma_1, \sigma_2, \sigma_3, \dots, \sigma_n$  respectively, then  $\sigma_0 + \sigma_1 + \sigma_2 + \dots + \sigma_n$

$$= -\sum_{x=i}^{x=n} \sigma_x \quad \dots(4)$$

Equations (1) to (4) are applicable only to a simple model just considered, of course trapped charges may not necessarily confine themselves around plane layers. It is, however, apparent from the above equations that unless the built up trapped charges are of such a magnitude that opposite kinds can completely neutralise the fields due to them, there would always remain some residual charge on the electrodes (iso-charge).

Now, in course of time, a charge layer may have its  $\sigma$  changed after its formation largely through phonon interactions between quantum states of the trapped carriers and those of the lattice vibrations. A quick change of these charge densities may however result from a fresh exposure of the activated sample stored under dark cover, to light, as the result of a process known as radiation induced depolarization of the activated sample.

The study of time variation of dielectric constant of the activated samples is meaningful which may reveal valuable informations about the carriers and the nature of traps within the dielectric. The results of the present set of experiments indicate that the thermo-magnetic treatment of the experimental sample is somewhat less potent in producing change in the permittivity as compared to the photo-magnetic action. Moreover, in the thermally treated sample, the permittivity shows a slow and steady decay after reaching a peak in course of about two weeks' time. Such a rate of decay is rather slower than in an optically activated sample. On heating a dielectric or irradiating it with light or radioactive rays the charge carriers tend to diffuse themselves if they are generated nonuniformly within the bulk material. Although the mobilities of such excess carriers are hampered by the presence of large number of traps and defects present in the polycrystalline materials, their motions, in the presence of external magnetic field may be expressed by the equation.

$$\frac{dp}{dt} = ev \times B - \frac{p}{\tau}, \quad \dots(5)$$

where  $e$ ,  $v$ ,  $p$  and  $\tau$  are the charge, diffusion velocity, momentum and relaxation time of the carrier respectively, while  $B$  is the magnetic induction.<sup>5</sup>

The presence of the magnetic field along a specified direction would bring some definite pattern in the trapping of the migrating charges at the defects and grain boundaries of the crystallities, resulting in non homogeneous separation of monopolar charges (electrons and holes). The quantum states of these trapped charges are, however, under continuous interactions with the vibrational states of the lattice even when the activated sample is stored in darkness. The sample which is thermally unshielded, faces low order of charge detrapping due to continuous phonon-charge interactions. However, a fresh exposure to light of the sample previously kept under darkness results in an enhanced detrapping of electrons and holes. The detrapped charges may recombine directly at the recombination centers or they move into conduction and valence bands and behave like free carriers. These free carriers may migrate towards the electrodes to recombine with the image charges. Apparently, the depolarisation of the activated sample follows the processes of detrapping.

ACKNOWLEDGEMENT

Thanks are due to Biren Roy Trust, Behala, for financial assistance.

REFERENCES

1. A Rose *R C A Rev* **12** (1951) 362 *Phys Rev* **97** (1955) 322
2. J F Fowler *Proc R Soc London A* **236** (1956) 464
3. S D Chatterjee and T C Bhadra *Phys Rev* **98** (1955) 1728
4. B M Agarwal and C S Bhatnagar *Indian J pure appl phys* **11** (1973) 413–416
5. P S Kireev *Semiconductor Physics* Mir Publishers (1975) 531–532

## VIBRATIONAL SPECTRUM AND NORMAL COORDINATE TREATMENT OF ACETOPHENONE

S MOHAN T J BHOOPATHY and K G RAVIKUMAR

Division of Applied Sciences, Anna University, Madras Institute of Technology,  
Madras-600 044, India

(Received 28 December 1984; after revision 8 April 1985)

The laser Raman spectrum of Acetophenone from 50-4000cm<sup>-1</sup> has been recorded. The fundamental frequencies are assigned and normal coordinate analysis has been carried out for this molecule with the aid of point mass model, using the kinetic constants method. Further using the values of the present potential constants, other molecular constants, viz., compliance constants, vibrational mean amplitudes, Coriolis coupling constants and centrifugal distortion constants have also been evaluated, for this molecule.

**Key Words :** Laser Raman Spectrum; Molecular Dynamics; Acetophenone

### INTRODUCTION

THE Raman spectrum of Acetophenone has been reported by Kohlrausch.<sup>1</sup> The infrared spectral data of this compound is also on record.<sup>2-4</sup> No attempt, however, appears to have been made to subject this molecule to a detailed normal coordinate treatment, perhaps due to its unsymmetric shape. This paper presents the laser Raman spectrum and normal coordinate analysis of Acetophenone. Wilson's FG matrix method coupled with kinetic constants method has been applied to evaluate the force constants of Acetophenone. Using these force constants, the other molecular constants, viz., compliance constants, vibrational mean amplitudes, Coriolis coupling constants, and centrifugal distortion constants have also been evaluated.

### EXPERIMENTAL

Acetophenone has been obtained from BDH Laboratory chemicals (England). The laser Raman spectrum of this compound has been recorded on a CARY MODEL 82 laser Raman spectrophotometer in the region 50-4000cm<sup>-1</sup> and is presented in Fig. 1.

### THEORETICAL CONSIDERATIONS

The vibrational frequencies are assigned for Acetophenone assuming the phenyl group and the CH<sub>3</sub> group as point masses. The vibrational frequencies are reported in this present investigation on the basis of C<sub>2</sub> symmetry. For this molecule present assignment agree quite well with the earlier authors<sup>3,4</sup> except for C-X stretching 1000cm<sup>-1</sup> and R-C-X out of plane bending 162cm<sup>-1</sup>. They have assigned

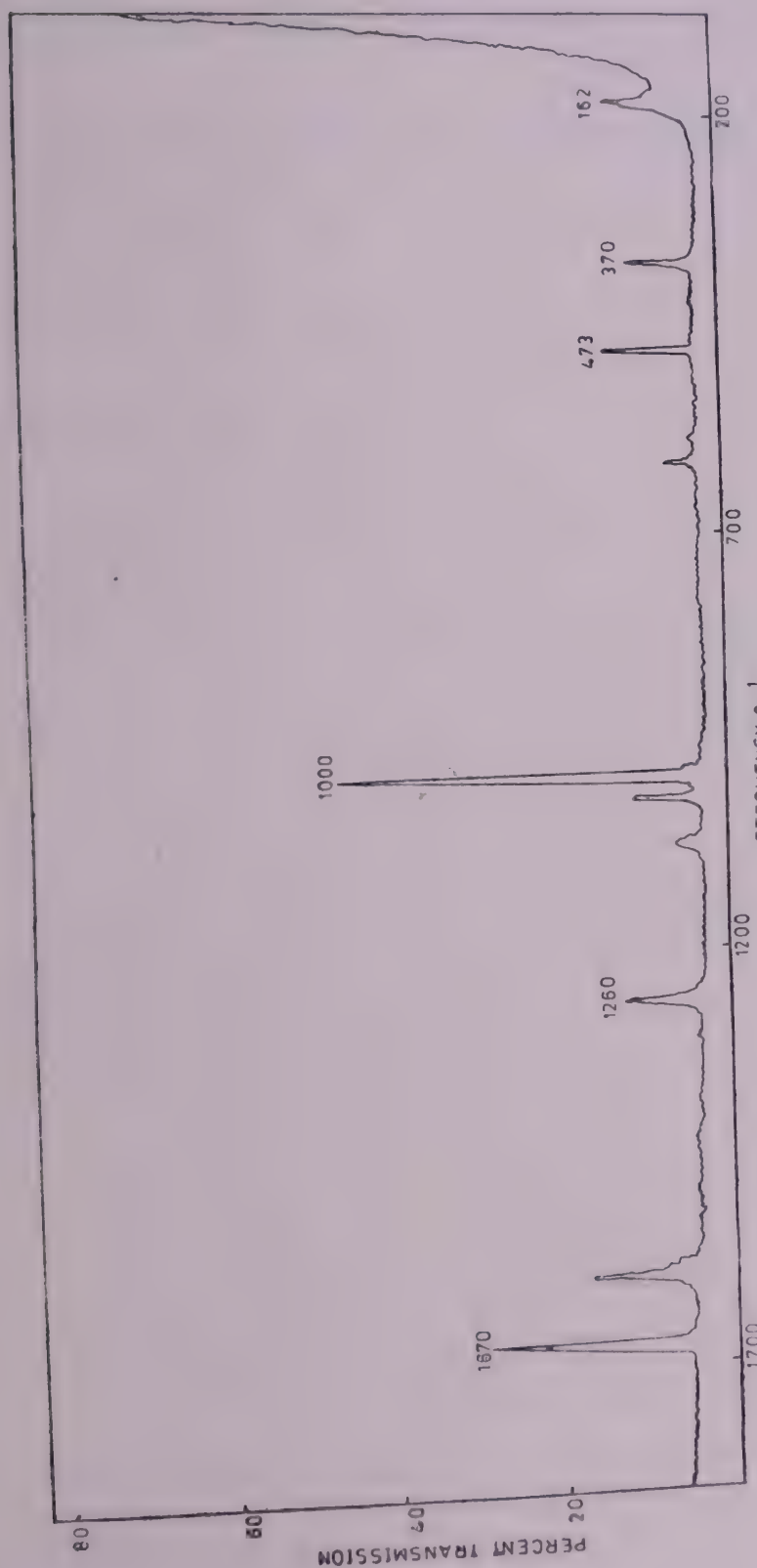


FIG 1 Laser Raman spectrum of acetophenone.

$957\text{cm}^{-1}$  and  $254\text{cm}^{-1}$  for C-X stretching and R-C-X out of plane bending respectively. The observed frequencies and assignments are listed in Table I.

TABLE I  
*Assignment of fundamental and combination Raman frequencies ( $\text{cm}^{-1}$ ) of acetophenone*

Frequency	Intensity <sup>+</sup>	Assignment
1670	S	$\nu_1$ (C = O stretching)
1580	M	$2\nu_2 - 2\nu_4$
1260	M	$\nu_2$ (C — R stretching)
1088	W	$\nu_2 - \nu_6$
1045	M	$2\nu_3 - 2\nu_4$
1000	VS	$\nu_3$ (C — X stretching)
620	W	$\nu_3 - \nu_5$
473	M	$\nu_4$ (R $\hat{C}$ X bending)
370	M	$\nu_5$ (R $\hat{C}$ X bending)
162	M	$\nu_6$ (R $\hat{C}$ X out of plane bending)

<sup>+</sup>VS : Very strong

S : Strong

M : Medium

W : Weak

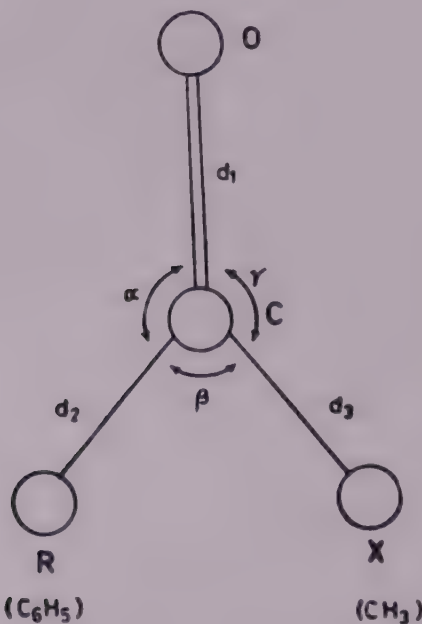


FIG 2 Planar configuration of acetophenone molecule

The planar configuration of this molecule is as shown in Fig. 2. The structural parameters, and symmetry coordinates used in this present investigation have been taken from Glasston<sup>5</sup> and Allen *et al.*<sup>6</sup> The most general quadratic valence force field is adopted in the present work and hence the following elements of F-matrix are obtained from the expression  $F = u\tilde{f}u$ .

In plane vibrations :—

$$\mathbf{F}_{11} = f_{\alpha_1}$$

$$\mathbf{F}_{12} = \frac{1}{\sqrt{2}} (f_{d_1 d_2} + f_{d_1 d_3})$$

$$\mathbf{F}_{13} = \frac{1}{\sqrt{2}} (f_{d_1 d_2} - f_{d_1 d_3})$$

$$\mathbf{F}_{14} = \frac{1}{\sqrt{6}} (\sqrt{\epsilon} f_{d_{1\alpha}} - 2\sqrt{\eta} f_{d_{1\beta}} + \sqrt{\pi} f_{d_{1\gamma}})$$

$$\mathbf{F}_{15} = \frac{1}{\sqrt{2}} (\sqrt{\epsilon} f_{d_{1\alpha}} - \sqrt{\pi} f_{d_{1\gamma}})$$

$$\mathbf{F}_{22} = \frac{1}{2} (f_{d_2} + f_{d_3} + 2f_{d_2 d_3})$$

$$\mathbf{F}_{23} = \frac{1}{2} (f_{d_2} - f_{d_3})$$

$$\mathbf{F}_{24} = \frac{1}{\sqrt{22}} [\sqrt{\epsilon}(f_{d_{2\alpha}} + f_{d_{3\alpha}}) - 2\sqrt{\eta}(f_{d_{2\beta}} + f_{d_{3\beta}}) + \sqrt{\pi}(f_{d_{2\gamma}} + f_{d_{3\gamma}})]$$

$$\mathbf{F}_{25} = \frac{1}{2} [\sqrt{\epsilon}(f_{d_{2\alpha}} + f_{d_{3\alpha}}) - \sqrt{\pi}(f_{d_{2\gamma}} + f_{d_{3\gamma}})]$$

$$\mathbf{F}_{33} = \frac{1}{2} (f_{d_2} + f_{d_3} - 2f_{d_2 d_3})$$

$$\mathbf{F}_{34} = \frac{1}{\sqrt{12}} [\sqrt{\epsilon}(f_{d_{2\alpha}} - f_{d_{3\alpha}}) - 2\sqrt{\eta}(f_{d_{2\beta}} - f_{d_{3\beta}}) + \sqrt{\pi}(f_{d_{2\gamma}} - f_{d_{3\gamma}})]$$

$$\mathbf{F}_{35} = \frac{1}{2} [\sqrt{\epsilon}(f_{d_{2\alpha}} - f_{d_{3\alpha}}) - \sqrt{\pi}(f_{d_{2\gamma}} - f_{d_{3\gamma}})]$$

$$\mathbf{F}_{44} = \frac{1}{6} [\epsilon f_\alpha + 4\eta f_\beta + \pi f_\gamma - 4\sqrt{\epsilon\eta} f_{\alpha\beta} + 2\sqrt{\epsilon\pi} f_{\alpha\gamma} - 4\sqrt{\eta\pi} f_{\beta\gamma}]$$

$$\mathbf{F}_{45} = \frac{1}{\sqrt{12}} [\epsilon f_\alpha - \pi f_\gamma - 2\sqrt{\epsilon\eta} f_{\alpha\beta} + 2\sqrt{\eta\pi} f_{\beta\gamma}]$$

$$\mathbf{F}_{55} = \frac{1}{2} [\epsilon f_\alpha + \pi f_\gamma - 2\sqrt{\epsilon\pi} f_{\alpha\gamma}]$$

Out of plane vibration :

$$\mathbf{F}_{66} = f_\delta,$$

where

$$\epsilon = d_1 d_2; \quad \pi = d_1 d_3; \quad \eta = d_2 d_3.$$

The notation of force constants as well as the kinetic constants are indicated below:

<i>Nature of the Constant</i>	<i>Force Constant</i>	<i>Kinetic Constant</i>
CO stretching	$f_{d_1}$	$k_{d_1}$
CR stretching	$f_{d_2}$	$k_{d_2}$
CX stretching	$f_{d_3}$	$k_{d_3}$
CO/CR interaction	$f_{d_1 d_2}$	$k_{d_1 d_2}$
CO/CX interaction	$f_{d_1 d_3}$	$k_{d_1 d_3}$
CR/CX interaction	$f_{d_2 d_3}$	$k_{d_2 d_3}$
OCR bending	$f_\alpha$	$k_\alpha$
RCX bending	$f_\beta$	$k_\beta$
XCO bending	$f_\gamma$	$k_\gamma$
OCR/RCX interaction	$f_{\alpha \beta}$	$k_{\alpha \beta}$
OCR/XCO interaction	$f_{\alpha \gamma}$	$k_{\alpha \gamma}$
RCX/XCO interaction	$f_{\beta \gamma}$	$k_{\beta \gamma}$
CO/OCR interaction	$f_{\alpha_1 \alpha}$	$k_{\alpha_1 \alpha}$
CO/RCX interaction	$f_{\alpha_1 \beta}$	$k_{\alpha_1 \beta}$
CO/XCO interaction	$f_{\alpha_1 \gamma}$	$k_{\alpha_1 \gamma}$
CR/OCR interaction	$f_{\alpha_2 \alpha}$	$k_{\alpha_2 \alpha}$
CR/RCX interaction	$f_{\alpha_2 \beta}$	$k_{\alpha_2 \beta}$
CR/XCO interaction	$f_{\alpha_2 \gamma}$	$k_{\alpha_2 \gamma}$
CX/OCR interaction	$f_{\alpha_3 \alpha}$	$k_{\alpha_3 \alpha}$
CX/RCX interaction	$f_{\alpha_3 \beta}$	$k_{\alpha_3 \beta}$
CX/XCO interaction	$f_{\alpha_3 \gamma}$	$k_{\alpha_3 \gamma}$
Out of plane bending	$f_s$	$k_s$

The elements of kinetic energy matrix have been obtained using Wilson's method<sup>7</sup> for non-degenerate vibration and they are given below:

In plane vibration :

$$\mathbf{G}_{11} = \mu_c + \mu_0$$

$$\mathbf{G}_{12} = 1/\sqrt{2} \mu_c (\cos \alpha + \cos \gamma)$$

$$\mathbf{G}_{13} = 1/\sqrt{2} \mu_c (\cos \alpha - \cos \gamma)$$

$$\mathbf{G}_{14} = -\sqrt{3}/2 \mu_c \left[ \frac{\sin \alpha}{d_2} + \frac{\sin \gamma}{d_3} \right]$$

$$\mathbf{G}_{15} = 1/\sqrt{2} \mu_c \left[ \frac{\sin \gamma}{d_3} - \frac{\sin \alpha}{d_2} \right]$$

$$\mathbf{G}_{22} = 1/2 (\mu_R + \mu_x) + \mu_c (1 + \cos \beta)$$

$$\mathbf{G}_{23} = 1/2 (\mu_R - \mu_x)$$

$$G_{24} = \sqrt{3}/2 \mu_c \left[ \frac{1}{d_2} + \frac{1}{d_3} \right] \sin \beta$$

$$G_{25} = \frac{\mu_c}{d_1} (\sin \gamma - \sin \alpha) + \frac{\mu_c}{2} \left[ \frac{1}{d_2} - \frac{1}{d_3} \right] \sin \beta$$

$$G_{33} = \frac{1}{2} \mu_R + \frac{1}{2} \mu_x + \mu_c (1 - \cos \beta)$$

$$G_{34} = \frac{\sqrt{3}}{2} \mu_c \left[ \frac{1}{d_3} - \frac{1}{d_2} \right] \sin \beta$$

$$G_{35} = -\frac{\mu_c}{d_1} (\sin \alpha + \sin \gamma) - \frac{\mu_c}{2} \left[ \frac{1}{d_2} + \frac{1}{d_3} \right] \sin \beta$$

$$G_{44} = \frac{3}{2d_2^2} (\mu_R + \mu_c) + \frac{3}{2d_3^2} (\mu_c + \mu_x) - \frac{3}{d_2 d_3} \mu_c \cos \beta$$

$$G_{45} = \frac{\sqrt{3}}{2d_2^2} (\mu_R + \mu_c) - \frac{\sqrt{3}}{2d_3^2} (\mu_c + \mu_x) + \frac{\sqrt{3}\mu_c}{d_1} \left[ \frac{\cos \gamma}{d_3} - \frac{\cos \alpha}{d_1} \right]$$

$$G_{55} = \frac{2}{d_1^2} (\mu_c + \mu_0) + \frac{1}{2d_2^2} (\mu_c + \mu_R) + \frac{1}{2d_3^2} (\mu_c + \mu_x)$$

$$- \frac{2\mu_c}{d_1 d_2} \cos \alpha - \frac{2\mu_c}{d_1 d_3} \cos \gamma + \frac{\mu_c}{d_2 d_3} \cos \beta$$

### Out of Plane Vibration

$$G_{66} = \frac{\mu_0}{d_1^2} + \frac{\mu_R \sin^2 \gamma}{d_2^2 \sin^2 \beta} + \frac{\mu_x \sin^2 \alpha}{d_3^2 \sin^2 \beta} + \mu_c \left[ \frac{-1}{d_1} - \frac{\sin \gamma}{d_2 \sin \beta} \right. \\ \left. - \frac{\sin \alpha}{d_3 \sin \beta} \right]^2$$

Here  $\mu$ 's are reciprocals of masses of atoms indicated by the respective suffixes.

The  $G$ -matrix elements are utilized to determine kinetic constants.<sup>8,9</sup> The kinetic constants have been employed here to solve the  $5 \times 5$  vibrations problem associated with  $A'$  type vibration of the acetophenone molecule.

Using  $F$ -matrix elements, force constants can be evaluated. The compliance constants are also determined for this molecule by the Decius method.<sup>10</sup> The mean square amplitude matrix elements<sup>11</sup> may be obtained, using the normal coordinate transformation matrix- $L$  from the relation  $\Sigma = L \Delta L'$  and hence bonded, non-bonded mean amplitudes of vibration at 298.16 K are calculated.

The Coriolis matrix elements  $C_i^\alpha$  ( $\alpha = x, y, z$ ) are obtained by the vector method of Meal and Polo<sup>12</sup> and are given below :

$C^\alpha$  elements :

$$C_{16}^\alpha = 0$$

$$\mathbf{C}_{26}^z = \frac{\mathbf{L}}{\sqrt{2}} (\sin \alpha - \sin \gamma) + \mathbf{M} - \mathbf{N}$$

$$\mathbf{C}_{36}^z = \frac{\mathbf{L}}{\sqrt{2}} (\sin \alpha + \sin \gamma) + \mathbf{M} + \mathbf{N}$$

$$\mathbf{C}_{46}^z = 3\mathbf{L} \left[ \frac{d_3 \cos \alpha - d_2 \cos \gamma}{\sqrt{6} d_2 d_3} \right] + \mathbf{P} - \mathbf{Q}$$

$$\mathbf{C}_{56}^z = \mathbf{L} \left[ \frac{d_3 \cos \alpha + d_2 \cos \gamma}{\sqrt{2} d_2 d_3} - \frac{\sqrt{2}}{d_1} \right] - \frac{\sqrt{2} \mu_0}{d_1^2} + \frac{\mathbf{P}}{\sqrt{3}} + \frac{\mathbf{Q}}{\sqrt{3}}$$

$\mathbf{C}^v$  elements :

$$\mathbf{C}_{16}^v = \mathbf{L} + \frac{\mu_0}{d_1}$$

$$\mathbf{C}_{26}^v = \frac{\mathbf{L}}{\sqrt{2}} (\cos \alpha + \cos \gamma) + \frac{\mathbf{P} d_2}{\sqrt{3}} + \frac{\mathbf{Q} d_3}{\sqrt{3}}$$

$$\mathbf{C}_{36}^v = \frac{\mathbf{L}}{\sqrt{2}} (\cos \alpha - \cos \gamma) + \frac{\mathbf{P} d_2}{\sqrt{3}} - \frac{\mathbf{Q} d_3}{\sqrt{3}}$$

$$\mathbf{C}_{46}^v = -3\mathbf{L} \left[ \frac{d_2 \sin \gamma + d_3 \sin \alpha}{\sqrt{6} d_2 d_3} \right] - \frac{\sqrt{3} \mathbf{M}}{d_2} - \frac{\sqrt{3} \mathbf{N}}{d_3}$$

$$\mathbf{C}_{56}^v = -\frac{\mathbf{L}}{\sqrt{2}} \left[ \frac{\sin \alpha}{d_2} - \frac{\sin \gamma}{d_3} \right] - \frac{\mathbf{M}}{d_2} + \frac{\mathbf{N}}{d_3}$$

where

$$\mathbf{L} = -\mu_e \left[ \frac{1}{d_1} + \frac{\sin \gamma}{d_2 \sin \beta} + \frac{\sin \alpha}{d_3 \sin \beta} \right]$$

$$\mathbf{M} = \mu_R (\sin \alpha \sin \gamma / \sqrt{2} d_2 \sin \beta)$$

$$\mathbf{N} = \mu_s (\sin \alpha \sin \gamma / \sqrt{2} d_3 \sin \beta)$$

$$\mathbf{P} = 3\mu_R (\sin \gamma \cos \alpha / \sqrt{6} d_2^2 \sin \beta)$$

$$\mathbf{Q} = 3\mu_s (\sin \alpha \cos \gamma / \sqrt{6} d_3^2 \sin \beta)$$

The zeta matrix elements are evaluated from the matrix relation  $\zeta^\alpha = \mathbf{L}^{-1} \mathbf{C}^z (\mathbf{L}^{-1})^1$ , where  $\mathbf{L}$  is the normal coordinate transformation matrix. Cyvin *et al.*<sup>13</sup> have reformulated the theory of rotational distortion by introducing certain new elements  $T_{\alpha\beta,\gamma}$  instead of partial derivatives of inertia tensor components  $J_{\alpha\beta,\gamma}$ , of Kivelson and Wilson,<sup>14,15</sup> The quantities  $t_{\alpha\beta\gamma\delta}$  have been obtained using Cyvin's relation and hence,  $\tau_{\alpha\beta\gamma\delta}$  values have been evaluated.

## RESULTS AND DISCUSSION

In the present investigation, the fundamental vibration frequencies of Acetophenone are assigned to 1670, 1260, 1000, 473, 370 and 162 cm<sup>-1</sup>. The vibrational representation of a planar *AXYZ* type molecules belonging to  $\mathbf{C}_s$  symmetry gives rise to  $\Gamma = 5A' + A''$ , all the modes being Infrared and Raman active. By taking into

account the earlier work,<sup>3,4</sup> the bands at 1670, 1260, 1000, 473, 370 and 162 cm<sup>-1</sup> are assigned to C = 0 stretching, C - R stretching, C - X stretching, RCO bending, R $\tilde{C}$ X bending and R $\tilde{C}$ X out of plane bending respectively.

### Normal Coordinate Analysis

A normal coordinate analysis of acetophenone has been carried out following Wilson's FG-matrix method on the basis of Cs-symmetry, using a general quadratic potential function. The molecular kinetic constants and a set of force constants have been reported in the present work.

The kinetic constants, the force constants, compliance constants are listed in Table II. Both the interaction kinetic constants and interaction potential constants viz.,  $k_{\alpha\beta}$ ,  $k_{\alpha\gamma}$ ,  $k_{\beta\gamma}$ ,  $k_{d_1\beta}$ ,  $k_{d_1\gamma}$ ,  $k_{d_2\gamma}$ ,  $k_{d_3\alpha}$ ,  $f_{\alpha\beta} f_{\alpha\gamma}$ ,  $f_{d_1\beta}$ ,  $f_{d_1\gamma}$ ,  $f_{\beta\gamma}$ ,  $f_{d_2\gamma}$ ,  $f_{d_3\alpha}$  are uniquely negative for this molecule. The stretching force constant C = 0 is in the expected range. This confirm the correctness of the assignment made in the present investigation. It may be added that all the force constants of acetophenone are available for the first time in the present work. The compliance constants naturally show the trend opposite to that of the force constants.

TABLE II

*Kinetic constants ( $10^{-23}$  g), force constants ( $10^5$  dynes/cm) and compliance constants ( $10^{-5}$  (dynes/cm) $^{-1}$ ) of acetophenone*

	<i>k</i> Kinetic constants ( $10^{-23}$ g)	<i>f</i> Force constants ( $10^5$ dynes/cm)	<i>c</i> Compliance constants ( $10^{-5}$ (dynes/cm) $^{-1}$ )
$d_1$	1.8312	11.4142	0.0952
$d_2$	4.1906	11.2739	0.1100
$d_3$	2.8117	7.6238	0.1526
$d_1d_3$	1.1001	2.9680	-0.0255
$d_1d_3$	0.2134	0.6206	-0.0032
$d_2d_3$	0.7592	2.1909	-0.0334
$\alpha$	0.9555	0.4607	0.2644
$\beta$	0.5302	0.2414	0.6660
$\gamma$	0.3346	0.1593	0.8223
$\alpha\beta$	-0.5634	-0.2661	0.0035
$\alpha\gamma$	-0.3331	-0.1651	-0.3584
$\beta\gamma$	-0.0116	0.0017	-0.5339
$d_{1\alpha}$	0.4759	0.2262	-0.0082
$d_{1\beta}$	-0.3294	-0.1509	0.0241
$d_{1\gamma}$	-0.1130	-0.0597	-0.0176
$d_{2\alpha}$	0.4977	0.2465	-0.0461
$d_{2\beta}$	0.3163	0.1449	-0.0382
$d_{2\gamma}$	-0.8211	-0.3942	0.0855
$d_{3\alpha}$	-0.9209	-0.4390	0.0662
$d_{3\beta}$	0.5515	0.2526	-0.0335
$d_{3\gamma}$	0.3099	0.1587	-0.0288
$\delta$	0.3471	0.0323	30.9391

The valence mean square amplitudes and the bonded, nonbonded vibrational mean amplitudes at 298.16 K of this molecule are given in Table III. From the table, it may be seen that the mean amplitudes for the bonded as well as non-bonded distances obtained in the present investigation are in the characteristic ranges for C—O, C—R, C—X vibrations.

TABLE III

*Valence mean square amplitudes ( $10^{-3} \text{ Å}^2$ ) and bonded and nonbonded vibrational mean amplitudes ( $10^{-2} \text{ Å}$ ) of acetophenone at 298.16 K*

<i>Valence Mean Square Amplitudes (<math>10^{-3} \text{ Å}^2</math>)</i>					
$\sigma_{d_1}$	1.5595	$\sigma_a$	1.9194	$\sigma_{d_1\alpha}$	-0.1485
$\sigma_{d_2}$	1.5660	$\sigma_B$	2.4353	$\sigma_{d_1\beta}$	0.4872
$\sigma_{d_3}$	2.1407	$\sigma_\gamma$	3.8757	$\sigma_{d_1\gamma}$	-0.3737
$\sigma_{d_1d_2}$	-0.5349	$\sigma_{a\beta}$	-0.0062	$\sigma_{d_2\alpha}$	-0.7848
$\sigma_{d_1d_3}$	-0.2087	$\sigma_{a\gamma}$	-0.0022	$\sigma_{d_2\beta}$	-0.3920
$\sigma_{d_2d_3}$	-0.9292	$\sigma_{B\gamma}$	-1.9386	$\sigma_{d_2\gamma}$	1.1812
<i>Bonded and Nonbonded Vibrational Mean Amplitudes (<math>10^{-2} \text{ Å}</math>)</i>					
<i>Bonded</i>			<i>Nonbonded:</i>		
$1_{d_1}(C - O)$	:	3.9491	$1_p(O..R)$	:	5.2085
$1_{d_2}(C - R)$	:	3.9572	$1_q(R..X)$	:	5.4808
$1_{d_3}(C - X)$	:	4.6267	$1_r(O..X)$	:	5.1125

The Coriolis coupling constants and centrifugal distortion constants are given in Table IV. The high values of the constants  $\zeta_{36}^x$ ,  $\zeta_{16}^y$ ,  $\zeta_{56}^y$  in this molecule suggest that the coupling between the vibrations concerned is more significant than others. The centrifugal distortion constants of this molecule are found to be in the expected range. The Coriolis coupling constants and centrifugal distortion constants are presented here for the first time.

TABLE IV

*The Coriolis coupling constant and centrifugal distortion constants (kHz) of acetophenone*

*Coriolis Coupling Constants:*

$\zeta_{16}^x = -0.1581$	$\zeta_{16}^y = -0.5089$
$\zeta_{26}^x = -0.3484$	$\zeta_{26}^y = 0.2662$
$\zeta_{36}^x = -0.6711$	$\zeta_{36}^y = 0.1810$
$\zeta_{46}^x = 0.2335$	$\zeta_{46}^y = 0.3952$
$\zeta_{56}^x = 0.1615$	$\zeta_{56}^y = 0.5078$

*Centrifugal Distortion Constants (kHz)*

$D_J = 3.5220$	$R_s = -1.0460$
$D_K = 4.7532$	$R_b = -0.5846$
$D_{JK} = -6.1443$	$\delta_J = -2.3359$

## CONCLUSION

A partial vibrational analysis of Acetophenone using the vibrational frequencies obtained from laser Raman Spectrum is available on the basis of  $C_s$  symmetry in the present study.

## ACKNOWLEDGEMENT

One of the authors (TJB) is thankful to UGC for the financial assistance.

## REFERENCES

1. K W F Kohlrausch *Raman Spektren* J W Edward Bros Inc Ann Arbor Michigan (1945) 383
2. H W Randall R G Fowler Fusin Nelson and J R Dangle *Infrared Determination of Organic Structures* Van Nostrand Inc. New York (1949)
3. H W Thompson and P Torkington *J chem Soc* (1945) 640
4. R S Rasmussen and R R Brattain *J Am chem Soc* 71 (1949) 1073
5. S Glasston *Chem Soc Ann Rep* 33 (1935) 134
6. P W Allen and L E Sutton *Acta Cryst* 3 (1950) 46
7. E B Wilson J C Decius and P Cross *Molecular Vibration* McGraw-Hill New York (1975)
8. S Mohan and K G Ravikumar *Acta Phys Pol* 62A (1982) 133
9. S Mohan and S Rajaraman *Indian J pure appl Phys* 90 (1982) 148
10. J C Decius *J chem Phys (USA)* 38 (1963) 241
11. S J Cyvin *Molecular Vibrations : Mean Square Amplitudes* Elsevier Amsterdam (1968)
12. J H Meal and S R Polo *J chem Phys (USA)* 24 (1956) 1119, 1126
13. S J Cyvin B N Cyvin and G Hagen *Z Naturforsch A (Ger)* 23 (1968) 1649
14. D Kivelson and E B Wilson (Jr) *J chem Phys (USA)* 20 (1953) 1575
15. D Kivelson and E B Wilson (Jr) *J chem Phys (USA)* 21 (1954) 1229
16. E V Rao *Ph D thesis* Osmania University (1964)

## INFRARED ABSORPTION SPECTRA OF SOME 8-AMINO-QUINOLINE SOLID COMPLEXES IN CORRELATION WITH COORDINATION BOND-LENGTH

MORSI M ABOU SEKKINA\* and S M EL-HELBAWY

Chemistry Department, Faculty of Science, Tanta University, Tanta, Egypt

(Received 23 May 1985)

The mode of bonding between  $\text{Cu}^{+2}$ ,  $\text{Ni}^{+2}$  and  $\text{Co}^{+2}$  and 8AQ in the solid complexes is studied by IR spectrophotometry. The shift of the band due to groups involved in coordination is utilized in estimating the coordination bond length. The value of C = N bond obtained amounts to 3.2–3.5 Å for 8AQ complexes. The value of coordination bond length of copper complexes is shorter than the corresponding value of the nickel and cobalt complexes. This is attributed to the increase of the strength of electrostatic field of copper ion as a result of its smallest ionic radius and its many *d*-electrons and thus would be its greater tendency for complex formation than the other metal ions involved.

**Key Words :** Infrared Absorption Spectra; 8-Aminoquinoline Solid Complex; Co-ordination Bond Length

### INTRODUCTION

THE infrared spectra of 8-aminoquinoline and its complexes were studied in an effort to obtain information regarding the type of bonding between the ligand and metal ions. Vibrations attributable to  $\text{-NH}_2$  group are observed for free 8AQ at 3440, 3340 $\text{cm}^{-1}$  (asym. and sym.  $\text{NH}_2$  stretching vibrations), 1615 $\text{cm}^{-1}$  ( $\text{NH}_2$  bending vibration), 1330 $\text{cm}^{-1}$  ( $\nu_{\text{C-NH}_2}$ ) and 760 $\text{cm}^{-1}$  (rocking vibration of the amino-group). The  $\text{NH}_2$ -stretching vibrations increase in intensity and suffer red shift upon coordination. This has previously been observed with related complexes in which coordination to an amino-nitrogen takes place<sup>1,2</sup>. Jensen and Nielsen<sup>3</sup>, assigned the bands at 1620 and 1580 $\text{cm}^{-1}$  to the vibration modes of the  $\text{NH}_2$  group partially coupled with the vibrations of the aromatic ring. The  $\text{NH}_2$  bending vibration shifts to lower frequency upon coordination, in accordance with the previous foundation on related materials.<sup>4,5</sup>

8AQ has a medium to strong band near 1340 $\text{cm}^{-1}$  which is probably a C–N stretching band. It may be significant that in the spectrum of all complexes studied, this band is shifted to a lower frequency (from 1339 $\text{cm}^{-1}$  to 1315 $\text{cm}^{-1}$ ). This is what would be expected, because the lonepair of the  $\text{NH}_2$  group is engaged when 8-aminoquinoline functions as a neutral ligand and accordingly, the double bond character of the *c*- $\text{NH}_2$  bond should be diminished.<sup>3</sup>

\*For correspondence.

Coordination of 8AQ through the formation of the chelate ring causes the appearance of the wagging frequency for  $-\text{NH}_2$  group<sup>1,2,6</sup> as broad and strong band at  $1020\text{-}1065\text{cm}^{-1}$  for the complexes studied.

As a result of chelation, the absorption band at  $1500\text{cm}^{-1}$  becomes the most intense in entire spectrum, these changes can be attributed to aromatic  $\text{C}=\text{C}$  and  $\text{C}=\text{N}$  vibrations indicating that chelation may take place through coordination with nitrogen of the ring.

From  $650$  to  $300\text{cm}^{-1}$ <sup>7</sup> the spectra of lanthanide chelates and pure ligand are similar in common. Several new weak to medium absorptions occur in chelates which could be probably attributed to coordinated water wagging and  $\text{M}-\text{OH}_2$  stretching,<sup>8-10</sup> (all of the absorptions are broad). In lanthanide complexes, new bands appear between  $220\text{-}260\text{cm}^{-1}$  and these are assigned to the stretching vibrations of lanthanon nitrogen coordinate bond.<sup>11</sup>

For complexes of transition metals, the band observed at  $470\text{-}530\text{cm}^{-1}$  could be assigned to  $\text{MNH}_2$  vibration since<sup>6,12,13</sup> this band cannot be observed for free 8AQ organic ligand.

## EXPERIMENTAL

### (i) Preparation of Metal Complexes of 8-Aminoquinoline (8AQ)

Hydrated metal chloride was reacted with 8AQ (as pure chemical from Eastman Organic Chemicals) in 1 : 2 molar ratio using absolute ethanol as solvent, and refluxed if necessary. The product was washed several times with absolute ethanol, dried and kept in vacuum desiccator.<sup>12</sup>

### (ii) Analysis of the Solid Complexes

The metal ion concentrations were estimated by EDTA titrations.<sup>14</sup> Analysis of C, H were determined in the micro-analytical unit-(Mansoura University, Egypt).

#### (a) Analysis of $[\text{Cu}(\text{C}_9\text{H}_8\text{N}_2)_2\text{Cl}_2 \cdot 2\text{H}_2\text{O}]$ Solid Complex :

$\text{Cu}$ {	Calc. 20.193%	C {	Calc. 47.47%	H {	Calc. 4.40%
found 20.969 %		Found 47.96 %		Found 4.60 %	

#### (b) Analysis of $\text{Ni}(\text{C}_9\text{H}_8\text{N}_2)_2\text{Cl}$ Solid Complex :

$\text{Ni}$ {	Calc. 14.046%	C {	Calc. 51.73%	H {	Calc. 3.82%
found 13.28 %		Found 52.30 %		Found 4.01 %	

#### (c) Analysis of $\text{Co}(\text{C}_9\text{H}_8\text{N}_4)\text{Cl}_2 \cdot 3\text{H}_2\text{O}$ Solid Complex :

$\text{Co}$ {	Calc. 12.45%	C {	Calc. 45.75%	H {	Calc. 4.693%
foun 12.27 %		Found 45.0 %		Found 5.00 %	

(iii) *Infrared Absorption Spectra Measurements*

The IR absorption spectra of the organic ligands as well as those of the corresponding complexes were recorded in the solid state on a UNICAM SP 1000 infrared spectrophotometer using the KBr disc technique within the region  $4000\text{--}200\text{cm}^{-1}$  at room temperature.

### RESULTS AND DISCUSSION

The IR spectra of the complexes of transition metal ions (Cu(II), Ni(II) and Co(II)) with 8-aminoquinoline (8AQ) are scanned as KBr discs as in Fig. 1. The characteristic band frequencies are listed in Table I.

For 8AQ complexes, the  $-\text{NH}_2$  stretching vibrations increase in intensity and suffer red shift upon coordination. This has been previously observed with related complexes in which coordination to an amino-nitrogen takes place.<sup>1,2</sup> As a result of chelation with 8AQ, the absorption band at  $1500\text{cm}^{-1}$  becomes the most intense entire spectrum. These changes can be attributed to aromatic C=C and C=N vibrations indicating that chelation may take place through coordination with nitrogen of the ring.

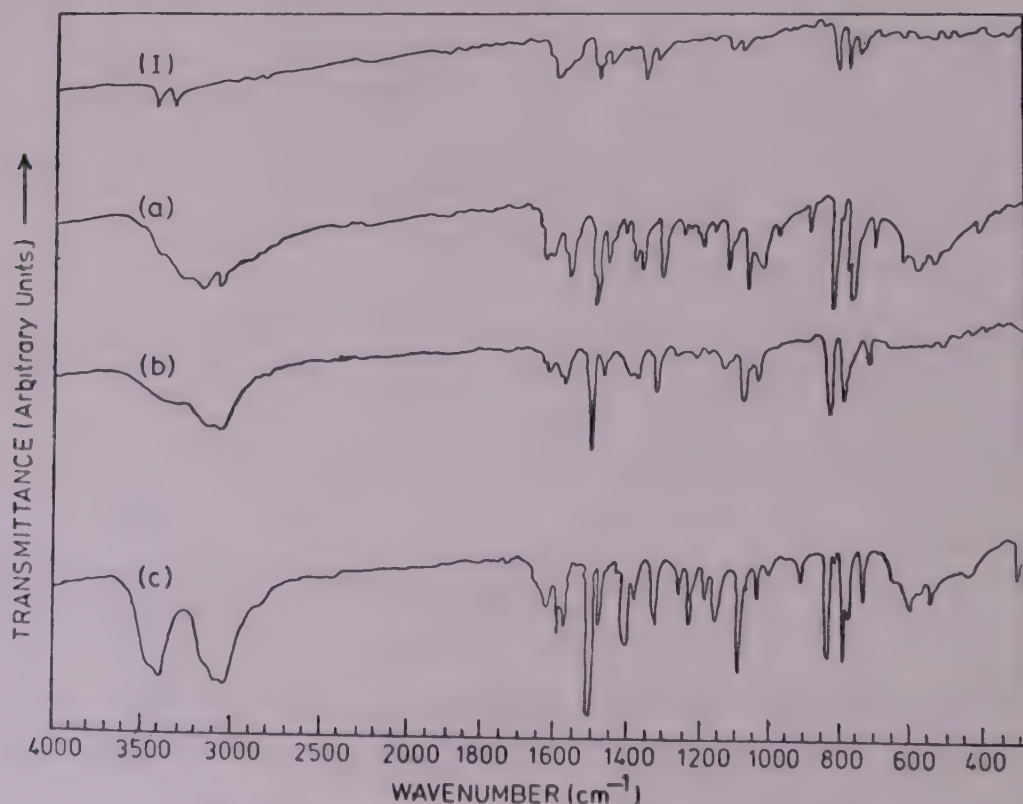


FIG 1 Infrared Absorption Spectra of :

- (I) 8 AQ.
- (a)  $\text{Co-(8 AQ)}_2 \text{Cl}_4 \cdot 3\text{H}_2\text{O}$  Complex.
- (b)  $\text{Ni-(8 AQ)}_2 \text{Cl}_4$  Complex.
- (c)  $\text{Cu-8 AQ} \cdot \text{Cl}_4 \cdot 2\text{H}_2\text{O}$  Complex.

TABLE I

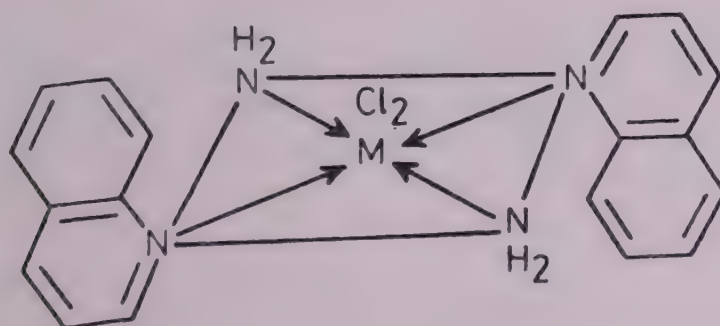
*Characterization and assignment of the infrared absorption spectral bands for 8-aminoquinoline and its complexes in the solid state*

Materials	Frequency ( $\text{cm}^{-1}$ )					
	$\nu\text{NH}_2$ asym.	$\nu\text{NH}_2$ sym.	$\nu\text{C}=\text{N}$	$\nu\text{C}-\text{N}$	$\delta\text{NH}_2$	$\text{WNH}_2$
8AQ	3440 <sup>m</sup>	3340 <sup>m</sup>	1630	1325 <sup>m</sup>	1620 1580	—
Cu.8AQ. $\text{Cl}_2\cdot\text{Cl}_2\cdot 2\text{H}_2\text{O}$	3380	3240	1615	1318	1585 1590	1030 1065
Co(8AQ) <sub>2</sub> . $\text{Cl}_2\cdot 3\text{H}_2\text{O}$	3330	3240	1618	1315	1580 1590	1030 1060
Ni(8AQ) <sub>2</sub>	3320	3270	1620	1318	1580 1590	1030 1050

*W* = Wagging vibration

*m* = Medium

According to the above data, together with results of chemical analysis of the solid complexes, the following structure is suggested at present :



M = Cu(II), Ni(II) and Co(II)

The foregoing results and discussion on 8AQ denote that as a result of their chelation, the C = N bands are apparently shifted to lower wavenumbers. Also other bands suffer some displacements in their positions. It is, however, of interest to mention that the magnitude of frequency shifts was dependent on the nature of both transition metal ion and ligand involved in chelation.

This was essentially ascribed to the change in the strength of the electrostatic fields of the metal ion and the position of the vibration dipoles.<sup>15</sup> Since all metal ions under investigation have the same charge, thus the distance between the metal ion and coordinating groups would be the main factor affecting band shifts, that is to say the coordination bondlength. The magnitude of frequency shift has been used and established elsewhere<sup>15</sup> in determining the distance between the metal ion and coordinating groups, which is approximately equivalent

to the length of coordination bond. The programme given by these authors<sup>15</sup> is summarised and based on the following :

According to Karagounis and Peter<sup>16</sup> the shifts in the IR spectra of organic ligands, on coordination with metal ions, are comparable to those due to absorption on salt substrate. Thus, both case can be treated in more or less the same manner. The change in dipole moment ( $\Delta\mu$ ) of the vibrating group under the influence of the electrostatic fields is given by the relation

$$\Delta\mu = \alpha f \quad \dots(1)$$

in which  $\alpha$  = bond polarizability

$f$  = field strength in electrostatic units.

The value of  $\Delta\mu$  can be determined from the change in charge density ( $\Delta e$ ),

$$\Delta\mu = l \Delta e, \quad \dots(2)$$

where  $l$  = length of the dipole (bond length).

From relations (1) and (2), one obtains :

$$\alpha f = l \Delta e \quad \dots(3)$$

where  $\Delta e$  should be given in electrostatic units.

The value of  $\Delta e$  can be determined from knowledge of the frequency shift of the band ( $\Delta\nu$ ) and the shift due to complete transfer of one electron from the bond. This latter is equivalent to half the difference between the frequency of the band due to a single bond ( $\nu_{s-s}$ ) and a double bond ( $\nu_{s=s}$ ). Accordingly :

$$\frac{\Delta e}{e} = \frac{2\Delta\nu}{\nu_{s=s} - \nu_{s-s}}, \quad \dots(4)$$

where  $\frac{\Delta e}{e}$  is the number of electrons transferred from the bond under the field effect. Thus,

$$\Delta e = \frac{2 \Delta \nu}{\nu_{s=s} - \nu_{s-s}} \quad \dots(5)$$

from relations (3) and (5), the following may be derived :

$$\alpha f = \frac{2 \Delta \nu l}{\nu_{s=s} - \nu_{s-s}} \quad \dots(6)$$

and  $f = \frac{2l}{\alpha(\nu_{s=s} - \nu_{s-s})} \quad \dots(7)$

Using this relation, the field strength at the position of the vibrating dipole can be calculated from the frequency shift. The variation of the field strength ( $f$ ) with the distance ( $r$ ) on the surface of the salt lattice is given by the Hückel relation (17) :

$$f = \frac{32\pi Z_e}{a^2} \cdot \exp \left( -2\pi \sqrt{\frac{2r}{a}} \right), \quad \dots(8)$$

where,  $Z_e$  = charge of the positive ion and  $a$  = lattice constant.

From (7 and 8) :

$$f = \left( \frac{32\pi\alpha}{a^2} \right) \left( \frac{v_{x-y} - v_{x-y}}{v_{x-y}} \right) \cdot \exp \left( -2\pi \sqrt{\frac{2r}{a}} \right).$$

The relation denotes that  $\log \Delta\nu$  would be a linear function of  $(r)$ , as shown in the calibration curves (Fig. 2).<sup>2,3</sup> The value of  $(r)$  can be directly calculated or determined graphically. The values of  $(r)$  for some complexes of 8-aminoquinoline with  $\text{CuCl}_2$ ,  $\text{NiCl}_2$  and  $\text{CoCl}_2$  are given in Table II.

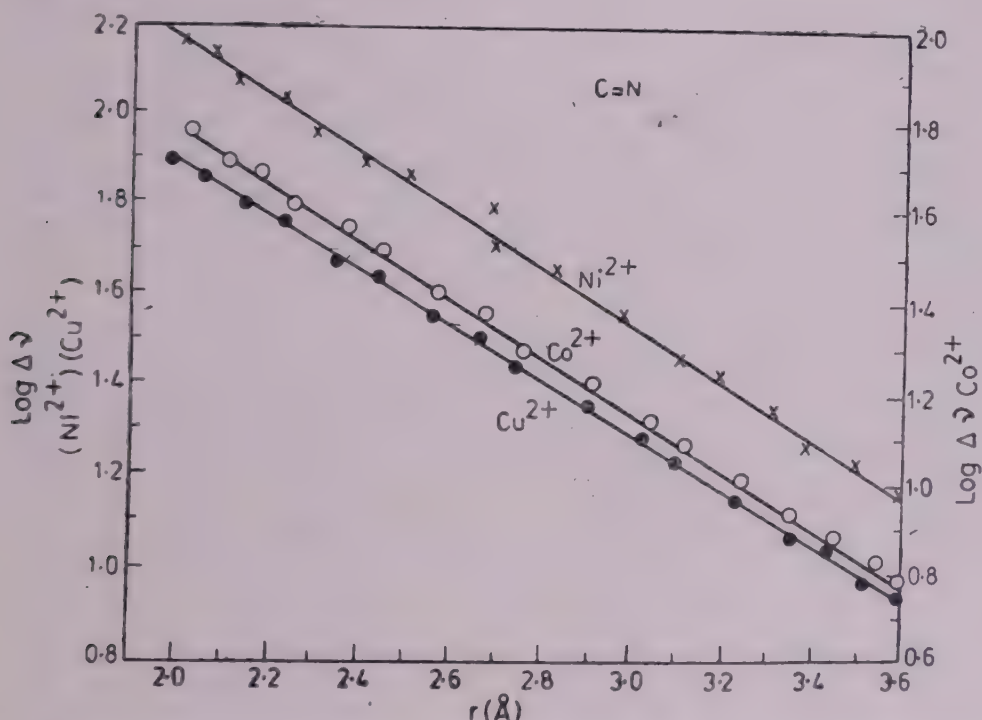


FIG 2 A diagrammatical representation for  $\log \Delta\nu$ -coordination bond length relationship.

TABLE II

*Band shift and the obtained value of coordination bond length for solid chelates with 8-aminoquinoline (8AQ)*

Material	$v(\text{cm})^{-1}$	$\Delta\nu \text{cm}^{-1}$	C=N	
			$\log \Delta\nu$	$r(\text{\AA})$
Ligand 8AQ	1630	—	—	—
Cu(II) complex	1615	15	1.1761	3.256
Ni(II) complex	1620	10	1.0000	3.511
Co(II) complex	1618	12	1.0792	3.500

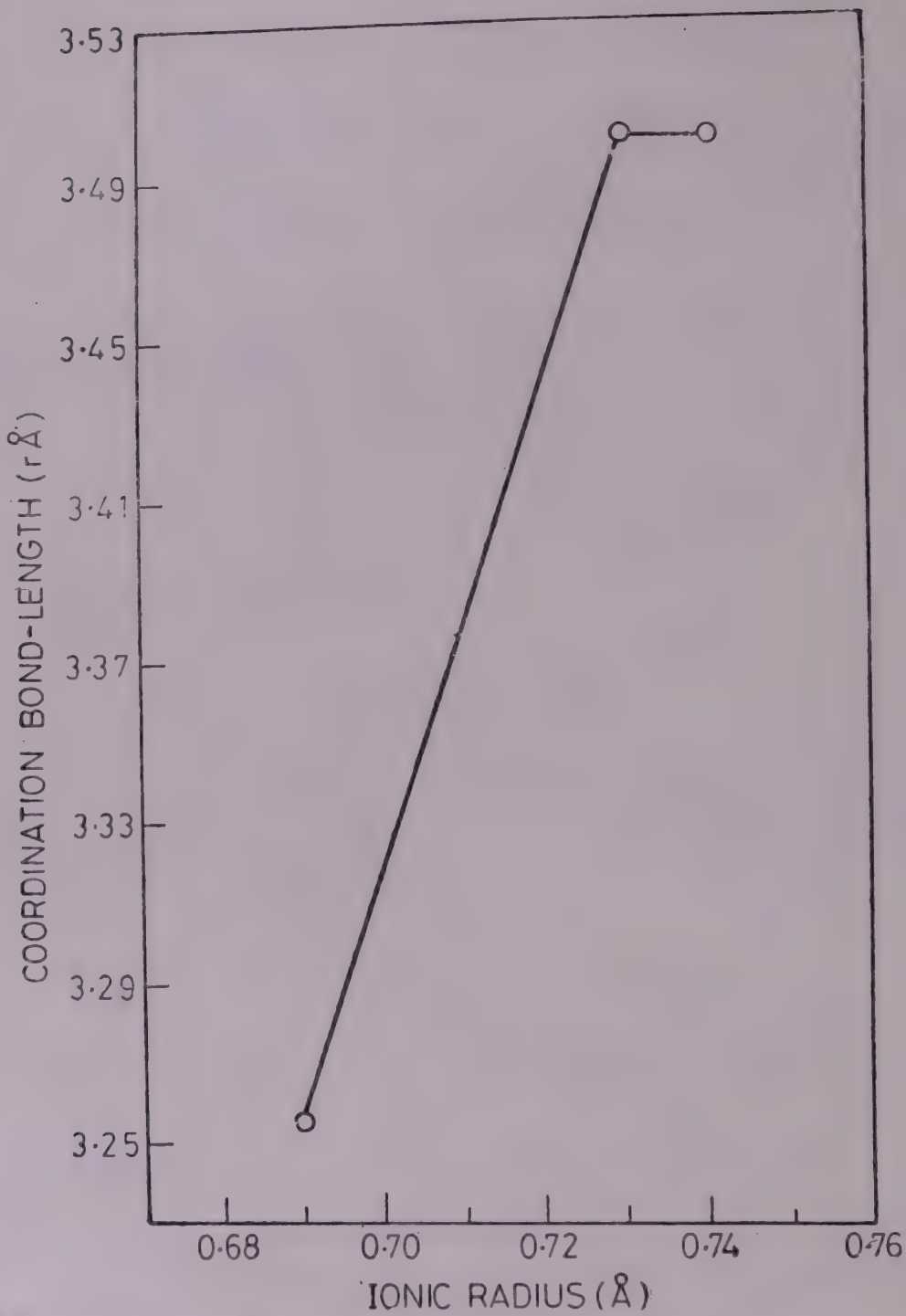


FIG 3 Relationship between coordination bond length of  $\text{Cu}^{+2}$ ,  $\text{Ni}^{+2}$  and  $\text{CO}^{+2}$  complexes with 8-aminoquinoline and ionic radii of the  $\text{Cu}^{+2}$ ,  $\text{Ni}^{+2}$  and  $\text{CO}^{+2}$  transition metals.

From Table II, one can conclude that for 8AQ, the  $\text{C} = \text{N}$  coordination bond length of the copper complex has a value shorter than the corresponding values for either nickel or cobalt complexes. This could be attributed to the increase of the strength of the electrostatic field of copper ion, as a result of the smaller ionic radius

of copper ion that for either Co(II) or Ni(II) ions (Fig. 3). Further contribution to this explanation is the greater number of d-electrons in Cu(II) ions than for either Ni(II) ions. The latter two ions have great similar ionic radii and thus their replacement with one another has no consistent effect on the coordination bond-lengths (Fig. 3 and Table II).

## REFERENCES

1. M P Coakley *Appl Spectra* **t18**(5) (1964) 149
2. L J Basile D L Kovacic and J R Ferraro *Inorg Chem* **t6**(2) (1967) 406
3. K A Jensen and P H Nielsen *Acta Chem Scand* **18**(1) (1964) 1
4. M A Jungbauer and C Curran *Spectrochim Acta* **21** (1965) 641
5. M A Coakley *Spectrochim Acta* **21** (1965) 1948
6. J Casabo J Ribas and J Bartroli *Rev Chim Miner* **t13** (1976) 149
7. L J Bellamy *The Infrared Spectra of Complex Molecules* Methuen Co. London (1962) p. 281
8. J Gamo *Bull chem Soc Japan* **34** (1961) 760, 765, 1430, 1433
9. J Fujita K Nakamoto and M Kobayashi *J Am chem Soc* (1956) 963
10. R Lofont *C R Hebd Seanc Acad Sci Paris* **244** (1957) 1481
11. J R Ferrare D L Kovacic and L J Basile *Inorg Chem* **5** (1966) 391
12. G M Barrow R H Koneger and F J Basolo *Inorg nucl Chem* **2** (1956) 340
13. E P Bertin I Nakagawa S Mizushima T J Lane and J V Quagliane *J Am chem Soc* **80** (1958) 525
14. J Welcher Frank *The Analytical Uses of Ethylene diaminetetraacetic Acid* D von Nostrand Company Inc Princeton-New Jersey-Toronto-London-New York (1961) 23.
15. I M Issa R M Issa Y M Temerk and M M Ghoneim *Egypt J Chem* **18** No. 1 (1975) 1
16. G Karagounis and O Peter *Z electrochem Ber Bunsenges phys Chem* **63** (1959) 1170
17. E Hückel *Adsorption and Kapillar Condensation* Leipzig (1968) 126

## ELECTROMAGNETIC FIELDS OF TRANSIENT SIGNALS ABOVE EVAPORATION DUCT

SAMIRA T BISHAY

*Department of Applied Mathematics, Faculty of Science, Ain-Shams University,  
Cairo, Egypt*

(Received 29 October 1984; after revision 4 October 1985)

The transient field of an atmospheric surface duct is studied when the distance between receiving and transmitting end is arbitrarily chosen. The application of two integral transforms to the wave equation of Hertzian vector—a Laplace transform in time and a two-dimensional Fourier transform in the horizontal coordinates in space—leads to an integral representation of the solution of the wave equation in transform space, considering initial, boundary and transition conditions. This integral representation determines the electromagnetic field in the ionosphere, which consists of a reflected wave which is superimposed upon the given incident wave.

**Key Words :** Electromagnetic Field; Transient Signals; Evaporation Duct;  
Hertzian Vector

### INTRODUCTION

For the last thirty years, the correlation between the propagation of electromagnetic waves in the atmosphere and meteorological conditions has been investigated by radiometeorologists. Sommerfeld<sup>1</sup> calculated the electromagnetic radiation from an electric vertical dipole, located above the plane interface of two media. Early attempts to get the transient response of a dielectric half-space were made by several authors; Gerjouy,<sup>2</sup> Friedrichs and Keller,<sup>3</sup> and Friedlander,<sup>4</sup> Poritsky,<sup>5</sup> generalizing Weyl's method,<sup>6</sup> expressed the primary field of the source in terms of a complex integral over plane waves. Pekeris and Alterman<sup>7</sup> have modified Cagniard's method<sup>8</sup> in solving a special integral equation occurring in propagation problems of electromagnetic and seismic pulses. Frankena<sup>9</sup> and De Hoop and Frankena<sup>10</sup> gave a further modification of Cagniard's method.

This paper treats the special problem of propagation of an electromagnetic impulse in an abnormal stratification of the upper ionosphere, the so-called surface duct. Kahan and Eckart<sup>11</sup> assumed a discontinuous drop in the otherwise constant refractive index at the upper duct boundary. The earth is assumed to be an ideal conductor and ideally plane. Bishay<sup>12</sup> extended the use to the steady-state duct propagation theory developed by the previous authors to calculate the field in the ionosphere above the duct. Now, we wish to apply this theory to transient excitation when no restrictions on the distance between the receiving and the transmitting end are made. We have used the method of De Hoop and Frankena<sup>10</sup> for the solution of our duct problem. Thus, the transient field of a dielectric half-space

situated above a dielectric layer and bounded by an infinitely conducting plane has been calculated.

### FORMULATION OF THE PROBLEM

We consider a dielectric layer of relative permittivity  $\epsilon_2$  overlying on the infinitely conducting plane earth which is confined by the plane  $z = 0$  of a Cartesian coordinate system  $(x, y, z)$ . At the height  $h$ , this permittivity decreases discontinuously to the value  $\epsilon_1$  (duct model of Kahan and Eckar).<sup>11</sup> The relative permeability  $\mu$  is assumed to be constant throughout the half-space  $z > 0$ . We refer to the layer as medium 2 and to the half-space  $z > h$  as medium 1. The potentials and the fields which belong to the two media are marked by the corresponding indices. The source of the field is assumed to be a vertical electric dipole in medium 1 at the point  $x = y = 0, z = d > h$ , whose moment is given by  $C \cdot F(t) \cdot \mathbf{e}_z$ . The vector  $\mathbf{e}_z$  denotes the unit vector in the  $z$ -direction,  $t$  is the time variable,  $C$  is some arbitrary constant to which we give the value  $\mu_0, \mu, \mu_0$  being the vacuum permeability. Regarding  $F(t)$ , we make the causality assumption  $F(t) = 0$  for  $t > 0$ .

The radiation field of this vertical electric dipole can be expressed in terms of the  $z$ -component of the Hertz vector  $\boldsymbol{\pi}$   $(x, y, z; t)$  denoted by  $\boldsymbol{\pi}_i(x, y, z; t)$   $i = 1, 2$ . This component fulfills the following wave equation

$$\Delta^2 \boldsymbol{\pi}_i - \frac{1}{v_i^2} \frac{\partial^2 \boldsymbol{\pi}_i}{\partial t^2} = \begin{cases} -\delta(x, y, z - d) F(t) & \text{for } i = 1 \\ 0 & \text{for } i = 2 \end{cases} \quad \dots(1)$$

where  $v_1$  denotes the phase velocity in medium 1.

### MATHEMATICAL FORMULATION

As mentioned above, at  $x = 0, y = 0, z = d$  ( $d > h$ ) a vertical electric dipole starts to radiate at the instant  $t = 0$ , it is assumed that prior to this instant all field quantities vanish identically. It is well-known, that the electromagnetic field generated by this vertical dipole can be derived from a Hertzian vector  $\boldsymbol{\pi}$  of which only the  $z$ -component is different from zero. The electric field vector  $\mathbf{E}$  and the magnetic field vector  $\mathbf{H}$  are expressed in terms of  $\boldsymbol{\pi}$  through the relations.

$$\mathbf{E} = \operatorname{grad} \operatorname{div} \boldsymbol{\pi} - \mu \epsilon \frac{\partial^2 \boldsymbol{\pi}}{\partial t^2}, \mathbf{H} = \epsilon \operatorname{curl} \frac{\partial \boldsymbol{\pi}}{\partial t}. \quad \dots(2)$$

In the region  $z > h$ , we write

$$\boldsymbol{\pi} = (\boldsymbol{\pi}_0 + \boldsymbol{\pi}_1) \mathbf{e}_z \quad (z > h), \quad \dots(3)$$

where  $\boldsymbol{\pi}_0$  yields the incident wave, while  $\boldsymbol{\pi}_1$  accounts for the reflected wave. Similarly, in the region  $0 < z < h$ , we write

$$\boldsymbol{\pi} = \boldsymbol{\pi}_2 \mathbf{e}_z,$$

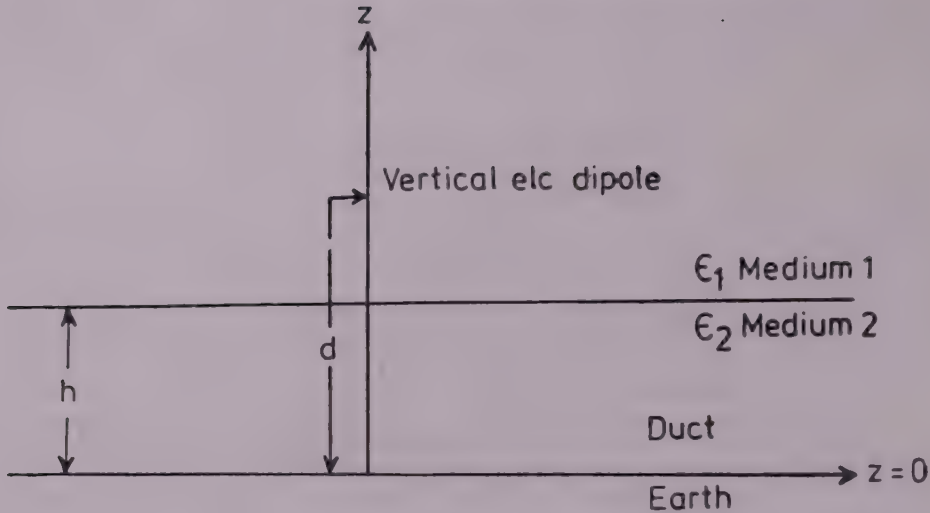


FIG 1 Geometry of the problem.

where  $\pi_2$  yields the refracted field and consist of an incident and reflected waves from the conducting plane  $z = 0$ . At any interior point of the appropriate half-space  $\pi_1 = \pi_1(x, y, z; t)$  and in the medium  $\pi_2 = \pi_2(x, y, z; t)$  are assumed to be continuous together with their first and second order partial derivatives.

#### METHOD OF SOLUTION

The starting point is the wave equation (1). The first step is the application of a Laplace transform with respect to time, which yields a three dimensional Helmholtz equation in the spatial coordinates for the  $\pi_i(x, y, z; s)$ .

$$\nabla^2 \pi_1(x, y, z; s) - \frac{s^2}{\gamma_1^2} \pi_1 = -\delta(x, y, z - d) f(s) \quad \dots(5)$$

$$\nabla^2 \pi_2(x, y, z; s) - \frac{s^2}{\gamma_2^2} \pi_2 = 0 \quad \dots(6)$$

$f(s)$  is the Laplace transform of  $F(t)$ . This step uses the initial conditions that  $\pi_i$  and its time derivative are zero for  $t$  equal to zero. The next step is to introduce the two-dimensional Fourier transforms  $\pi_i(x, y, z; s)$  with respect to  $x$  and  $y$ . Let :

$$U_i(\alpha, \beta; z; s) = \int_{-\infty}^{\infty} \int_{-\infty}^{\infty} \exp(-is(\alpha x + \beta y)) \pi_i(x, y, z; s) dx dy \quad \dots(7)$$

Then equations (5), (6) lead to a one-dimensional Helmholtz equations in the height coordinate  $z$  for the Fourier-transformed field.

$$\frac{\partial^2 U_1}{\partial z^2} - s^2 \gamma_1^2 U_1 = -\gamma(z - d) f(s) \quad \dots(8)$$

$$\frac{\partial^2 U_2}{\partial z^2} - s^2 \gamma_2^2 U_2 = 0 \quad \dots(9)$$

where  $\gamma_i^2 = \alpha^2 + \beta^2 + V_i^{-2}$ ,  $i = 1, 2$  with  $\operatorname{Re} \gamma_i \geq 0$ .

Here,  $\alpha$  and  $\beta$  are variables in the transform space of the two-dimensional Fourier transform.

The solutions that remain bounded as  $|z| \rightarrow \infty$  can be written as :

$$U_1 = \frac{f(s)}{2s} A_1 \exp(-s\gamma_1(z+d)) \quad \dots(10)$$

and

$$U_2 = \frac{f(s)}{2s} (A_2 \exp(s(\gamma_2 z - \gamma_1 d)) + B_2 \exp(-s(\gamma_2 z - \gamma_1 d))). \quad \dots(11)$$

The functions  $A_1(\alpha, \beta)$ ;  $A_2(\alpha, \beta)$  and  $B_2(\alpha, \beta)$  follow from the boundary conditions at the interfaces.

If  $U_1$  and  $U_2$  were known,  $\pi_1$  and  $\pi_2$  could be determined from the inversion integral.

$$\pi_i(x, y, z; s) = \frac{s^2}{4\pi^2} \int_{-\infty}^{\infty} \int_{-\infty}^{\infty} \exp(i(\alpha x + \beta y)) U_i(\alpha, \beta, z', s) d\alpha d\beta. \quad \dots(12)$$

The corresponding representation of  $\pi_0(x, y, z'; s)$  is known to be<sup>14</sup>

$$\begin{aligned} \pi_0(x, z, y', s) &= \frac{s f(s)}{8\pi^2} \int_{-\infty}^{\infty} \int_{-\infty}^{\infty} \exp(i(\alpha x + \beta y)) \frac{e}{\gamma_1} \\ &\quad - s \gamma_1 |z - d| d\alpha d\beta. \end{aligned} \quad \dots(13)$$

From these results the Hertzian vector in the ionosphere and the duct will be determined as integral-representations as:

$$\begin{aligned} \pi &= \frac{sf(s)}{8\pi^2} \int_{-\infty}^{\infty} \int_{-\infty}^{\infty} \left( \frac{\exp(-s\gamma_1 |z - d|)}{\gamma_1} \right) \\ &\quad - \frac{\exp(-s\gamma_1(d+z))(1+C_{12}) \exp(-2s\gamma_1(h-d))}{\gamma_1(1+C_{12} \exp(-2s\gamma_1 h))} \\ &\quad \exp(is(\alpha x + \beta y) d\alpha d\beta), \end{aligned} \quad \dots(14)$$

where

$$C_{12}(\alpha, \beta) = \frac{\gamma_1(\alpha, \beta) - \gamma_2(\alpha, \beta)}{\gamma_1(\alpha, \beta) + \gamma_2(\alpha, \beta)}. \quad \dots(15)$$

A similar expression can be derived for  $\pi_2(x, y, z', s)$ . The first term of the integrand in (14) is the potential due to the primary field, the second term denotes the diffracted field, and  $C_{12}$  correspond to the Fresnel reflection coefficient.

## CONCLUSION

An exact solution has been provided for the transient field of a dielectric layer as, for example, an atmospheric duct layer valid for arbitrary distance between receiving and transmitting end. To this end, we used a method originally given by Cagniard<sup>8</sup> and modified by De Hoop and Frankena<sup>10</sup> extending it to the present case of more complex geometry and to source position in the medium of smaller refractive index.

## REFERENCES

1. A Sommerfeld *Ann Phys* **28** (1909) 665
2. E Gerjouy *Comm pure appl Math* **6** (1953) 73
3. K O Friedrichs and J B Keller *J appl phys* **26** (1955) 961
4. F G Friedlander *Sound Pulses* Cambridge University Press Cambridge (1958)
5. H Poritsky *Br J appl phys* **6** (1955) 421
6. H Weyl *Ann Phys* (1919) 481
7. C L Pekeris and Z Alterman *J appl phys* **28** (1957) 1317
8. L Cagniard *Réflexion et Réfraction des ondes Seismiques Progressive* Gauthier-Villard, Paris (1939)
9. H J Frankena *Appl Sci Res* **B8** (1960) 357
10. A T De Hoop and H J Frankena *Appl Sci Res* **B8** (1960) 369
11. T Kahan and G Eckart *Ann Phys* **5** (1950) 641
12. S T Bishay *Ain Shams Sci Bull* **23B** (1981) 51
13. D S Jones *The Theory of Electromagnetism* Pergamon Press Oxford (1964)
14. A T De Hoop *Appl Sci Res* **B8** (1960) 349

## VIBRATIONAL SPECTRA OF SOME SOLID 8-HYDROXY- QUINOLINE METAL COMPLEXES IN CORRELATION WITH THEIR COORDINATION BOND LENGTH AND TYPE OF METAL ION

MORSI M ABOU SEKKINA and S M EL HELBAWY

Chemistry Department, Faculty of Science, Tanta University, Tanta, Egypt

(Received 23 May 1985)

The IR absorption spectra of metal complexes of 8HQ compared with those of 8HQ organic ligand, gave an idea about the nature of bonds taking part during complexation. The shift of the band due to groups involved in coordination is utilised in estimating the coordination bond length. The value of C=N bond obtained amounts to 3.4–3.5 Å for 8HQ complexes. The value of coordination bond length of copper(II) complexes is shorter than the corresponding values for nickel(II) and cobalt(II) complexes. This is attributed to the increase of the strength of electrostatic field of copper ion as a result of its smallest ionic radius and its many *d*-electrons.

**Key Words :** Vibrational Spectra; Solid 8-Hydroxyquinoline Metal Complexes; Coordination Bond Length

### INTRODUCTION

THE fundamental absorption bands characteristic for the essential groups in 8HQ are observed at  $3480\text{cm}^{-1}$  (OH-stretching vibration :  $\nu_{\text{OH}}$ ),  $1380\text{cm}^{-1}$  (OH deformation mode :  $\delta_{\text{OH}}$ ),  $1630\text{cm}^{-1}$  ( $\nu_{\text{C}-\text{N}}$ ),  $1330\text{cm}^{-1}$  ( $\nu_{\text{C}-\text{N}}$ ) and  $1095\text{cm}^{-1}$  ( $\nu_{\text{C}-\text{O}}$ ). The band  $3480\text{cm}^{-1}$  due to  $\nu_{\text{OH}}$  stretching vibration<sup>1</sup> disappears in the spectra of all complexes indicating that the OH-group is involved in complex formation. This deduction is supported by the disappearance of the band  $1380\text{cm}^{-1}$  due to  $\delta_{\text{OH}}$  in the IR spectra of all complexes.<sup>1</sup> Thus, the bonding of the metal ions to 8HQ takes place through covalent linkage with the phenolic oxygen.<sup>1</sup> The band near  $1630\text{cm}^{-1}$  which can be assigned to the C=N group is shifted to lower frequency in the spectra of chelates. Also the same behaviour is observed for  $\nu_{\text{C}-\text{N}}$  band. Thus, the bonding of the metal ions to 8HQ takes place through coordination bond with the nitrogen atoms of the ring.<sup>1</sup> In the spectra of all the 8HQ chelates studied, a strong peak appears at about ( $1095\text{--}1110\text{cm}^{-1}$ ). This peak may be ascribed to the C-O stretching frequency at the –C–O–M cite.<sup>2</sup> A weak intensity band at around  $400\text{cm}^{-1}$  which is absent in the ligand molecule is observed in all complexes of 8HQ with transition metal ions, this arises from some sort of metal chelates ring vibration essentially that of the M–O bond.<sup>3–5</sup>

\*For correspondence.

## EXPERIMENTAL

## (i) Preparation of Metal Complexes of 8-Hydroxyquinoline (8-HCl)

A solution of metal chloride 0.01 mol in ethanol was mixed with 0.02 mol of 8HQ (supplied from Cambrian Chemicals) in ethanol and refluxing if necessary. The complexes so formed are separated out as solids, then filtered off, washed several times with absolute alcohol, dried and kept in a vacuum desiccator.<sup>2</sup>

## (ii) Analysis of the Solid Complexes

The metal ion concentrations were estimated by EDTA titration.<sup>6</sup> C, H analysis were determined in the micro-analytical unit (Mansoura University, Egypt).

(a) Analysis of  $[\text{Cu}(\text{C}_9\text{H}_6\text{NO})_2]$  Solid Complex :

$\text{Cu}$	{ Calc. 18.058 %	$\text{C}$	{ Calc. 61.447 %	$\text{H}$	{ Calc. 3.43 %
	{ found 17.13 %		{ found 63.63 %		{ found 5.02 %

(b) Analysis of  $[\text{Ni}(\text{C}_9\text{H}_6\text{NO})_2]$  Solid Complex :

$\text{Ni}$	{ Calc. 16.915 %	$\text{C}$	{ Calc. 62.291 %	$\text{H}$	{ Calc. 3.48 %
	{ found 15.88 %		{ found 66.60 %		{ found 5.55

(c) Analysis of  $[\text{Co}(\text{C}_9\text{H}_6\text{NO})_2]$  Solid Complex :

$\text{Co}$	{ Calc. 16.836 %	$\text{C}$	{ Calc. 62.302 %	$\text{H}$	{ Calc. 3.483 %
	{ found 15.93 %		{ found 56.60 %		{ found 5.30 %

## (iii) Infrared Absorption Spectra Measurements

The IR absorption spectra of the organic ligand as well as the corresponding solid complexes were recorded in the solid state on UNICAM SP-1000 infrared spectro-photometer using the KBr disc technique within the region  $4000\text{-}200\text{cm}^{-1}$ .

## RESULTS AND DISCUSSION

The complexes involved in this investigation were those of transition metal ions Cu(II), Ni(II) and Co(II) with 8-hydroxyquinoline (8HQ). The wave numbers corresponding to peak absorption and their band assignments for complexes studied are collected in Table I, while representative spectra is given in Fig. 1.

For 8HQ, the band  $3480\text{cm}^{-1}$  due to  $\nu_{\text{OH}}$  stretching vibration disappears in the spectra of all complexes indicating that the OH-group is involved in complex formation. This is supported by the disappearance of the band  $1380\text{cm}^{-1}$  due to  $\delta_{\text{OH}}$  in the IR spectra of those complexes. Thus, the bonding of the metal ions to

TABLE I

*Characterization and assignments of the infrared absorption spectral bands of 8-hydroxyquinoline (8HQ) and its solid complexes*

Materials	Frequency ( $\text{cm}^{-1}$ )				
	$\nu_{\text{OH}}$	$\nu_{\text{C=N}}$	$\delta_{\text{OH}}$	$\nu_{\text{C-N}}$	$\nu_{\text{O-O}}$
8HQ	3480 <sup>b</sup>	1630	1380	1330	1095 <sup>a</sup>
$\text{Cu-(8HQ)}_2$	—	1620	—	—	1110
$\text{Ni-(8HQ)}_2$	—	1618	—	1330	1105
$\text{Co-(8HQ)}_2$	—	1618	—	1325	1110

*s*=strong    *b*=broad

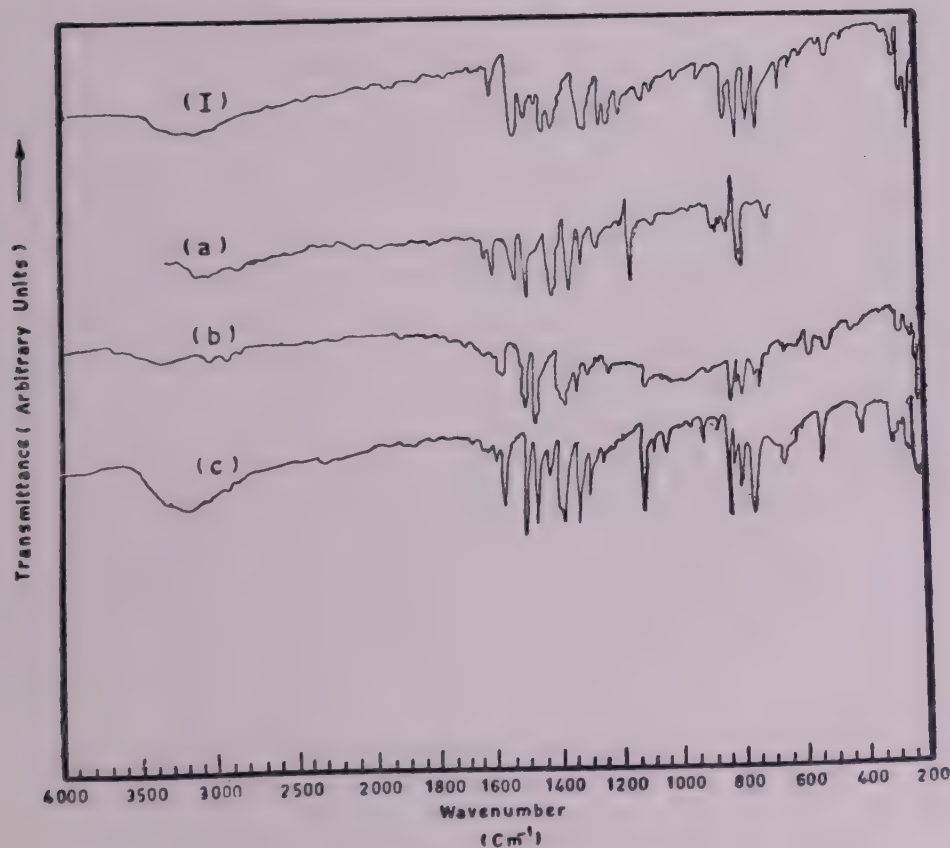
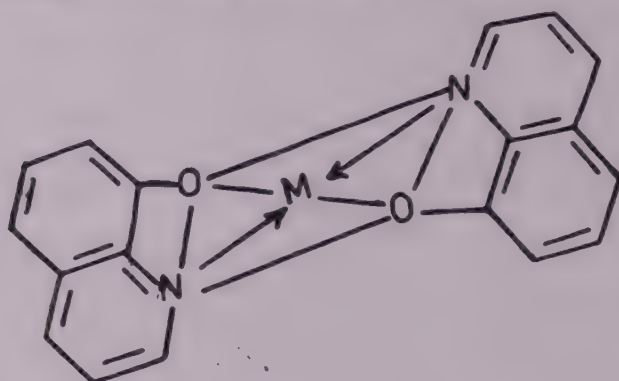


FIG 1 Infrared absorption spectra

- (I) 8HQ
- (a)  $\text{Cu-(8HQ)}_2$  Complex
- (b)  $\text{Ni-(8HQ)}_2$  Complex
- (c)  $\text{Co-(8HQ)}_2$  Complex

8HQ takes place through covalent linkage with the phenolic oxygen. The band near  $1630\text{cm}^{-1}$  which can be assigned to the  $\text{C-N}$  group is red shifted (to lower frequency) in the spectra of chelates. Also the same behaviour is covered for  $\nu_{\text{C-N}}$  band. Thus, the bonding of the metal ions to 8HQ takes place through coordination with the nitrogen of the ring.

According to the above data together with the results of chemical analysis of the solid complexes, the following structure is recommended at present :



### M=Cu(II), Ni(II) and Co(II)

The foregoing results and discussion on 8HQ denote that as a result of their chelation, the C = N bands are apparently shifted to lower wavenumbers. Also other bands suffer some displacements in their position. It is, however, of interest to mention that the magnitude of frequency shifts was dependent on the nature of both transition metal ion and ligand involved in chelation. This was essentially ascribed to the change in the strength of the electrostatic field of the metal ion and the position of the vibrating dipoles.<sup>7</sup> Since all metal ions under investigation have the same charge, thus the distance between the metal ion and coordinating groups would be the main factor affecting band shifts, that is to say the coordination bond length. The magnitude of frequency shifts has been used and established elsewhere<sup>7</sup> in determining the distance apart between the metal ion and coordinating groups, which is approximately equivalent to length of the coordination bond length. According to Karagounis and Peter,<sup>8</sup> the shifts in the IR spectra of organic ligands, on coordination to metal ions, are comparable to those due to absorption on salt substrate. The scheme given by Issa *et al.*<sup>7</sup> can be treated in more or less the same manner.

The value of the coordination bond length (*r*) can be determined from the relation<sup>9</sup>

$$\Delta\nu = \left( -\frac{32\pi\alpha}{a^2} \right) \left( \frac{\nu_{x-y} - \nu_{z-y}}{l} \right) \exp \left( -2\pi \sqrt{\frac{2r}{a}} \right),$$

where       $\alpha$  = bond polarisability,

$\Delta\nu$  = shift in the oscillator frequency  
 $(\nu_{\text{ligand}} - \nu_{\text{complex}}),$

$a$  = lattice constant of the metal salt used,

$\nu_{x-y}$  = frequency of the oscillator with single bond,

$\nu_{z-y}$  = frequency of the oscillator with double bond

and       $l$  = length of the oscillator coordinated to metal ion.

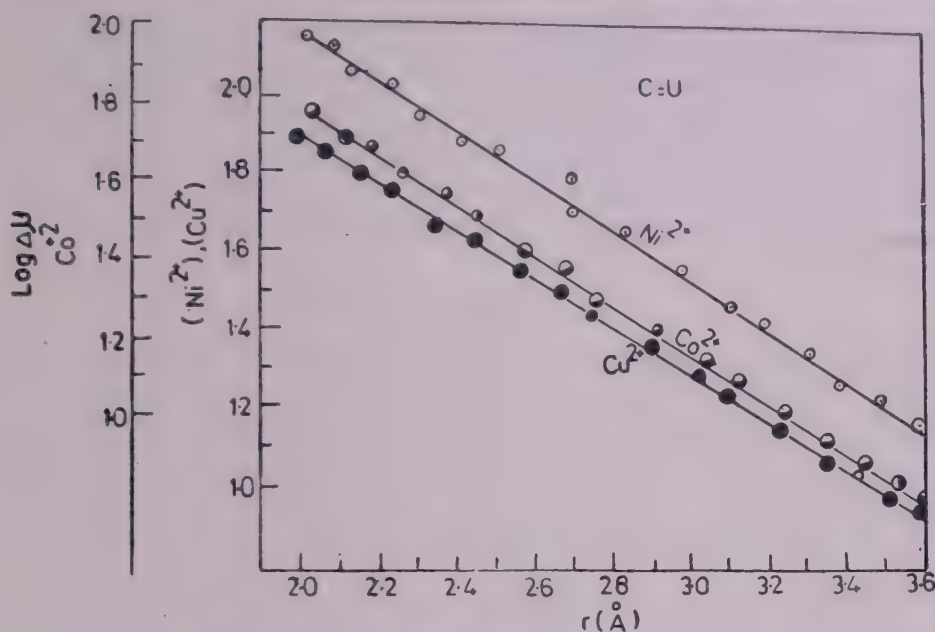
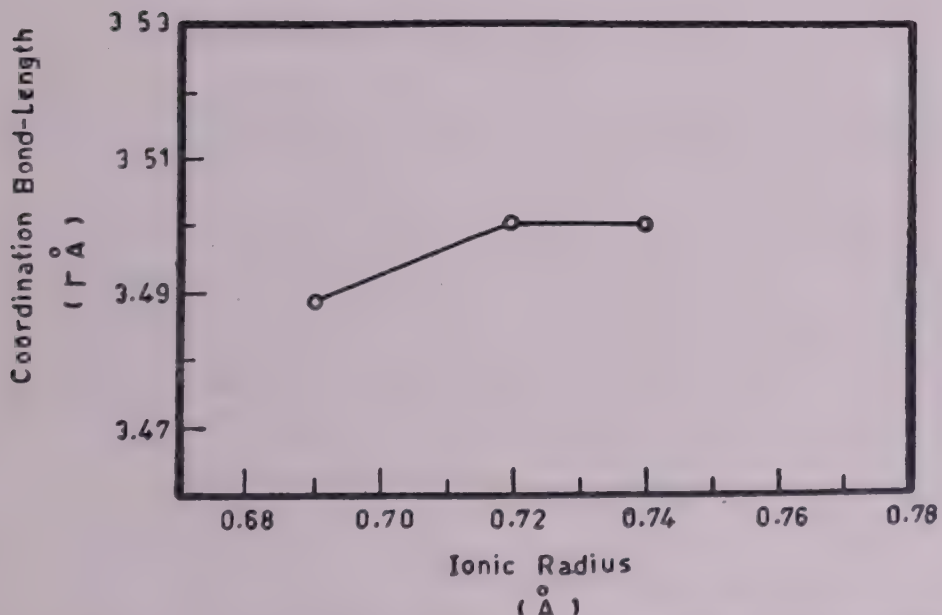


FIG 2

FIG 3 Relationship between coordination bond length of Cu<sup>2+</sup>, Ni<sup>2+</sup> and Co<sup>2+</sup> complexes with 8-hydroxyquinoline and the ionic radii of the Cu<sup>2+</sup>, Ni<sup>2+</sup> and Co<sup>2+</sup> transition metals.

This relation denotes that  $\log \Delta\nu$  would be a linear function of  $(r)$ , as shown in the calibration curves (Fig. 2). Values of  $(r)$  can be directly computed or determined graphically. The values of  $(r)$  for some coordinated compounds under investigation are given in Table II. From Table II, one can conclude that for 8HQ, the C=N coordination bond length of the copper (II) complex has a value shorter than the corresponding values for either Ni(II) or Co(II) complexes. This could

be attributed to the increase of the strength of electrostatic field of copper ion, as a result of the smaller ionic radius of copper ion than for the others ( $\text{Co}^{2+}$  and  $\text{Ni}^{2+}$ ) as shown in Fig. 3. Further contribution to our view is the greater number of  $d$ -electrons in Cu(II) ions than for either Ni(II) or Co(II) ions. The latter two ions have great similar ionic radii and thus their replacement with one another has no consistent effect on the coordination bond length (see Table II).

TABLE II

*Band shift and the obtained values of coordination bond length for some solid chelates with 8-hydroxyquinoline (8HQ)*

Material	C=N		$\log \Delta\omega$	$(r \text{ \AA})$
	$\nu_{(\text{cm}^{-1})}$	$\Delta\nu_{(\text{cm}^{-1})}$		
Ligand 8HQ	1630	—	—	—
Cu(II) complex	1620	10	1.00	3.488
Ni(II) complex	1618	12	1.0792	3.500
Co(II) complex	1618	12	1.0792	3.500

## REFERENCES

1. I M Issa R M Issa and R M Awadallah *Egypt J Chem* **18**(2) (1975) 215
2. R G Charles H Freiser R Friedel L E Hilliard and W D Johnston *Spectrochim Acta* **8** (1956) 1
3. K Nakamoto and A E Martell *J chem Phys* **32** (1960) 588
4. K Nakamoto P J McCarthy A Ruby and A E Martell *J Am chem Soc* **83** (1961) 1066
5. K Nakamoto Y Morimoto and A E Martell *J phys Chem Ithaca* **66** (1962) 346
6. J Welcher Frank *The Analytic Uses of Ethylene Diaminetetraacetic Acid* D von Nostrand Company Inc Princeton—New Jersey—Toronto—London—New York (1961) 11
7. I M Issa R M Issa Y M Temark and M M Ghoneim *Egypt J Chem* **18** (1975) No. 11
8. G Karagounis and O Peter *J Electrochem Ber Bunsenges phys Chem* **63** (1959) 1170
9. M M Abou Sekkina and S M El-Helbawy *Egypt J Chem* **8** (1984)

## SPECTRA OF SAMARIUM COMPLEXES

V RAMESH BABU and S BUDDHUDU

*Spectroscopic Laboratories, Department of Physics, S.V. University  
College of Arts and Science, Tirupati-517 502, India*

(Received 26 August 1985)

The ultraviolet(uv)-visible absorption spectra of Sm(III) ion in  $\text{NH}_4\text{Cl}$ ,  $(\text{NH}_4)_2\text{NO}_3$ ,  $\text{SmCl}_3$  and  $\text{Sm}(\text{NO}_3)_3 \cdot 6\text{H}_2\text{O}$  solutions have been studied. For the observed eleven energy levels, the energies ( $E$ ) and oscillator strengths ( $f$ ) have been measured. By a least-squares fit method, the experimental intensities of the observed bands are found to be in agreement with the theoretical values. The values of Judd-Ofelt ( $T_\lambda$ ) and bonding ( $\delta$ ) for the Sm(III) complexes are reported in this short note paper. From the bonding parameter ( $\delta$ ) values, the natures of bonding of these samarium complexes have been suggested.

**Key Words :** Energy Levels; Judd-Ofelt Intensity; Bonding Parameters

### INTRODUCTION

RECENTLY, we have reported the optical absorption spectra of rare earth elements such as Pr(III),<sup>1</sup> Nd(III),<sup>2</sup> Tm(III) and Er(III),<sup>3</sup> and Ho(III)<sup>4</sup> ions in ammonium solution complexes. As there has been no detail available in the literature on the spectra of samarium complexes, the present work has been taken up and the results thus obtained are reported in this paper.

### EXPERIMENTAL STUDIES

Samarium solution complexes were prepared by adding 0.2 mole per cent of samarium chloride and samarium nitrate to the saturated solutions of  $\text{NH}_4\text{Cl}$  and  $\text{NH}_4\text{NO}_3$ . In addition to these two complexes, two more solutions complexes were also prepared by mixing of same mole per cent in aquo region. The spectra recording were carried out in the uv-visible regions. From this recorded spectral features about eleven bands were observed in all the four solution complexes. From the spectra of these complexes the band intensity values were measured from the following expression:<sup>5</sup>

$$f_{\text{expt}} = 4.32 \times 10^{-9} \int \epsilon dv,$$

where  $\epsilon$  is the extinction coefficient and  $dv$  is the band-width at half height. The extinction coefficient  $\epsilon$  is evaluated from<sup>5</sup>

$$\epsilon = A/CL,$$

where  $A$  is the absorbance (optical density),  $C$  is the concentration of the sample and  $L$  is the optical path-length (Cell-Length). In the present work, the values of  $C$  and  $L$  are 0.2 mole per cent and 1cm respectively.

## RESULTS AND DISCUSSION

Assignments to the observed bands for the Sm(III) ion in four different solutions have been made according to the theoretical interpretation of Reisfeld.<sup>6</sup> The measured energies of the bands (in  $\text{cm}^{-1}$ ) are given in Table I, alongwith the assignments.

TABLE I  
*Experimentally determined energies of the observed levels of  $\text{Sm}^{3+}$  solution complexes*

Energy levels from $^5\text{H}_{5/2}$	Sm (III)				
	$\text{NH}_4\text{Cl}$ $E(\text{cm}^{-1})$	$\text{NH}_4\text{NO}_3$ $E(\text{cm}^{-1})$	$\text{SmCl}_3$ $E(\text{cm}^{-1})$	$\text{Sm}(\text{NO}_3)_3 \cdot 6\text{H}_2\text{O}$ $E(\text{cm}^{-1})$	Aquo <sup>b</sup> $E(\text{cm}^{-1})$
$^4\text{D}_{7/2}$	29146	29104	29189	29146	29100
$^4\text{D}_{3/2}$	27693	27693	27731	27693	27700
$^4\text{P}_{7/2}$	26838	26766	26838	26802	26750
$^4\text{L}_{15/2}$	25700	25700	25700	25700	25650
$^4\text{P}_{5/2}$	24993	24900	24993	24931	24950
$^4\text{P}_{3/2}$	24148	24003	24119	24061	24050
$^4\text{G}_{9/2}$	22773	22721	22773	22721	22700
$^4\text{I}_{13/2}$	21663	21592	21616	21639	21600
$^4\text{M}_{15/2}$	20981	20959	20959	20981	20800
$^4\text{G}_{7/2}$	20215	20095	20115	20115	20050
$^4\text{G}_{5/2}$	17237	17237	17478	17387	17900

By applying the Judd-Ofelt theory<sup>5</sup> the measured intensities of the observed bands are compared with the computed theoretical values. These values are presented in Table II. The evaluated Judd-Ofelt intensity ( $T_2$ ,  $T_4$  and  $T_6$ ) parameters are presented in Table II.

TABLE II  
*Judd-Ofelt ( $T_2$ ,  $T_4$ ,  $T_6$ ) and bonding ( $\delta$ ) parameters for Sm(III) solution complexes*

Parameter	Sm(III)			
	$\text{NH}_4\text{Cl}$	$\text{NH}_4\text{NO}_3$	$\text{SmCl}_3$	$\text{Sm}(\text{NO}_3)_3 \cdot 6\text{H}_2\text{O}$
$T_2 \times 10^6$	8.88399	50.609	75.4976	25.0674
$T_4 \times 10^6$	0.39308	1.147	0.6681	0.6547
$T_6 \times 10^6$	0.39958	1.565	1.0331	0.7838
$\delta$	0.06201	0.256	—	—

According to Tandon *et al.*<sup>7</sup> and Sinha,<sup>8</sup> the bonding nature of the ion studied may be covalent or ionic, depending on the positive or negative sign of the bonding parameter ( $\delta$ ). Table III gives the values of ' $\delta$ ' for Sm(III) :  $\text{NH}_4\text{Cl}$ ,  $\text{NH}_4\text{NO}_3$ . From this Table, it appears that the bonding may be covalent for the

two ammonium complexes. Similar such bonding natures have earlier been reported for Pr(III),<sup>1</sup> Nd(III),<sup>2</sup> Tm(III) and Er(III)<sup>3</sup> and Ho(III)<sup>4</sup> in ammonium solution complexes.

TABLE III

*Experimentally measured and calculated band intensities ( $f \times 10^6$ ) for  $\text{Sm}^{3+}$  solution complexes*

Energy Levels from ${}^*H_{5/2}$	Sm (III)							
	NH <sub>4</sub> Cl		NH <sub>4</sub> NO <sub>3</sub>		SmCl <sub>3</sub>		Sm (NO <sub>3</sub> ) <sub>3</sub> , 6H <sub>2</sub> O	
	$f_{\text{expt.}}$	$f_{\text{cal.}}$	$f_{\text{expt.}}$	$f_{\text{cal.}}$	$f_{\text{expt.}}$	$f_{\text{cal.}}$	$f_{\text{expt.}}$	$f_{\text{cal.}}$
${}^4D_{7/2}$	0.6185	0.4424	1.9700	1.7251	1.8502	0.0391	1.1781	0.8656
${}^4D_{5/2}$	0.3899	0.2976	2.1209	0.9378	0.7675	0.0243	1.2013	0.5245
${}^4P_{7/2}$	0.4743	0.8223	2.5167	3.1957	1.4361	0.0787	1.1146	1.6054
${}^4L_{15/2}$	0.1428	0.0617	0.5464	0.2414	0.4429	0.0062	0.2801	0.1208
${}^6P_{3/2}$	1.6256	1.6144	4.5546	4.8122	2.7215	0.1125	2.6387	2.7486
${}^6P_{5/2}$	0.3664	0.2497	1.4871	0.7245	0.9114	0.0176	0.5517	0.4143
${}^6G_{9/2}$	0.2252	0.0547	0.7139	0.2407	1.0782	0.0318	0.4025	0.1227
${}^4I_{13/2}$	0.3119	0.2229	0.9445	0.8449	0.6070	0.0256	0.4654	0.4285
${}^6M_{15/2}$	0.6813	0.2592	1.9701	1.0072	1.2175	0.0317	1.1151	0.5050
${}^6G_{7/2}$	0.0316	0.1058	0.0976	0.5269	0.2102	0.0339	0.0561	0.2655
${}^6G_{5/2}$	0.0699	0.0353	0.3756	0.1889	0.7486	0.0156	0.1357	0.0956

## ACKNOWLEDGEMENTS

The help rendered by Professor S V J Lakshman, FNASC is gratefully acknowledged by the authors. One of the authors (SB) expresses thanks to the UGC, New Delhi for a minor research grant.

## REFERENCES

1. S V J Lakshman and S Buddhudu *Phys Chem Solids* **43** (1982) 849
2. S V J Lakshman and S Buddhudu *Acta Physica Hung* **34** (1983) 231
3. C K Jayasankar *PhD Thesis* S V University Tirupati (1984)
4. Ch Gopinath and S Buddhudu *JQSRT* **35** (1986) (*In press*)
5. W T Carnall J P Hessler and F J Wanger *J chem Phys* **82** (1978) 2152
6. R Reisfeld *J non-cryst Solid* **30** (1979) 337
7. S P Tandon S S L Surana and R C Mathur *J phys C* **8** (1975) 2323
8. S P Sinha *Spectrochim Acta* **22** (1966) 57
9. W T Carnall P R Fields and K Rajnak *J chem phys* **49** (1966) 4424

## DISTRIBUTION OF STRESS IN THE NEIGHBOURHOOD CRACK IN A TRANSVERSELY ISOTROPIC SOLID

P CHOWDHURY and SUKLA MAITY

Department of Mathematics, Presidency College, Calcutta, India

(Received 17 December 1984)

The distribution of stress produced in the interior of a transversely isotropic solid by the opening of a crack under the action of pressure to its surface is considered. The case in which the pressure is constant over the entire crack, is also considered and the stress components Griffith Crack calculated and shown graphically.

**Key Words :** Stress Distribution; Griffith Crack; Transversely Isotropic Solid; Fracture

### INTRODUCTION

THE distribution of stress in the neighbourhood of a Griffith crack in an elastic body is of importance in the theory of fracture. Sneddon<sup>1</sup> has considered in detail the distribution of stress in the neighbourhood of a penny-shaped crack when it is opened under the action of pressure on its surface. The solution of the same problem in an isotropic solid has been discussed by Green,<sup>2</sup> Payne<sup>3</sup> and others. In this paper the distribution of stress produced in the interior of a semi-infinite transversely isotropic solid by the opening of penny-shaped crack under the action of variable pressure is considered. The case when the pressure is constant over the entire surface of the crack is also considered. The stress components are tabulated and the distribution of stress is shown graphically.

For a penny-shaped crack occupying the circle  $r^2 = x^2 + y^2 = a^2$  in the plane  $Z = 0$  of a infinite solid there is symmetry about the  $Z$ -axis, so the cylindrical coordinates  $(r, \theta, Z)$  may be employed. In this coordinate system the displacement vector assumes the form  $(u, \theta, w)$  and the stress in the interior of the medium is specified completely by the stress components  $rr, \theta\theta, zz, rz$ , the remaining components being identically zero.

It may now be assumed that the distribution of stress in the neighbourhood of the crack is the same as that produced in the interior of the semi-infinite transversely isotropic solid  $z > 0$  by the boundary conditions.

- (i)  $rz = 0$ , for all values of  $r$
- (ii)  $zz = -p(r/a)$ ,  $r < a$
- (iii)  $w = 0$ ,  $r > a$

on the plane  $z = 0$ .

In the first instant we assume that the applied internal pressure  $p$  is a function of  $r$ ; the case of a constant internal pressure will be examined later. The only restriction on the function  $p(r)$  imposed is such that the integral

$$\int_0^a rp(r) J_0(\xi r) dr$$

exists for all real values of the parameter  $\xi$ .

### SOLUTION OF THE GENERAL EQUATIONS

In a transversely isotropic solid  $z \geq 0$  with  $Z$ -axis as the axis of elastic symmetry the stress-strain relations are

$$\begin{aligned} rr &= C_{11}e_{rr} + C_{12}e_{\theta\theta} + C_{13}e_{zz}, \\ \theta\theta &= C_{12}e_{rr} + C_{11}e_{\theta\theta} + C_{13}e_{zz}, \\ zz &= C_{13}(e_{rr} + e_{\theta\theta}) + C_{33}e_{zz} \end{aligned} \quad \dots(1)$$

and  $rz = C_{44}e_{rz}$ ,

where  $C_{11}$ ,  $C_{12}$  etc. are elastic constants.

The strain components in terms of displacements are

$$e_{rr} = \frac{\partial u}{\partial r}, \quad e_{\theta\theta} = \frac{u}{r}, \quad e_{zz} = \frac{\partial w}{\partial z}$$

$$\text{and } e_{rz} = \frac{\partial u}{\partial z} + \frac{\partial w}{\partial r} \quad \dots(2)$$

and the equations of equilibrium  $x$  reduce to

$$\frac{\partial}{\partial r}(rr) + \frac{\partial}{\partial z}(rz) + \frac{1}{r}(rr - \theta\theta) = 0$$

$$\text{and } \frac{\partial}{\partial r}(rz) + \frac{\partial}{\partial z}(zz) + \frac{1}{r}(rz) = 0 \quad \dots(3)$$

Substituting the values of the stress components in the two equations of (3), we obtain

$$C_{11}\left(\frac{\partial^2 u}{\partial r^2} + \frac{1}{r}\frac{\partial u}{\partial r} - \frac{u}{r^2}\right) + C_{44}\frac{\partial^2 w}{\partial z^2} + (C_{13} + C_{44})\frac{\partial^2 w}{\partial r \partial z} = 0 \quad \dots(4)$$

and

$$C_{44}\left(\frac{\partial^2 w}{\partial r^2} + \frac{1}{r}\frac{\partial w}{\partial r}\right) + C_{33}\frac{\partial^2 w}{\partial z^2} + (C_{13} + C_{44})\frac{\partial}{\partial z}\left(\frac{\partial u}{\partial r} + \frac{u}{r}\right) = 0 \quad \dots(5)$$

Let us assume  $u = \frac{\partial \phi}{\partial r}$ ,  $w = \lambda \frac{\partial \phi}{\partial z}$  where  $\phi$  is a function of  $r$ ,  $z$  and  $\lambda$  is some constant.

Eqnate (4) is satisfied if

$$C_{11} \left( \frac{\partial^2 \phi}{\partial r^2} + \frac{1}{r} \frac{\partial \phi}{\partial r} \right) + [C_{44} + \lambda(C_{13} + C_{44})] \frac{\partial^2 \phi}{\partial z^2} = 0 \quad \dots(6)$$

and equation (5) will be satisfied if

$$(C_{13} + C_{44} + \lambda C_{44}) \left( \frac{\partial^2 \phi}{\partial r^2} + \frac{1}{r} \frac{\partial \phi}{\partial r} \right) + \lambda C_{33} \frac{\partial^2 \phi}{\partial z^2} = 0 \quad \dots(7)$$

The two equations of (6) and (7) will give a non-zero solution only if they are identical and this happens if

$$\frac{\lambda(C_{13} + C_{44}) + C_{44}}{C_{11}} = \frac{\lambda C_{33}}{\lambda C_{44} + C_{13} + C_{44}} = m^2 \text{ (say)} \quad \dots(8)$$

Then  $\phi_1$  and  $\phi_2$  are the solutions of

$$\left( \frac{\partial^2}{\partial r^2} + \frac{1}{r} \frac{\partial}{\partial r} + m_i^2 \frac{\partial^2}{\partial z^2} \right) \phi_i = 0; \quad i = 1, 2, \quad \dots(9)$$

where  $m_i^2$  are the roots of the equation

$$C_{11}C_{44}m^4 + \left( 2C_{13}C_{44} + C_{13}^2 - C_{11}C_{33} \right) m^2 + C_{33}C_{44} = 0 \quad \dots(10)$$

The roots  $m_i^2$  are real or complex depending on the five elastic constants  $C_{11}$ ,  $C_{13}$ ,  $C_{33}$ , ...etc. They are real, for example in the case of Magnesium but are conjugate complex for Zinc.

The components of displacement are given by

$$u = \frac{\partial}{\partial r} (\phi_1 + \phi_2), \quad w = \frac{\partial}{\partial z} (\lambda_1 \phi_1 + \lambda_2 \phi_2), \quad \dots(11)$$

where  $\lambda_1, \lambda_2$  are the two values of  $\lambda$  corresponding to  $m_1^2$  and  $m_2^2$  respectively.

In the case of a semi-infinite solid  $Z \geq 0$  assumed free from disturbances at infinity, we are interested in the solution of the equation (9) which tends to zero as  $Z$  tends to infinity, so that the appropriate solution of the equation (9) are

$$\left. \begin{aligned} \phi_1 &= \int_0^\infty A e^{-\alpha z/m_1} J_0(\alpha r) d\alpha \\ \phi_2 &= \int_0^\infty B e^{-\alpha z/m_2} J_0(\alpha r) d\alpha \end{aligned} \right\} \quad \dots(12)$$

where  $A$  and  $B$  are arbitrary functions of  $\alpha$  only to be determined from the boundary conditions.

The stress components are given by

$$\begin{aligned} rr &= \left( C_{11} \frac{\partial^2}{\partial r^2} + C_{12} \frac{1}{r} \frac{\partial}{\partial r} \right) (\phi_1 + \phi_2) \\ &\quad + C_{13} \frac{\partial^2}{\partial z^2} (\lambda_1 \phi_1 + \lambda_2 \phi_2), \end{aligned}$$

$$\begin{aligned} \theta\theta &= \left( C_{12} \frac{\partial}{\partial r^2} + C_{11} \frac{1}{r} \frac{\partial^2}{\partial r} \right) (\phi_1 + \phi_2) \\ &\quad + C_{13} \frac{\partial^2}{\partial z^2} (\lambda_1 \phi_1 + \lambda_2 \phi_2), \end{aligned}$$

$$\begin{aligned} zz &= C_{13} \left( \frac{\partial}{\partial r^2} + \frac{1}{r} \frac{\partial^2}{\partial r} \right) (\phi_1 + \phi_2) \\ &\quad + C_{33} \frac{\partial}{\partial z^2} (\lambda_1 \phi_1 + \lambda_2 \phi_2) \end{aligned}$$

and

$$rz = C_{41} \frac{\partial^2}{\partial r \partial z} [(1 + \lambda_1) \phi_1 + (1 + \lambda_2) \phi_2]. \quad \dots(13)$$

Inserting the values of  $\phi_1$  and  $\phi_2$  from (12) we obtain from relations (11) and (13)

$$\begin{aligned} rr &= (C_{11} - C_{12}) \int_0^\infty \alpha^2 (A e^{-\alpha z/m_1} + B e^{-\alpha z/m_2}) \frac{J_1(\alpha r)}{\alpha r} d\alpha \\ &\quad + \int_0^\infty \alpha^2 \left[ A e^{-\alpha z/m_1} \left( \frac{\lambda_1 C_{13}}{m_1^2} - C_{11} \right) + B e^{-\alpha z/m_2} \left( \frac{\lambda_2 C_{12}}{m_2^2} - C_{11} \right) \right] \\ &\quad \times J_0(\alpha r) d\alpha \quad \dots(14) \end{aligned}$$

$$\begin{aligned} \theta\theta &= (C_{12} - C_{11}) \int_0^\infty \alpha^2 (A e^{-\alpha z/m_1} + B e^{-\alpha z/m_2}) \frac{J_1(\alpha r)}{\alpha r} d\alpha \\ &\quad + \int_0^\infty \alpha^2 \left[ A e^{-\alpha z/m_1} \left( \frac{\lambda_1 C_{13}}{m_1^2} - C_{12} \right) + B e^{-\alpha z/m_2} \left( \frac{\lambda_2 C_{13}}{m_2^2} - C_{12} \right) \right] \\ &\quad \times J_0(\alpha r) d\alpha \quad \dots(15) \end{aligned}$$

$$\begin{aligned} zz &= \int_0^\infty \alpha^2 \left[ A \left( \frac{C_{33}\lambda_1}{m_1^2} - C_{13} \right) e^{-\alpha z/m_1} + B \left( \frac{C_{33}\lambda_2}{m_2^2} - C_{13} \right) e^{-\alpha z/m_2} \right] \\ &\quad \times J_0(\alpha r) d\alpha \quad \dots(16) \end{aligned}$$

$$rz = C_{44} \int_0^\infty \alpha^2 \left[ \frac{1 + \lambda_1}{m_1} A e^{-\alpha z/m_1} + \frac{1 + \lambda_2}{m_2} B e^{-\alpha z/m_2} \right] J_1(\alpha r) d\alpha \quad \dots(17)$$

$$u = - \int_0^\infty \alpha (A e^{-\alpha z/m_1} + B e^{-\alpha z/m_2}) J_1(\alpha r) d\alpha \quad \dots(18)$$

$$w = - \int_0^\infty \alpha \left( \frac{\lambda_1 A}{m_1} e^{-\alpha z/m_1} + \frac{\lambda_2 B}{m_2} e^{-\alpha z/m_2} \right) J_0(\alpha r) d\alpha \quad \dots(19)$$

### PRESCRIBED NORMAL PRESSURE ACROSS THE SURFACE OF A PENNY-SHAPED CRACK

Let a penny-shaped crack, occupying a circular area  $r \leq a$  in the plane  $z = 0$  be opened out and deformed by a normal pressure defined by  $zz = -p(r/a)$  when  $z = 0$ . So the boundary surface  $z = 0$  is subjected to the boundary conditions as pointed out in the introduction.

$$rz = 0, \text{ for all values of } r \quad \dots(20)$$

$$zz = -p(r/a), \quad r < a \quad \dots(21)$$

$$w = 0, \quad r > a \quad \dots(22)$$

On the surface  $z = 0$  the normal and axial components of stress and the normal component of displacement are obtained from the relations (16), (17) and (19).

$$zz = \int_0^\infty \alpha^2 \left[ C_{33} \left( \frac{A \lambda_1}{m_1^2} + \frac{B \lambda_2}{m_2^2} \right) - C_{13}(A + B) \right] J_0(\alpha r) d\alpha \quad \dots(23)$$

$$rz = C_{44} \int_0^\infty \alpha^2 \left[ \frac{1 + \lambda_1}{m_1} A + \frac{1 + \lambda_2}{m_2} B \right] J_1(\alpha r) d\alpha \quad \dots(24)$$

$$w = - \int_0^\infty \alpha \left( \frac{\lambda_1 A}{m_1} + \frac{\lambda_2 B}{m_2} \right) J_0(\alpha r) d\alpha \quad \dots(25)$$

From the relation (24) and the condition (20) we obtain

$$B(\alpha) = -k_1 A(\alpha), \quad \dots(26)$$

where

$$k_1 = \frac{1 + \lambda_1}{1 + \lambda_2} \cdot \frac{m_2}{m_1}. \quad \dots(27)$$

With this value of  $B(\alpha)$  the relations (23) and (25) reduce to

$$[zz]_{z=0} = \int_0^\infty \alpha^2 k_2 A(\alpha) J_0(\alpha r) d\alpha \quad \dots(28)$$

and

$$[\nu]_{z=0} = - \int_0^\infty \alpha k_3 A(\alpha) J_0(\alpha r) d\alpha, \quad \dots(29)$$

where

$$k_2 = \left( \frac{C_{33}\lambda_1}{m_1^2} - C_{13} \right) - \left( \frac{C_{33}\lambda_2}{m_2^2} - C_{13} \right) k_1, \quad \dots(30)$$

and

$$k_3 = \frac{\lambda_1}{m_1} - \frac{\lambda_2}{m_2} k_1.$$

Introducing dimensionless variable  $\eta = \alpha a$ ,  $\rho = r/a$  and  $\alpha k_3 A(\alpha) = f(\eta)$  and using the conditions (21), (22) we obtain from relations (28) and (29) the pair of integral equations

$$\left. \begin{aligned} \int_0^\infty \eta f(\eta) J_0(\rho\eta) d\eta &= g(\rho), \quad 0 < \rho < 1, \\ \int_0^\infty f(\eta) J_0(\rho\eta) d\eta &= 0, \quad \rho > 1 \end{aligned} \right\} \quad \dots(31)$$

where

and

$$\left. \begin{aligned} \int_0^\infty f(\eta) J_0(\rho\eta) d\eta &= 0, \quad \rho > 1 \end{aligned} \right\}$$

$$g(\rho) = - \frac{a^2 k_3}{k_2} p(\rho).$$

The dual integral equations of the type (31) have been considered by Titchmarsh<sup>4</sup> and Busbridge<sup>5</sup>; the solutions of the pair (31) can be derived from Busbridge's analysis in the form

$$f(\eta) = \frac{2}{\pi} \int_0^1 \mu \sin \mu \eta d\mu \int_0^1 \frac{\rho g(\rho \mu)}{\sqrt{1 - \rho^2}} d\rho \quad \dots(32)$$

With this value of  $f(\eta)$  the components of stresses and displacements are obtained from relations (14) to (19).

#### PREScribed NORMAL DISPLACEMENT ON THE SURFACE $Z = 0$

We consider the problem of determining the distribution of stress in a semi-infinite transversely isotropic medium bounded by the plane  $z = 0$  when the surface value of the normal component of the displacement vector is prescribed for all values of  $r$ . So the boundary conditions are

$$rz = 0, \text{ for all values of } r \quad \dots(33)$$

$$\left. \begin{array}{l} w = w(r), \quad r < a \\ = 0, \quad \quad r > a \end{array} \right\} \quad \dots(34)$$

Substituting the conditions (34) into the equation (29)

$$\int_0^\infty \alpha A(\alpha) J_0(\alpha r) d\alpha = \begin{cases} -\frac{1}{k_3} w(r), & r < a \\ 0, & r > a \end{cases}$$

Inverting the result by means of Hankel inversion theorem

$$A(\alpha) = -\frac{1}{k_3} \int_0^\infty r w(r) J_0(\alpha r) d\alpha. \quad \dots(35)$$

Denoting the integral on the R.H.S. of (35) by  $w(\alpha)$  then, from (28)

$$[zz]_{z=0} = -\frac{k_2}{k_3} \int_0^\infty \alpha^2 w(\alpha) J_0(\alpha r) d\alpha. \quad \dots(36)$$

Equation (36) gives the value of the applied pressure on the circle  $r < a$  which must be applied to maintain the prescribed surface displacement. For example, if it is assumed that

$$w(r) = \epsilon \left( 1 - \frac{r^2}{a^2} \right),$$

then from equation (35) it follows that

$$w(\alpha) = \frac{2\epsilon}{\alpha^2} J_2(a\alpha)$$

and so by equation (36) that the normal component of the surface stress is given by the expression

$$[zz]_{z=0} = -\frac{2k_2}{k_3} \epsilon \int_0^\infty J_2(a\alpha) J_0(\alpha r) d\alpha. \quad \dots(37)$$

Using the recurrence relation

$$J_2(a\alpha) = J_0(a\alpha) - \frac{2}{a} \frac{\partial}{\partial \alpha} J_1(a\alpha)$$

after integration by parts it is found that

$$\int_0^\infty J_0(\alpha r) J_2(a\alpha) d\alpha = \int_0^\infty J_0(\alpha r) J_0(a\alpha) d\alpha - \frac{2r}{a} \int_0^\infty J_1(\alpha r) J_1(a\alpha) d\alpha. \quad \dots(38)$$

Sneddon<sup>1</sup> has shown that by Gubler's formula<sup>6</sup> value of the first integral can be found in the usual notation for elliptic integrals<sup>7</sup> and for the second integral can be evaluated by making use of Neumann's result and the same is expressed in terms of complete elliptic integrals. So

$$[zz]_{z=0} = -\frac{4}{\pi a} \frac{k_2}{k_3} \epsilon f(\rho), \quad \dots(39)$$

where the function  $f(\rho)$  is defined by the equation

$$f(\rho) = \frac{1 + \rho^2}{1 + \rho} K(k) - K(\rho) - (1 + \rho) E(k)$$

in which

$$\rho = r/a \text{ and } k^2 = 4\rho/(1 + \rho^2).$$

Result (39) gives the value of applied pressure which is required to maintain the prescribed surface displacement. It appears therefore that in case of isotropic material the constant factor in the expression for  $[zz]_{z=0}$  is  $E/(1 - \sigma^2)$  whereas in case of transversely isotropic material the constant factor is  $2k_2/k_3$ , where  $K_2, K_3$  are the expressions in (30) involving elastic constants in a transversely isotropic material.

#### PREScribed CONSTANT PRESSURE ON THE SURFACE OF THE CRACK

The normal component of surface displacement is obtained from the relation (29) by substituting the value of  $f(\eta)$  from (32)

$$[w]_{z=0} = -\frac{2}{a\pi} \int_0^\infty \sin \mu \eta J_0(\rho \eta) d\eta \int_0^1 \mu d\mu \int_0^1 \frac{\rho g(\rho \mu)}{\sqrt{1 - \rho^2}} d\rho, \quad \dots(40)$$

By making use of the result<sup>8</sup>

$$\int_0^\infty \sin \mu \eta J_0(\rho \eta) d\eta = \begin{cases} 0, & \rho > \mu \\ (\mu^2 - \rho^2)^{-1/2}, & \rho < \mu. \end{cases}$$

The expression of  $[w]_{z=0}$  in relation (40) reduces to

$$[w]_{z=0} = \frac{2ak_3}{\pi k_2} \int_p^1 \frac{\mu d\mu}{\sqrt{\mu^2 - \rho^2}} \int_0^1 \frac{x p(x\rho)}{\sqrt{1 - x^2}} dx, \rho < 1 \quad \dots(41)$$

If it be supposed that the applied pressure  $p(r/a)$  is constant over a circular area of radius  $c < a$ , then

$$p(r/a) = \begin{cases} p_0, & 0 < r < c \\ 0, & c < r < a. \end{cases} \quad \dots(42)$$

Substituting into the equation (41) we obtain the expression

$$w = \frac{2ak_3p_0}{\pi k_2} (a^2 - r^2)^{1/2} \{1 - (1 - c^2/a^2)^{1/2}\} \quad \dots(43)$$

If  $\epsilon$  be the normal displacement at the centre of the crack then from (43) by putting  $r = 0$

$$\epsilon = \frac{2a^2k_3p_0}{\pi k_2} \{1 - (1 - c^2/a^2)^{1/2}\}$$

So the equation (43) may be written in the form

$$\frac{w^2}{\epsilon^2} + \frac{r^2}{a^2} = 1$$

showing that for all values of  $C \leq a$  the crack resulting from the application of the pressure as given in (42) is ellipsoidal in shape provided that the applied pressure is constant.

In the case where the applied pressure  $p(r/a)$  is a constant  $p_0$  over the entire surface area  $r \leq a$  of the crack, we obtain from the equation (32)

$$f(\eta) = \frac{2a^2k_3p_0}{\pi k_2} \frac{d}{d\eta} \left( \frac{\sin \eta}{\eta} \right). \quad \dots(44)$$

Substituting the value for  $f(\eta)$  into the equation (28) it follows that the normal component of stress across the plane  $z = 0$

$$[zz]_{z=0} = \frac{2p_0}{\pi} \left\{ \rho \int_0^\infty \sin \eta J_1(\rho\eta) d\eta - \int_0^\infty \frac{\sin \eta}{\eta} J_0(\rho\eta) d\eta. \right.$$

By means of the results<sup>6</sup>

$$\int_0^\infty \frac{\sin \eta}{\eta} J_0(\rho\eta) d\eta = \begin{cases} \sin^{-1}(1/\rho), & \rho \geq 1 \\ \frac{\pi}{2}, & \rho \leq 1 \end{cases}$$

$$\int_0^\infty \rho \sin \eta J_1(\rho\eta) d\eta = \begin{cases} (\rho^2 - 1)^{-1/2}, & \rho > 1 \\ 0, & \rho < 1 \end{cases}$$

It is verified that  $[zz]_{z=0} = -p_0$  when  $\rho < 1$  and for the value of the normal component of the surface stress when  $\rho > 1$  we obtain the expression

$$[zz]_{z=0} = -\frac{2p_0}{\pi} \left[ \sin^{-1}(1/\rho) - \frac{1}{\sqrt{\rho^2 - 1}} \right]. \quad \dots(45)$$

It is seen that when  $\rho \rightarrow \pm 1$ ,  $[zz]_{z=0} \rightarrow \infty$ . It, therefore, appears that plastic flow occurs at the ends of the crack to relieve the infinite stress at those two points.

In discussing the half-space problem we are interested in calculating the energy  $W$  of the crack and the stress intensity factor  $K$  at the tip of the crack. The stress intensity factor is given by

$$\begin{aligned}
 K &= \lim_{\rho \rightarrow 1^+} \sqrt{2(\rho - 1)} z z(\rho, 0), \quad \rho > 1 \\
 &= \lim_{\rho \rightarrow 1^+} \sqrt{2(\rho - 1)} \left[ -\frac{2p_0}{\pi} \left\{ \sin^{-1}(1/\rho) - \frac{1}{\sqrt{\rho^2 - 1}} \right\} \right] \\
 &= 2p_0/\pi
 \end{aligned}$$

The result is the same as that in an isotropic material.

The energy of the crack is given by

$$\begin{aligned}
 W &= 2\pi \int_0^1 \rho p_0 w(\rho, 0) d\rho \\
 &= \frac{4ak_3 p_0^2}{k_2} \int_0^1 \rho \sqrt{1 - \rho^2} d\rho \\
 &= \frac{4ak_3 p_0^2}{3k_2}
 \end{aligned}$$

Hence, it appears that the above result differs in the case of an isotropic body.

### STRESSES IN THE INTERIOR OF THE MEDIUM

The evaluation of the stress components in the interior of the medium may be obtained from the relations (14) to (17) and the displacement components from 18 to (19) by using the relations (26) and (44),

$$\begin{aligned}
 zz &= \frac{2p_0}{\pi k_2} \int_0^\infty \left[ \left( \frac{c_{33}\lambda_1}{m_1^2} - c_{13} \right) (e^{-\xi_1 \eta} - e^{-\xi_2 \eta}) + k_2 e^{-\xi_2 \eta} \right] \\
 &\quad \times \left( \cos \eta - \frac{\sin \eta}{\eta} \right) J_0(\rho \eta) d\eta \\
 &= \frac{2p_0}{\pi k_2} [k_4 \{c_1^0(\rho, \zeta_1) - c_1^0(\rho, \zeta_2) - s_0^0(\rho, \zeta_1) + s_0^0(\rho, \zeta_2)\} \\
 &\quad + k_2 \{c_1^0(\rho, \zeta_2) - s_0^0(\rho, \zeta_2)\}] \quad \dots(46)
 \end{aligned}$$

$$\begin{aligned}
 \text{and } rz &= \frac{2c_{44}p_0}{\pi k_2} \frac{1 + \lambda_1}{m_1} \int_0^\infty \left( \cos \eta - \frac{\sin \eta}{\eta} \right) (e^{-\xi_1 \eta} - e^{-\xi_2 \eta}) J_1(\rho \eta) d\eta \\
 &= \frac{2c_{44}p_0}{\pi k_2} \frac{1 + \lambda_1}{m_1} [c_1^1(\rho, \zeta_1) - c_1^1(\rho, \zeta_2) - s_0^1(\rho, \zeta_1) + s_0^1(\rho, \zeta_2)], \quad \dots(47)
 \end{aligned}$$

where

$$\zeta_1 = \frac{z}{am_1} = \frac{\zeta}{m_1}, \quad \zeta_2 = \frac{z}{am_2} = \frac{\zeta}{m_2}, \quad \rho = \frac{r}{a}, \quad k_4 = \frac{c_{33}\lambda_1}{m_1^2} - c_{13} \quad \dots(48)$$

and the notations  $c_n^m$ ,  $s_n^m$  denote the integrals

$$c_n^m(\rho, \zeta) = \int_0^\infty \eta^{n-1} e^{-\zeta \eta} J_m(\rho \eta) \cos \eta d\eta$$

$$\text{and } s_n^m(\rho, \zeta) = \int_0^\infty \eta^{n-1} e^{-\zeta \eta} J_m(\rho \eta) \sin \eta d\eta.$$

Writing in the general case,

$$w_1 = \zeta_1 + i, \quad w_2 = \zeta_2 + i$$

$$\text{then } z_n^m = c_n^m - i s_n^m = \int_0^\infty \eta^{n-1} e^{-w_j \eta} J_m(\rho \eta) d\eta \quad (j = 1, 2)$$

and the integral  $z_n^m$  can be evaluated by means of the formula

$$\int_0^\infty \eta^{n-1} e^{-w_j \eta} J_m(\rho \eta) d\eta = \begin{cases} \frac{(n-m+1)}{(w_j^2 + \rho^2)^{n/2}} P_{n-1}^m \left( \frac{w_j}{\sqrt{w_j^2 + \rho^2}} \right), & (m \leq n-1) \\ \frac{(n+m-1)!}{(w_j^2 + \rho^2)^{n/2}} P_{n-1}^{-m} \left( \frac{w_j}{\sqrt{w_j^2 + \rho^2}} \right), & (m > n-1), \end{cases}$$

where  $P_n^m$  denotes the associated Legendre function.

In this way we obtain the results

$$Z_1^0 = (\rho^2 + w_j^2)^{-1/2}, \quad Z_2^0 = w_j(\rho^2 + w_j^2)^{-3/2},$$

$$Z_0^1 = \frac{1}{\rho} \{(\rho^2 + w_j^2)^{1/2} - w_j\}, \quad Z_1^1 = \frac{1}{\rho} - \frac{w_j}{\rho \sqrt{w_j^2 + \rho^2}}$$

$$\text{and } Z_2^1 = \rho(\rho^2 + w_j^2)^{-3/2}$$

Adopting the notations

$$r_1^2 = 1 + \zeta_1^2, \quad r_2^2 = 1 + \zeta_2^2,$$

$$\zeta_1 \tan \theta_1 = 1, \quad \zeta_2 \tan \theta_2 = 1,$$

$$R_1^2 = (\rho^2 + \zeta_1^2 - 1)^2 + 4\zeta_1^2,$$

$$R_2^2 = (\rho^2 + \zeta_2^2 - 1)^2 + 4\zeta_2^2,$$

$$2\zeta_1 \cot \phi_1 = \rho^2 + \zeta_1^2 - 1$$

$$\text{and } 2\zeta_2 \cot \phi_2 = \rho^2 + \zeta_2^2 - 1$$

... (49)

and equating real and imaginary parts we obtain the formula

$$C_1^0(\rho, \zeta_1) = R_1^{-1/2} \cos \frac{\phi_1}{2},$$

$$C_1^0(\rho, \zeta_2) = R_2^{-1/2} \cos \frac{\phi_2}{2},$$

$$S_1^0(\rho, \zeta_1) = R_1^{-1/2} \sin \frac{\phi_1}{2},$$

$$S_1^0(\rho, \zeta_2) = R_2^{-1/2} \sin \frac{\phi_2}{2},$$

$$C_0^1(\rho, \zeta_1) = \frac{1}{\rho} \left( (R_1^{1/2} \cos \frac{\phi_1}{2} - \zeta_1) \right),$$

$$C_0^1(\rho, \zeta_2) = \frac{1}{\rho} \left( R_2^{1/2} \cos \frac{\phi_2}{2} - \zeta_2 \right),$$

$$S_0^1(\rho, \zeta_1) = \frac{1}{\rho} \left( 1 - R_1^{1/2} \sin \frac{\phi_1}{2} \right),$$

$$S_0^1(\rho, \zeta_2) = \frac{1}{\rho} \left( 1 - R_2^{1/2} \sin \frac{\phi_2}{2} \right),$$

$$C_1^1(\rho, \zeta_1) = \frac{1}{\rho} - \frac{r_1}{\rho} R_1^{-1/2} \cos \left( \theta_1 - \frac{\phi_1}{2} \right),$$

$$\text{and } C_1^1(\rho, \zeta_2) = \frac{1}{\rho} - \frac{r_2}{\rho} R_2^{-1/2} \cos \left( \theta_2 - \frac{\phi_2}{2} \right). \quad \dots(50)$$

Integrating the expressions for  $Z_1^0$  and  $Z_0^1$  with respect to  $w$  it being assumed in both cases that  $\rho \neq 0$ , we obtain with the help of notation (49) by equating the imaginary parts

$$S_0^0(\rho, \zeta_1) = \tan^{-1} \frac{R_1^{1/2} \sin \frac{\phi_1}{2} + r_1 \sin \theta_1}{R_1^{1/2} \cos \frac{\phi_1}{2} + r_1 \cos \theta_1}$$

$$\text{and } S_0^0(\rho, \zeta_2) = \tan^{-1} \frac{R_2^{1/2} \sin \frac{\phi_2}{2} + r_2 \sin \theta_2}{R_2^{1/2} \cos \frac{\phi_2}{2} + r_2 \cos \theta_2} \quad (\rho \neq 0). \quad \dots(51)$$

With the help of the recurrence formula

$$J_{n-1}(z) + J_{n+1}(z) = \frac{2n}{z} J_n(z) \quad \dots(52)$$

we obtain the further relation

$$Z_n^2 = \frac{2}{\rho} Z_{n-1}^1 - Z_n^0.$$

Hence,

$$C_1^2 = \frac{2}{\rho} C_0^1 - C_1^0,$$

$$C_1^2(\rho, \zeta_1) = \frac{2}{\rho^2} \left( R_1^{1/2} \cos \frac{\phi_1}{2} - \zeta_1 \right) - R_1^{-1/2} \cos \frac{\phi_1}{2}$$

$$\text{and } C_1^2(\rho, \zeta_2) = \frac{2}{\rho_2} \left( R_2^{1/2} \cos \frac{\phi_2}{2} - \zeta_2 \right) - R_2^{-1/2} \cos \frac{\phi_2}{2} \quad \dots(53)$$

By using the recurrence relation (52) and following the method of deducing  $S_0^0$  as obtained in relation (51) we get by equating imaginary parts.

$$S_0^2 = \frac{1}{\rho} (C_0^1 - \zeta S_0^1).$$

Therefore,

$$\begin{aligned} S_0^2(\rho, \zeta_1) &= \frac{1}{\rho^2} \left[ \left( R_1^{1/2} \cos \frac{\phi_1}{2} - \zeta_1 \right) - \zeta_1 \left( 1 - R_1^{1/2} \sin \frac{\phi_1}{2} \right) \right] \\ S_0^2(\rho, \zeta_2) &= \frac{1}{\rho_2} \left[ \left( R_2^{1/2} \cos \frac{\phi_2}{2} - \zeta_2 \right) - \zeta_2 \left( 1 - R_2^{1/2} \sin \frac{\phi_2}{2} \right) \right] \quad \dots(54) \end{aligned}$$

By use of the recurrence relation 52 and the relation (14), we get

$$\begin{aligned} rr &= (C_{11} - C_{12}) \int_0^\infty \alpha^2 A(\alpha) \left[ e^{-\alpha z/m_1} K_1 e^{-\alpha z/m_2} \right] \frac{J_0(\alpha r) + J_2(\alpha r)}{2} d\alpha \\ &\quad + \int_0^\infty \alpha^2 A(\alpha) \left[ e^{-\alpha z/m_1} \left( \frac{\lambda_1 C_{13}}{m_1^2} - C_{11} \right) - K_1 e^{-\alpha z/m_2} \right. \\ &\quad \times \left. \left( \frac{\lambda_2 C_{13}}{m_2^2} - C_{11} \right) \right] J_0(\alpha r) d\alpha \\ &= (C_{11} - C_{12}) \frac{p_0}{\pi k_2} \int_0^\infty \left( \cos \eta - \frac{\sin \eta}{\eta} \right) (e^{-\zeta_1 \eta} - K_1 e^{-\zeta_2 \eta}) \\ &\quad \times [J_0(\rho \eta) + J_2(\rho \eta)] d\eta \\ &\quad + \frac{2p_0}{\pi k_2} \int_0^\infty \left( \cos \eta - \frac{\sin \eta}{\eta} \right) [K_6(e^{-\zeta_1 \eta} - e^{-\zeta_2 \eta}) + k_5 e^{-\zeta_2 \eta}] J_0(\rho \eta) d\eta \end{aligned}$$

$$\begin{aligned}
&= (C_{11} - C_{12}) \frac{p_0}{\pi k_2} [C_1^0(\rho, \zeta_1) - K_1 C_1^0(\rho, \zeta_2) + C_1^2(\rho, \zeta_1) \\
&\quad - K_1 C_1^2(\rho, \zeta_2) - S_0^0(\rho, \zeta_1) + K_1 S_0^0(\rho, \zeta_2) - S_0^2(\rho, \zeta_2) \\
&\quad + K_1 S_0^2(\rho, \zeta_2)] + \frac{2p_0}{\pi K_2} [K_6 C_1^0(\rho, \zeta_1) + (K_5 - K_6) C_1^0(\rho, \zeta_2) \\
&\quad - K_6 S_0^0(\rho, \zeta_1) (K_5 - K_6) S_0^0(\rho, \zeta_2)] \quad \dots(55)
\end{aligned}$$

By using the notations given in (50), (51), (53), (54) the constants  $K_5$  and  $K_6$  are given by

$$K_5 = \left( \frac{\lambda_1 C_{13}}{m_1^2} - C_{11} \right) - K_1 \left( \frac{\lambda_2 C_{13}}{m_1^2} - C_{11} \right)$$

$$\text{and } K_6 = \frac{\lambda_1 C_{13}}{m_1^2} - C_{11}. \quad \dots(56)$$

### NUMERICAL RESULTS

We consider the case of Magnesium in which the roots of the equation (10) are real. The elastic constants are

$$\begin{aligned}
C_{11} &= 565, & C_{12} &= 232, & C_{13} &= 181, \\
C_{33} &= 587, & C_{44} &= 168.
\end{aligned}$$

Here, the constants are expressed in terms of an unit stress of  $10^9$  dynes/sq.cm. The roots of the equation (10) are

$$m_1^2 = 1.985, \quad m_2^2 = 0.524$$

and

$$\lambda_1 = 2.733, \quad \lambda_2 = 0.367 \quad \dots(57)$$

From these values of the elastic constants we obtain from relations (37), (30), (48), (56)

$$\begin{aligned}
K_1 &= 1.403, & K_2 &= 304.333, & K_3 &= 1.229, \\
K_4 &= 627.197, & K_5 &= -930.632, & K_6 &= -315.794 \quad \dots(58)
\end{aligned}$$

By means of the expressions of the relations (46), (47), (55), the components of stress at any point  $r = \rho a$ ,  $Z = \zeta a$  in the interior of the elastic body can be calculated for the prescribed values of elastic constants as noted above. The results of these calculations for the case where both  $\rho$  and  $\zeta$  assume a sequence of values are obtained. The variation of the various components of stress in certain planes is shown graphically in Figs. 1, 2, 3. The rapid decay of the stress component  $rr$  as  $Z$  increases is illustrated by Fig. 3. The variation with  $Z$  of the normal component of stress is much more gradual as is seen from Fig. 1.

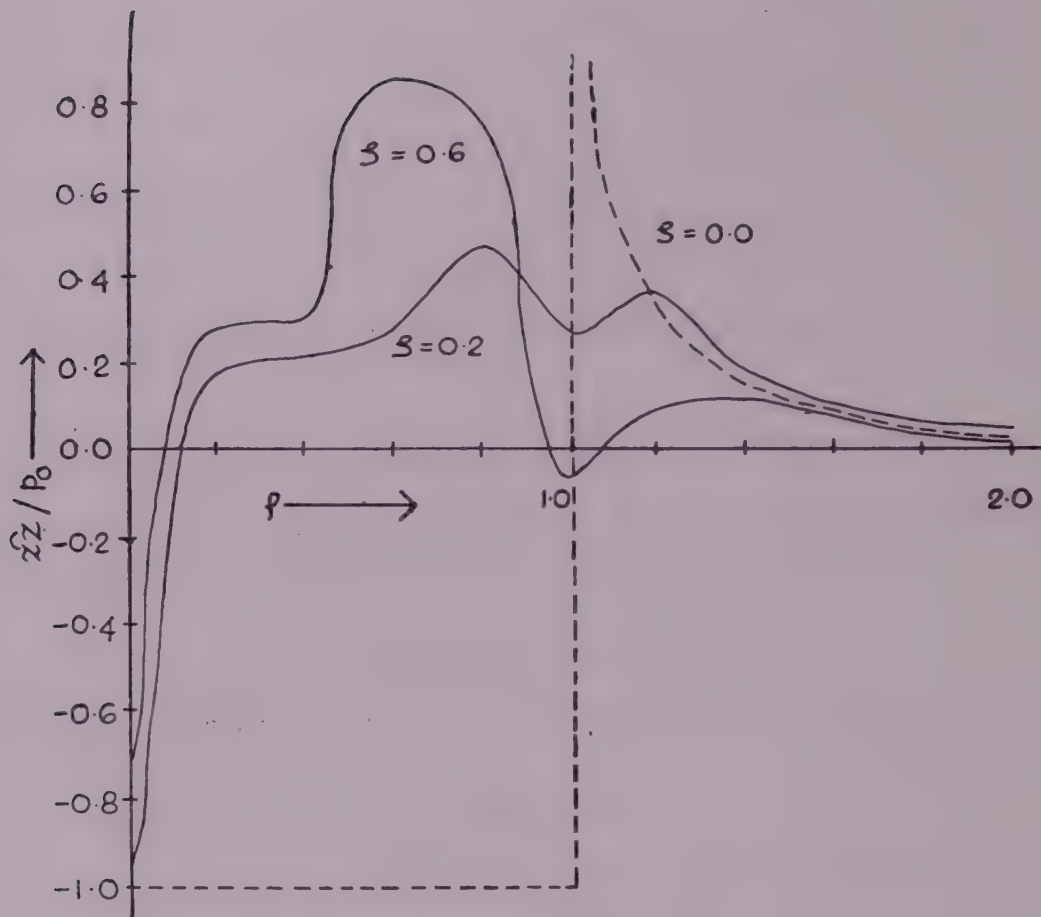


FIG 1 The variation of the normal component of stress  $zz$  with  $\rho$  and  $\zeta$ . The broken curve shows the variation of  $zz$  in the plane of the crack ( $z = 0$ ).

#### PRINCIPAL STRESSES

The principal stresses at any point are determined by the roots of the discriminating cubic

$$\begin{vmatrix} \lambda - rr & 0 & rz \\ 0 & \lambda - \theta\theta & 0 \\ rz & 0 & \lambda - zz \end{vmatrix} = 0 \quad \dots(59)$$

so that they are equal to

$$\theta\theta, \frac{1}{2}(rr + zz) \pm \left\{ \left( \frac{1}{2}rr - \frac{1}{2}zz \right)^2 + (rz)^2 \right\}^{1/2} \quad \dots(60)$$

With the values of the stress components the components of principal stress may readily be deduced from the formula (60). The numerical value of the principal shearing stress can then be determined from the fact that it is equal to one half of the algebraic difference between the maximum and the minimum components of the principal stress. So it is equal to

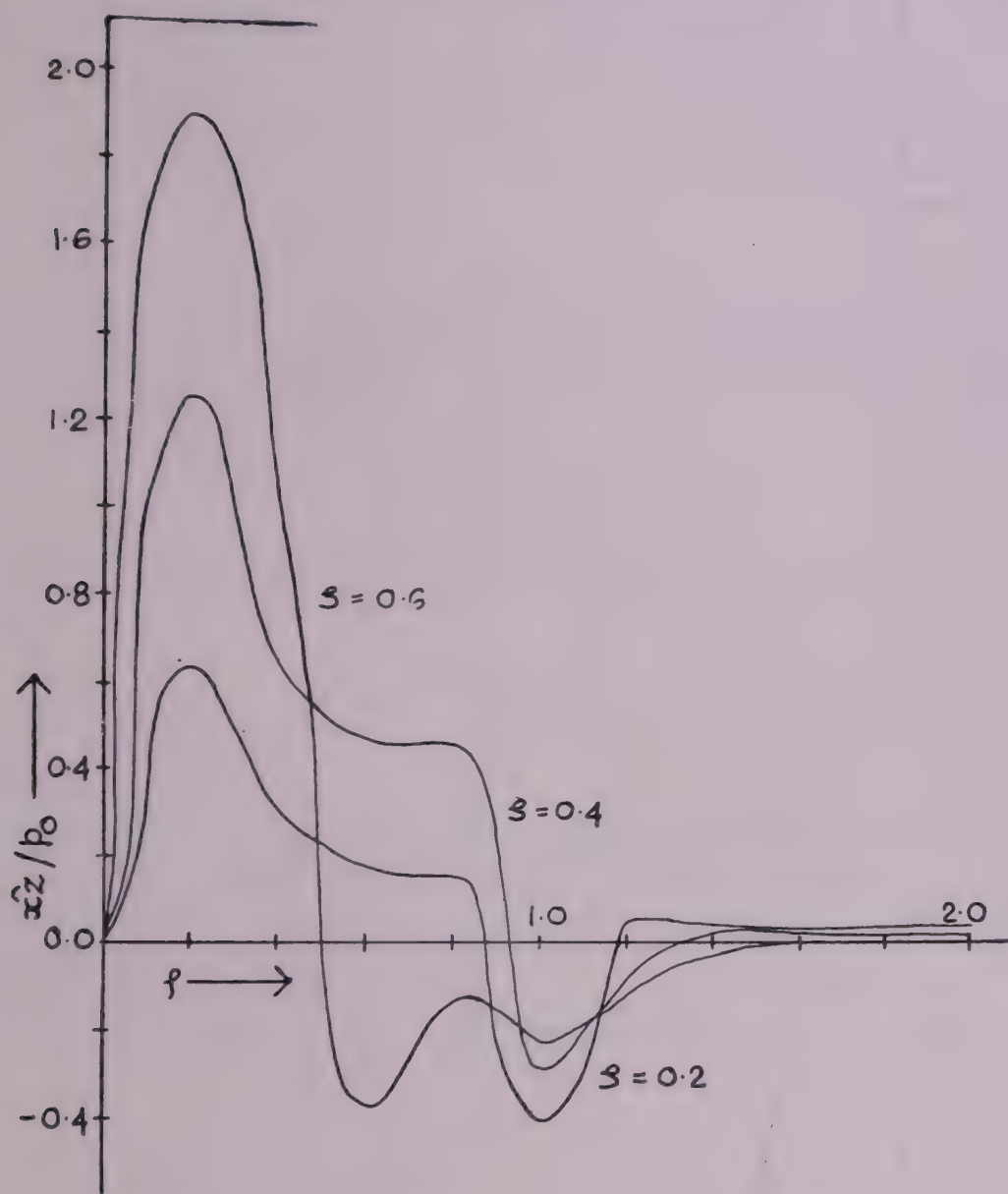


FIG 2 The variation of the shearing stress  $rz$  with  $\rho$  and  $\zeta$

$$\tau = \left\{ \left( \frac{1}{2} rr - \frac{1}{2} zz \right)^2 + (rz)^2 \right\}^{1/2} \quad (61)$$

The results of such a calculation are obtained and the variation of principal shearing stress in planes parallel to the plane of the crack exhibited graphically in Fig. 4.

The numerical work as exhibited in Figs 1, 2, 3 and 4 is done by computer.

#### NORMAL COMPONENT OF DISPLACEMENT

Since the normal component of stress  $zz$  is infinitely large at the edge of the crack it might appear that the displacement  $w$  should also be infinite in that region.

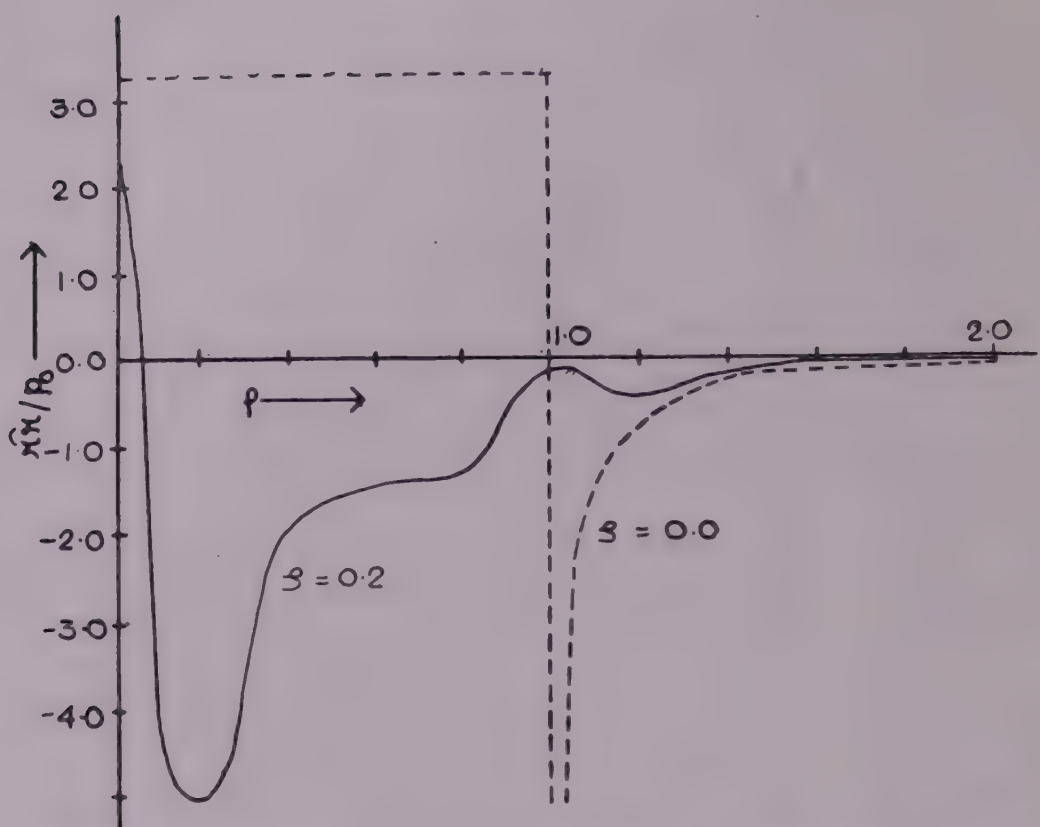


FIG 3 The variation of the radial component of stress  $\bar{\sigma}_{rr}$  with  $\rho$  and  $\zeta$ . The broken curve shows the variation of the curve  $rr$  in the plane of the crack ( $z = 0$ ).

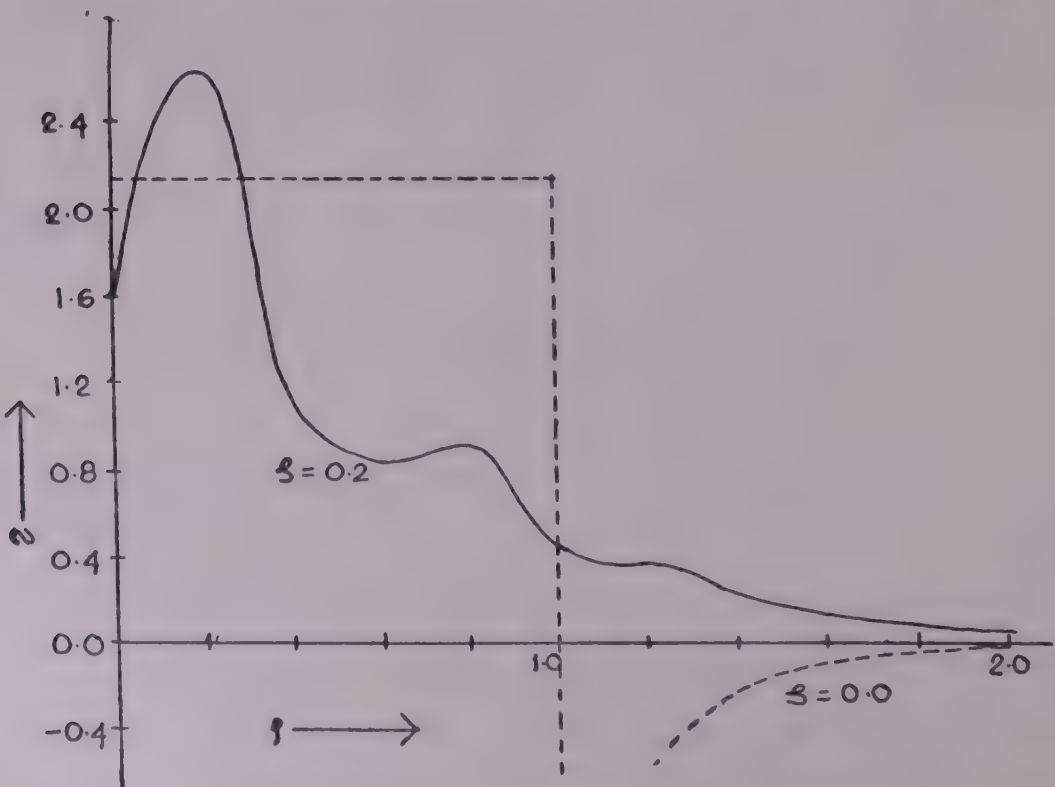


FIG 4 The variation of principal shearing stress  $\tau$  with  $\rho$  and  $\zeta$ . The broken curve shows the variation of  $\tau$  in the plane of the crack.

But this is not so as can be seen from an examination of equation for  $w$  as obtained from (19).

$$w = - \frac{2ap_0}{\pi K_2} \int_0^\infty \left( \frac{\cos \eta}{\eta} - \frac{\sin \eta}{\eta^2} \right) \left[ \frac{\lambda_1}{m_1} (e^{-r_1 \eta} e^{-r_2 \eta}) + K_3 e^{-r_2 \eta} \right] J_0(\rho \eta) d\eta \quad \dots(62)$$

In conclusion, we remark that the distribution of stress and displacement in the inferior and the vicinity of the crack due to loading on its surface is of great physical importance in fracture mechanics in care of modern structures composed of different alloys exhibiting anisotropic behaviour.

#### ACKNOWLEDGEMENT

We take this opportunity of expressing our gratitude to The University Grants Commission for their assistance in implementing this project.

#### REFERENCES

1. I N Sneddon *Proc R Soc London* **187A** (1946) 1009
2. A E Green *Proc Camb phil Soc* **45** (1949) 251
3. I E Payne *J SIAM* **1** (1953) 53
4. E C Titchmarsh *An Introduction to the Theory of Fourier Integrals* Oxford University Press (1937)
5. I W Busbridge *Proc London math Soc* **2** (1938) 44, 115
6. G N Watson *The Theory of Bessel Functions*, 2nd Edn Cambridge University Press (1944)
7. H A Elliott *Proc Camb phil Soc* **45** (1949) 621
8. R F S Hearmon *Rev mod Phys* **2** (1946) 18, 409
9. E Jahnke and F Emde *Tables of Functions* Teubner Leipzig (1938)

# DETERMINATION OF SOLAR ENERGY FLUCTUATIONS IN THE LOWER ATMOSPHERE USING SPECTRAL ANALYSIS TECHNIQUES

ERNEST C NJAU\*

*International Centre for Theoretical Physics, Trieste, Italy*

(Received 10 December 1984; after revision 9 September 1985)

An expression for the direct solar energy incident upon an arbitrary portion of the Earth's surface over an arbitrary duration of time ( $> 2$  days) has been formulated as a product of a continuous solar energy signal function and a correspondingly continuous time-dependent sampling function. The energy density spectrum of this product is then evaluated and its predictions compared with observations. Predicted periodicities agree well with both short-term and long-term observations. The implication of this work to meteorological and climatic studies is briefly discussed.

**Key Words :** Sun-Weather Relationships; Solar-Terrestrial Physics; Solar Energy Variations; Sun-Climate Links

## INTRODUCTION

THE study of solar energy fluctuations at and near the Earth's surface is relevant to meteorology, climatology, agriculture and related fields. Although much work has already been done in this area,<sup>1-5</sup> a complete description of the energy fluctuations in the lower atmosphere and/or on the Earth's surface has not yet been achieved.<sup>6-9</sup> The aim of this paper is to improve that description through a spectral analysis of the direct solar energy incident upon an arbitrarily chosen portion of the Earth's surface together with the atmosphere above that portion. As explained further below, the underlying rationale is that the results of the spectral analysis can be used in making useful predictions provided that certain characteristics of solar radiation are known. We have deliberately singled out direct solar energy for spectral analysis mainly because of the predominant influence which is wielded by this variable over climatic and meteorological phenomena. According to previous studies,<sup>1,10</sup> not only is the climate system driven primarily by solar-derived energy that is absorbed at the Earth's surface, but also solar radiation is undoubtedly the most important climatological variable to which many of the other variables are somehow correlated.

The analytical strategy adopted in this paper can be summarized as follows:

Let  $A$  denote an arbitrary part of the Earth's surface. Part  $A$  (together with the atmosphere above it) normally receives direct solar energy in a time-dependent

\*Permanent Address : Department of Physics, University of Dar es Salaam, P. O. Box 35063, Dar es Salaam, Tanzania.

discrete sequence because the Earth is constantly rotating about its axis in front of the relatively still sun. In other words, part  $A$  enters and leaves the day-side of our Earth in a continuously systematic sequence, and can, therefore, receive direct solar energy only when it is on the day-side. The solar energy "samples" that normally get into part  $A$  (and the atmosphere there upon) over a time period  $J$  ( $> 2$  days) can be equivalently obtained by assuming that part  $A$  is permanently in the day-side of a non-rotating Earth but that the direct energy getting into it (i.e.  $A$ ) is appropriately controlled by a certain time-dependent sampling process. In the next Section, we have formulated a realistic form of this time-dependent sampling process with reference to an arbitrary Earth location  $A$ . In addition, we have represented the solar energy continuously directed towards location  $A$  during the period  $J$  by an energy signal function that incorporates a constant-amplitude component and a variable component. Clearly, a product of the energy signal function and the corresponding sampling function yields a function for the actual solar energy that falls into location  $A$  over a period  $J$ . Now, the energy density spectrum of this product is obtained as the square of the Fourier transform of the same product. Finally, the features of the energy density spectrum are carefully examined with the aim of getting out details about energy fluctuations in location  $A$ .

In the next Section, the problem which is the subject of the paper is formulated in accordance with the strategy already summarized above. The formulation culminates in a general expression of the desired energy spectrum, which is then discussed briefly. Consequent to this, some predictions are made from the formulated energy density spectrum and compared with actual observations.

### FORMULATION

Theoretically the patterned sequence in which an Earth Location  $A$  (say) of arbitrary latitude  $k$  receives (net) direct solar energy does have some similarities with the patterned sequence in which a continuous energy signal is received in a regular manner by some sampling device. These similarities are displayed with further clarity in Table I wherein the symbol \* denotes convolution operation,  $j = \sqrt{-1}$ , and  $w$  denotes radian frequency. In Table I as well as the rest of the paper, we use "Location  $A$ " to refer to a portion of the Earth's surface together with the atmosphere directly above it. The similarity given in Table I signifies or implies that some of the analytical techniques used in conventional signal processing can be applied, with relevant modifications, to analyses pertaining to certain solar-terrestrial phenomena.

Let the continuous (net) solar irradiance directed from the sun towards the position of location  $A$  from time  $t = 0$  up to  $t = J$  be denoted by the function  $R_k(t)$ . It is logical to consider  $R_k(t)$  as being made up of a constant-amplitude component  $R_{0k}(t)$  as well as some time-variable components. In reality, the component  $R_{0k}(t)$  makes up more than about 85 per cent of  $R_k(t)$ .

We can thus express  $R_k(t)$  as follows :

TABLE I

<i>Conventional Sampling of a Time-Dependent Energy Signal</i>	<i>Direct Solar Energy Reception at Location A</i>
Availability of a continuous stretch of time-dependent energy signal $f_c(t)$	Sun emits continuous time-dependent energy stream $f(t)$ towards location A.
Signal $f_c(t)$ is sampled by some device which receives and records only discrete portions of $f_c(t)$	Location A receives directly only discrete samples of $f(t)$ since it is exposed to the sun discretely
Sampled data form a time-dependent signal $f_d(t)$	The portions of $f(t)$ that fall into location A form an energy signal $f_{Jk}(t)$
Exact transform-domain version of $f_d(t) = P(jw)^* F_d(jw)$ , where $F_d(jw)$ is the Fourier transform of the part of $f_c(t)$ involved and $P(jw)$ is the frequency response function of the sampling device	Exact transform-domain version of $f_{Jk}(t) = S_{Jk}(jw)^* E_p(jw)$ , where $E_p(jw)$ is the Fourier transform of the part of $f(t)$ involved and $S_{Jk}(jw)$ is the frequency response function of the relevant sampling mechanism

$$R_k(t) = R_{0k}(t) + \sum_{n=1}^L R_{nk}(t), \quad \dots(1)$$

where  $R_{nk}(t)$  is a regular function with period  $T_{nk}$ , and that  $R_{mk}(t)$  is not a harmonic of  $R_{nk}(t)$  for any values of  $m$  and  $n$  ( $\neq m$ ) equal to or less than the integral  $L$ . Owing to the Earth's rotational motion, location A will effectively receive energy from  $R_k(t)$  in samples, and the implicit sampling mechanism is characterized by a sampling window of variable shape and width as well as a fairly constant sampling interval  $\lambda$ . In this analysis, we have adopted sampling windows that are cosinusoidally-shaped or cosinusoidally-edged since these are fairly close to what actually takes place. Thus a typical sampling window is illustrated in Fig. 1 where portions A and B correspond to early morning hours and late evening hours, respectively.

On the basis of cosinusoidally-edged windows, location A will receive from  $R_k(t)$  discrete portions which altogether form an energy signal  $f_{ik}(t)$  that is expressed as follows :

$$f_{ik}(t) = \tau_k \Gamma_k(t) \sum_{n=0}^{N-1} \Phi_{ik}(n\lambda, I_k = 0) + \sum_{n=1}^L \tau_k R_{nk}(t) \left\{ \sum_{P=0}^{W_{nk}-1} \sum_{m=0}^{V_{nk}-1} \right. \\ \left. \text{equation contd.} \right.$$

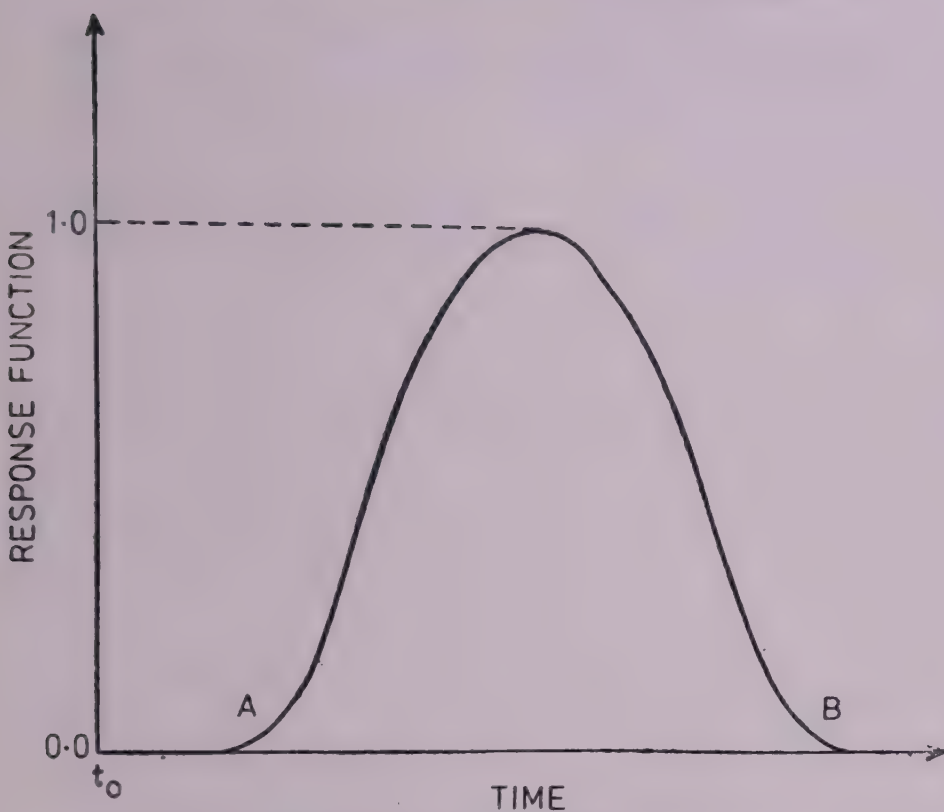


FIG. 1 A typical cosinusoidally-edged sampling window.

$$\times \Phi_{2k}(p\lambda + m\tau_{nk}, I_k = 0) + \sum_{p=W_{nk}}^{W_{nk}+Y_{nk}-1} \sum_{m=0}^{V_{nk}-1} \Phi_{3k}(t, I_k = 0) \\ \times \Phi_{2k}(p\lambda + mT_{nk}, I_k = 0) \Big\} + \Delta_k(t), \quad \dots(2)$$

where

$$\Delta_k(t) = \tau_k \Gamma_k(t) \sum_{n=0}^{N-1} [\Phi_{1k}(n\lambda, I_k) - \Phi_{1k}(n\lambda, I_k = 0)] + \sum_{n=1}^L \tau_k R_{nk}(t) \\ \times \left\{ \sum_{p=0}^{W_{nk}-1} \sum_{m=0}^{V_{nk}-1} [\Phi_{2k}(p\lambda + mT_{nk}, I_k) - \Phi_{2k}(p\lambda + mT_{nk}, I_k = 0)] \right. \\ + \sum_{p=W_{nk}}^{W_{nk}+Y_{nk}-1} \sum_{m=0}^{V_{nk}-1} \{ [\Phi_{3k}(t, I_k) - \Phi_{3k}(t, I_k = 0)] [\Phi_{2k}(p\lambda \\ + mT_{nk}, I_k) - \Phi_{2k}(p\lambda + mT_{nk}, I_k = 0)] \} \Big\};$$

$$\begin{aligned}\Phi_{1k}(n\lambda, I_k) &= \cos p_{0k}[y - (\sigma_{0k} + a_{0k}I_k(n\lambda))] [\psi(y) - \psi[y - (\sigma_{0k} \\ &\quad + a_{0k}I_k(n\lambda))]] \quad \text{when } 0 \leq y < \sigma_{0k} + a_{0k}I_k(n\lambda), \\ &= \psi[y - d_{2k}(n\lambda) + \frac{1}{2}(\sigma_{1k} + a_{1k}I_k(n\lambda))] - \psi[y - d_{2k}(n\lambda) \\ &\quad - \frac{1}{2}(\sigma_{1k} + a_{1k}I_k(n\lambda))] \quad \text{when } \sigma_{0k} + a_{0k}I_k(n\lambda) \leq y \leq d_{3k}(n\lambda), \\ &= \cos p_{1k}[y - d_{3k}(n\lambda)] [\psi[y - d_{3k}(n\lambda)] - \psi[y - d_{3k}(n\lambda) \\ &\quad - (\sigma_{4k} + a_{4k}I_k(n\lambda))]],\end{aligned}$$

when  $d_{3k}(n\lambda) < y \leq d_{3k}(n\lambda) + \sigma_{4k} + a_{4k}I_k(n\lambda)$ ,

$$= 0 \text{ (or undefined) otherwise;}$$

$$y = t - n\lambda;$$

$$\begin{aligned}\Phi_{2k}(p\lambda + mT_{nk}, I_k) &= \cos p_{0k}[\chi - (\sigma_{0k} + a_{0k}I_k(n\lambda))] [\psi(\chi) - \psi[\chi \\ &\quad - (\sigma_{0k} + a_{0k}I_k(n\lambda))]] \quad \text{when } 0 \leq \chi < \sigma_{0k} \\ &\quad + a_{0k}I_k(n\lambda), \\ &= \psi[\chi - d_{2k}(n\lambda) + \frac{1}{2}(\sigma_{1k} + a_{1k}I_k(n\lambda))] \\ &\quad - \psi[\chi - d_{2k}(n\lambda) - \frac{1}{2}(\sigma_{1k} + a_{1k}I_k(n\lambda))],\end{aligned}$$

when  $\sigma_{0k} + a_{0k}I_k(n\lambda) \leq \chi \leq d_{3k}(n\lambda)$ ,

$$\begin{aligned}&= \cos p_{1k}[\chi - d_{3k}(n\lambda)] [\psi[\chi - d_{3k}(n\lambda)] \\ &\quad - \psi[\chi - d_{3k}(n\lambda) - (\sigma_{4k} + a_{4k}I_k(n\lambda))]] \\ \text{when } &d_{3k}(n\lambda) < \chi \leq d_{3k}(n\lambda) + \sigma_{4k} + a_{4k}I_k(n\lambda), \\ &= 0 \text{ (or undefined) otherwise;}\end{aligned}$$

$$\chi = t - p\lambda - mT_{nk};$$

$$\Phi_{3k}(t, I_k) = 0$$

whenever  $(W_{nk}V_{nk} - 1)\lambda + d_{3k}[(W_{nk}V_{nk} - 1)\lambda]$   
 $+ \sigma_{4k} + a_{4k}I_k[(W_{nk}V_{nk} - 1)\lambda] \geq p\lambda + mT_{nk}, = 1$

whenever  $(W_{nk}V_{nk} - 1)\lambda + d_{3k}[(W_{nk}V_{nk} - 1)\lambda] + \sigma_{4k}$   
 $+ a_{4k}I_k[W_{nk}V_{nk} - 1)\lambda] < p\lambda + mT_{nk};$

$$\psi(t' - \chi) = \int_{-\infty}^{t' - \chi} \delta(t'') dt'';$$

$\Delta_k(t)$  = a term that gives the solar energy variations in a location of latitude  $k$  merely because days in that location are not of the same lengths as they are at the Equator;

$T_{nk}$  = period of the  $n$ th variable component of  $R_{nk}(t)$  as already noted in connection with equation (1);

$\sigma_{0k} + a_{0k} I_k(t) = d_{0k}(t)$  is the duration from local sunrise to the start of local noon (i. e. when the sun just reaches its highest altitude) in a day denoted by  $t$ . Note that  $\sigma_{0k}$  and  $a_{0k}$  are constants for a given value of  $k$ ;

$\sigma_{1k} + a_{1k} I_k(t) = d_{1k}(t)$  is the duration in which the sun remains at its highest altitude in a specified by i.e. in a day specified by  $t$ ;

$$d_{2k}(t) = d_{0k}(t) + \frac{1}{2} d_{1k}(t);$$

$$d_{3k}(t) = d_{0k}(t) + d_{1k}(t);$$

$\sigma_{4k} + a_{4k} I_k(t) = d_{4k}(t)$  is the duration from when the sun just starts moving off its highest altitude to local sunset on a day specified by  $t$ ;

$$P_{0k} = \frac{\pi}{2d_{0k}(t)};$$

$$P_{1k} = \frac{\pi}{2d_{1k}(t)};$$

$J = (N - 1) \lambda + d_{3k}[(N - 1) \lambda] + d_{4k}[(N - 1) \lambda]$  defines the integer  $N$  since  $J$ ,  $\lambda$ ,  $d_{3k}(t)$  and  $d_{4k}(t)$  have already been defined;

$\tau_k$  = a constant for a given value of  $k$ ;

$\Gamma_k(t)$  = continuous portion of  $R_{0k}(t)$  that extends from  $t = 0$  up to  $t = J$ ;

$V_{nk}$  = number of complete wavelengths contained in  $R_{nk}(t)$ ;

$T_{nk} = W_{nk} \lambda + \mu_{nk}$  defines  $W_{nk}$  since  $T_{nk}$ ,  $\lambda$  and  $\mu_{nk}$  are defined separately;

$$Y_{nk} = |\theta_{nk} - \Omega_{nk}| \frac{T_{nk}}{2\pi\lambda} + \delta_{nk};$$

$\theta_{nk}$  = initial phase of  $R_{nk}(t)$ ;

$\Omega_{nk}$  = final phase of  $R_{nk}(t)$ ;

$|\mu_{nk}| (< \lambda)$  = a constant for fixed values of  $n$  and  $k$ ;

$|\delta_{nk}| (< \lambda)$  = a constant for fixed values of  $n$  and  $k$ . Physically, the term  $\Phi_{1k}(n\lambda, I_k)$  shapes up the window with which location  $A$  samples out direct solar energy. The energy-density spectrum  $E_k(w)$  of  $f_{ik}(t)$  can be obtained after Fourier-transforming equation (2). Thus

$$\begin{aligned} E_k(w) &= \left| h_k S_{0k}(jw) * \left\{ \left[ \left[ \sigma_{0k} \exp(j \frac{1}{2} \sigma_{0k} w) \frac{\sin(\frac{1}{2} \sigma_{0k} w)}{\frac{1}{2} \sigma_{0k} w} \right] \right. \right. \right. \\ &\quad \left. \left. \left. * \left[ \frac{2H_{0k} \exp(j \sigma_{0k} w) \cos(\sigma_{0k} w)}{H_{0k}^2 - w^2} \right] + \sigma_{1k} \exp[j(\sigma_{0k} + \frac{1}{2} \sigma_{1k}) w] \right. \right. \\ &\quad \left. \left. \times \frac{\sin(\frac{1}{2} \sigma_{1k} w)}{\frac{1}{2} \sigma_{1k} w} + [\sigma_{4k} \exp[j(\sigma_{0k} + \sigma_{1k} + \frac{1}{2} \sigma_{4k}) w] \frac{\sin(\frac{1}{2} \sigma_{4k} w)}{\frac{1}{2} \sigma_{4k} w}] \right] \right\} \right| \\ &\quad \text{equations contd.} \end{aligned}$$

$$\begin{aligned}
& * \left[ \frac{2H_{1k} \exp [j(\sigma_{0k} + \sigma_{1k}) w] \cos (\sigma_{4k} w)}{H_{1k}^2 - w^2} \right] \right] \exp [j \frac{1}{2} (N-1) \lambda w] \\
& \times \frac{\sin (\frac{1}{2} N \lambda w)}{\sin (\frac{1}{2} \lambda w)} \} + \sum_{n=1}^L h_k S_{nk}(jw) * \left\{ \left[ \left[ \sigma_{0k} \exp (j \frac{1}{2} \sigma_{0k} w) \frac{\sin (\frac{1}{2} \sigma_{0k} w)}{\frac{1}{2} \sigma_{0k} w} \right] \right. \right. \\
& * \frac{2\sigma_{0k} \exp (j\sigma_{0k} w) \cos (\sigma_{0k} w)}{\sigma_{0k}^2 - w^2} + \sigma_{1k} \exp [j(\sigma_{0k} + \frac{1}{2} \sigma_{1k})] \frac{\sin (\frac{1}{2} \sigma_{1k} w)}{\frac{1}{2} \sigma_{1k} w} \\
& \left. \left. + \left[ \sigma_{4k} \exp [j(\sigma_{0k} + \sigma_{1k} + \frac{1}{2} \sigma_{4k}) w] \frac{\sin (\frac{1}{2} \sigma_{4k} w)}{\frac{1}{2} \sigma_{4k} w} \right] \right. \right. \\
& * \frac{2H_{1k} \exp [j(\sigma_{0k} + \sigma_{1k}) w] \cos (\sigma_{4k} w)}{H_{1k}^2 - w^2} \left. \right] \left[ \exp [j \frac{1}{2} (V_{nk} - 1) T_{nk} w] \right. \\
& \times \exp [j \frac{1}{2} (W_{nk} - 1) \lambda w] \times \frac{\sin (\frac{1}{2} V_{nk} T_{nk} w)}{\sin (\frac{1}{2} T_{nk} w)} \frac{\sin (\frac{1}{2} W_{nk} \lambda w)}{\sin (\frac{1}{2} \lambda w)} \\
& \left. \left. + \left[ \sigma_{0k} \exp (j \frac{1}{2} \sigma_{0k} w) \frac{\sin (\frac{1}{2} \sigma_{0k} w)}{\frac{1}{2} \sigma_{0k} w} \right] * \left[ \frac{2H_{0k} \exp (j\sigma_{0k} w) \cos (\sigma_{0k} w)}{H_{0k}^2 - w^2} \right] \right. \right. \\
& + \sigma_{1k} \exp [j(\sigma_{0k} + \frac{1}{2} \sigma_{1k}) w] \frac{\sin (\frac{1}{2} \sigma_{1k} w)}{\frac{1}{2} \sigma_{1k} w} + \left[ \sigma_{4k} \exp [j(\sigma_{0k} + \sigma_{1k} \right. \\
& \left. + \frac{1}{2} \sigma_{4k}) w] \frac{\sin (\frac{1}{2} \sigma_{4k} w)}{\frac{1}{2} \sigma_{4k} w} \right] * \left[ \frac{2H_{1k} \exp [j(\sigma_{0k} + \sigma_{1k}) w] \cos (\sigma_{4k} w)}{H_{1k}^2 - w^2} \right] \\
& \times \left[ \exp (jW_{nk} w) \exp [j \frac{1}{2} (Y_{nk} - 1) \lambda w] \frac{\sin (\frac{1}{2} Y_{nk} \lambda w)}{\sin (\frac{1}{2} \lambda w)} \right] \\
& \left. \left. + G_k(jw) \right\} \right|^2, \quad \dots(3)
\end{aligned}$$

where  $H_{0k} = P_{0k}(I_k = 0)$ ,  $H_{1k} = P_{1k}(I_k = 0)$ ,  $h_k$  = a constant for a given value of  $k$ ,  $S_{0k}(jw)$  = Fourier transform of  $R_{0k}(t)$ ,  $S_{nk}(jw)$  = Fourier transform of  $R_{nk}(t)$  and  $G_k(jw)$  is the Fourier transform of  $\Delta_k(t)$ . Equation (3) gives a convenient form of  $E_k(w)$  that expresses the significant variations or oscillations in  $f_{ik}(t)$ . Since all the parameters incorporated in equation (3) may be specified for a location at any latitude, this particular equation is thus a convenient tool for studying fluctuations in solar-derived energy at any Earth location and for any length of time that exceeds 48 hours.

## DISCUSSION

For an Equatorial location  $k = 0$  and hence  $\Delta_k(t) = G_k(jw) = 0$  in equations (2) and (3). This implies that the corresponding energy-density spectrum  $E_0(w)$  becomes equivalent to  $P_J(w)^2$ , where the expression for  $P_J(w)$  has been derived in reference.<sup>11</sup>

As shown in the latter reference, the sampling of the constant amplitude component  $R_{00}(t)$  does induce fluctuations in  $E_0(w)$  at radian frequencies  $w_{0n}$  and corresponding amplitudes  $A_{0n}$  that are given by the equations

$$w_{0n} \approx \left( \frac{2n + 1}{N\lambda} \right) \pi \quad \dots(4)$$

and

$$A_{0n} \approx \frac{h_0^2 R_{00}^2}{1 + (N^2 - 1) \sin^2 \left[ \left( \frac{2n + 1}{2N} \right) \pi \right]}, \quad \dots(5)$$

where  $R'_{00}$  is the magnitude of  $R_{00}(t)$  for  $0 \leq t \leq J$ , and  $n = 1, 2, 3, \dots$ . Theoretically some of these fluctuations can attain amplitudes as large as about 0.21  $R'_{00} \leq 0.2$  {Size of  $R_0(t)$  when  $0 \leq t \leq J$ } and hence can induce substantial forcing into the (lower) atmosphere. We should not forget that an ice age can after all be triggered simply by a prolonged decrease in the Earth-ward solar energy stream larger than a few per cent. Since the amplitude of  $R_{00}(t)$  is constant with time, the influence of this constant-amplitude term upon the fluctuations in  $E_0(w)$  depends on the frequency response function of the Earth location involved with respect to incoming solar energy. On the other hand, effects of the terms  $\sum_n R_{n0}(t)$

upon fluctuations in  $E_0(w)$  depends not only on the latter frequency response function but also on some processes inside the Sun.<sup>7,13</sup>

It is worth noting that predictions made from  $P_J(w)$ , which is equivalent to  $[E_0(w)]^{1/2}$ , have been shown<sup>11</sup> to yield good agreement with a number of long- and short-term lower atmospheric observations, some of which were made in places near but not exactly at the Equator. This apparent agreement implies that at least some of the significant (lower) atmosphere fluctuations result primarily from the natural fact that each location on the Earth samples out direct solar energy instead of receiving it continuously. We shall re-visit this issue later on.

In order to obtain a simplified version of  $E_k(w)$  for an arbitrary non-Equatorial location, one must obtain a simplified version of  $G_k(jw)$  unless the latter is justifiably neglected. However, it appears that a simplified and exact expression for  $G_k(jw)$  is rather tricky to get hold of because  $\Delta_k(t)$  incorporates some complicated "pulse-shape modulation" effects that consequently make the exact form of  $G_k(jw)$  a non-simple summation of terms. Nevertheless, approximate but realistic versions of  $G_k(jw)$  can be obtained for any value of  $k$ , and these will be of invaluable use in the study of relevant weather fluctuations.

The comparison mentioned earlier between observed variations in climatic/meteorological parameters and corresponding predictions made using our theory involved a total of 35 separate records of rainfall, wind speeds, humidity, geoclimatic data, water discharge of rivers and atmospheric temperature. The time-lengths of the records varied from a few days up to 260,000 years. A sample (i.e. 14 per cent) of these records is featured in Table II. In a total of 33 out of the 35

TABLE II  
*A comparison of observations and calculations made on the basis of the theory presented herein  
[after Njau (1984)]<sup>11</sup>*

METEOROLOGICAL PARAMETER	TIME LENGTH OF EXPERIMENTAL DATA	OBSERVED PERIOD OF FLUCTUATION	CALCULATED PERIOD OF FLUCTUATION	SOURCE OF EXPERI- MENTAL RESULTS/ DATA
(i) Temperature in California	1,000 years	670 years	667 years (largest amplitude variation)	Svalgaard <sup>12</sup>
(ii) Rainfall in 2 Tanzanian stations	30 years	19.5 years	20 years (largest amplitude variation)	Njau <sup>13</sup>
(iii) Geoclimatic records from Mexico and Texas	260,000 years	100,000 years	104,000 years (2nd largest amplitude variation)	Anderson <sup>17</sup>
(iv) Water discharge of Senegal river (this has been positively correlated with Sahelian rainfall <sup>18</sup> )	51 years	~ 30 years	34 years (largest amplitude variation)	Hastenbach and Kaczmarczyk <sup>19</sup>
(v) Worldwide marine temperature	119 years	83 years	80 years (largest amplitude variation)	Folland <i>et al.</i> <sup>14</sup>

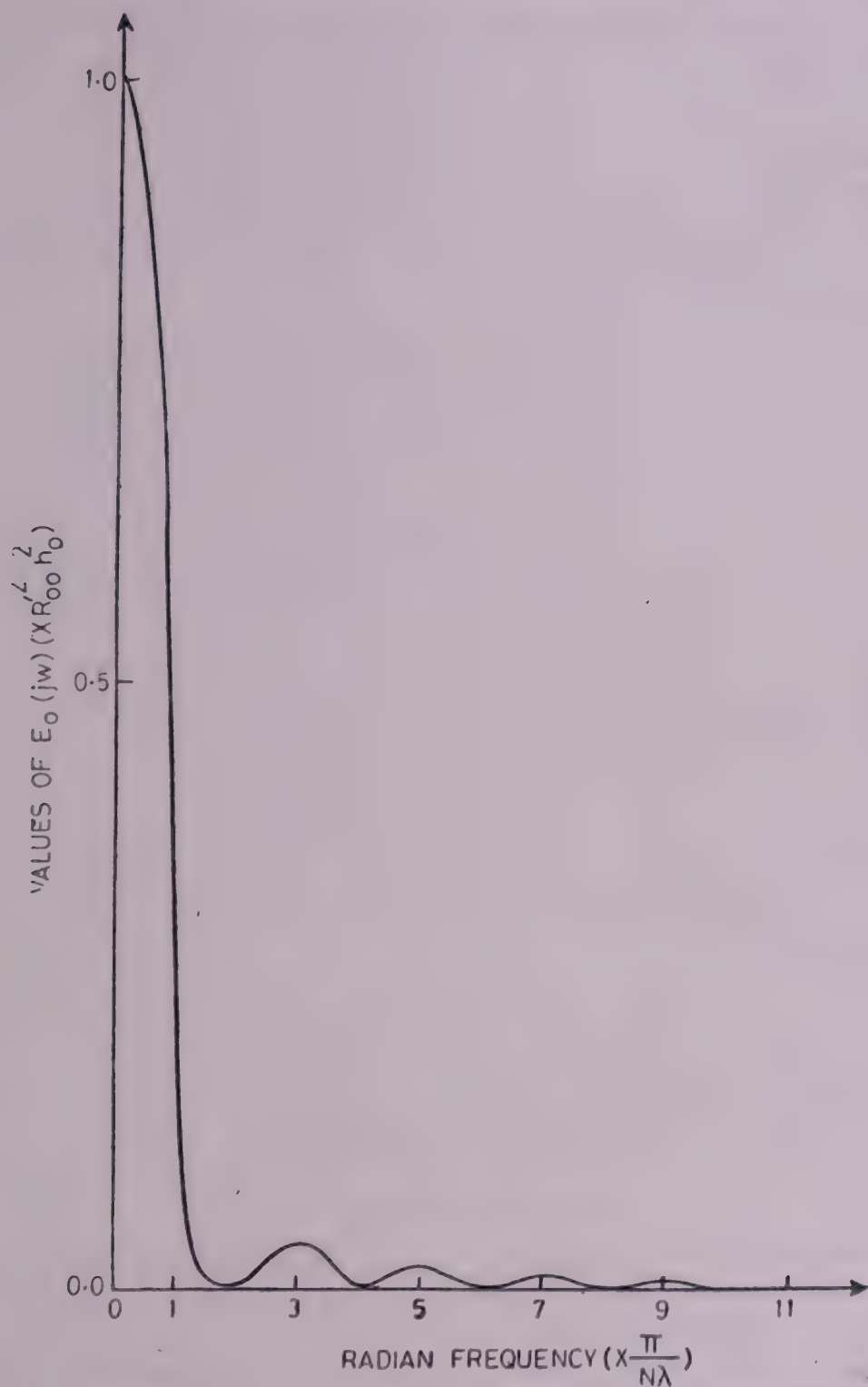


FIG 2 A plot of  $E_0(jw)$  vs.  $w$  that reveals the peaks corresponding to oscillations in  $E_0(jw)$ .

records the measured dominant periodicities agreed with the periodicities of the correspondingly largest-amplitude variations predicted by our theory to within less than 5 per cent. Note that according to equations (4) and (5), the largest-amplitude

variation for a given length of time has radian frequency  $w_{01}$  as well as amplitude  $A_{01}$  that are obtained when  $n = 1$  in equations (4) and (5), respectively. This has been illustrated graphically in Fig. 2 wherein  $E_0(iw)$  has been plotted against  $w$ . The peak for which  $w = 3\pi/N\lambda$  corresponds to the largest-amplitude oscillations. Now for the remaining 2 out of the 35 records, the predicted periodicities agreed with the observed periodicities to within 5–9 per cent. Our latest comparison involved 119 years long data of Worldwide marine temperature.<sup>14</sup> In this comparison, the dominant periodicity deduced from the data is 83 years while the dominant periodicity predicted by equation (4) is 80 years.

In a nutshell, the work presented in the paper can be divided into two parts. Firstly, we have developed an analytical expression for the (solar-derived) energy fluctuations in an arbitrary Earth location over an arbitrary period that exceeds two days. This expression is given by equation (3). Additionally, the reduced form of equation (3) has shown good agreement with recent observations<sup>14</sup> which are considered as the best estimate hitherto made of global climatic fluctuations of temperature at sea level. All in all, what comes out of this analysis is that the rotational motion of the Earth creates a solar-energy sampling process which plays a significant role in linking (the energy coming from) the Sun to fluctuations in the lower atmosphere. Since we know the features of the sampling process, we can easily predict energy fluctuations caused by the inevitable interaction between the constant-component of incoming solar energy and the sampling process. However, our formulation cannot help in predicting energy fluctuations caused by the interaction between the sampling process and the variable component of incoming solar energy unless the periodicities in this component are known. The usefulness of our formulation in this case is merely that after having knowledge of the periodicities in the variable component of incoming solar energy, the formulation can be used to predict energy fluctuations that are made harmonics of the latter periodicities by the sampling process.

Finally, it is worth nothing that the energy fluctuations discussed in this paper can have considerable effects upon weather changes because variations in solar-derived energy are in fact the ones primarily responsible for running the climatic system.<sup>10</sup> Besides, while the solar radiation variable is the most dominant climatic variable, many of the other variables are correlated to it.<sup>1</sup>

#### ACKNOWLEDGEMENTS

The author would like to thank Professor R Hide for suggestions that have greatly improved presentation of the paper and professor A H Cook for reading through the manuscript. Thanks are also due to Professor Abdus Salam, the International Atomic Energy Agency and UNESCO for hospitality at the International Centre for Theoretical Physics, Trieste, Italy.

#### REFERENCES

1. S Alterio S Barbaro and S Coppolino *Il Nuov Cim* **6C** (1983) 159
2. A B Pittock *Rev Geophys Space Phys* **16** (1978) 400

3. H H Lamb *Climate : Past, Present and Future* 1(1972) Methuen & Co Ltd London
4. W Bach J Pankrath and J Williams (Eds) *Interactions of Energy and Climate* D. Reidel Publishing Company Dordrecht Holland (1980)
5. A E J Ogilvie *Climatic Change* 6(1984) 131
6. A B Pittock *Q J R met Soc* 109(1983) 23
7. S Sofia and A S Endal *Comment Astrophys* 9(1982) 277
8. B Ponomaryov and R Ward *Int J Solar Energy* 1(1983) 379
9. D E Venne G D Nastrom and A D Belmont *J geophys Res* 88(1983) 11025
10. A Henderson-Sellers and M F Wilson *Rev Geophys Space Phys* 21(1983) 1743
11. E C Njau *ICTP (Trieste) int Rep IC/83/37* (1983); also published in *Proc Symp State of Physics and Mathematics in Africa*, Trieste Italy, 8-16 October 1984 (ICTP, Trieste 1985)
12. R T Wetherald and S Manabe *J atmos Sci* 32(1975) 2044
13. A A Ruzmaikin *Comment Astrophys* 9(N°2) (1981) 87
14. C K Folland D E Parker and F E Kates *Nature* 310(1984) 670
15. L Svalgaard *Physics of Solar Planetary Environments Proc of STP Symp* American Geophysical Union (1976)
16. E C Njau *Tanzania Not Rec* 81 & 82(1977)
17. R Y Anderson *J geophys Res* 87(1982) 7285
18. S Hastenrath and E B Kaczmarczyk *Tellus* 33(1981) 453
19. J P Palutikof J M Lough and G Farmer *Nature* 293(1981) 414

## COMPUTATION OF NEUTRON CROSS-SECTIONS AT 14 MeV FOR SOME MEDIUM MASS TRACE ELEMENTS

R S KHANCHI,\* K K MANOCHA,\*\* S K GUPTA,\*\*\* and R K MOHINDRA\*\*\*

\*Dyal Singh College, Karnal (Haryana)

\*\*Medical College, Rohtak (Haryana)

\*\*\*Physics Department, Kurukshetra University, Kurukshetra (Haryana), INDIA

(Received 21 May 1985)

An attempt had been made to compute all energetically possible primary and secondary neutron interaction cross-sections at 14 MeV with some medium mass trace elements,  $^{31}\text{P}$ ,  $^{32}\text{S}$ ,  $^{35}\text{Cl}$ ,  $^{39}\text{K}$ ,  $^{40}\text{Ca}$ ,  $^{55}\text{Mn}$ ,  $^{56}\text{Fe}$ ,  $^{60}\text{Co}$  and  $^{75}\text{As}$ . The calculations are based on the compound nucleus theory using optical model potential and Newton's shell dependent level density formula. The significant cross-sections tabulated are  $(n, p)$ ,  $(n, n')$ ,  $(n, \alpha)$ ,  $(n, np)$ ,  $(n, 2n)$ ,  $(n, n\alpha)$ ,  $(n, \alpha n)$ ,  $(n, pn)$  and these have been compared with the available experimental cross-sections. The agreement is reasonable in general with few large deviation. To assess the feasibility for trace elemental analysis of these isotopes, the induced activities/gm/unit flux via the appropriate reactions by 14 MeV neutrons have also been estimated and tabulated. Out of the large number of cross-sections computed here, only a few are amenable to experimental measurements and therefore these theoretical estimates can be quite useful in many nuclear design applications.

**Key Words :** Nuclear Physics; Neutron Cross-Sections; Medium Mass Trace Elements

### INTRODUCTION

At 14 MeV neutron laboratory energy, primary reactions like  $(n, p)$ ,  $(n, n')$  and  $(n, \alpha)$  are quite prominent. Secondary reactions of the type  $(n, 2n)$ ,  $(n, np)$ ,  $(n, n\alpha)$ ,  $(n, pn)$ ,  $(n, p\alpha)$  and  $(n, \alpha n)$  whenever possible by reaction energetics, also contribute significantly and some have quite large cross-sections. The compound nucleus theory based on Fermi gas and evaporation models with optical model potential has been used for evaluation of these cross-sections. The reactions of the type  $(n, np)$  &  $(n, pn)$  are quite different by reaction energetics and should have quite different cross-sections.

From these computed cross-sections one can readily estimate the value of induced activity per unit flux per gm of a sample (e. g.  $^{56}\text{Fe}$  in blood,  $^{75}\text{As}$  in hair, as trace elements). Such estimates can be very useful for the study of neutron activation analysis with conventional 14 MeV neutron generators, when experimental cross-sections are not available.

A knowledge of these detailed estimated interaction cross-sections presented here may also be useful for the design of fission and fusion nuclear devices. The

data on  $(n, p)$  and  $(n, \alpha)$  type reactions are important for making estimates of radiation damage to materials. Such estimated cross-sections acquire great importance when certain reactions are not possible to be measured easily and precisely in the laboratory because of target availability or complicated competing activities.

### CALCULATIONS AND RESULTS

The details of these calculations have been described earlier by Wadhwa and Mohindra,<sup>1</sup> for computation of primary and secondary reaction cross-sections based on compound nucleus model using the optical model potential parameters given by Mani *et al.*<sup>2</sup> for proton and neutron penetrabilities. For alpha-induced inverse reactions, the inverse cross-sections have been listed by Huizinga and Igo.<sup>3</sup> Shell-dependent level density formula due to Newton<sup>4</sup> as discussed by Wadhwa, Manocha and Mohindra<sup>5</sup> has been used in these evaluations. The formulae used for secondary cross-sections based on the evaporation theory have been reported earlier by Wadhwa and Mohindra.<sup>1</sup> The gamma-ray emission has been ignored in competition to particle emission in these computations. Recent values of separation energies listed by Wapstra and Bos<sup>6</sup> have been used. The computed cross-sections at 14 MeV neutron energy have been tabulated in Tables I and II along-with some of the available experimental cross-sections for comparison, from the listings of Borman *et al.*<sup>7</sup> The experimental  $(n, n')$  cross-sections have been taken from Cullen *et al.*<sup>8</sup>

The comparison between available experimental and our computed values is tolerable in general but in many cases [e.g.  $(n, n')$ ,  $(n, \alpha)$  reactions], the deviations are serious. This suggests that the theory needs great refinements to predict all such primary and secondary cross-sections with reasonable accuracy. This theory cannot even predict all the primary cross-sections listed here, with a fair degree of accuracy.

*Induced Activities* : The induced activity in micro-curies per unit neutron flux per gram of a sample containing e.g.  $^{75}\text{As}$  in equivalent to

$$\frac{0.693 \times \text{Number of atoms of } ^{75}\text{As} \times \sigma_{np}(\text{cm}^2) \times \text{Isotopic abundance}}{3.7 \times 10^4 \times T_{1/2} \text{ (seconds)}},$$

where  $T_{1/2}$  is the physical half life of the residual nucleus  $^{75}\text{Ge}^*$  in  $^{75}\text{As}$  ( $n, p$ )  $^{75}\text{Ge}^*$  reaction and = 79 minutes. The induced activities for all the nine trace elements under discussion here, have been listed in Table III for some typical reactions with appropriate half lives for laboratory measurements, using the computed cross-sections tabulated here. Relative comparison of the various induced activities is greatly simplified by these estimated cross-sections.

The calculated cross-sections for some of these reactions emitting charged particles have been profitably used for evaluating induced activities and hence radiation doses to man, Manocha and Mohindra,<sup>9</sup> using  $^{56}\text{Fe}$  ( $n, p$ )  $^{56}\text{Mn}^*$  reaction. Recently, it has been reported by Khanchi and Mohindra<sup>10</sup> that the estimates of

TABLE I  
*Computed cross-sections in mbs of  $^{31}P$ ,  $^{33}S$ ,  $^{35}Cl$ ,  $^{39}K$  and  $^{40}Ca$*

Sr. No.	Cross- Sections	$^{31}P$		$^{33}S$		$^{35}Cl$		$^{39}K$		$^{40}Ca$	
		Computed	Expt.	Computed	Expt.	Computed	Expt.	Computed	Expt.	Computed	Expt.
1.	$\sigma(n, n')$	265.8	600	232.3	400	499.4	—	630.7	850	840.7	—
2.	$\sigma(n, 2n)$	0.5	$5.1 \pm 0.45$	0	—	1.0	$3.4 \pm 1.5$	1.0	$2.5 \pm 0.3$	0	—
3.	$\sigma(n, np)$	101.9	$163 \pm 14$	60	$105 \pm 25$	349.4	—	482.8	$186 \pm 28$	366.4	$205 \pm 38$
4.	$\sigma(n, n\alpha)$	0	—	100.9	—	8.3	—	5.6	25	31.1	$23 \pm 6$
5.	$\sigma(n, p)$	247.4	$184 \pm 14$	142.2	$225 \pm 25$	192.8	$125 \pm 38$	333.7	$354 \pm 54$	181.4	$298 \pm 38$
6.	$\sigma(n, pn)$	99.3	—	15.9	—	95.0	—	205.3	—	64.7	—
7.	$\sigma(n, 2p)$	0	—	0.1	—	<1	—	<1	—	1.03	—
8.	$\sigma(n, p\alpha)$	0	—	0	—	<1	—	2.0	—	0.04	—
9.	$\sigma(n, \alpha)$	533.6	142	688.8	$109 \pm 16$	416.8	$121 \pm 20$	199.0	$84 \pm 12$	153.0	$138 \pm 20$
10.	$\sigma(n, \alpha n)$	2.6	—	50.0	—	26.2	—	4.8	—	1.4	—
11.	$\sigma(n, \alpha p)$	0	—	0	—	<1	—	13.2	—	0.005	—
12.	$\sigma(n, 2\alpha)$	0	—	0	—	0	—	0	$0.13 \pm 0.02$	0.08	—

TABLE II  
*Computed cross-sections in mbs of  $^{55}\text{Mn}$ ,  $^{56}\text{Fe}$ ,  $^{59}\text{Co}$  and  $^{75}\text{As}$*

Sr. No.	Cross- Sections	$^{55}\text{Mn}$		$^{56}\text{Fe}$		$^{59}\text{Co}$		$^{75}\text{As}$	
		Computed	Expt.	Computed	Expt.	Computed	Expt.	Computed	Expt.
1.	$\sigma(n, n')$	1245.3	—	1342.2	$950 \pm 140$	1251.5	—	1532.6	1610
2.	$\sigma(n, 2n)$	232.1	—	352.8	$440 \pm 90$	1066.3	$930 \pm 100$	115.6	$1070 \pm 43$
3.	$\sigma(n, np)$	430.2	—	11.7	$35 \pm 7$	0	—	227.7	—
4.	$\sigma(n, n\alpha)$	0	—	10.98	—	0	—	<1	—
5.	$\sigma(n, p)$	48.68	$43 \pm 7$	14.8	$109 \pm 9$	71.85	$82 \pm 8$	6.6	$35 \pm 7$
6.	$\sigma(n, pn)$	1.47	—	0.59	—	<1	—	5.96	—
7.	$\sigma(n, 2p)$	0	—	0	—	0	—	0	—
8.	$\sigma(n, p\alpha)$	0	—	0	—	0	—	0	—
9.	$\sigma(n, \alpha)$	43.02	$34 \pm 5$	61.94	$23 \pm 7$	59.34	$39 \pm 8$	0.9	$12 \pm 2.3$
10.	$\sigma(n, \alpha n)$	<1	—	1.57	—	0	—	<1	—
11.	$\sigma(n, \alpha p)$	0	—	0	—	0	—	0	—
12.	$\sigma(n, 2\alpha)$	0	—	0	—	0	—	0	—

TABLE III  
*Evaluation of induced activity for some trace elements using computed cross-sections*

Sr. No.	Nuclear Reaction	$T_{1/2}$ of Residual nucleus	Induced activity C1/gm per unit neutron flux
1.	$^{31}\text{P}(n, p) ^{31}\text{Si}^*$	2.62 hrs	$9.5 \times 10^{-14}$
2.	$^{31}\text{P}(n, \alpha) ^{28}\text{Al}^*$	2.31 min	$4.0 \times 10^{-13}$
3.	$^{32}\text{S}(n, p) ^{32}\text{P}^*$	14.28 days	$1.0 \times 10^{-16}$
4.	$^{35}\text{Cl}(n, 2n) ^{34}\text{Cl}^*$	1.56 Sec	$3.1 \times 10^{-13}$
5.	$^{39}\text{K}(n, 2n) ^{38}\text{K}^*$	7.71 min	$1.3 \times 10^{-16}$
6.	$^{40}\text{Ca}(n, \alpha) ^{37}\text{Ar}^*$	35.1 days	$2.4 \times 10^{-16}$
7.	$^{56}\text{Fe}(n, p) ^{56}\text{Mn}^*$	2.57 hrs	$3.1 \times 10^{-17}$
8.	$^{55}\text{Mn}(n, p) ^{55}\text{Cr}^*$	3.6 min	$1.54 \times 10^{-15}$
9.	$^{55}\text{Mn}(n, \alpha) ^{52}\text{V}^*$	3.75 min	$2.2 \times 10^{-16}$
10.	$^{59}\text{Co}(n, \alpha) ^{56}\text{Mn}^*$	2.57 min	$4.3 \times 10^{-16}$
11.	$^{75}\text{As}(n, p) ^{75}\text{Ge}^*$	79 min	$1.6 \times 10^{-17}$

induced activity of  $^{75}\text{Ge}^*$  from  $^{75}\text{As}(n, p) ^{75}\text{Ge}^*$  reaction at 14 MeV can be used for the trace elemental analysis of  $^{75}\text{As}$  in samples of hair, nail and diseased liver.

It has been established by Manocha *et al.*<sup>11</sup> that reasonable estimates of maximum permissible dose of 14 MeV neutrons to man can be obtained by using such calculated cross-sections. Evaluated cross-sections listed here can play useful role in several nuclear design, radiation damage and shielding problems at low energies in the range say 5–20 MeV. Computations at around 14 MeV neutron energies have been undertaken because enormous cross-section data is available from 14 MeV neutron generators, for comparison.

## ACKNOWLEDGEMENT

One of the authors (RSK) is grateful to University Grants Commission, New Delhi for research grant.

## REFERENCES

- 1 B S Wadhwa and R K Mohindra *Nucl Sci Engng (USA)* **56** (1975) 96
- 2 G S Mani M A Melkanoff and Iori *Rep CEA* No. 2379 (Saclay, France (1963); (b) *ibid Rep CEA* No. 2380 (Saclay France) (1963)
- 3 J R Huijzena and G IgO *Nucl Phys* **29** (1962) 462
- 4 T D Newton *Canad J Phys* **34** (1956) 804
- 5 B S Wadhwa K K Manocha and R K Mohindra *Indian J pure appl Phys* **12** (1974) 645
- 6 A H Wapstra and K Bos *Atomic Data and Nuclear Data Tables (USA)* **19** (1977) No. 3
- 7 M Borman T Neurt H and W Scobal *Handbook of Neutron Cross-Sections* IAEA Austria 1974
- 8 D E Cullen R J Howerton S T Perkins and M H Mac Gregor *Major Neutron Induced Interaction Cross-sections UCRL-50400 7 and 8* Lawrence Livermore Laboratory, University of California, USA (1976)
- 9 K K Manocha and R K Mohindra *J Rad Res Japan* **18** (1977) 165
- 10 R S Khanchi and R K Mohindra *Proc Indian natn Sci Acad* **50A** (1984) 382
- 11 K K Manocha H K Sahajwani and R K Mohindra *Indan J Radiol* **35** (1981) 52

## RARE-EARTH CHELATES OF DIBASIC TRIDENTATES POSSESSING NITROGEN AND OXYGEN DONOR SITES

SUNITA BHATIA, PREETI MEHTA and R K MEHTA

Department of Chemistry, University of Jodhpur, Jodhpur-342001, INDIA

(Received 12 November 1984; after revision 15 April 1985)

The stability constants and thermodynamic parameters of the lanthanon chelates of o-( $\alpha$ -benzoylmethyl-benzylidene imino) benzene sulphonic acid ( $H_2BB$ ) and 2-( $\alpha$ -benzoylmethyl benzylidene imino) ethane sulphonic acid ( $H_2BE$ ) have been determined using the Calvin-Bjerrum pH-titration technique as employed by Irving and Rossotti in aqueous media ( $\mu = 0, 1m, 0.05$  and  $0.01M NaClO_4$ ) at  $25 \pm 0.05$ ,  $35 \pm 0.05$  and  $45 \pm 0.05$  °C. The order of stability constants is found to be : La(III) < Ce(III) < Pr(III) < Nd(III) < Sm(III) < Gd(III) < Tb(III) < Dy(III) < Ho(III). The magnetic, conductance and infra spectra of the solid chelates have also been studied.

**Key Words :** Lanthanon chelates of o-( $\alpha$ -benzoylethyl-benzylidene imino) benzene sulphonic acid ( $H_2BB$ ) and 2-( $\alpha$ -benzoylmethyl benzylidene imino) ethane sulphonic acid ( $H_2BE$ ).

### INTRODUCTION

METAL chelates of some tridentate Schiff bases have been studied in these laboratories.<sup>1,2,3</sup> A survey of the literature<sup>4</sup> indicates that no systematic study of the chelates of o-( $\alpha$ -benzoylmethyl benzylidene imino) benzene sulphonic acid ( $H_2BE$ ) and 2-( $\alpha$ -benzoylmethyl benzylidene imino) ethane sulphonic acid ( $H_2BE$ ) with La(III), Ce(III), Pr(III), Nd(III), Sm(III), Gd(III), Tb(III), Dy(III) and Ho(III) have been carried out. It was therefore considered interesting to perform physico-chemical investigations on these chelates. The results of these studies are discussed in this communication.

### EXPERIMENTAL

#### Materials

La(III), Ce(III), Pr(III), Nd(III), Sm(III), Gd(III), Tb(III), Dy(III), and Ho(III) nitrates and EDTA were of analytical reagent grade. Dibenzoyl methane was a Fluka product. Orthanilic acid (L.R.) and Taurine were BDH product. A digital pH-meter type DPH-77 (Unitech), equipped with a glass-calomel electrode assembly was used.

The ligands o-( $\alpha$ -benzoylmethyl benzylidene imino) benzene sulphonic acid ( $H_2BB$ ) and 2-( $\alpha$ -benzoylmethyl benzylidene imino) ethane sulphonic acid were synthesised respectively from dibenzoyl methane and orthanilic acid or taurine by the methods already reported.<sup>2</sup> The solid lanthanon chelates were prepared by an earlier method.<sup>3</sup>

For potentiometric studies Irving-Rossotti technique<sup>5</sup> was followed. For this purpose the following mixtures (total volume 25ml) were prepared and their low ionic strengths ( $\mu = 0.1M$ ,  $0.05M$  and  $0.01M$   $NaClO_4$ ) were maintained. These mixtures were titrated against  $0.1M$   $NaOH$  and the titration curves had the usual shapes. (1) 5.0ml  $0.01M$   $HClO_4$  + 2.5ml  $1.0M$   $NaClO_4$  + 17.5ml water (2) 5.0ml  $0.01M$   $HClO_4$  + 10.0ml  $0.01M$   $H_2BB$  or  $H_2BE$  + 2.5ml  $1.0M$   $NaClO_4$  + 7.5ml water (3) 5.0ml  $0.01M$   $HClO_4$  + 10.0ml  $0.01M$   $H_2BB$  or  $H_2BE$  + 2.0ml  $0.01M$  metal-ion solution + 2.5ml  $1.0M$   $NaClO_4$  + 5.5ml water.

### RESULTS AND DISCUSSION

The dissociation constants ( $\log K_1^H$  and  $\log K_2^H$  of  $H_2BB$  (at  $0.1\text{ NaClO}_4$ ) are 7.13 and 9.85 at  $25^\circ C$ , 6.78 and 9.43 at  $35^\circ C$  and 6.39 and 9.03 at  $45^\circ C$  and of  $H_2BE$  7.15 and 10.0 at  $25^\circ C$  6.81 and 9.55 at  $35^\circ C$  and 6.45 and 9.05 at  $45^\circ C$ , respectively. Stability constants ( $\log K_1$  and  $\log K_2$ ) of its rare earth chelates are shown in Table I.

TABLE I  
*Dissociation constants of  $H_2BB$  and  $H_2BE$  and stability constants of their rare-earth chelates at  $0.1M\text{ NaClO}_4$*

Ligand/Metal chelates	$pH$ -range	$\log K_H^1 \log K_1$			$\log K_H^2 \log K_2$		
		$25^\circ$	$25^\circ$	$35^\circ$	$45^\circ$	$25^\circ$	$35^\circ$
$H_2BB$		7.13	6.78	6.39	9.85	9.43	9.03
( $H_2BE$ )		(7.15)	(6.81)	(6.45)	(10.00)	(9.55)	(9.05)
La(III)	5.40–6.85 (6.85–8.40)	6.83 (6.35)	7.11 (8.68)	7.46 (9.00)	5.46 (6.90)	5.78 (7.25)	6.09 (7.60)
Ce(III)	5.65–7.30 (7.15–8.60)	7.22 (8.55)	7.56 (8.86)	7.92 (9.18)	5.68 (7.19)	5.99 (7.53)	6.30 (7.85)
Pr(III)	6.10–7.50 (7.40–8.75)	7.56 (8.74)	7.88 (9.05)	8.18 (9.39)	6.00 (7.49)	6.39 (7.80)	6.72 (8.09)
Nd(III)	6.40–8.15 (7.55–8.90)	8.00 (8.89)	8.40 (9.29)	8.81 (9.61)	6.43 (7.59)	6.76 (7.90)	7.08 (8.20)
Sm(III)	6.85–8.55 (7.70–9.00)	8.51 (8.98)	8.89 (9.21)	9.25 (9.56)	6.87 (7.76)	7.20 (8.02)	7.57 (8.35)
Gd(III)	6.99–8.95 (7.90–9.20)	8.93 (9.15)	9.28 (9.50)	9.66 (9.89)	7.01 (7.99)	7.40 (8.32)	7.72 (8.62)
Tb(III)	7.45–9.30 (8.10–9.45)	9.38 (9.40)	9.71 (9.79)	10.03 (10.08)	7.52 (8.12)	7.92 (8.45)	8.25 (8.75)
Dy(III)	7.80–9.70 (8.25–9.60)	9.79 (9.55)	10.15 (9.90)	10.47 (10.22)	7.90 (8.27)	8.23 (8.63)	8.56 (8.95)
Ho(III)	8.00–9.95 (8.40–9.80)	10.15 (9.75)	10.50 (10.10)	10.83 (10.43)	8.18 (8.45)	8.49 (8.79)	8.80 (9.10)

The values given in the parenthesis refer to those of  $H_2BE$ .

From Table I it is apparent that stability of the rare-earth chelates increases with rise of temperature. The stability of the chelates increases with decreasing ionic size of the metal ions, i.e. La(III) < Ce(III) < Pr(III) < Nd(III) < Sm(III) < Gd(III) < Tb(III) < Dy(III) < Ho(III), which is in agreement with the findings of Stagg and Powell.<sup>6</sup> The thermodynamic stability constants have been obtained by extrapolation of the experimentally obtained constants to zero ionic strengths and their values along with other related parameters are summarised in Table II.

The  $\Delta G^\circ$  of all the chelates have more negative values at 45° than at 35° and 25°. It is also observed that  $\Delta H^\circ$  is positive in all the cases. This suggests that some steric strain exists around the metal ion in the fused rings. The positive values of  $\Delta S^\circ$  suggest that entropy term is favourable for the formation of the chelates.

In terms of Harned's relation the values of the  $\theta^\circ$  (the temperature at which  $pK_m^H$  is minimum) and  $pK_m^H$  ( $pK_m^H$  at  $t = 0$ ) for the ligand ( $H_2BB$ ) were found to be 800 and -13.1 and for ( $H_2BE$ ) 867.94 and -18.37, respectively.

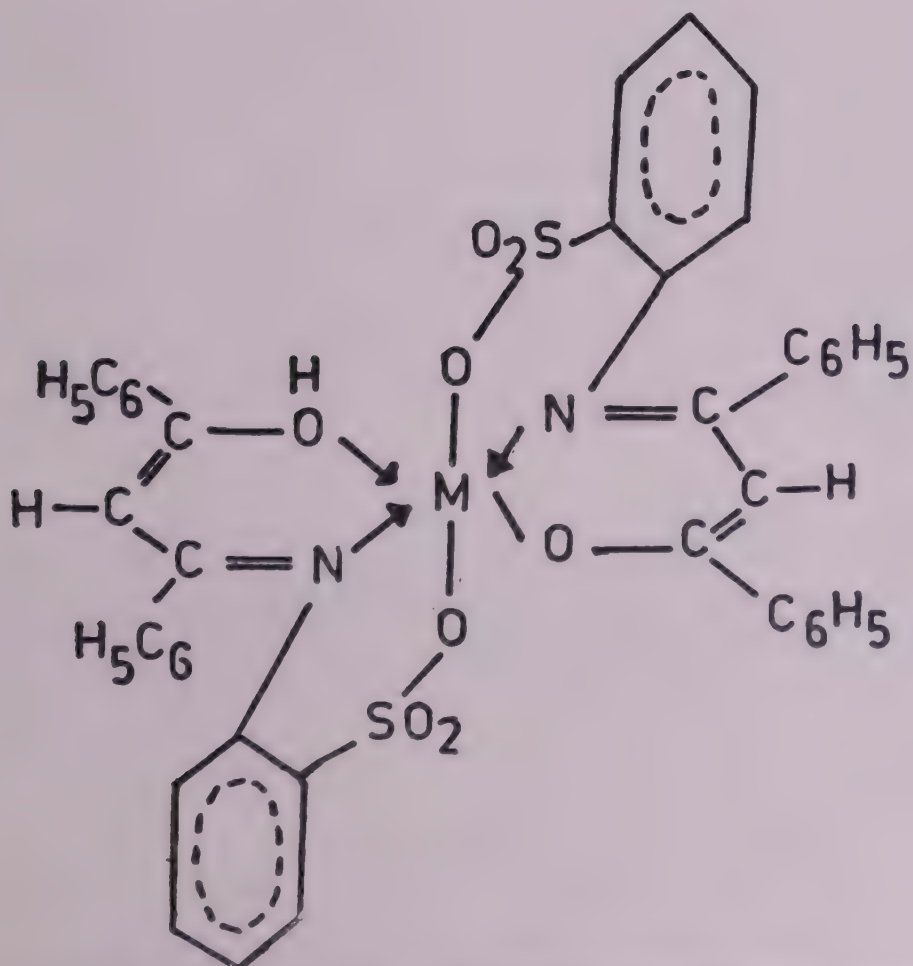


FIG 1 Structure of rare earth chelates of *o*-( $\alpha$ -benzoylmethyl benzylidene imino) benzene sulphonic acid ( $H_2BB$ )       $M = \text{La, Ce, Pr, Nd, Sm, Gd, Tb, Dy or Ho}$ .

TABLE II

*Average stability constants and thermodynamic parameters of rare-earth chelates of o-( $\alpha$ -benzoylmethyl benzylidene imino) benzene sulphonic acid and 2-( $\alpha$ -benzoylmethyl benzylidene imino) ethane sulphonic acid*

Metal chelate	log $\beta^\circ$			$-\Delta G^\circ$ K. Joule mole $^{-1}$			$\Delta H^\circ$ K. Joule mole $^{-1}$ at 35 °C	$\Delta S^\circ$ Joule mole $^{-1}$ at 35 °C
	25°	35°	45°	25°	35°	45°		
La(III)	14.80 (16.50)	15.12 (16.83)	15.45 (17.09)	84.45 (94.15)	89.17 (99.26)	94.06 (104.06)	58.97 (53.53)	98.05 (148.47)
Ce(III)	15.00 (17.00)	15.40 (17.39)	15.77 (17.70)	85.59 (97.00)	90.82 (102.56)	96.02 (107.78)	69.86 (68.51)	68.05 (126.79)
Pr(III)	16.30 (18.04)	16.67 (18.45)	17.00 (18.82)	93.01 (102.94)	98.31 (108.81)	103.51 (114.60)	63.51 (70.77)	112.99 (123.51)
Nd(III)	17.01 (18.21)	17.39 (18.59)	17.76 (18.90)	97.06 (103.91)	102.56 (109.64)	108.14 (115.08)	68.05 (62.60)	112.04 (152.73)
Sm(III)	17.55 (18.60)	17.90 (18.92)	18.29 (19.25)	100.14 (106.13)	105.57 (111.58)	111.37 (117.21)	67.14 (58.97)	124.77 (170.81)
Gd(III)	17.80 (18.90)	18.15 (19.27)	18.60 (19.67)	101.57 (108.30)	107.04 (113.65)	113.26 (119.77)	72.58 (69.86)	111.88 (142.18)
Tb(III)	19.12 (19.41)	19.48 (19.80)	19.90 (20.12)	109.10 (110.76)	114.88 (116.77)	121.17 (122.51)	70.77 (64.42)	143.21 (169.97)
Dy(III)	19.35 (19.49)	19.72 (19.92)	20.08 (20.25)	110.41 (111.21)	116.30 (117.48)	122.27 (123.30)	66.23 (68.95)	162.56 (157.56)
Ho(III)	19.69 (19.90)	20.00 (20.27)	20.38 (20.63)	112.35 (113.55)	117.95 (119.54)	124.09 (125.62)	62.60 (66.23)	179.71 (173.08)

The values given in the parenthesis refer to those of 2-( $\alpha$ -benzoylmethyl benzylidene imino) ethane sulphonic acid.

Lanthanum chelate was found diamagnetic whereas the rest paramagnetic. From the magnetic moments which are very close to spin-only values, it is apparent that in these compounds there is no metal-metal bonding and, hence, no spin-exchange occurs and they exist as monomer. Negligibly small conductance values ( $3.23\text{--}6.30 \text{ ohm}^{-1} \text{ cm}^2 \text{ mole}^{-1}$ ) of the compounds suggest them to be non electrolytes.

#### I.R. Spectra

In the I.R. spectra of  $H_2BB$  and  $H_2BE$  five bands were observed in the ranges 3360–3370, 1670–1690, 1630–1640, 1610–1620 and 1100–1130  $\text{cm}^{-1}$ , which correspond to  $\nu_{\text{O-H}}$ ;  $\nu_{\text{C=O}}$ ;  $\nu_{\text{C=C}}$ ;  $\nu_{\text{C=N}}$  and  $\nu_{\text{SO}_3\text{OH}}$ , respectively. In the metal chelates the  $\nu_{\text{C-H}}$  is lowered to 1580–1590  $\text{cm}^{-1}$  suggesting involvement of azomethine nitrogen in chelation. The disappearance of the band in the range 1100–1130  $\text{cm}^{-1}$  suggest

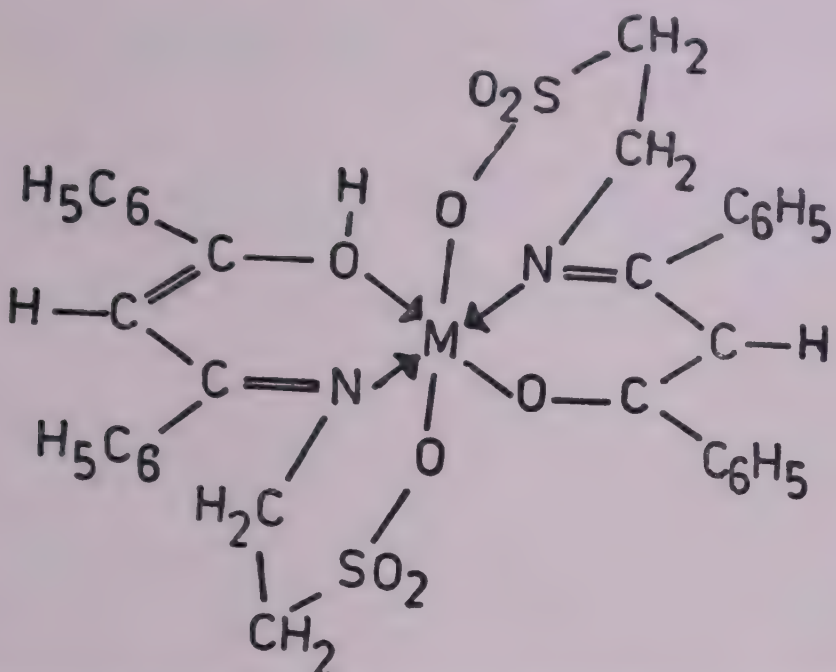


FIG 2 Structure of rare earth chelates of 2-( $\alpha$ -benzylidene imino) ethane sulphonic acid ( $H_2BE$ )  
 $M = La, Ce, Pr, Nd, Sm, Gd, Tb, Dy$  or  $Ho$ .

elimination of sulphonic group in chelation. Appearance of bands in the ranges 510–530 and 410–420 cm<sup>-1</sup> indicate  $M-O$  and  $M-N$  bands, respectively.

Based on the above evidences an octahedral structure is suggested for the lanthanon chelates as shown in Figs. 1 and 2.

#### ACKNOWLEDGEMENT

The authors are thankful to U. G. C. (India) for grant of fellowship to one of them (S.B.).

#### REFERENCES

- 1 R S Shekhawat N K Sankhla and R K Mehta *Polish J Chem* **54** (1980) 391
- 2 R P Mathur and R K Mehta *J prakt Chem* **325** (1981) 847
- 3 K G Sharma R P Mathur and R K Mehta *J less-common Metals* **80** (1981) 91
- 4 F A Cotton *Progress in Inorganic Chemistry* Intersci Publ **7** (1966) 88
- 5 J Bjerrum *Metal Amine Formation in Aqueous Solution* P Hasses and Sons Copenhagen **14a-36b** (1957) pp. 20, 114.
- 6 W R Stagg and J E Powell *Inorg Chem* **6** (1964) 242

## KINETICS OF ALKALI CATALYSED CATECHOL-FORMALDEHYDE REACTION

H C MALHOTRA\* and P S JASSAL

Department of Chemistry, University of Delhi, Delhi-110007, INDIA

(Received 15 December 1984; after revision 25 July 1985)

Kinetic study of the reaction of catechol-formaldehyde was carried out at temperatures 65, 70, 75 and 80 °C and at  $4.2 \times 10^{-3}$ N,  $10.2 \times 10^{-3}$ N,  $16.2 \times 10^{-3}$ N and  $22.2 \times 10^{-3}$ N concentrations of sodium hydroxide. Reaction follows an overall second order rate kinetics. Rate of the reaction increases as the concentration of the alkali catalyst increases. Overall rate constant  $k$ , has been resolved into stepwise rate constants  $k_1$  and  $k_2$ , for the formation of monomethylol and dimethylol products. Rate equations for various possible steps have been given and the concentrations of the methylols formed have been determined. Arrhenius parameters and entropy of activation for the reaction are calculated by using the transient kinetics. The experimental and calculated values of the overall rate constant  $k$  are well within the experimental error.

**Key Words :** Chemical Kinetics; Catechol-Formaldehyde Reaction; Arrhenius Parameters; Entropy of Activation

### INTRODUCTION

RESINOUS and non-resinous products formed by the reaction of various phenols and formaldehyde find large number of industrial applications. Once the utility of these products have been established, studies usually of an empirical nature have to be initiated in an effort to develop resinous and non-resinous products suited to each new application. However, as technology is developing and the applications of these materials are very much on the increase, it is desirable to know the exact factors controlling the properties of catechol-formaldehyde products, their mode of formation etc. Earlier investigations were mainly concerned with the detection of major phenolic resins. A few workers made kinetic investigations of various phenols—formaldehyde reaction extensively.<sup>1-9</sup> A thorough review of literature reveals that not even a single kinetic study has been made on the catechol-formaldehyde reaction.

In our present work, we have made a comprehensive kinetic study of catechol-formaldehyde reaction at 65, 70, 75 and 80 °C, using different concentrations of sodium hydroxide as catalyst. All the reactions were studied in 50 per cent (v/v) methanol-water media. The functionality i.e. the available reactive ortho and para positions of catechol, has been taken into consideration while suggesting the rate equations.

\*For correspondence.

## EXPERIMENTAL

*Materials and Method*

- (a) *Materials*: Catechol used for rate studies was a E. Merck product and it was further purified by recrystallization. Formalin (37.5 per cent solution in H<sub>2</sub>O) sodium thiosulphate, potassium iodide, iodine and sodium bisulphite were B.D.H. products. Other chemicals—sodium hydroxide, methanol, cyclohexane and ethyl acetate were of A.R. or C.P. quality. German thermostat (model NBE) maintained within  $\pm 0.05$  °C, was used for rate studies.
- (b) *Method*: Reaction mixture was placed in 100 ml round bottom flask fitted with a water condenser. The flask was suspended in the thermostat maintained at the desired temperature. After equilibration, 5 ml of the reaction mixture was taken and placed in an ice-bath to freeze the reaction. Formaldehyde was estimated by the usual sodium bisulphite method and catechol was determined spectrophotometrically using diazotised-*p*-nitro aniline as an indicator.

## RESULTS AND DISCUSSION

Results of kinetic studies at different temperatures and at different concentrations of sodium hydroxide are reported in Table I. Catechol-formaldehyde reaction obeys

TABLE I  
Overall second order rate constants for various sodium hydroxide concentrations at different temperatures

Initial [catechol] = 0.418M

Temp. °C	[NaOH] $\times 10^{-3}N$	[HCHO] (M)	Second order rate constant (litre/mole-sec)
65	4.20	0.4151	$1.86 \times 10^{-6}$
	10.20	0.4032	$4.32 \times 10^{-6}$
	16.10	0.4175	$1.84 \times 10^{-5}$
	22.20	0.4075	$3.92 \times 10^{-5}$
70	4.20	0.4332	$4.11 \times 10^{-6}$
	10.20	0.4125	$6.41 \times 10^{-6}$
	16.20	0.4172	$2.62 \times 10^{-5}$
	22.20	0.4256	$6.30 \times 10^{-5}$
75	4.20	0.4067	$7.54 \times 10^{-6}$
	10.20	0.4283	$9.37 \times 10^{-6}$
	16.20	0.4183	$4.78 \times 10^{-5}$
	22.20	0.4038	$9.21 \times 10^{-5}$
80	4.20	0.4056	$1.21 \times 10^{-5}$
	10.20	0.4171	$3.27 \times 10^{-5}$
	16.20	0.4043	$6.79 \times 10^{-5}$
	22.20	0.4332	$1.93 \times 10^{-4}$

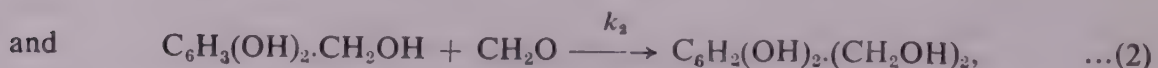
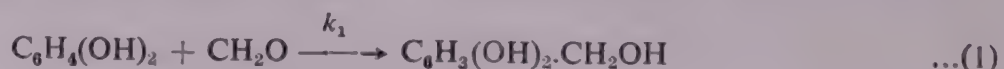
an overall second order rate kinetics and it is further proved by the linear plot of  $\log(b/na)(na-y)/(b-y)$  vs. time. Rate of the reaction increases as the concentration of alkali increases as it is obvious from Table I. Arrhenius parameters and entropy of activation have been calculated by the linear plots of  $\log k/T$  vs.  $1/T$  (Table II). From Table II, it can be seen that as the concentration of alkali increases, the value of activation energy and entropy of activation decreases appreciably.

TABLE II  
*Activation parameters at various sodium hydroxide concentration for the overall reaction*

[NaOH] $\times 10^{-3} N$	$\Delta E$ (K. cal mole $^{-1}$ )	$\log A$ (Litre mole $^{-1}$ sec $^{-1}$ )	$\Delta S^\neq$ (Cal. deg $^{-1}$ mole $^{-1}$ )
4.20	35.64	14.72	+ 20.16
10.20	31.53	12.31	+ 9.15
16.20	22.46	7.22	- 14.17
22.20	18.31	4.96	- 24.53

### *Calculation of Stepwise Rate Constants*

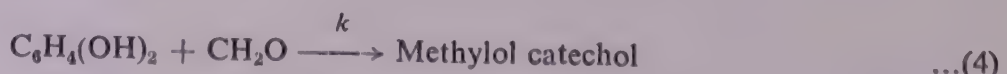
The alkali catalysed catechol-formaldehyde reaction proceeds according to the following equations :



where  $k_1$  and  $k_2$  are the stepwise rate constants for the formation of monomethylol catechol and dimethylol catechol. The overall rate expression is given by equation (3) :

$$k = \frac{2.303}{t(na - b)} \log \frac{b}{na} \cdot \frac{(na - y)}{(b - y)}, \quad \dots(3)$$

where  $a$  and  $b$  are the initial concentrations of catechol and formaldehyde, respectively and  $y$  is the amount of formaldehyde reacted during time interval ' $t$ '.  $n$  is the functionality of catechol ( $= 2$ ).



The rate of disappearance of catechol and formaldehyde is given by :

$$-\frac{d(a - x)}{dt} = nk(a - x)(b - y); \quad \dots(5)$$

and

$$-\frac{d(b - y)}{dt} = k(na - y)(b - y), \quad \dots(6)$$

where  $x$  is the amount of the catechol disappeared at time  $t$  and  $k$  is the overall rate constant. Dividing equation (6) by equation (5) and integrating :

$$y = na - na^{(n-1)/n}(a - x)^{1/n} \quad \dots(7)$$

The rate of formation of monomethylol catechol and dimethylol catechol is given by :

$$\frac{dx}{dt} = k_1(a - x)(b - y) \quad \dots(8)$$

and

$$\frac{dc}{dt} = k_2(x - c)(b - y); \quad \dots(9)$$

also

$$\frac{dy}{dt} = \frac{dx}{dt} + \frac{dc}{dt} \quad \dots(10)$$

or

$$\frac{dy}{dt} = k_1(a - x)(b - y) + k_2(x - c)(b - y), \quad \dots(11)$$

where  $c$  is the amount of monomethylol catechol disappeared at time  $t$ . Dividing equation (9) by equation (8), a first order differential equation is obtained :

$$\frac{dc}{dx} + \frac{u}{a-x} \cdot C = \frac{u}{a-x} \cdot x, \quad \dots(12)$$

where  $u = k_2/k_1$ . The integrating factor for this linear differential equation is given by

$$\begin{aligned} \text{I.F.} &= \exp \left( \int \frac{u}{a-x} \cdot dx \right) \\ &= \frac{1}{(a-x)^u} \end{aligned} \quad \dots(13)$$

Multiplying both sides of equation (12) by  $1/(a - x)^u$ , we get :

$$\frac{1}{(a-x)^u} \cdot \frac{dc}{dx} + \frac{u}{(a-x)^{1+u}} \cdot C = \frac{u}{(a-x)^{1+u}} \cdot x \quad \dots(14)$$

or

$$\frac{d}{dx} \cdot C \frac{1}{(a-x)^u} = \frac{ux}{(a-x)^{u+1}} \quad \dots(15)$$

Integrating equation (14) and putting the limits when  $t = 0$ ,  $x = 0$  and  $c = 0$ , we get :

TABLE III  
*Concentrations of various methylol-catechol at temperature 65 °C*

[NaOH] × 10 <sup>-3</sup> N	Time (sec)	Concentration (mole/litre)		
		y	x	c
4.20	16200	.0132	.0128	.00010
	23400	.0176	.0163	.00016
	30600	.0214	.0199	.00024
	37800	.0246	.0237	.00034
10.20	14400	.0217	.0207	.00026
	20400	.0291	.0282	.00049
	26400	.0361	.0347	.00075
	32400	.0436	.0418	.00109
16.20	9000	.0527	.0502	.00160
	14400	.0777	.0751	.00370
	19800	.1020	.0992	.00668
	25200	.1251	.1237	.01078
22.20	6000	.0751	.0735	.00354
	9600	.0967	.0941	.00597
	13200	.1283	.1258	.01118
	16800	.1635	.1607	.01930

$$C = x + \frac{a - x}{1 - u} - \left[ \frac{a^{1-u}}{1-u} (a - x)^u \right] \quad \dots(16)$$

or

$$C = \frac{1}{1-u} [a - xu - a^{1-u}(a - x)^u] \quad \dots(17)$$

Finally, on dividing equation (11) by equation (8) and using equation (12), a differential equation (18) with separate variable is obtained :

$$\frac{dy}{dx} = 1 + \left( \frac{u}{a-x} \right) \cdot x - \frac{u \cdot c}{a-x} \quad \dots(18)$$

or

$$y = x + u \int \frac{x}{a-x} \cdot dx - u \int \frac{c}{a-x} \cdot dx + I_0. \quad \dots(19)$$

We know that :

$$\int \frac{x}{a-x} \cdot dx = -a \log(a-x) - x$$

$$\begin{aligned} \int \frac{c}{a-x} \cdot dx &= \frac{1}{1-u} \left[ -a \log(a-x) + ua \log(a-x) + ux \right. \\ &\quad \left. + \frac{a^{1-u}}{u} \cdot (a-x)^u \right] \end{aligned}$$

TABLE IV

*Stepwise rate constants at different concentrations of sodium hydroxide and at different temperatures*

Temp. °C	[NaOH] × 10 <sup>-3</sup> N	Stepwise rate constants (litre mole <sup>-1</sup> sec <sup>-1</sup> )	
		$k_1$	$k_2$
65	4.20	$3.72 \times 10^{-6}$	$1.93 \times 10^{-6}$
	10.20	$8.64 \times 10^{-6}$	$4.49 \times 10^{-6}$
	16.20	$3.68 \times 10^{-5}$	$1.91 \times 10^{-5}$
	22.20	$7.86 \times 10^{-5}$	$4.08 \times 10^{-5}$
70	4.20	$8.22 \times 10^{-6}$	$4.27 \times 10^{-6}$
	10.20	$12.82 \times 10^{-6}$	$6.66 \times 10^{-6}$
	16.20	$5.24 \times 10^{-5}$	$2.72 \times 10^{-5}$
	22.20	$12.60 \times 10^{-5}$	$6.55 \times 10^{-5}$
75	4.20	$15.08 \times 10^{-6}$	$7.84 \times 10^{-6}$
	10.20	$18.74 \times 10^{-6}$	$9.74 \times 10^{-6}$
	16.20	$9.56 \times 10^{-5}$	$4.97 \times 10^{-5}$
	22.20	$18.42 \times 10^{-5}$	$9.58 \times 10^{-5}$
80	4.20	$2.42 \times 10^{-5}$	$1.26 \times 10^{-5}$
	10.20	$6.54 \times 10^{-5}$	$3.40 \times 10^{-5}$
	16.20	$13.56 \times 10^{-5}$	$7.05 \times 10^{-5}$
	22.20	$3.86 \times 10^{-4}$	$2.01 \times 10^{-4}$

Putting the values of the integrals in equation (19), we get :

$$y = x + u [-a \log (a - x) - x] - \frac{u}{1-u} - a \log (a - x) \\ + ua \log (a - x) + ux + \frac{a^{1-u}}{u} (a - x)^u + I_0 \quad \dots(20)$$

The value of the integration constant  $I_0$  is determined by putting the limits, when  $t = 0$ ,  $x = 0$  and  $y = 0$ , then equation (20) is reduced to :

$$y = a + x + \frac{u}{1-u} (a - x) - \frac{a^{1-u}}{1-u} \cdot (a - x)^u \quad \dots(21)$$

If the ratio of the reaction rate constants  $u$  is determined, then from equations (17) and (21), we can determine the concentrations of all the species present at any stage in the system.

Comparing equations (7) and (21) :

$$na - na^{(n-1)/n} \cdot (a - x)^{1/n} = a + x + \frac{u}{1-u} (a - x) - \frac{a^{1-u}}{1-u} (a - x)^u \\ \dots(22)$$

TABLE V  
*Experimental and calculated values of k at 65 °C*

[NaOH] × 10 <sup>-2</sup> N	Time (sec)	k (litre mole <sup>-1</sup> sec <sup>-1</sup> )	
		Experimental	Calculated
4.20	16200	1.35 × 10 <sup>-6</sup>	1.35 × 10 <sup>-6</sup>
	23400	2.17 × 10 <sup>-6</sup>	2.18 × 10 <sup>-6</sup>
	30600	2.04 × 10 <sup>-6</sup>	2.05 × 10 <sup>-6</sup>
	37800	1.88 × 10 <sup>-6</sup>	1.88 × 10 <sup>-6</sup>
10.20	14400	4.65 × 10 <sup>-6</sup>	4.67 × 10 <sup>-6</sup>
	20400	4.26 × 10 <sup>-6</sup>	4.27 × 10 <sup>-6</sup>
	26400	4.13 × 10 <sup>-6</sup>	4.16 × 10 <sup>-6</sup>
	32400	4.22 × 10 <sup>-6</sup>	4.25 × 10 <sup>-6</sup>
16.20	9000	1.93 × 10 <sup>-6</sup>	1.95 × 10 <sup>-6</sup>
	14400	1.84 × 10 <sup>-6</sup>	1.86 × 10 <sup>-6</sup>
	19800	1.75 × 10 <sup>-6</sup>	1.76 × 10 <sup>-6</sup>
	25200	1.82 × 10 <sup>-6</sup>	1.79 × 10 <sup>-6</sup>
22.20	6000	4.26 × 10 <sup>-6</sup>	4.28 × 10 <sup>-6</sup>
	9600	3.60 × 10 <sup>-6</sup>	3.61 × 10 <sup>-6</sup>
	13200	3.74 × 10 <sup>-6</sup>	3.73 × 10 <sup>-6</sup>
	16800	4.10 × 10 <sup>-6</sup>	4.05 × 10 <sup>-6</sup>

Putting the values of  $x$  in equation (22) and by using the method of successive approximations, the value of  $u$  is evaluated to be :

$$u = \frac{k_2}{k_1} = 0.52.$$

From equations (5) and (8), it has been found that  $k_1 = nk$ . Thus  $k_1$  was calculated with the help of the overall rate constant  $k$ . From a knowledge of  $k_1$  and  $u$ , the values of  $k_2$  were calculated. The values of the stepwise rate constants are given in Table IV. By using the calculated values of  $c$ ,  $k_1$  and  $k_2$ , overall rate constant  $k$  has been calculated at 65 °C. These calculated values of  $k$  compare well within experimental values (Table V) at the same temperature and different concentrations of alkali catalyst.

$k_1$  and  $k_2$  are the rate constants corresponding to the formation of intermediates monomethylol and dimethylol catechol, which could be used in laminates, surface coatings and adhesives etc.

This study clearly reveals various factors controlling the formation of mono and dimethylol intermediates. The investigation could, however, be extended to the formation of epoxyresins having outstanding property of binding metals, glasses and ceramics, by mixing bisphenols obtained by combination of catechol-formaldehyde with epichlorohydrin in presence of base. The present fundamental study, is therefore, likely to be of much significance in industry.

## ACKNOWLEDGEMENT

One of the authors (PSJ) is thankful to CAS, Department of Chemistry, University of Delhi, Delhi, for the award of a research fellowship.

## REFERENCES

1. A A Zavitsas *J Polymer Sci* **6**(1968) 2541
2. A G Ryabukhin *Vysokomol Soedin* **A11**(11) (1969) 2562
3. J I De Jong and J De Jong *Recl Trav Chem* **72** (1953) 497
4. T T Jones *J Soc Chem Ind* **65** (1946) 264
5. S R Finn and G J Lewis *J Soc Chem Ind* **69** (1950) 129
6. M M Sprung *J Am chem Soc* **63** (1941) 334
7. H C Malhotra and V K Gupta *J appl Polymer Sci* **22** (1978) 343
8. H C Malhotra and V P Tyagi *J macromol Sci Chem* **A16** (6) (1981) 1183
9. K Auwers *Ber* **40** (1907) 2524

## EFFECTS OF TEMPERATURE AND SOIL MOISTURE ON THE KINETICS OF PHOSPHATE FIXATION IN ALKALINE ALLUVIAL SOILS

P P BISWAS\* AND GEETANJALI GHOSH

Nuclear Research Laboratory, Indian Agricultural Research Institute,  
New Delhi-110 012, INDIA

(Communicated by S P Raychaudhuri, FNA)

(Received 3 July 1985)

An investigation on phosphate fixation in alkaline alluvial soils revealed that the amount of P recovered in Olsen's extractant declined sharply as the reaction temperature increased gradually from 5 to 45 °C. On the other hand, the variation in soil moisture levels between 1/3rd and 3 bar had little effect on phosphate fixation. The P fixing capacity, however, increased at a decreasing rate with the rise in soil fertilizer reaction time irrespective of the temperature and soil moisture treatments. A mathematical model in the following form was proposed to describe the phosphate fixation in soil :—

$$FF = \alpha D^\beta t^\gamma,$$

where  $FF$  = fraction P fixed,  $D$  = reaction time in days,  $t$  = temperature (°C)  
 $\alpha$ ,  $\beta$  and  $\gamma$  are coefficients.

The soil with higher  $\alpha$  value was found to be associated with lower temperature and rate coefficients. The model gave a reasonably good description of P fixation in soils and hence can be used to estimate long term availability of applied P at a given temperature under optimum soil moisture condition.

**Key Words :** Phosphate Fixation; Kinetics; Temperature; Soil Moisture;  
Alkaline Alluvial Soil

### INTRODUCTION

THE rate and extent of phosphate fixation in soil is of prime interest from the standpoint of long term fertilization practice. But due to the complexity of reaction process, it is very difficult to draw a generalised kinetic model for phosphate fixation from the results of a specific soil condition. However, in all the kinetic studies, a two stage process was observed—a fast initial reaction followed by a slower step.<sup>1-3</sup> The influence of some important extrinsic variables like soil moisture and temperature on phosphate reaction kinetics is also not well understood. Hence, the aim of this paper is to use a simple laboratory technique based on the established soil test method (olsen-P) for available P, to evaluate phosphate fixation in alkaline alluvial soils and from this to predict the residual value of added P under a given range of moisture and temperature variability.

\*Present Address : National Institute of Horticulture for Northern Plains, B-117, Indiranagar Lucknow-226 016.

## MATERIALS AND METHODS

Surface samples (0–15cm) from two alkaline soils (Typic Ustocrept) of different P status were collected from two blocks of Union Territory of Delhi *viz* Todapur and Alipur. The general characterization of the soils used was made by usual methods<sup>4</sup> and is presented in Table I.

TABLE I  
*General characteristics of the soils*

Soil	Textural Class	pH (1 : 2.5)	%O.C.	%Clay	CEC me/100 g	Olsen P (ppm)	Total P%	Free Fe <sub>2</sub> O <sub>3</sub> %	Free CaCO <sub>3</sub> %
Todapur	Sandy loam	8.2	0.34	15	8.32	3.25	0.04	0.60	Traces
Alipur	Sandy loam	8.0	0.86	13	13.57	8.56	0.09	0.25	0.85

The air-dried, ground soil samples were passed through 0.5mm sieve and incubated in polythene container for several days (7, 21, 35, 56 and 84 days) with 0, 50, 75, 100 and 125  $\mu\text{g P/g}$  of soil (added as a solution of DAP) under (i) for  $\gamma$  moisture levels corresponding to  $\frac{1}{3}$ ,  $\frac{1}{2}$ , 1 and 3 bar at 30 °C and (ii) four temperature treatments *viz* 5, 20, 30 and 45 °C with a moisture level equivalent to 1/3 bar moisture tension. The tops of the containers were covered with fully stretched perforated polythene sheet to facilitate aeration. The loss of soil moisture was replenished as and when required by the addition of distilled water. After the lapse of each incubation period, the availability of P was determined according to the extraction procedure given by Olsen *et al.*

## RESULTS AND DISCUSSION

The results pertaining to P fixing capacity (fraction fixed, FF) of the soils at different treatment combinations were given in Tables II and III. The values of FF *i.e.* the proportion of the added P which is not extractable in Olsen's reagent was calculated from the slope (Fractional recovery, FR) of the linear regression equation relating absolute quantity of P recovered to P added ( $r^2$  value in each case was significant at 0.01 level), using the relationship  $FF = 1 - FR$ .<sup>3</sup> It was noted that the fixation of phosphorus increased with increase in soil fertilizer reaction time and with rise in temperature (Table II which corroborates the findings reported by other workers.<sup>6-8</sup> The amount of P recovered declined sharply as the reaction temperature increased gradually from 5 to 45 °C. The values ranged from 0.61 at 5 °C to 74 at 45 °C with 7 days of incubation and 0.77 to 0.87 after 84 days in Todapur soil. Such figures for Alipur soil were 0.39 to 0.66 and 0.55 to 0.81 respectively. At higher temperature, the P fixing capacity

TABLE II

*Fraction P fixed (FF) at different incubation time and temperature in two soils*

Tempera- ture (°C)	Todapur Soil			Incubation time in days			Alipur Soil			
	7	21	35	56	84	7	21	35	56	84
5	0.61	0.66	0.70	0.73	0.77	0.39	0.41	0.46	0.52	0.55
20	0.68	0.70	0.72	0.77	0.79	0.42	0.45	0.54	0.58	0.61
30	0.71	0.76	0.78	0.81	0.82	0.53	0.57	0.65	0.70	0.72
45	0.74	0.77	0.84	0.86	0.87	0.66	0.71	0.75	0.81	0.81

beyond 56 days did not vary appreciably indicating the rapid attainment of equilibrium due to faster rate of fixation under such situation.

A rise in P fixation with the increase in duration of contact between fertilizer and soil could be explained from the viewpoint of formation of relatively stable reaction products as time progressed. The slower rate of fixation at lower temperature may be the result of reduced reaction velocity as shown by Arrhenius equation.<sup>9</sup> Robinson<sup>10</sup> suggested that the slower mobility of phosphate ions towards P sorbing sites reduces the extent of P fixation considerably. A lower temperature could also cause the equilibrium between fertilizer and reaction products to shift in the direction of exothermic reaction where heat is evolved and  $\Delta H$  is negative.<sup>9</sup> It is thus expected that such a shift in equilibrium may favour the formation of reaction products which are more available. Moreover, the temperature may influence the availability of reaction products by altering the crystal size and consequently the specific surface of these products. The rate of crystal growth of a number of compounds has been found to decrease with fall in temperature.<sup>11</sup>

From a perusal of Table III, a slight increase in P fixation with rise in soil water content from 3 to 1 bar tension was observed for both the soils throughout the incubation period tried. Further rise in soil water contents above 1 bar had little effect on P fixation as was also reported by Sharpley and Ahuja.<sup>12</sup> The reduced P fixation at lower moisture may result from a fall in the rate of P diffusion to fixation sites<sup>13</sup> or from a reduction in the amount of P sorbing complexes such as

TABLE III

*Fraction P fixed (FF) at different incubation time and soil moisture levels in two soils*

Soil moisture (Bar)	Todapur Soil			Incubation time in days			Alipur Soil			
	7	21	35	56	84	7	21	35	56	84
1/3	0.71	0.76	0.78	0.81	0.82	0.53	0.57	0.65	0.70	0.72
1/2	0.73	0.77	0.77	0.83	0.82	0.52	0.62	0.66	0.71	0.74
1	0.73	0.75	0.77	0.79	0.82	0.50	0.56	0.61	0.69	0.73
3	0.68	0.73	0.76	0.78	0.79	0.46	0.51	0.55	0.62	0.68

amorphous Fe and Al hydroxides and Ca, precipitated at lower soil water content as was suggested by Sharpley and Ahuja.<sup>12</sup>

Overall appraisal of the results indicated that P fixation was markedly affected by the temperature treatments. The water content within the upper available soil moisture range (1/3 to 3 bar) had little effect on the P fixing capacity of the soil. Therefore, attempt was made to incorporate the effect of time and temperature in one expression to predict the P fixing capacity of the soil from the following proposed mathematical model :

$$FF = \alpha D^\beta t^\gamma, \quad \dots(1)$$

where  $D$  in the reaction time (in days),  $t$  is the temperature in °C, and  $\alpha$ ,  $\beta$  and  $\gamma$  are co-efficients. The values of  $FF$ ,  $D$  and  $t$  were fitted into equation (i) in a manner similar to that for fitting a multiple regression equation after logarithm transforation to estimate the values of different coefficients for each soil.

From a perusal of the coefficients given in Table IV, it appeared that the soil with higher value of  $\alpha$  (amount fixed after 1 day at 1 °C) had comparatively lower rate and temperature coefficients ( $\beta$  and  $\gamma$ , respectively) than the soil of smaller  $\alpha$  value. This seemed that higher the value of  $\alpha$ , the slower will be the subsequent rise in phosphate fixation with the increase in reaction time and temperature. In Todarpur soil, the values of  $\beta$  and  $\gamma$  were found to be more or less same indicating that the extent of variation in P fixation caused by the two factors viz., reaction time and temperature were equal. On the contrary, in low P fixing Alipur soil, the temperature showed somewhat greater influence than the reaction time on P fixation as seen from higher values of  $\gamma$  than  $\beta$ . The model also suggested that the rate of P fixation is inversely related with time ( $\beta < 1$ ).

TABLE IV

*Calculated coefficients ( $\alpha$ ,  $\beta$  and  $\gamma$ ) of the model of phosphate fixation  
( $FF = \alpha D^\beta t^\gamma$ ) in two soils*

Soil	$\alpha$	$\beta$	$\gamma$
Todapur	0.48	0.071	0.073
Alipur	0.20	0.133	0.201

$FF$  = fraction P fixed;  $D$  = reaction time in days;  $t$  = temperature in °C

The ratios of the predicted  $FF$  and observed  $FF$  values at different time-temperature treatment combinations for both the soils have been presented in Table V. The ratios did not deviate appreciably from unity which implied the close resemblance between observed and predicted  $FF$  values. A highly non significant 't' test (at 1 per cent level of significance) between the experimental results and those predicted from the model also indicated that the model satisfactorily described the P fixing ability of the soils and thereby can be used to calculate

TABLE V  
*Ratios between the predicted and observed FF values for two soils under different time and temperature treatments*

Temperature (°C)	7	21	Incubation time in days		
			35	56	84
5	1.02 (0.92)	0.99 (1.02)	0.99 (0.98)	0.99 (0.92)	1.04 (0.93)
20	1.00 (1.14)	1.06 (1.24)	1.06 (1.11)	1.03 (1.10)	1.04 (1.10)
30	0.99 (0.98)	1.00 (1.05)	1.01 (1.00)	1.01 (0.99)	1.02 (1.01)
45	0.99 (0.86)	1.03 (0.93)	0.96 (0.93)	0.98 (0.93)	1.00 (0.98)

Values within brackets are for Alipur soil

the residual value of added phosphorus as the product of  $(1 - \widehat{FF})$  and the amount of P added at any particular time and temperature under adequate soil moisture level. In addition, it appears that the coefficients  $\alpha$ ,  $\beta$  and  $\gamma$  may be useful to characterise the P fixation in different soils.

#### REFERENCES

1. G E C Mattingly *Tech Bull* **20** Ministry of Agriculture, Fisheries & Food, London (1971) 16
2. J N Barrow *Soil Sci* **118** (1974) 380-386
3. O Ayodele and A A Agboola *Soil Sci Soc Am J* **45** (1981) 462-464
4. M L Jackson *Soil Chemical Analysis* Prentice Hall of India Pvt Ltd New Delhi (1967)
5. S R Olsen C V Cate F S Watanabe and L A Dean *Estimation of Available Phosphorus and with Sodium Biocarbonate* US Department of Agriculture Circular (1954) 939
6. J N Barrow and T C Shaw *Soil Sci* **119** (1975) 190-197
7. S K Sanyal and D L Deb *J nucl agric Biol* **5** (1976) 54-60
8. M Velayutham and M N Court *Indian Soc Soil Sci Bull* **12** (1979) 305-311
9. S Glasstone *Text Book of Physical Chemistry* D Van Nostrand Company Inc New York Edn 2 (1954)
10. R R Robinson *J Am Soc Agron* **34** (1942) 301-306
11. A van Hook *Am Chem Soc Monogr* No 152 Reinhold Publishing Corp New York (1961)
12. A N Sharpley and L R Ahuja *Soil Sci* **133** (1982) 350-355
13. K Lawton and J A Vomocil *Proc Soil Sci Soc Am* **18** (1954) 26-32

## AN APPRAISAL OF THE MANGANESE ORE DEPOSITS OF GOA, INDIA

A G DESSAI

*Department of Geology, University of Poona, Pune-411 007, INDIA*

(Received 18 March 1985)

The manganese ore deposits of Goa are associated with the metasediments of the Precambrian Dharwar Supergroup. They are localised in highly weathered phyllites and occur as pockets in the lateritised portions, in the fracture and shear zones in the phyllites, in the lithomarge below them and also with a zone of powdery ore below the lithomarge. The powdery ore, at places grades downwards into hard and compact massive ore, occurring as lenses in the phyllites.

Microscopic examination, G. T. A., D. T. A. and X-ray diffraction studies of the ores reveal the presence of braunite, jacobsite, psilomelane, pyrolusite, manganite and nsutite as the main constituents. Of these braunite and jacobsite represent the original metamorphosed ores whereas the other minerals are supergene alteration products.

**Key Words :** Manganese Ores of Goa; Metasediments; Precambrian Dharwar Supergroup; Phyllites; Lithomarge; Braunite; Jacobsite; Psilomelane; Pyrolusite Manganite; Nsutite.

### INTRODUCTION

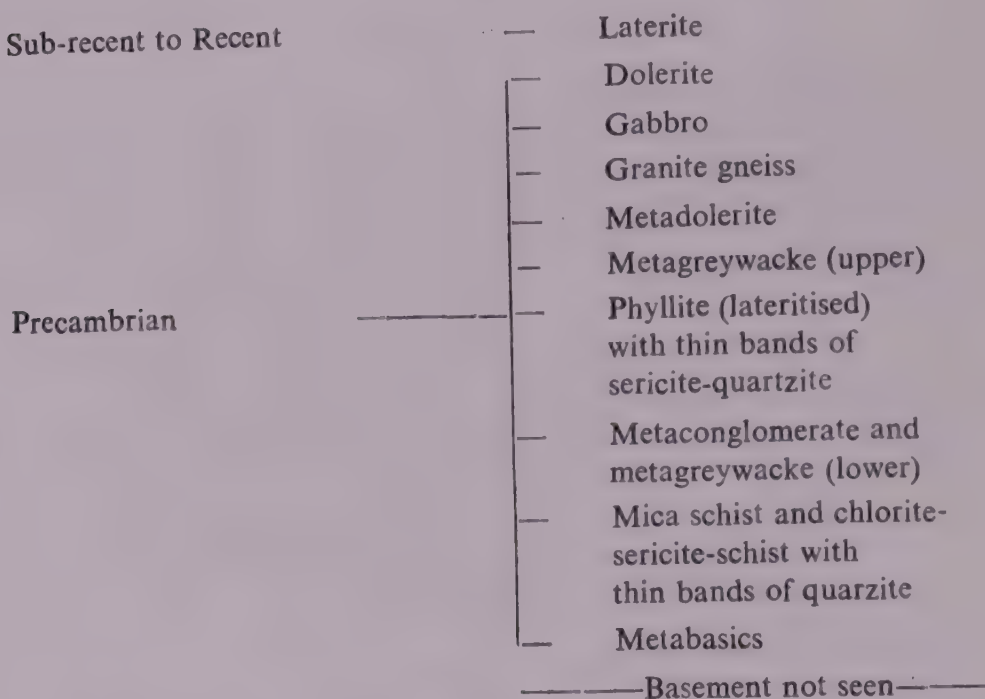
THE manganese ore deposits of Goa that have been exploited for over four decades, are mainly located in the southeastern part of the territory with some sporadic occurrences located in the northern and central Goa (Fig. 1). Though the deposits were being exploited since a very long time they remained academically neglected for quite sometime. Recently, these deposits were investigated with regard to their geological setting, mode of occurrence controls of ore localisation and mineralogy.<sup>1-3</sup> In the present paper, a genetic model for these deposits, has been proposed in the light of some recent findings.

### GEOLOGICAL SETTING

The southern part of the territory of Goa, forms a part of the Indian Peninsular shield which is predominantly occupied by the granite gneisses and schistose rocks. The former were referred to as Basement Complex whereas the latter were called ancient schistose formations by Fermor,<sup>4</sup> and constitute the Precambrian Dharwar Supergroup. The earliest reference to the geology of the area is by Foote<sup>5</sup> who assigned the rocks exposed in the area to the Dharwar System. Later, Maclarens<sup>6</sup> gave the name 'Castle Rock Band' to the schistose rocks of Goa. Subsequently, the area was studied by Fermor<sup>7</sup> and Dunn<sup>8</sup> and a summary of their work is given by Pascoe.<sup>9</sup> Gokulam<sup>10</sup> studied the area particularly to investigate the iron ore deposits.

The mineralogy of the iron ores has been studied by Majumdar<sup>11</sup> and Dessai.<sup>12</sup> Recently, the mineralogy of the manganese ore deposits was investigated by Dessai and Deshpande.<sup>13</sup>

Field investigations, assisted by the study of aerial photographs, have shown that the following generalised stratigraphic succession is present in the area:



The metabasics are the ultrabasic and basic lava flows which have been metamorphosed to give rise to serpentinites and serpentine-tremolite-schists.<sup>14</sup> The pelitic schists have, on the basis of the predominant mineral constituents, been classified as mica-schists and chlorite-sericite-schists. They are overlain by the metaconglomerates which contain ellipsoidal pebbles of quartzite in a matrix of chlorite and quartz. They grade into metagreywacke with coarse grained fragments of quartz in a fine grained chloritic matrix.

The area is structurally very complex since two or three tectonic episodes have been superimposed on one another. Interpretation of aerial photos on 1:60,000 scale indicates that the rock formations have been folded into plunging anticlines and synclines with their axes trending almost N-S. They have also suffered deformation during a second episode which has resulted in cross folds with axes trending almost E-W. A complicated pattern of joints, fractures and shear zones, as observed in the field and on the aerial photographs was produced during these tectonic disturbances. A lineament map of the area prepared from aerial photointerpretation is presented in Fig. 2. Ground truth collection has shown that the lineaments in general correspond to the direction of shear and fracture zones or strike of the phyllites.<sup>15,16</sup>

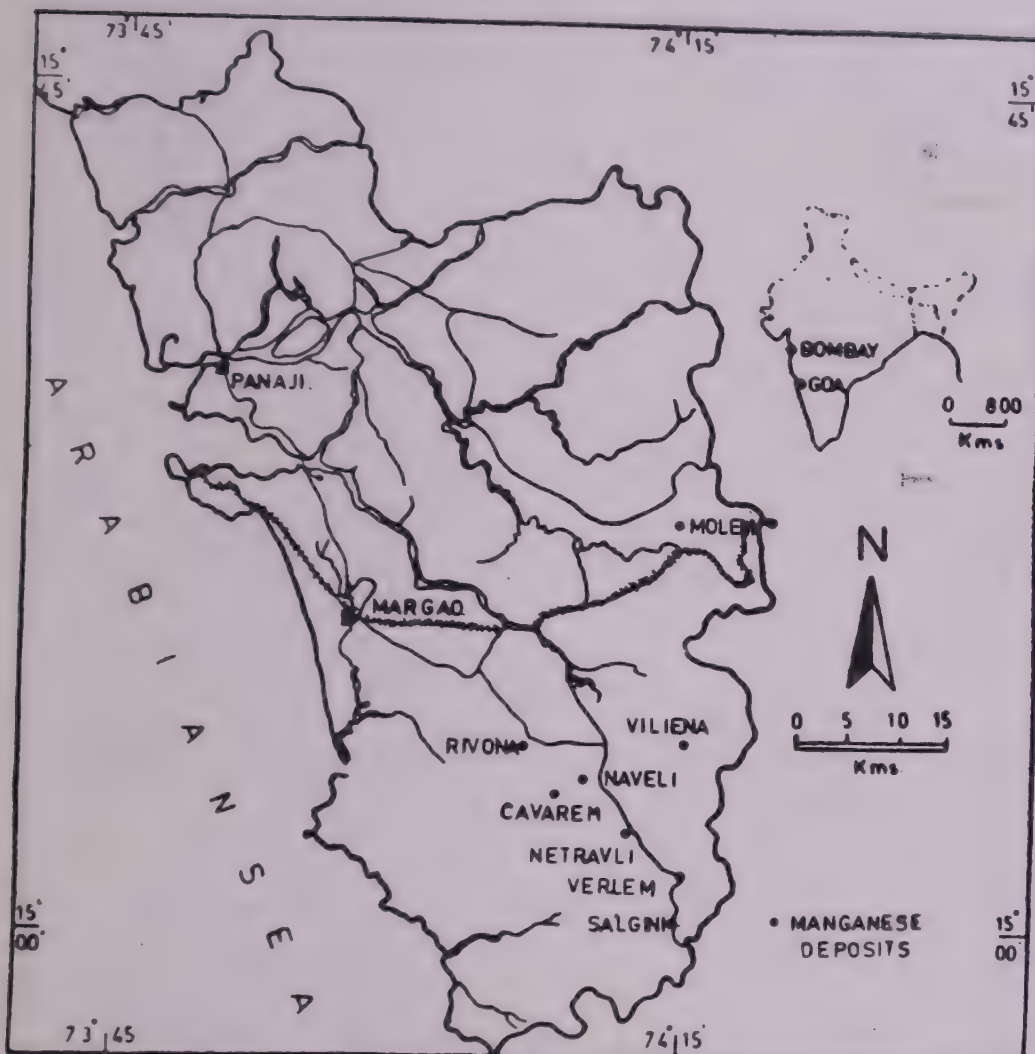


FIG 1 Map showing locations of manganese ore deposits from Goa.

#### MODE OF OCCURRENCE OF THE MANGANESE ORE DEPOSITS

The manganese ore deposits in the area are entirely restricted to phyllites which have been extensively laterised. The ore is found as boulders and concretions or as pockets and lenses of varying dimensions in the lateritised phyllites. In some cases, below the laterite zone, highly weathered phyllites are seen. These have sometimes retained their folded character even after their alteration to lithomarge. The crests of the anticlines of such folds show the presence of manganese ore, usually concretionary, occupying the highly brecciated portions. The zone of lithomarge is followed downward by a zone of wad of varying thickness and this at depth usually grades into a zone of powdery ore. A parent rock rich in manganese is rarely seen below the zone of powdery ore. In other cases, the country rock is traversed by shear zones and the ore is found in the crushed, fractured and brecciated portions looking very much similar to a breccia with angular fragments of chert bound together by the manganese oxides.

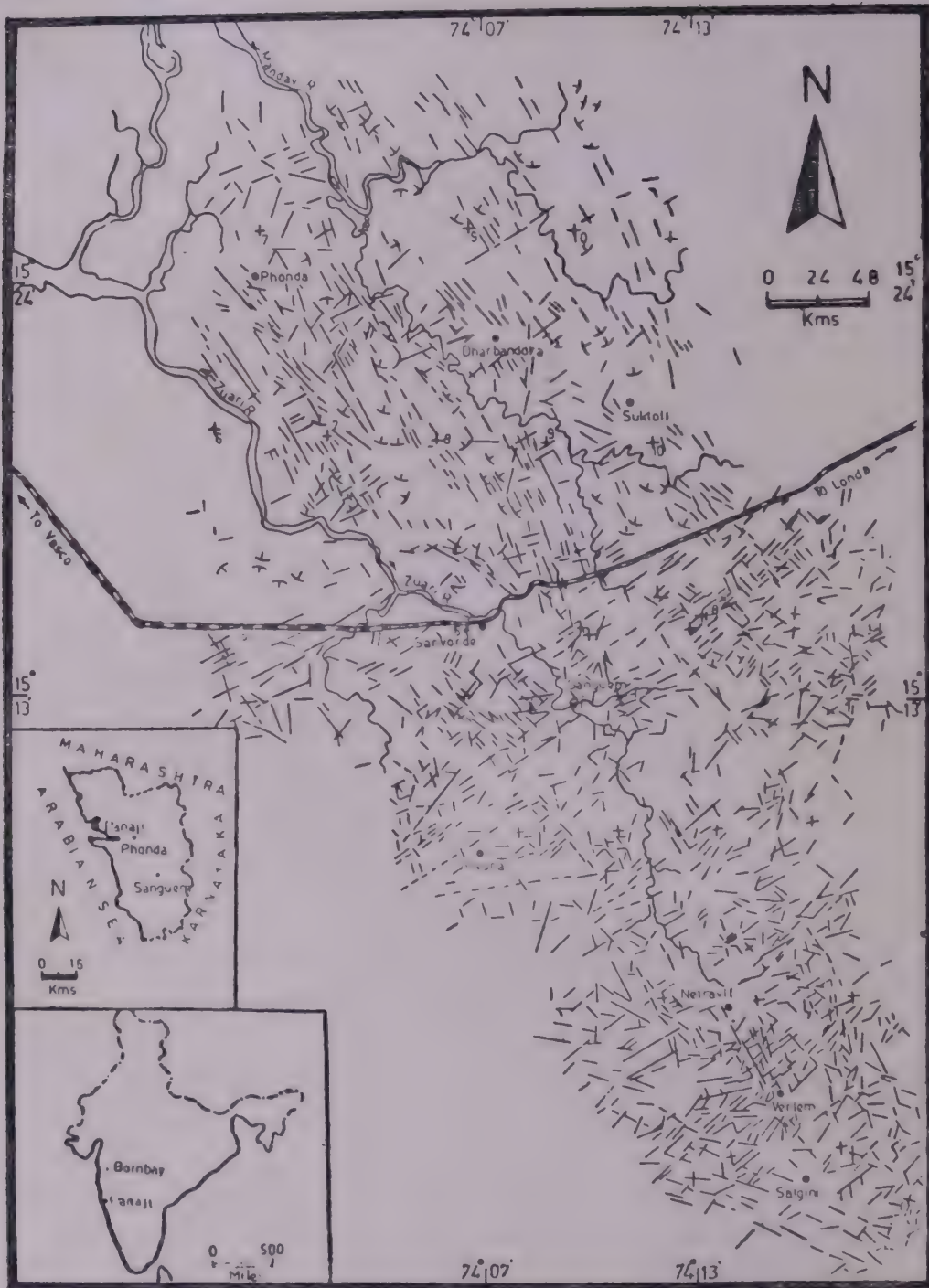


FIG 2 Lineament map of part of Goa based on aerial photointerpretation.

#### CONTROLS OF LOCALISATION

From the above description it will be clear that the manganese ore deposits are confined to certain environments. These environments have thus acted as controls of localisation for these deposits. One feature that is common to all the three types of deposits is that they all occur in phyllites. The lateritoid deposits<sup>7</sup> are followed

in depth either by secondary deposits in the fracture and shear zones or by wad or by a zone of powdery ore<sup>3</sup>. This indicates that their localisation is controlled by either the shear zones or the presence of wad or powdery ore at depth. It is found that many of the mining pits that are being worked for the ore, when plotted on the lineament map are aligned in a direction which is either parallel to the shear zone or to the strike of the phyllites.

Some of the ore in the zone of lithomarge is found to be present in the fracture or shear zones forming breccia-type deposits, while at other times manganese ore is deposited in the fractured regions along the crests of the plunging anticlines giving rise to breccia-pipe-like bodies.

The powdery ore zone is rarely seen to grade into manganiferous phyllite or protore. These zones are much longer than they are wide, extend laterally parallel to the strike of the rocks and taper at both ends. It may therefore, be suggested that the localization of powdery ore zone is controlled by the presence of bands or lenses of the protore below it.

#### STRUCTURES AND TEXTURES

Manganese ores, from different environments, show concretionary, botryoidal, mammillary, stalactitic, box work, banded, columnar and brecciated textures in hand specimen. All the three types of textures like open space filling textures, colloidal textures and replacement textures<sup>17-19</sup> are shown by the deposits. Open space filling textures include crustification, cockade or ring structure, comb structure, fracture and pore fillings and cataclastic structure. In colloidal textures are found colloform texture (Plate I, Fig. 1), rotund or spheroidal bodies, pellet texture (Plate I, Fig. 2), and shrinkage cracks (Plate I, Fig. 3). The replacement textures include diffused penetration and selective replacement (Plate I, Fig. 4).

#### MINERALOGY AND PARAGENESIS

Microscopic examination of the ores revealed the presence of braunite, jacobsite, psilomelane, pyrolusite, manganite and nsutite as the main manganese ore minerals and goethite and quartz as the gangue minerals.

The primary minerals, braunite and jacobsite, are found to have been replaced by psilomelane. The secondary mineral pyrolusite occurs as tabular crystals or as needles replacing psilomelane and manganite. The coarse grained crystals of pyrolusite show fracturing due to chemical brecciation.<sup>20</sup> Manganite occurs as metacrysts or well-developed prismatic crystals with pyramidal terminations, sometimes forming a stellate arrangement, replacing pyrolusite. It is also found replaced by younger pyrolusite. Nsutite consists of fine dusty looking aggregates or folted masses of fine delicate needles. It is seen to replace psilomelane, pyrolusite and manganite. Sometimes veins of nsutite traverse rock fragments which are enclosed in the base of nsutite. Goethite usually occurs as a constituent of colloform bands

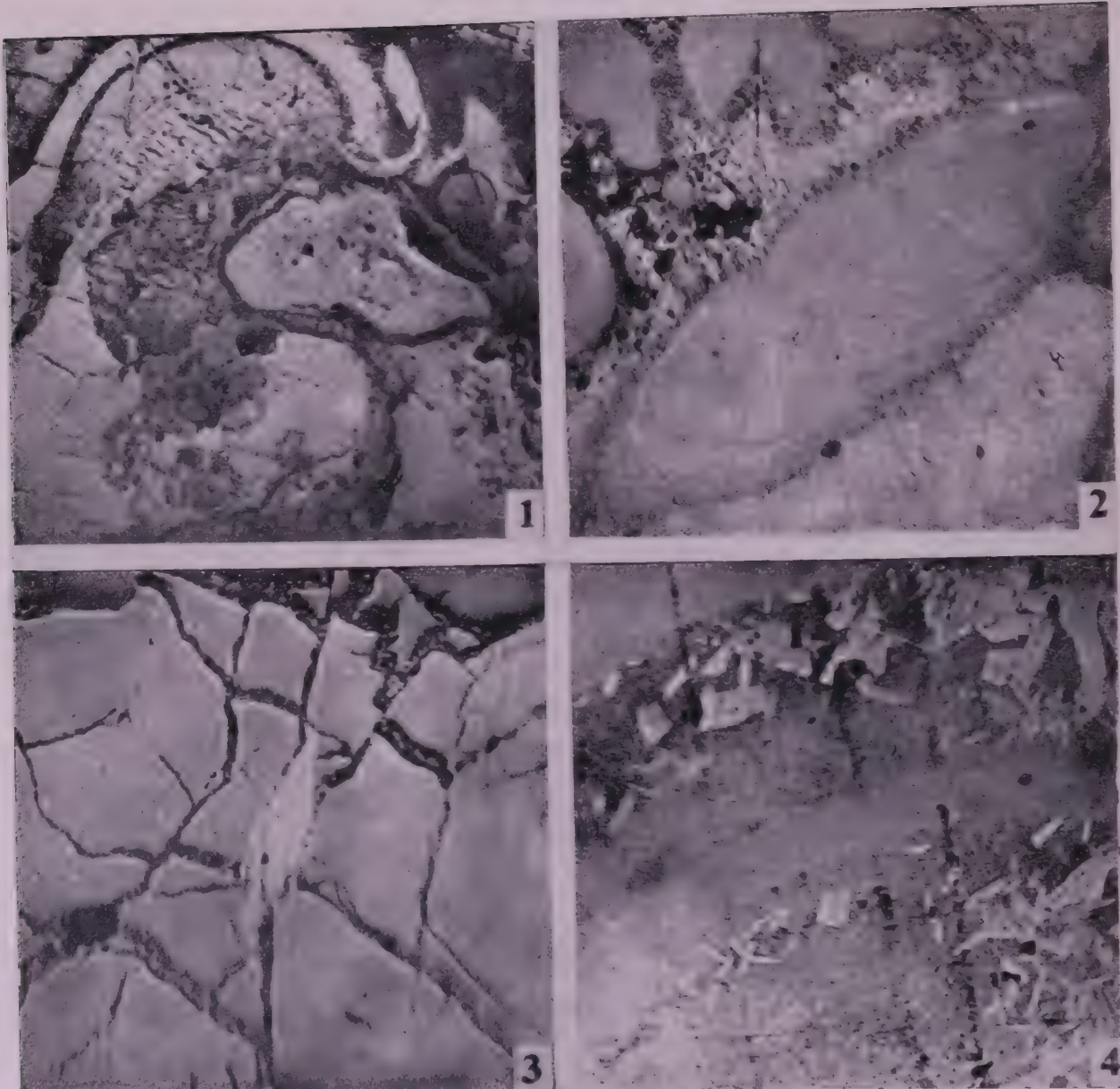


## PLATE I

FIG 1 A reniform body showing colloform banding. The bands are made up of pyrolusite (light grey), quartz (dark) and goethite (grey). X 60

The central portion of the cavity is occupied by quartz and goethite. Radiating cracks are formed by syneresis. X 55.

FIG 2 Ellipsoidal pellets of psilomelane with partial development of inner bands. They show replacement from outside by nsutite. X 60.

FIG 3 Shrinkage cracks in psilomelane formed due to dehydration. X 45.

FIG 4 Selective replacement of bands of pyrolusite (dusty grey) by tabular crystals of manganite. X70.

while quartz is found as a member of colloform bands as well as a fracture filling mineral.

These ore minerals belong to two different phases of mineralization. The older phase is represented by the primary deposits or protore (metamorphosed), found below the zone of powdery ore. The protore is represented by a richly manganeseiferous phyllite containing braunite and jacobsite. These two have been subsequently replaced by psilomelane. The second phase is represented by secondary deposits constituting the ores in the powdery ore zone, breccia zone and laterite zone. The breccia zone deposits are formed mostly by cavity filling in different phases of mineralisation separated from one another by intermineralisation fracturing.

The paragenetic sequence of the minerals, deciphered on the basis of their mutual relationship, is as follows:—

	Metamorphic	Supergene and Colloidal
Braunite	—	
Jacobsite	—	
Quartz	—	—
Psilomelane	—	
Goethite	—	
Pyrolusite—I	—	
Manganite		—
Nsutite		—
Pyrolusite-II	—	

#### GTA, DTA, X-RAY AND CHEMICAL ANALYSIS

The manganese ores were subjected to gravimetric and differential thermal analyses. The curves obtained from these studies indicated major endothermic peaks between 300 and 400 °C, 600 and 700 °C, 800 and 900 °C and 900 and 1000 °C. On comparing these curves with those published in the literature<sup>21-30</sup> the manganese minerals are identified as manganite, pyrolusite, psilomelane and cryptomelane or their mixtures.<sup>31</sup>

Powder X-ray diffraction analysis of some of the samples confirmed the presence of manganite, pyrolusite, psilomelane, cryptomelane and nsutite.

The manganese ore samples from all the three zones, i.e. lateritic zone, shear and fracture zone and powdery ore zones were subjected to chemical analysis. These analyses (Table I) show that the maximum MnO<sub>2</sub> is in the ores from the lateritic zone and minimum in the ores from the breccia zone, while the silica content is higher in the breccia zone than in the other two zones. The phosphorus content is very low in the ores from all the three zones. Some samples of manganese ore have also been analysed for minor elements. Ni varies between 500 and 675 ppm, Co varies between 250 and 350 ppm while Cr, Pb, Zn and Ag are present in traces only.

#### GENESIS

In proposing a genetic model for these deposits certain characteristic features of the deposits should be considered. The deposits are localised within phyllites which

TABLE I  
*Chemical analyses of the manganese ores from Goa, India*

	MnO <sub>2</sub>	MnO	Fe <sub>2</sub> O <sub>3</sub>	SiO <sub>3</sub>	Al <sub>2</sub> O <sub>3</sub>	TiO <sub>4</sub>	CaO	MgO	P <sub>2</sub> O <sub>5</sub>	Loss on ignition	Total	Total Mn
1	98.02	—	0.62	0.07	0.10	0.02	—	—	0.02	0.32	99.17	61.93
2	88.11	2.3	3.2	0.32	1.34	0.03	0.07	0.03	0.01	4.45	99.86	57.45
3	72.46	1.8	8.68	3.65	3.23	0.03	0.06	0.01	0.21	9.46	99.59	47.17
4	72.01	1.85	6.81	2.19	4.37	0.03	0.05	0.03	0.02	12.00	99.36	46.93
5	76.25	1.52	7.65	1.45	1.23	0.06	0.06	0.05	0.19	11.40	99.86	49.35
6	50.10	1.80	13.10	24.80	1.20	0.07	0.10	0.06	0.08	8.40	99.71	33.04
7	65.49	1.64	2.84	10.64	2.80	0.03	0.08	0.05	0.13	16.58	100.28	47.65
8	69.62	1.72	5.82	5.48	1.94	0.02	0.06	0.04	0.12	15.98	100.80	45.32
9	76.88	1.50	9.70	2.40	0.82	0.08	0.08	0.03	0.12	7.98	99.60	49.73
10	71.70	1.58	14.21	2.65	0.87	0.07	0.08	0.04	0.09	8.60	99.89	46.52
11	75.62	1.68	9.68	2.33	0.41	0.04	—	—	0.14	9.68	99.76	48.78
12	73.23	1.14	11.48	2.20	2.44	—	0.06	0.04	—	9.30	99.89	47.15
13	73.11	1.98	9.46	1.23	5.00	0.11	0.08	0.03	0.51	9.32	100.83	47.72
14	71.26	2.38	9.31	2.35	2.65	0.03	0.08	0.01	0.12	11.58	99.17	47.86
15	70.32	1.49	11.62	1.82	3.26	0.05	0.04	0.04	0.18	10.94	99.76	45.58

Samples 1 to 5 Laterite zone

Samples 6 to 10 breccia zone

Samples 11 to 15 powdery zone

are lateritised to a depth of more than 100m from the surface. They occur within laterite but are found only in certain regions. The laterite duricrust is followed at depth by a zone of saprolite in which manganese ore is confined to shear zones traversing it or along the crests of the antiformal structures. The saprolites grade into a zone of wad which in turn grades into a zone of powdery ore. The latter extends parallel to the strike of the phyllites. The ore bodies extend parallel to the strike and extend along the dip of the phyllites. The ores in the laterite and the fracture zones show open-space-filling colloidal structures whereas those in the zones of wad and powdery ore exhibit replacement textures. The zone of powdery ore grades into a dull, black, hard and compact maganiferous phyllite.

In his classic work on the manganese ore deposits of India, Fermor<sup>7</sup> suggested that the Goa deposits were formed by residual concentration during the process of lateritisation, the manganese being derived from the phyllites in which it was disseminated. Had this been the case, the deposits should have been present throughout the lateritised region. Roy<sup>32</sup> agreed with Fermor<sup>7</sup> and suggested that in the absence of manganese silicates and sulphides below the supergene concentrations, the manganese must have been supplied by phyllites in which it was disseminated. However, the present study has shown that manganese-rich protores do exist in the form of lenses within the phyllites. Such lenses are made up of metamorphic minerals such as braunite and jacobsite. They have the same attitude as the phyllites and exist at different levels with respect to the erosional surface. On weathering the protore will be subjected to the process of supergene enrichment by *in situ* oxidation and residual concentration. This is in agreement with the observations made by Straczek<sup>33</sup> and Mahadevan and Krishna Rao<sup>34</sup> respectively in the case of gondite and kodurite type deposits. From the thickness of saprolite it is seen that the process of lateritisation has operated for more than 100 metres. The process of lateritisation indicates alternating wet and dry seasons during which the ground water table fluctuated. Due to such fluctuations the protore will be oxidised and will become porous in the capillary zone of the zone of aeration and suspended water above the water table (Fig. 3).

It is possible to visualise the environmental conditions leading to the decomposition of protore from a study of abrasion pH measurements which appear to approach equilibrium conditions. The abrasion pH of fresh phyllite rich in chlorite or sericite is in the range of 7 to 8. As the phyllite alters to saprolite containing kaolinite as the dominant mineral<sup>35</sup> the abrasion pH value is around 5. Under high pH conditions, mica undergoes disilication with the formation of kaolinite<sup>36</sup> in well drained near surface environments. As weathering progresses the percentage of kaolinite in the lithorelicts increases. Kaolinite acts as an acid in the weathering system and therefore abrasion pH decreases from 8 in fresh rock to 5 in the saprolite zone. The abrasion pH also increases with depth in the weathered profile. In the top horizon of the saprolite the pH is about 5 and increases downwards reaching a value between 7 and 8 in slightly weathered phyllites due to predominance of mica or chlorite. Under low pH conditions manganese is taken into solution and the same is precipitated in environments of high pH.

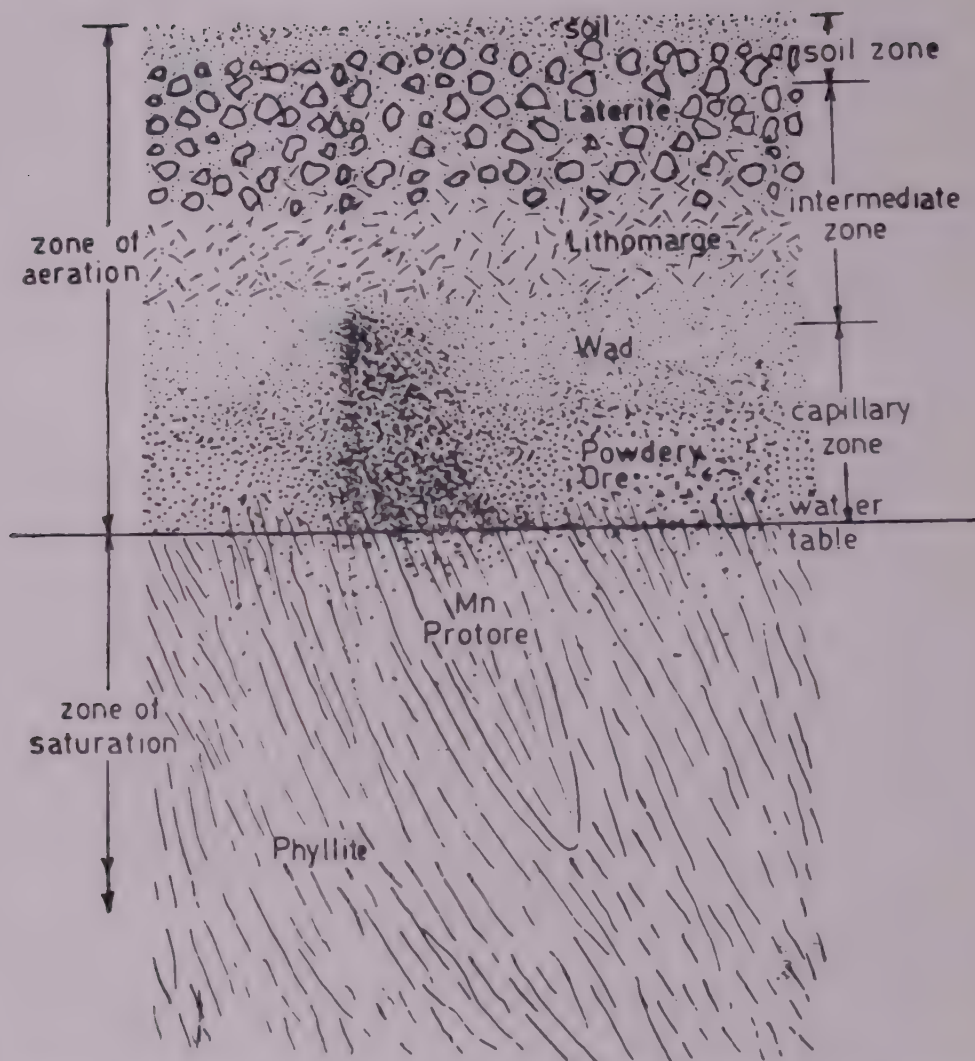


FIG 3 Schematic section showing a lense of manganese protore within phyllite. The protore undergoes enrichment during lateritisation.

Due to seasonal fluctuations of the ground water table the Eh and pH of waters will vary. In dry season the waters are acidic with low Eh and therefore manganese from the protore will be dissolved. During the following wet season, addition of fresh waters of higher Eh and pH will bring about precipitation of manganese within saprolites giving rise to wad. Thus wad will continue thickening during alternating wet and dry seasons, and the zone of powdery ore will extend downwards.

Wherever the phyllites are traversed by fracture zones, the manganese in solution will be deposited in cavities to give rise to open-space-filling deposits.<sup>37</sup> The ores in such cases show banded structures and intermineralisation fracturing and fracture filling by manganese oxide, goethite or quartz. Thus the solutions came up in pulses and deposited the different ore minerals. At places where such mineralised fracture zones are exposed at the surface residual concentration along such

zones would give deposits in the zone of laterite. The collomorphic structures exhibited by the ore minerals indicate their deposition in colloidal state at low temperature. The other possibility as pointed out by Herzenberg<sup>38</sup> is that waters carrying manganese may have changed from solution at depth to colloidal solutions in near surface environments.

### CONCLUSIONS

The manganese ore deposits of Goa have been derived as a result of secondary enrichment of manganese-rich protores that are found as lenses within the phyllites. The ores are found as pockets within laterite, in the fracture and shear zones in the saprolites below the laterite and as a zone of powdery ore below the lithomarge. The powdery ore zone at places grades into manganese-rich protore.

The deposits have resulted by (i) residual concentration of manganese protores in the zone of laterite (ii) oxidation, secondary enrichment and replacement of lithomarge giving rise to zones of wad and powdery ore and (iii) by open-space-filling in fracture and shear zones.

### ACKNOWLEDGEMENTS

Thanks are due to the Head, Department of Geology, University of Poona for laboratory facilities.

### REFERENCES

- 1 G G Deshpande and A G Dessai *Curr Sci* **46** (1977) 523-524
- 2 G G Deshpande and A G Dessai *Berg Huttenmann Monatsh* **123** (1978) 466-468
- 3 A G Dessai and G G Deshpande *Geoviews* **5** (1979) 21-22
- 4 L L Fermor *Mem geol Surv India* **70** (1936) 68
- 5 R B Foote *Mem geol Surv India* **12** (1876)
- 6 J M Maclarem *Geol Surv Ind Rec* **34** (1904) 96-131
- 7 L L Fermor *Mem geol Surv India* **37** (1909)
- 8 J A Dunn *Rec geol Surv India* **76** (1942) 1-53
- 9 E H Pascoe *A Manual of Geology of India and Burma* Govt of India New Delhi **1** (1965) 485
- 10 A R Gokulam *Bull geol Surv India* **37** (1972) 1-186
- 11 A K Majumdar *Min Wealth* **1** (1965) 14-20
- 12 A G Dessai *J Min metal Fuel* **28** (1981) 166-69
- 13 A G Dessai and G G Deshpande *Recent Res Geol* **5** (1978) 271-283
- 14 A G Dessai and G G Deshpande *N Jp Miner Aph* **135** (1979) 209-220
- 15 A G Dessai and G G Deshpande *Proc Symp Remote Sensing for Hydrology, Agriculture and Mineral Resources* (1977) 157-159
- 16 A G Dessai and V V Peshwa In : *Hidden Wealth : Mineral Exploration Techniques in Tropical Forest Areas* Association of Geoscientists for International Development (Eds D J C Laming and A K Gribbs) (1982) 170-175
- 17 E S Bastin *Mem geol Soc Am* **45** (1950) 1-101
- 18 P Ramdohr *Proc Symp Manganese 20th int. geol Congr Mexico* (1956) 19-73
- 19 P Ramdohr *The Ore Minerals and their Intergrowths* Pergamon Press London (1969) 1174
- 20 F J Sawkins *Econ Geol* **64** (1968) 613-617

- 21 J L Kulp and J N Perfetti *Min Mag* **29** (1950) 239-251
- 22 B L Sreenivas *Min Mag* **31** (1957) 605-606
- 23 S Kilpadi and G G Deshpande *J Univ Geol Soc Nagpur* **1** (1958) 9-11
- 24 M Fleischer *Am Miner* **45** (1960) 176-187
- 25 M Fleischer W E Richmond and H T Evans Jr *Am Miner* **47** (1962) 4758
- 26 W K Zwicker W O J Groeneveld Meijer and H W Jaffe *Am Miner* **47** (1962) 246-266
- 27 C Naganna *Proc Indian Acad Sci* **58** (1963) 16-28
- 28 L S Dent Glasser and I B Smith *Min Mag* **35** (1964) 327-334
- 29 D R Das Gupta *Min Mag* **35** (1965) 131-319
- 30 M J Wilson M L Berrow and W J McHardy *Min Mag* **37** (1970) 618-623
- 31 A G Dessai and G G Deshpande *Min Metal Fuels* **26** (1978) 193-196
- 32 S Roy *Econ Geol* **63** (1968) 760-786
- 33 J A Straczek *Proc Symp Manganese 20th int geol Congr Mexico* **4** (1956) 63-96
- 34 C Mahadevan and J S R Krishna Rao *Proc Symp Manganese 20th int geol Congr Mexico* **4** (1956) 134-138
- 35 A G Dessai *J geol Soc India* **25** (1984) 598-603
- 36 S A Norton *Econ Geol* **68** (1973) 353-361
- 37 H L James C E Dutton F J Pettijohn and K L Wier *US geol Surv Prof Pap* **570** (1968) 1-134
- 38 E Herzenberg *Econ Geol* **31** (1936) 761-766

## PRECAMBRIAN OF INDIA—POSSIBLE SOURCE OF EVIDENCE FOR EARLY LIFE

VIVEK NAVALE, RAMACHANDRAN SURESH and CYRIL PONNAMPERUMA, FNA

*Laboratory of Chemical Evolution, University of Maryland,  
College Park, Maryland 20742, USA*

(Received 19 February 1985; after revision 2 December 1985)

When did life begin? This question is of fundamental importance in the study of terrestrial evolution. An interdisciplinary approach to the problem has highlighted the relationship between the development of the earth and the evolution of its biosphere. The presence of molecular fossils in the ancient rocks can provide valuable information about the origin and early evolution of life. Investigations carried out in many parts of the world have provided strong evidence for morphological and chemical forms of life from the various time planes of the Precambrian period.

India provides a unique opportunity for further studies as it is easily accessible and unexplored. The presence of the very ancient rocks makes it further more exciting. There is an evident need for applying the geological, geochronological, paleobiological and organogegeochemical studies to specific areas of interest. Such a programme may enable one to narrow the gap between chemical and biological evolution.

**Key Words :** Precambrian; Terrestrial, Chemical and Biological Evolution; Biosphere; Molecular Fossils

### INTRODUCTION

ON the planet earth the rock record is evidenced by the oldest metasedimentary sequence of the Isua-Godthab of Western Greenland, which has been radiometrically dated at 3.8Ga. Recent paleobiological and organic geochemical studies were carried out on these rocks to ascertain the earliest evidence of life. The presence of morphological remains such as stromatolites or microfossils could not be established although the isotopic studies of the organic carbon revealed a wide variability, indicating that isotopic fractionation had occurred. Since the isotopic shifts could not all be accounted for by metamorphism, there is little doubt that biological control of the terrestrial carbon cycle had been established by Isua times.<sup>1,2</sup> In retrospect, the 3.5Ga sediments of the Warwoona group of Western Australia account for the presence of stromatolites and the existence of complex microbiota associated with it.<sup>3</sup> The microbiota indicate that biological evolution had preceded the period, probably close to the Isua period. The discovery further stimulates the search for the earliest life in the Archaean sediments and subsequent interpretation of various microbial ecosystems in the Precambrian.

### EVIDENCE FOR LIFE IN PRECAMBRIAN SEDIMENTS

Another significant event in the evolutionary history of the earth is the creation of the oxygenic atmosphere which resulted in a complex interplay of the various biogeochemical processes. The study of early life on earth will help the understanding of the paleobiochemistry of these organisms and the paleoenvironments prior to origin and evolution of life. In the Precambrian sediments evidence for life can be broadly categorized into two sections : (1) chemical and (2) morphological.<sup>4</sup>

Chemical evidence seeks to investigate the following parameters :

- a.* Extractable organic matter ;
- b.* Insoluble organic matter;
- c.* Stable isotope evidence; and
- d.* Paleoenvironmental significance of banded iron formation.

Morphological evidence includes the study of :

- a.* Stromatolites ;
- b.* Microfossils—(*i*) filamentous and (*ii*) spheroidal ; and
- c.* Algal megafossils.<sup>5</sup>

Integration of the above data provides a comprehensive knowledge of life in the entire prephanerozoic period of the earth.

#### *Sedimentary Organic Matter*

Sedimentary organic matter has been observed to be of two types: extractable and insoluble.

*Extractable Organic Matter*—Extractable organic matter is composed largely of a volatile geolipid fraction of the organic matter which has been preserved in the sediments with minor alteration. The organic compounds are commonly referred to as chemical, or molecular, fossil. A chemical fossil has been defined as an organic compound in the geosphere whose structure suggests an unambiguous link with a known natural product.<sup>6</sup> The notion of the biological marker compounds has been central to the search for chemical traces of life in the Precambrian for the last two decades.

A variety of compounds has been reported from the Precambrian sediments.<sup>7</sup> They include alkanes (branched and cyclic), steranes, fatty acids, porphyrins, carbohydrates and amino acids. Among them, the most recent discovery of the five nitrogenous bases—adenine, cytosine, thymine, guanine and uracil from the McArthur shales, Western Australia—has demonstrated beyond doubt that the geological record bears the imprints of the primary constituents of life.<sup>8</sup>

*Insoluble Organic Matter*—The rather inert, insoluble organic matter in the sediments is termed “kerogen”. This type of organic matter is formed during the

diagenesis of sediments involving condensation and polymerization reactions, which result in the formation of complex macromolecules.

In recent years studies on the Precambrian kerogens have been carried out by the analytical pyrolysis technique.<sup>8,9</sup> The pyrolysis products included alkanes, alkenes and alkadienes and aromatic hydrocarbons.

### *Stable Isotope Studies*

The elements hydrogen, carbon, oxygen, nitrogen and sulphur are predominantly cycled in the atmosphere and hydrosphere by the various biogeochemical pathways of living organism. Carbon prominently figures as being one of the primary constituents of life. Biological fractionation by photosynthesis results in the enrichment of lighter isotope of carbon  $^{12}\text{C}$ . Stable isotopic studies carried on various Precambrian rocks has shown a wide range of values of  $^{13}\text{C}$  ranging from  $-20$  to  $-320$  per mill. The interpretation of the data requires the understanding of the geochemical history of the sediments.

### *Banded Iron Formation*

The presence of banded iron formation in the Precambrian was described as an evidence of oxygenic atmosphere as a result of photosynthesis.<sup>10</sup> In recent years, the geological evidence has shown that terrestrial oxidation occurred prior to and synchronous with the deposition of banded iron ore formation. Therefore, the idea of direct relationship between photosynthetic oxygen and precipitated iron is at best debatable.

### *Stromatolites*

Stromatolites are organosedimentary structures produced by sediment trapping, binding and precipitation resulting from metabolic activity and growth of organisms, primarily blue-green algae. They have been reported all over the world from the Precambrian sediments. The prominent Archaean stromatolites are from Bulawayan, Rhodesia, and the North Pole, Pilbara region of Western Australia. The presence of these structures is an indication of biological activity as evident from the modern analogous mats in the coastal environment of the Shark Bay of Australia.

### *Spheroidal and Filamentous Microfossils*

A large number of spheroidal and filamentous microstructures has been reported from stromatolites and cherts of the Precambrian. These microfossils show morphological resemblance to the prokaryotes. In the late proterozoic period certain large megascopic algal remains and macroscopic spheroids like *Chuaria* have been reported from various parts of the world. These structures are considered to be "algal megafossils".

## PRECAMBRIAN ROCKS OF INDIA

The Precambrian rocks of India occupy nearly two thirds of the Indian subcontinent, encompassing the peninsular, extrapeninsular and to some extent the basement rocks of the Indo-gangetic alluvium.

The extrapeninsular region of India comprises a polymetamorphic tectonic history imprinted by the Himalayan orogeny. The Himalayas are a result of the innumerable geological processes represented in sediments of various geological ages. The peninsular India on the other hand is dominated by the rocks of the Precambrian period which have been tectonically stable for a long period of time. The distribution of the Precambrian rocks in the Indian subcontinent is presented in Map 1.<sup>11</sup> Gupta<sup>11</sup> has reviewed the stratigraphy of the Precambrian rocks of India.

The geochronological investigations on the various formations of India have been represented on a geological map of the country in Map 2.<sup>12</sup> Sarkar<sup>13</sup> reviewed the Precambrian stratigraphy and geochronology of peninsular India.

The Indian subcontinent provides an unique opportunity as the Precambrian rocks are generally well exposed and easily accessible. There is also evidence for the remnants of the oldest crust. Radiometric dating of eight tonalite samples of the Singhbum province of India has revealed age determinations as old as 3.8 G. yr,<sup>14</sup> which can be correlated with the Isua metasediments of Western Greenland.

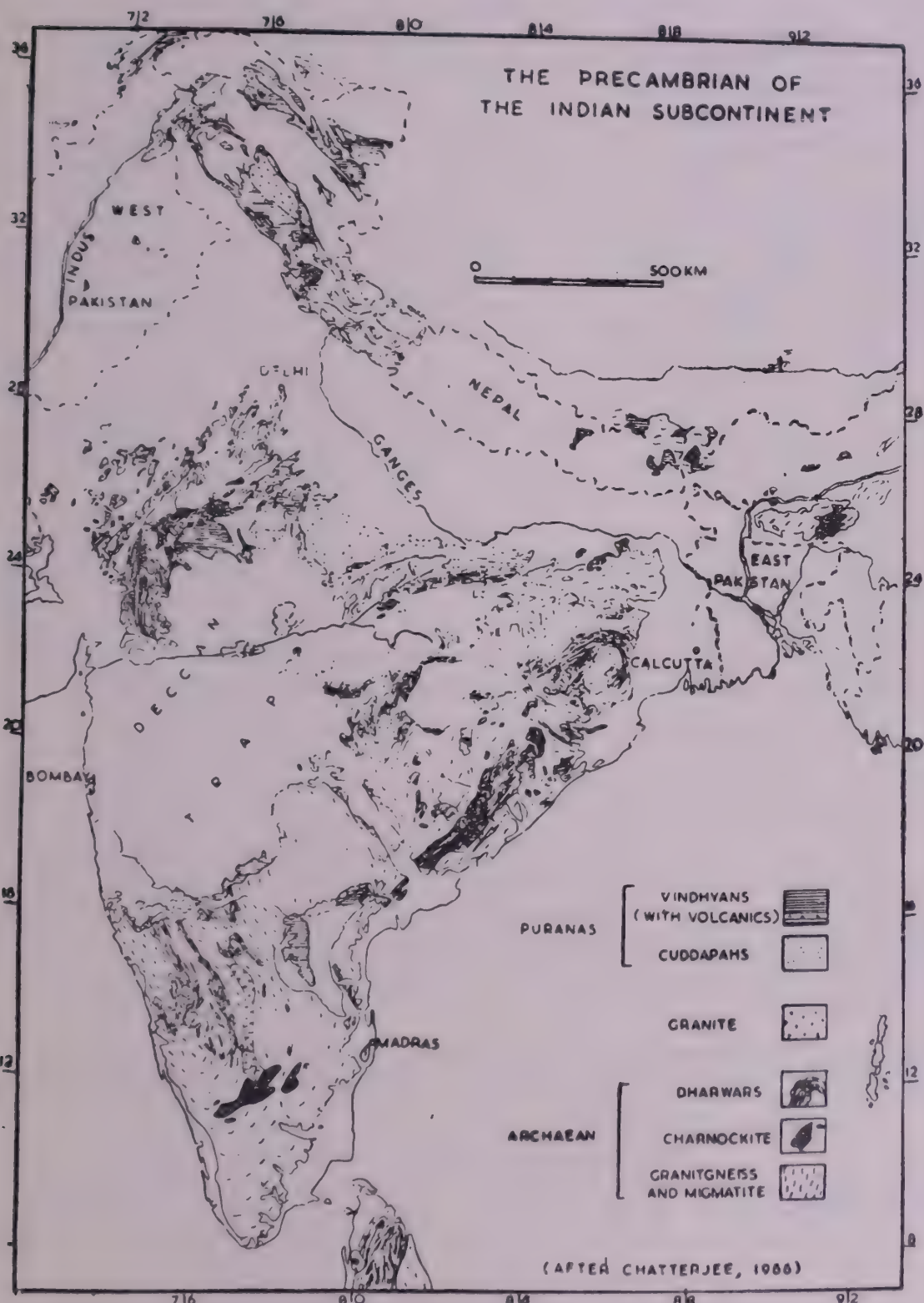
A critical appraisal of the data on the Indian Precambrian rocks highlights the lack of reliable radiometric studies for many areas. This makes selection of the area and interpretation of the data difficult. Precambrian microfossils from India have been reviewed by Prasad,<sup>15</sup> Sastry,<sup>16</sup> Raha and Sastry.<sup>17</sup> The reports of Archean microfossils are scarce; although there are several proterozoic microfossil reports, many of the areas need systematic investigation.<sup>17</sup> Certain reports of microfossils give different ages for the same stratigraphic horizon. There is an evident need for organic geochemical studies. Radhakrishna<sup>18</sup> has discussed the gaps in this field and has stressed the need for paleobiological and organogeochanical investigations in India.

In view of the studies in Precambrian life and paleobiology, a geochronological column is presented in Table I. The column incorporates radiometric data, lithology, biological evidence such as stromatolites and microfossils from the sediments as old as 3.5 Ga. The different time planes provide a unique opportunity for detailed studies of stromatolite morphologies, the various microbial communities, and the associated geochemical fossils which reflect the nature of life in the Precambrian. The area selected for the description have been based on the following criteria :

1. rock formations which have undergone less deformational history and metamorphism;
2. undoubted stratigraphic horizons having reliable dates; and
3. fossiliferous rocks with a prospective for organogeochanical work.

#### ARCHEAN ROCKS OF INDIA

Archean rocks are widely distributed in the eastern and southern parts of India. In eastern India the rocks are represented in Bihar and Orissa states of the Singhbum region.



MAP I

TABLE I

AGE $\times 10^9$	FORMATION	LITHOLOGY	DATA Ref.
3.5	Sargur Group	Chert	Microbiota <sup>19</sup>
2.6	Chitradurga	Chert	Microbiota <sup>20</sup>
2.6	G. R. Formation	Shale	Microbiota <sup>21</sup>
2.5	Iron Ore Group (Singhbhum)	Chert	Stromatolite <sup>22-24</sup>
2.5	Bababudhan Group	Banded Iron Ore	Microbiota <sup>25</sup>
2.4 to 1.5	Bijawar Formation	Dolomite	Stromatolite <sup>26-27</sup>
2.0	Aravalli Supergroup	Phosphorites	Stromatolite <sup>28-33</sup>
1.4	Cuddapah	Limestone	Stromatolite <sup>34-42</sup>
1.4 to 0.9	Vindhyan Supergroup	Limestone	Stromatolite <sup>43-49</sup>
1.4	Lower Vindhyan		
0.9	Upper Vindhyan		
1.4	Kaladgi Group	Limestone	Stromatolite <sup>49-50-51</sup>
1.1	Pakhal Group	Silicified	Stromatolite <sup>52-53</sup>
	Delhi Supergroup		Stromatolite
0.9	Bhima Group	Shale	Algal Structures <sup>54-55</sup>
	Kurnool Group	Dolomite	Stromatolite <sup>56</sup>

*Archaean Rocks of Eastern India*

The Archean rocks of eastern India are exposed in Orissa and Bihar states and can be subdivided into the following areas from south to north :

- a. Singhbhum-Keonjar-Sundargarh-Bonai-Mayurbhanj;
- b. Ranchi-Muri; and
- c. Hazaribagh-Gaya-Monghyr.

Three major groups of rocks—Gangpur, Iron ore and Kolhan groups are recognized with a well marked, 200km long copper belt thrust zone separating the low grade metamorphic rocks of the south from high grade metamorphic rocks to the north. On the basis of extensive structural and stratigraphic data accompanied by the various radiometric dates, Sarkar<sup>13</sup> proposed a revised stratigraphic succession which is as follows :

South of Copper Belt Thrust Zone in Singhbhum,  
N. Mayurbhanj and N. Keonjhar

North of Copper Belt Thrust Zone in  
Singhbhum

*End of Singhbhum Orogenic Cycle (c. 0.85 Ga)*

- |  |  |
|--|--|
| Newer Dolerites (c. 1.6–0.95 Ga)                     | Soda Granite Granophyre Chakradharpur                      |
| Mayurbhanj Granite (c. 1.2 Ga)?                      | Granite Gneiss Kuilapal Granite                            |
| Gabbro-anorthosite (c. 1.47 Ga)                      |  |
| Ultramafic intrusions Kalhan Group (c. 1.5–1.6 Ga)   |  |
| .....Unconformity.....                               |  |
| Jagannathpur Dhanjori-Simlipal Lavas (c. 1.6–1.7 Ga) | Dalma lavas with intertrappean reworked lava conglomerates |
| Quartzite conglomerate                               |  |

<i>Dhanjori Group</i>	
<i>Unconformity</i>	
Chaibasa Formation	
.....Unconformity.....	Dhalbhumi Formation—Singhbhum Group
Singhbhum Granite (c. 2.95 Ga)	Chaibasa Formation (sed. 2.0–1.7 Ga)
Iron Ore Orogeny	
Iron Ore Group	
.....Unconformity.....	
Older Metamorphic Gneiss (c. 3.2 Ga)	
O.M. Orogeny	
Older Metamorphic Group	
.....Basement (c. 3.3 Ga)	

### *Older Metamorphics*

The older metamorphic group is composed of calc-magnesian metasediments, argillites and arenites, tonalitic gneisses with basic intrusives. The rocks have undergone amphibolite facies of metamorphism.

### *Iron-ore Group*

The Iron-ore group of rocks unconformably overlies the older metamorphics. The lithology of rocks is comprised of limestone, shales (often phyllitic and grading to mica schists), quartzite, sandstones hematite beds, hematite quartzites. A basal conglomerate horizon rests upon the quartzites and quartz horblende mica schists.

In the Koira Valley in Keonjar and Bonai, the shales are manganiferous and are associated with hematite quartzites which have alternating layers of chert, jasper and hematite. The stratigraphy of the Koira group is as follows :

### *Kolhan Group*

Koira group	<i>Mixed facies formation</i> —undifferentiated sequence of multicolor manganiferous shale, dolomite chert
	<i>Upper shale formation</i> —banded shale member-red and white Black shale member with Black pyritiferous argillite
	<i>Banded iron formation</i> —Chert-shale member finely banded Jaspilite and coarsely banded Jaspilite member
	<i>Volcanic formation</i> —shaly member basic lava member Basal sandstone Quartzite formation

### *Singhbhum and Bonai Granites with Infolded Supracrustals*

*Paleobiological Investigations*—Stromatolites and associated microbiota have been reported from the Iron-ore group of Singhbhum province,<sup>22–24</sup> Grant *et al.*<sup>24</sup> reported the first record of stromatolites from the Koira group (iron ore series) of Bihar-Orissa, India.

The stromatolites reported are from the mixed facies formation, within two different lithologies, chert and dolomite. There are four main types: domal, Laminar, oncolitic and clavate. The first two types are reported to be present in cherts.

The author in his discussions has indicated that the siliceous stromatolites observed are primary in nature and no replacement phenomenon is discernible; probably microfossils resembling *Eospaera* and *Hurnosporia* have been identified. Stromatolites of the area require detailed study. The absolute age of the Koira group is uncertain. It has been assigned an age between 1.6 and 2.7 G.yr.

#### *Archaean Rocks of South India*

The Dharwar Supergroup of rocks of Karnataka State, South India, form several prominent schist belts in an otherwise granitic and gneissic terrain. The central part of the craton consists of a greenstone—gneissic complex characterized by green-schist to amphibolite facies and enclosed by a mobile belt of granulites and migmatite gneisses. The Northern part of the basin is covered by upper proterozoic Kal'dagi sediments and the Deccan traps. The Western side is bounded by the Arabian Sea. Gowda and Srinivasan<sup>57</sup> have discussed the history of concepts as applied to the rocks of Dharwar Supergroup. Srinivasan and Sreenivas,<sup>58,59</sup> Radhakrishna and Vasudev,<sup>60</sup> Ramakrishnan *et al.*,<sup>61</sup> Naqvi *et al.*<sup>62</sup> have enumerated

**Closepet Granite (2.38–2.0 Ga)**

**Chitradurga Granite (2.45 Ga)**

Manganiferous phyllites

Ankeritic limestones

**Ranibennur group (?)**

Greywackes

Chloritic phyllites

Agglomerate, tuffs, pillow lavas

Ferruginous & manganiferous cherts

Dolomites and limestones

Phyllites

Orthoquartzites

Banded magnetite quartzites

Argillites

**Chitradurga group**

Mafic lavas

Orthoquartzites

Conglomerates

**Bababudan group**

II event

c. 2.6 Ga

I event

c. 2.95 Ga

**Peninsular Gneisses**

**Granites, granodiorites**

**tonalities & granitic gneisses**

**Sargur group**

Interbedded mafic and ultramafic

Metalavas, Anorthosite pods

Magnetite Quartzites, Graphitic Schists

Kyanite-Staurolite Schists, Cordierite

Graulites, Crystalline Limestones &

Dolomites, Fuchsite Quartzites, etc.

**Basement C. 3.2 Ga (?)**

schemes for stratigraphic classifications for the entire Dharwar supergroup of rocks. The table on p. 1040 by Radhakrishna and Vasudev<sup>60</sup> gives a succession of the sediments in the area.

Viswanathiah and Ramakrishnan<sup>63</sup> identified a group of sediments associated with the lava flows in the Sargur region, named "Sargur high grade schist complex." The rocks of the Sargur Group are characterized by high grade metamorphism ranging from amphibolite to lower granulite facies. Lenses of anorthosite and anorthositic gabbro are abundant. Quartzites are often fuchsitic and characteristically bedded with sedimentary baryte. Structurally, the sediments are more deformed, with tight folds, steep plunges and complicated fold interference patterns. The Sargur sediments and the peninsular complex represent the older episodes of the region.

The Bababudan Group is well developed in the arc shaped Bababudan mountains and is predominantly volcanic. The basement gneissic complex is overlain by basal orthoquartzite which is succeeded by a thick succession of mafic lava flows unconformably overlain by argillites and massive beds of banded quartz magnetite rocks. The sequence is of shallow water platformal deposition. Sedimentary structures like ripple marks and cross bedding in quartzites also suggest shallow water depositional environment. The rocks have been subjected to green schist facies to lower amphibolite facies of metamorphism.

The Chitradurga Group is geosynclinal in character with a higher proportion of sediments. It starts with a basal conglomerate, orthoquartzites, phyllites, limestones and dolomites followed by banded ferruginous and manganeseiferous quartzites and cherts. Pillow lavas are abundant. Greywackes and cherts are extensively developed and marked by volcanic activity. Banded pyritiferous cherts have undergone a low grade of metamorphism of green schist facies.

Ranibennur Supa-Dandeli group of rocks is exposed to the North of Chitradurga Group of rocks characterized by greywackes and chlorite phyllites. The beds are least disturbed with gentle dips and are represented in North Kanara and Dharwar districts. A horizon of ankeritic limestones, ankeritic magnetite quartzites and manganeseiferous phyllites are exposed from a younger manganese iron ore belt in the Supa-Dandeli region. The low grade of metamorphism and less structural deformation of the sediments from the area offers a potential site for the investigation of early evidence of life.

*Radiometric Studies in the Region*—Geochronological investigations have been carried out in various parts of the area. The early Precambrian sediments of South India represent a time span of 3.5 to 2.5 Ga. Several radiometric dating reports in recent years support this view. Certain Conglomerates from Kaldurga in Tarikere Valley forming a part of Shimoga belt date  $3.25 \pm 0.15$  Ga.<sup>64</sup> The Sargur schist belt has been assigned an age older than 3.2 Ga, possible remnant of the Archaean protocrust.<sup>65</sup> Balasubramanyan<sup>66</sup> advocated a minimum age of 3.2 Ga to the Archaean tonalitic gneisses and granites from South Kanara. Certain other rocks of the region are the Champion gneiss and

the peninsular gneisses. The Rb-Sr radiometric investigations of the gneisses provide age estimates of  $2.95 \pm 0.11$  Ga with an initial Sr/Sr ratio of  $0.706 \pm 0.004$ .<sup>64</sup> Beckinsale *et al.*<sup>67</sup> dated gneisses from the Holenarasipur area giving an age of 3.36 to 3.10 Ga. Drury<sup>68</sup> dated metavolcanic lava flows at the base of the Kudremukh west coast belt by the Sm-Nd method, giving an age of 3.0 Ga. According to him the Kudremukh belt rests unconformably upon gneisses dated at 3.3 Ga. by an Rb-Sr method. Janardhan and Vidal<sup>69</sup> dated the gneisses from Gundlupet area which forms a part of the Sargur Group at an age of 2.83 Ga. They conclude that the age indicates the metamorphic event and sediments of the Sargur Group are still older. Chitradurga granites have also been dated,<sup>70</sup> giving an age of 2.65 Ga. The radiometric data discussed so far conclusively demonstrates that the Dharwar Supergroup is the rocks of Archaean age. The Arachean rocks of South India may provide a prospective site for evidence of early life.

*Paleobiological Investigations in Dharwar*—Gowda and Srinivas<sup>21</sup> have reported acritarchs which have been considered by others<sup>42</sup> as putative ‘pseudofossils’, mineralogical artifacts.<sup>42</sup> This calls for the reexamination of the rocks for the supposed microfossils in thin section as their importance lies in the fact that it would represent an early proterozoic non-stromatolitic biota.

Venkatachala *et al.*,<sup>71</sup> reported the presence of *Leiosphaerida agglutinata*, *L. dhakshinii*, *L. insigna concentrites muricatus*, *Protoleiosphaeridium sp.* *Granomarginata sp.* and *Vavosphaendium reticulatum* from the Dharwars of Karnataka. These reports and some others were based on studies of objects detected in acid resistant residues; these are questionable as they provide no direct evidence of the relationship between the microstructures detected and the original (undissolved) rock matrix.<sup>42</sup>

Viswanathiah and Venkatchalapathy<sup>25</sup> reported the presence of microbiota from the Bababudan group. The authors have described an assemblage of microfossils present in thin sections of the cherts.

Suresh<sup>20</sup> and Suresh *et al.*,<sup>72</sup> provided additional information on the Dodguni microbiota from the Chitradurga schist belt. These fossils were examined in thin sections of the cherts.

## PROTEROZOIC ROCKS OF INDIA

Proterozoic rocks representing various time planes are exposed in different parts of India (Table I and Map 3).<sup>16</sup> The various proterozoic basins are discussed below :

### *Aravalli Supergroup of Rajasthan*

The Aravalli sediments of India behold many geological formations of different ages. They are broadly categorized as :

Rialo Group;

Aravalli and Gwalior Supergroups :

Banded gneissic complex; and  
Bundelkhand granite and associated rocks.

#### RADIOMETRIC STUDIES OF THE ARAVALLI SUPERGROUP

Sarkar<sup>18</sup> has considered the end of Aravalli orogeny between 0.95 and 1.5Ga. The Pb isotope age of Aravalli schists near Udaipur was found to be and K-Ar age of gneiss 50km South of Udaipur was found to be 1.59Ga. Crawford<sup>73</sup> assigned the commencements of Aravalli Orogeny between 2.5 and 2.59Ga.

#### *Geology and Paleobiological Investigations*

Banerjee<sup>28,29</sup> reported stromatolitic colonies in and around the Udaipur area : Kanpur, Matoon, Dhamdhar, Jhamarkotra, Sameta, Dakamkotra, Neemuch Mata, Badgaon; all them are located between 2 to 25km. Generalized stratigraphic succession established by Banerjee<sup>28,29</sup> is as follows :

*Udaipur formation*—lithic quartzite, flaggy quartzite and current bedded orthoquartzite. greywacke and phyllite, sandy phyllite, calcareous phyllite.

orthoquartzite, brecciated calcareous quartzite, marble and carbon phyllite.

impure marble, dolomitic limestone with rolled and rewash-ed fragmental phosphorite and biothermal phosphorite.

*Matoon formation*—sandy phyllite, schist, orthoquartzite, brecciated quartzite, dolomite, marble, fragmental phosphorite, locally biothermal phosphorite.

impure marble, carbon phyllite with small garnets, mangani-ferous dolomite, intruded by granite.

buff, reddish white and brown orthoquartzite with inter-calated phyllite and chlorite schist at the top.

*Debari formation*—metaconglomerates and coarse arkose, meta arkose, meta conglomerate.

.....Shears.....Local faults.....

Bhilwara group (Banded gneissic complex)

The stromatolites have been reported in lower and middle part of Matoon formation. The author reported two assemblages in the lower and middle units of the Matoon.

(a) *Baicalica and Minjaria*—1.0–1.3Ga.

(b) *Collenia Columaris*—1.65–1.85Ga.

*Baicalica* is middle Riphean in age; *Minjaria* on the other hand is the lower part of upper Riphean. The report of the phosphorite bearing horizon is also

confined in the dolomitic limestone of the Matoon formation, which is abundant in brecciated cherty rocks and bluish gray dolomites interbedded with stromatolitic columns.

The depositional environment of the phosphorite bearing strata of Udaipur appear to be related to a facies change from argillaceous and silico-argillaceous shale and phyllite into calcareous or arenaceous. It appears to have been deposited close to an area of abrupt shallowing of the basin. Sedimentary structures such as load casts, convolutely laminated shaly horizon superimposed directly over the current bedded, pebbly orthoquartzites, followed by algal dolomitic phosphorite, have been reported.

Certain microfossils have been observed in thin sections. Banerjee<sup>28,29</sup> has reported the presence of filamentous bodies of *Baicalica* assemblage characteristic of middle Riphean age preserved in a phosphate carbonate chert matrix.

The area is suitable for detailed organic geochemical and paleobiological research. The association of phosphorite with stromatolites makes it more interesting and the reported environment of deposition by Banerjee<sup>28,29</sup> is of shallow water marginal sedimentation.

The occurrence of two different types of stromatolitic assemblage needs a detailed investigation.

#### *Cuddapah Basin of Andhra Pradesh, South India*

The Cuddapah basin represents the middle Proterozoic sequence of sediments. The crescent shaped basin (Map 3) has been extensively studied. Lithologically, it comprises alternating quartzites and shales. The classification of the Cuddapah Supergroup is as follows :

Krishna Group	Srisailam quartzites Kolamnala shales Irlakonda quartzites
Nallamalai Group	Cumbum shales Bairenkonda quartzites
Cheyair Group	Tadpatrisha shales Pulivendla quartzites
	.....Unconformity.....
Papagni Group	Vempalle shales and limestones Gulcheru quartzites
	.....Eparchean Unconformity.....
Archaeans	Gneisses and Schists

#### *Radiometric Studies of the Cuddapah Supergroup*

Crawford<sup>73</sup> reported the ages of the lavas in the Vempalle Formation to be  $1.32 \pm 0.6$  Ga. The Rb-Sr whole rock isochron age of these lavas gives an age of

1.25Ga whereas the intrusive dolerites are  $0.98 \pm 0.11$ Ga. According to Crawford<sup>73</sup> the Cuddapahs can be correlated with lower Vindhyanas. Crawford and Compston<sup>74</sup> dated the base of the basin to be 1.7Ga and the top at  $0.98 \pm 0.11$ Ga.

### *Paleobiological Investigations*

Rao<sup>31</sup> reported stromatolites *Conophyton*, *Kussiella*, *Colomnella* in the Vempalle Formation of the Cuddapah Supergroup. The latter two are reported in the Tadpatri by various workers. Prasad and Verma<sup>38</sup> have reported *Collenia rajurkarii* in the upper part of Vempalle strata. *Conophyton* has been reported from the Cumbum Formation.<sup>41</sup> A large assemblage of structurally preserved microorganisms was identified including *Archaeorestis barghoorn*, *Corymbococcus awramik*, *Eostriion barghoorn* which were similar to the forms of the Gunflint Formation of Canada.

Schopf and Prasad<sup>12</sup> account a diverse assemblage of originally preserved unicellular and filamentous microorganisms from the *Collenia* bearing Vempalle Formation. According to them, it represents the oldest stromatolitic microbiota known in India.

### *Pakhal Group of Andhra Pradesh*

The Pakhals represent a conspicuous stratigraphic sequence in the Pranhita Godavari Valley. The stratigraphic position of the Pakhals in the area is as follows :

Gondwana Supergroup	
Purana Supergroup	Sullavai Group Pakhal Group
	Undifferentiated basement complex

### *Geology and Paleobiological Investigations*

Chaudhuri<sup>52</sup> reported stromatolites from the Mallampalli Subgroup. A generalized stratigraphic succession is presented to indicate the various lithologies present.

Pandikunta shale (450')	slate with bedded limestone
Mallampalli Subgroup	
Pandikunta limestone (8050')	cherty limestone with interbedded purple limestone
Mallampalli conglomerate (100')	Ferruginous silicerudite (local) Arkose arkosic conglomerate

Non-conformity

Archaean	Granite and gneisses, etc.
----------	----------------------------

The upper calcareous Pandikunta Formation has stromatolites *Colonella*, *Conophyton* and *Kussiella* were assigned.<sup>52</sup> He assigned the stromatolites to various groups: types LLH, SH and SS depending on whether the base of the structure is attached to the substratum or not. Each of the three groups has been divided into various subgroups.

The dominant lithology of the Pandikunta Formation is limestone and dolomite. The carbonate rocks occur as well developed, fairly persistent beds. Glauconitic sandstone and few lenses of shales are found associated with it. The beds containing stromatolites are light gray, buff purple and light pink, weathered black, fine grained, massive dolomitic limestone. Sedimentary structures like small scale bedding and ripple marks characterize the different lithotypes.

The depositional sedimentary environment occurred, according to Basumallick<sup>75</sup> in a marine epineritic condition evidenced by the presence of glauconite, bedded chert, moderate to well sorted arenites, secondary growth of potash feldspar and high magnesia content of the carbonates. The formation has been dated 1.4 Ga based on K-Ar ratio in glauconitic sandstones.

#### *Vindhyan Supergroup*

The Vindhyan Supergroup has a wide geographical distribution encompassing the border of three states : Rajasthan, Madhya Pradesh and Uttar Pradesh : these are representatives of the Northern part of India. The area has been extensively investigated by various workers and the broad division of the stratigraphic units is as follows :

Rewa Group	Upper Bhander Sandstones
150–300m	Sirbu Shales
	Lower Bhander Sandstones
	Lower Bhander Limestones
	Ganurgarh Shales
Kaimur Group Upper	Upper Rewar Sandstones
150–300m	Jhiri Shales
	Lower Rewar Sandstones
	Panna Shales
	Kaimur Sandstones (Dhandhraul Quartzites)
	Upper Kaimur Congolmerates (Scarp Sandstones)
	Bijaigarh Shales
	Upper Quartzite
	Silicified Shales
	Lower Quartzites
	Rohtas Formation
	Kheinijua Formation—Glauconite Sandstone, Fawn Limestone, Olive Shales
Semri Group	Porcellanite Formation
300–1,000m	Basal Formation
	Kajrahat Limestone Conglomerates

The classic area for the study of rocks is the Semri group in the Sone Valley, Mirzapur. Lithologically, the rocks belonging to this group comprise dolomitic limestones, which at places are intercalated with bands of rhyolitic tuffs and glauconitic sand stones.

Bhargava,<sup>76</sup> on the basis of the studies performed in the North and West of Sidhrie, concluded that the environment of the deposition of the lower Vindhyan is a shallow marine environment ranging from intertidal to epineritic zones. The lower Vindhyan are unconformably overlain by the Kaimurs in the Mirzapur District, represented by Bijagarh shales, which comprise carbonaceous, pyritiferous, micaceous, siltstone of bleached or yellow colour representing an euxinic facies. The pyrite bearing horizon near Bijagarh is about 10m thick but it thins out eastward and westward.<sup>77</sup>

The Rewa group succeeds the Kaimur group, lithologically composed of red shales and sandstones. The Bhander group, which constitutes the youngest division of the Vindhyan supergroup and comprises a thick succession of shales, limestones, dolomites and sandstones. Geologically, the rocks of the Vindhyan supergroup are ideally suited for detailed organic geochemical and paleobiological work.

#### *Radiometric studies of the Vindhyan Supergroup*

The geochronological data available indicate that the base of the lower Vindhyan may have a minimum age of 1.4Ga and the base of upper Vindhyan can be demarcated at above 1.14Ga.<sup>78</sup>

Misra<sup>77</sup> gave a time span of 1.4Ga to 0.9Ga for the Vindhyan by the evidence provided by various stromatolitic horizons. The Glauconitic sandstone is dated to be  $1.11 \pm 0.06$  Ga,<sup>79</sup> which is thus of late or early middle Riphean age.

#### *Paleobiological Studies of the Vindhyan*

Jones<sup>80</sup> reported the presence of black, carbonized, wrinkled, discoidal bodies from the Suket shales exposed at Rampura in the Neemuch District of M.P. The organic remains were assigned to the genus *Obolella* and later considered resembling *Chauria circularis*. Workers were disputed on the plant or animal origin of these organic discs. Chapman<sup>81</sup> attributed these discs as representatives of two new genera : *Fermoria* and *Protobolella*. Sahni and Srivastava<sup>82</sup> suggested evidence supporting the algal nature of *Fermoria*. Misra<sup>83</sup> contended that the material was of inorganic origin, a colloidal precipitation of mineral matter. Palynological investigations in the area were carried out by a number of workers, and revealed a microfloral assemblage--*Leiosphaerida*, *Retisphaerodium*, *Lacunalites*, *Tasmanites*, *Gloeocapsmorphia*, etc. However, in all probability the microfloral assemblage which indicates Cambrian and Ordovician age appears post depositional and may not represent the time period of deposition.

Kumar<sup>48</sup> recorded an assemblage of *Kussiella Russiensis*, *K. dalensis*, *Collenia symmetrica*, *Colonella* and *Conophyton* from the Kajrahat limestone (basal members of the Semri group) and *Conophyton gorganicus* and *Collonella columnaris* from

the Fawn limestone of the Vindhyan. The report suggests an early Riphean age for the lower part and middle Riphean age for the upper part of the Semri group.

The Bhander group has reports of *Collenia baicalica*,<sup>47</sup> *Crytozoon Occidentalis*,<sup>53</sup> *Baicalia baicalica*, *B. Satnesis* and *Maiharia maiharensis*,<sup>48</sup> *Tunguissa*, *Boxonia* from different parts of the Vindhyan.

#### *Bijawar Group, Madhya Pradesh, India*

The Bijawars underlie the Vindhyan supergroup and are exposed as a series of outcrops from Bundelkhand to the South of the Narmada (see Map 3). Lithologically, this group consists of 240m thick succession on horizontally or gently dipping beds of quartzites interbedded with limestones and hornstones breccia which are not uniformly distributed. In the Joga area, Hoshangabad District, the dolomites contain stromatolites *Conophyton* (*cylindricus*) and *Collenia columnaris* (*colonnella*).<sup>27</sup> No systematic study has been carried out. The Bundelkhand granite which underlines the Bijawars has been dated 2.37Ga by Sarkar.<sup>84</sup> The Bijawars has been dated by Rb-Sr isochron of whole rock at 2.41–1.51Ga.<sup>84</sup>

#### *Kaladgi and Bhima Basins of Karnataka State, South India*

The Kaladgis are exposed along the southern border of the Deccan trap country, extending 150km; at places they are covered by the Deccan traps (see Map 3). It rests unconformably on gneisses and schists with little or no metamorphism. Viswanathiah *et al.*<sup>85</sup> have classified the Kaladgi group.

#### Badami Group

Unconformity.....		
Kaladgi Group	Mudhol Formation	Machkhandi-granite
		Laksanhalli-dolerite
		Nirlasperi-breccia
		Vajramatti-quartz-arenite
		Yadhatti argillite
		Retlur limestones
		Jalikatti-argillite
		Chikshellikari limestone
Lokapur Formation		Chitrabhanukot dolomite
		Manoli-argillite
		Makut-breccia
		Bili-quartz-arenite
Bagalkhot Formation		Salagundi conglomerate
Unconformity.....		
		Dharwar Supergroup

### Paleobiological Investigations

Stromatolites belonging to *Collenia* group were identified by Viswanathiah and Gowda.<sup>86</sup> Raha and Sastry<sup>17</sup> contended that there is lack of detailed systematic studies and have recognized *Colonella-Kussiella* assemblage in the Kaladgi group.

Apart from the stromatolites, Venkatachala and Rawat<sup>51</sup> and Viswanathiah et al.<sup>85</sup> have recorded the occurrence of a rich assemblage of acritarchs from the Chikshellikeri limestone and Chitrabhanukot dolomite of the Lokapur formation. The fossil assemblage reported includes *Microtaenia*, *Protoliosphaeridium*, *problematicum*, *Spumiosa alara*, *Leiosphaeridia aglutinata*, *L. dhakshimii*, *Retisphaeridium dichamerum*, etc. Radiometric data are lacking from the area.

### Bhima Group Karnataka

The Bhima group is well developed in the Gulbarga and Bijapur districts of Karnataka state and part of Andhra Pradesh occupying an area of about 4,200 sq. km. The group is subdivided into three units :

Upper (100m)	Black, blue, buff and purple shales with local sandstones at the bottom and flaggy limestone at the top.
Middle (165m)	Creamy, gray, bluish buff and flaggy limestones.
Lower (110m)	Sandstones, green and purple shales. The bottom beds are conglomeratic whereas the topmost beds are often calcareous.

### Paleobiological Studies

The area has been studied by various workers who have reported a host of palynofossils and late proterozoic index fossil *Chauria Circularies Walcott* from the lower Bhima shales.<sup>54</sup>

Salujha, Rehman and Arora,<sup>87</sup> Venkatachala and Rawat<sup>51</sup> and Viswanathiah et al.<sup>55</sup> reported an assemblage of microflora. Salujha, Rehman and Arora<sup>87</sup> state that Bhima group may range from Cambrian to Ordovician in age. The assemblage representing different ages conclusively does not define a time period.

Suresh and Gowda<sup>54</sup> upon investigations carried out on the samples collected from the Gulbarga district, Karnataka, reported a palynofossil assemblage of sphaeromorphs associated with *Leiosphaerida*, *Tasminites*, and *Hystrichosphene*. On the basis of characteristic index fossil *Chauria Circularis*, a late proterozoic age is suggested. There are no reports of stromatolites.

There is no record of any radiometric investigations. Schnitzer<sup>56</sup> on the basis of lithology and various cycles of sedimentation has considered it to be equivalent to the Kurnools in age.

### Kurnool Supergroup of Andhra Pradesh, South India

The Cuddapah sediments in the parts of Kundair Valley and Palnad tract of Andhra Pradesh are conformably overlain by the rocks of the Kurnool supergroup.

Lithologically, it comprises sandstones, shales, limestones and quartzites. The best succession of this supergroup is exposed in the Kurnool area where it is subdivided into four units :

Kurnool Supergroup	
Group	Formation
Kundair	Nandyal shales, Koilkunta limestone
Panaim	Pinnacled quartzites
Jamalmadugu	Plateau quartzites
Banganpalli	Auk shales, Narji limestone
	Banganpalli sandstone

Schnitzer<sup>56</sup> on the basis of four cycles (A, B, C, D) of sedimentation recorded various units of this supergroup. All cycles culminate in a red series (red beds, red claystone, red shales). He has reported the occurrence of stromatolitic limestones, forming large reef complexes from cycles B and C (Nargi Formation). The stromatolites are silicified, showing the presence of radiolarites in the chert bands.

It is noted that the stromatolites differ in form and character from those found in rocks of Cuddapah and Chattisgarh supergroups.

Salujha, Rehman and Arora<sup>87</sup> have recorded the occurrence of microplankton from different stratigraphical horizons. The forms include *Archaeasavosina pellucida*, *Lophosphaeridium bellus*, *L. Kurnodi*, *Dictyotidium sp.*, etc.

#### *Age of the Kurnool Supergroup*

Systematic radiometric studies are lacking. Sarkar<sup>88</sup>, reported a whole rock age 0.453 Ga for the Auk shales. Palynofossil assemblage renders a late Precambrian to Cambrian age. Schnitzer<sup>56</sup> has considered it to be the equivalent of the Bhima group as evidenced by identical lithology, sedimentation pattern and palynological assemblage.

#### *Chattisgarh Supergroup*

The sediments are deposited in an intracratonic basin between South India and the Vindhyan. Schnitzer<sup>56</sup> proposed a classification scheme for this supergroup. The base of it is marked by Chandapur quartzite, which is disconformably overlain by a succession of rocks belonging to the Raipur group. Raipur succession has been assigned to five cycles of sedimentation which begin with dark limestones and extend into "red beds". Stromatolites are extensively developed and particularly larger in size in the fifth cycle of sedimentation. Jairaman and Banerjee<sup>89</sup> have reported stromatolites in the limestones from the Raipur area of the Chattisgarh basin. The forms described are *Gymnosolen*, *Inzeria*, *Tungussia*, *Cryptozoan occidentalis*. The late proterozoic Chattisgarh sediments are correlated with Kurnool supergroup.

### CONCLUSION

The Precambrian rocks of India represent a vast area of time and space. The oldest dated sediments from the eastern part of India provide an opportunity to study the early chemical evolutionary events from this part of the earth. Although there are many reports of stromatolites from the Proterozoic basins, systematic work is needed in many areas. Reports of Archean life forms are rare. Reliable radiometric data are needed in many areas. Organogeochemical data are lacking.

### REFERENCES

1. M Schidlowski In: *Stable Isotopes* (Eds Schmidt, Forstel and Heinzinger) Elsevier Amsterdam (1982) 95
2. C C Walters *Organic Geochemistry of the 3800 Million Year Old Metasediments from Isua, Greenland Ph D Thesis* University of Maryland College Park USA (1981)
3. J W Schopf and M R Walter *Origin and Evolution of Earth's Earliest Biosphere* (Ed Schopf) Princeton University Press Princeton (1983)
4. J W Schopf *Ann Rev Earth Planet Sci* **3** (1975) 213
5. S M Awarmik *Minerals Deposit and Evolution of Biosphere* (Ed Holland and Schidlowski) Springer-Verlag Berlin New York (1982) 67
6. A S Mackenzie S C Brassell G Eglington and J R Maxwell *Sci* **217** (1982) 491
7. D M McKirdy D J McHugh and J W Tardiff *Biochemistry of Ancient and Modern Environments* (Ed Trudinger, Walter and Ralph) Springer-Verlag Berlin (1980) 187
8. C Ponnampерuma *Organic Compounds in Carbonaceous Chondrites Abstr* 186th ACS National Meeting Washington D C USA (1983) and unpublished results.
9. R P Philip and D van de Meent *Precamb Res* **20** (1983) 3
10. P Cloud *Econ Geol* **68** (1973) 1135
11. V J Gupta *Precambrian Stratigraphy of India* Hindustan New Delhi (1977)
12. M N Saxena and J A Miller *Curr Sci* **41** (3) (1972) 108
13. S N Sarkar *Indian J Earth Sci* **7**(1) (1980) 11
14. A R Basu S L Ray A K Saha and S N Sarkar *Sci* **212** (26) (1981) 1502
15. K N Prasad *Geol Surv India Misc Publ* **44** (1980) 11
16. M V A Sastry *Geol Surv India Misc Pubc* **44** (1980) 3
17. P K Raha and M V A Sastry *Precamb Res* **18** (10) (1982) 293
18. B P Radhakrishna *J geol Soc India* **23** (1982) 313
19. M N Viswanathiah V Venkatchalapathy and A P Mahalakshamma *J geol Soc India* **17** (1) (1976) 112
20. R Suresh *J geol Soc India* **23** (1982) 267
21. S S Gowda and T N Sreenivasa *J geol Soc India* **10** (1969) 201
22. R K Avasthy *Geol Surv India Misc Pub* **44** (1980)
23. P K Maithy and R K Avasthy *J geol Soc India* **23** (1982) 263
24. P R Grant V M Murthy and S Sengupta *Geol Surv India Misc Publ* **44** (1980)
25. M N Viswanathiah and V Venkatachalam *J geol Soc India* **21** (1980) 16
26. M S Balasundaram and T M Mahadevan *Rec geol Surv India* **2** (1972) 127
27. M Krishnamurthy *M P J geol Soc India* **13** (1972) 183
28. D M Banerjee *Geol Soc Am Bull* **82** (1971) 2319
29. D M Banerjee *J geol Soc India* **12** (1971) 349
30. D S Chauhan *Dokl Akad Nauk SSSR* **208** (1975) 1429
31. D S Chauhan *Geol Surv India Misc Publ* **44** (1980) 128
32. Mukti Nath and V N Sant *Curr Sci* **36** (23) (1967) 638

33. C S Raja Rao G C Iqbaluddin and R K Mathur *Curr Sci* **37** (10) (1968) 560
34. M R S Rao *Curr Sci* **13** (3) (1943) 75
35. R Vaidhyanathan *Curr Sci* **30** (6) (1961) 221
36. M N Viswanathiah and B V G Rajulu *Curr Sci* **32** (10) (1963) 510
37. M N Viswanathiah and A N Aswahanarayana *Indian Min* **8** (1967) 62
38. K N Prasad and K K Verma *A P J Indian geol Sci Assoc* **7** (1967) 95
39. F Lotze *Nue Jahrb Geol Palaeontol Monash* **11** (1967) 677
40. S R Sharma and C N Rao *J Indian geol Sci Assoc* **2** (1969) 102
41. B Bhaskara Rao and M N Gururaja *Geol Surv India Misc Publ* **44** (1980) 38
42. J W Schopf and K N Prasad *Precamb Res* (1978) 347
43. J B Auden *Mem geol Surv India* **62** (1933) 141
44. A K Dutta *Sci Cult* **18** (7) (1953) 328
45. S M Mathur K Narain and J P Srivastava *Rec geol Surv India* **87** (1962) 819
46. M Krishnamohan *N Jb geol Palaeont Abstr* **130** (1968) 335
47. K S Valdiya *J Geol Soc India* **10** (1969) 1
48. S Kumar *J Palaeontol Soc India* **19** (1976) 24
49. V B Khilnani *O Jl Min métal Soc India* **40** (1968) 1
- 49a. B V G Rajulu and M J C Gowda *J Sedim Petrol* (1968) 1039
50. M N Viswanathiah and T R Sreedhara Murthy *Curr Sci* **41** (5) (1972) 171
51. B S Venkatachala and M S Rawat *Geophytology* **3** (1) (1973) 26, 107
52. A Chaudhuri *Palaeogeogr Palaeoclimatol Palaeoecol* **7** (1970) 208
53. K K Verma and G Barman *Seminar on Recent Advances in Geology Rajasthan and Gujarat, Jaipur—On the Stromatolites from the Upper Vindhyan of Rajasthan India* (1973)
54. R Suresh and S S Gowda *Proc IX Indian Coll Micropal Strat* (1981) 127
55. M N Viswanathiah V Venkatachalapathy and D Doddaiyah *Geol Surv India Misc Publ* **45** (1979) 17
56. W A Schnitzer *Erlang Geol Abhandlung* **85** (1971) 1
57. S S Gowda and R Srinivasan *History of the Concepts of Precambrian Geology as applied in the Mysore Area of India* (Ed Kupsch and Sarjeant) Geol Assoc CANADA Spec Paper **19** (1979) 81
58. R Srinivasan and B L Sreenivas *Indian Min* **9** (1968) 182
59. R Srinivasan and B L Sreenivas *J geol Soc India* **11** (1972) 75
60. B P Radhakrishna and V N Vasudev *J geol Soc India* **18** (1977) 10
61. M Ramakrishnan M N Viswanatha and J Swaminath *J geol Soc India* **17** (1976) 97
62. S M Naqvi V Divakara Rao and Harinarain *Precamb Res* **6** (1978) 323
63. M N Viswanatha and M Ramakrishnan *Indian Min* **16** (1976) 48
64. V S Venkatsubramanian and R Narayanswamy *J geol Soc India* **15** (2) (1974) 77; **15** (3) 318
65. P Venkataramana *Precam Res* **19** (1982) 51
66. M N Balasubramanyan *Archean Geochem* Elsevier Amsterdam (1978) 59
67. R D Beckinsale S A Drury and R W Holt *Nature* **283** (1980) 469
68. S A Drury *Geochim Cosmochim Acta* **47** (1983) 317
69. A S Janardhan and P H Vidal *J geol Soc India* **239** (11) (1982) 578
70. B Chadwick M Ramakrishnan M N Viswanatha and V Srinivasa Murthy *Precamb Res* **16** (1981) 31
71. B S Venkatachala L L Bhandari A N Chaube and M S Rawat *The Palaeobotanist* **21** (1) (1973) 1
72. R Suresh and S S Gowda *Curr Sci* **52** (1983) 71
73. A R Crawford *J geol Soc India* **22** (1969) 557
74. A R Crawford and W Compston *J geol Soc London* **125** (1983) 351

75. S Basumallick *J geol Soc India* **8** (1967) 130
76. M Bhargava *Bull Indian geol Assoc* **4** (3-4) (1971) 3
77. R C Misra *Pres Addr Geology Section 56th Indian Sci Congr* (1961) 1
78. A I Tugarinov L L Shamin G A Kazakov and M M Arakelyants *Geokhim* **6** (1965) 652
79. A Vinogradov and A I Tugarinov *Proc 22nd int geol congr* **10** (1964) 515
80. H C Jones *Rec geol Surv India* **38** (1909) 66
81. F Chapman *Rec geol Surv India* **69** (1935) 164
82. M R Sahni and R N Srivastava *Curr Sci* **23** (1954) 39
83. R C Misra *J pal Soc Geol* **2** (1957) 54
84. S N Sarkar *Dhanbad* (1968) 1
85. M N Viswanathiah V Venkatachalapathy and A P Mahalakshmamma *J geol Soc India* **11** (4) (1975) 378
86. M N Viswanathiah and M J C Gowda *J geol Soc India* **11** (1970) 378
87. S K Salujha K Rehman and C M Arora *J Palynol* **8** (1972) 123
88. S K Sarkar *Sci Cult* **30** (1964) 527
89. R Jairaman and D M Banerjee *Geol Surv India Misc Publ* **44** (1980)



## Procedure for submitting manuscript

**General :** Manuscripts should be sent, *in triplicate* (with 3 sets of illustrations, *one original and two photocopies*) to the *Editor of Publications, Proceedings A, Indian National Science Academy, Bahadur Shah Zafar Marg, New Delhi-110 002.*

Submission of the manuscript will be held to imply that it has not been previously published in any form and is not under consideration for publication elsewhere.

**Presentation :** Articles should be as brief as full documentation allows. They should not usually exceed 12 printed pages (approx. 12,000 words). Review articles may be upto 20 pages. Papers must be written clearly and concisely with consistency in style and spelling (spellings should be according to Oxford Dictionary), and typed double spaced with ample margins on durable bond paper. The usual format is: 'Abstract', 'Key words', 'Introduction', 'Materials and Methods', 'Results', 'Discussion', and 'Acknowledgement' (if any) and 'References'.

**Classification :** The exact classification of the paper (e.g., Astrophysics, Inorganic, Organic and Physical Chemistry, Seismology etc.) should be provided at the top of the manuscript.

**Title :** Title should be brief, specific and informative of the subject discussed. It should not begin with such general words as 'The', 'A', 'Study', 'Effect'. If a paper forms part of a series, this may be indicated through a symbol in the title and a footnote "This is paper X in series. Paper on IX is ref .....". The preceding paper must then be included in the list of references.

**Running Title :** Should not exceed 50 characters (including spaces).

**Keywords :** Up to five important key words should be provided for indexing and for information retrieval.

**Abbreviations :** Non-standard abbreviations used five or more times in the text should be listed in the footnote. Define where first mentioned followed by abbreviation in parentheses. Subsequently, the abbreviations should be used. However, these should be kept to a minimum and should not be used in the titles, key words or abstract.

**Abstract :** The abstract (typed on a separate page) should summarize the principal findings within 250 words.

**Text :** The paper must be divided into sections preferably starting with 'Introduction' and ending with 'Discussion' (or 'Acknowledgement', if any). All measurements must be given in SI units. Avoid numbers at the beginning of a sentence or spell them out. The scientific names of plants, minerals, and animals should be underlined. Authors of name of taxa should be cited at the first mention of a taxon, but not elsewhere. Accepted common names of plants and animals should neither be capitalized nor placed within quotation marks. Words and phrases of foreign origin in common use need not be underlined (e.g., *et al.*, *viz.* e.g.,

i.e., etc.) whereas the rest should be underlined (e.g., *in vitro*, *in situ*).

**Tables :** All tables must be numbered serially in roman numerals and placed at the end. The table should have brief titles (*underlined*) and contents should be self-explanatory. Non-standard abbreviations should be used sparingly and defined at the bottom of the table. Also details of the experiment (not mentioned in the text) may be indicated below the table.

**Illustrations :** Original drawings (in India ink in clean uniform lines on tracing paper or Bristol paper) and sharp photographs (with high contrast and glossy prints) numbered in arabic numerals should be provided. Illustrations on reduction must fit into a minimum of 6.5cm and a maximum of 12.5cm width. Labelling of figures should therefore be done keeping in view the reduction (blow-up) into (6.5cm or 12.5cm). Magnification should be indicated in the legend be scale or figures (x .....). For composite figures, mounting should be done carefully with even spacing in between. Illustrations should be supported with cardboard to avoid damage in transit.

**References :** References in the text should be cited by number. References at the end of the paper should be listed by number, author's name, name of journal (*underlined* and abbreviated according to the *World List of Scientific Periodicals* Butterworths, London), Vol. no., year of publication and page no. References to book should include : name of author, title of the book (*underlined*), name of editor if any, preceded by 'Ed(s)', place of publication, publisher, year of publication chapter or pages referred to. References to thesis, the degree, the year for which submitted, the university and the place. Sample citations are given below :

### For periodicals

1. R H Fox *Fund Math* 34(1947) 278

### For books

1. H Rund *The Differential Geometry of Finsler Spaces* Springer-Verlag Berlin (1953) p 283

**Proofs :** Proofs will be sent to the author(s) and should be returned to the Editor within 48 hours. Major corrections or alterations will be accepted only at author's expense.\* If proofs are not returned within the specified time, they will be read in the Editorial Office and print-ordered.

**Reprints :** Fifty reprints will be supplied free of charge to the authors. Additional copies should be ordered on the order-form accompanying the proofs. Payment for extra reprints must accompany the order-form.

\*The recompensation cost will be charged to the author. In case the author desires to withdraw the paper, he shall pay towards the composition charges, if the paper has already been type-set.

# Proceedings of the Indian National Science Academy

Vol. 51, Part A, No. 6

NOVEMBER 1985

## CONTENTS

	Page
<i>Sisir Kumar Mitra Memorial Lecture—1984 : Secologanin Derived Bio-Dynamic Indole Alkaloids (Mrs) Asima Chatterjee FNA</i>	905
Thermo- and Photo-Magnetic Effects in Poly-Crystalline Meta Dinitrobenzene involving Time-Variation of Dielectric Constant A K Chatterjee and S D Chatterjee FNA	929
Vibrational Spectrum and Normal Coordinate Treatment of Acetophenone S Mohan T J Bhoopathy and K G Ravikumar	936
Infrared Absorption Spectra of Some 8-Aminoquinoline Solid Complexes in correlation with Coordination Bond-Length Morsi M Abou Sekkina and S M El-Helbawy	946
Electromagnetic Fields of Transient Signals above Evaporation Duct Samira T Bishay	954
Vibrational Spectra of Some Solid 8-Hydroxyquinoline Metal Complexes in correlation with their Coordination Bond Length and Type of Metal Ion Morsi M Abou Sekkina and S M El Helbawy	959
Spectra of Samarium Complexes V Ramesh Babu and S Buddhudu	965
Distribution of Stress in the Neighbourhood Crack in a Transversely Isotropic Solid P Chowdhury and Sukla Maity	968
Determination of Solar Energy Fluctuations in the Lower Atmosphere Using Spectral Analysis Techniques Ernest C Njau	986
Computation of Neutron Cross-Sections at 14 MeV for Some Medium Mass Trace Elements R S Khanchi, K K Manocha, S K Gupta, and R K Mohindra	998
Rare-Earth Chelates of Dibasic Tridentates Possessing Nitrogen and Oxygen Donor Sites Sunita Bhatia, Preeti Mehta and R K Mehta	1003
Kinetics of Alkali-catalysed Catechol-Formaldehyde Reaction H C Malhotra and P S Jassal	1008
Effects of Temperature and Soil Moisture on the Kinetics of Phosphate Fixation in Alkaline Alluvial Soils P P Biswas and Geetanjali Ghosh	1016
An Appraisal of the Manganese Ore Deposits of Goa, India A G Dessai	1021
Precambrian of India—Possible Source of Evidence for Early Life Vivek Navale, Ramachandran Suresh and Cyril Ponnamperuma FNA	1033